Using Surface Chemistry to Facilitate Silicon Nanocrystal Applications

by

Muhammad Amirul Islam

A thesis submitted in partial fulfillment of the requirements for the degree of

Doctor of Philosophy

Department of Chemistry
University of Alberta

Abstract

Quantum dots (QDs) have drawn substantial attention in multidisciplinary research in science, technology, and biomedicine during the last three decades. However, the toxicity of heavy metals and the depleting earth abundance of some elements common to QDs have prompted the development of alternative non-toxic and abundant QDs. To date, silicon nanocrystals (SiNCs) have shown promise as a safer and a readily available alternative to common QDs partly because silicon is abundant, non-toxic, and the workhorse material in electronic devices. However, controlling SiNC surface chemistry remains an important challenge to the widening of the scope of their applications in optoelectronics, catalysis, bioimaging, and drug delivery. This thesis will present attempts to tailor SiNC surface chemistry in a targeted fashion to facilitate applications.

Chapter 1 will present the fundamentals of QDs highlighting the current state of SiNC research including a brief summary of material synthesis, surface modification, physicochemical properties, and prototype applications. Chapter 2 describes the exploration of the Lewis acidic nature of chloride-terminated SiNCs (Cl-SiNCs), chloride-terminated silicon wafers (Cl-SiWF), and silicon tetrachloride ($SiCl_4$) for the synthesis of poly (3-hexylthiophene) (P3HT) *via* oxidative coupling of 5-chloromagnesio-2-bromo-3-hexylthiophene monomer. This study provides an insight into the reactivity of the silicon-based species that can potentially be applied for the synthesis of valuable materials. The details of the synthesis, characterization, and optical properties of SiNC and P3HT hybrid functional material (HFM) is described in Chapter 3. This study demonstrates an effective procedure for grafting conducting polymers from semiconductor SiNCs with direct interfacial contact and provides a valuable understanding of the benefits of this attachment on the optoelectronic properties of the resulting HFM. Chapter 4 presents a study of reactivity of hydride-terminated SiNCs (H-SiNCs) with phosphorus pentachloride (PCl_5) and the subsequent functionalization of SiNCs with alkenes/alkynes at room temperature. This investigation offers a

straightforward method for the efficient functionalization of SiNCs exhibiting minimal surface oxidation and impressively high photoluminescence quantum yield that are essential for their optoelectronic applications.

Finally, Chapter 5 describes a summary of the experimental chapters and some future directions related to SiNC surface modifications for targeted applications in optoelectronics, catalysis, bioimaging, and drug delivery.

Preface

This thesis is an original work by Muhammad Amirul Islam. The research was conducted under the supervision of Professor Jonathan G. C. Veinot at the Department of Chemistry, University of Alberta.

A version of Chapter 2 has been published as Islam, M. A.; Purkait, T. K.; Veinot, J. G. C., "Chloride Surface Terminated Silicon Nanocrystal Mediated Synthesis of Poly(3-hexylthiophene)", *J. Am. Chem. Soc.,* **2014**, *136*, 15130–15133. I designed the project, performed the experiments, carried out the data analysis, and wrote the first draft of the manuscript. T. K. Purkait assisted with material characterization such as TEM, FT-IR, UV-Vis, and PL of chloride-terminated silicon nanocrystals, as well as manuscript writing. J. G. C. Veinot supervised the research and composed up to the final version of the manuscript.

A version of Chapter 3 has been published as Islam, M. A.; Purkait, T. K.; Mobarok, M. H.; Höehlein, I. M. D.; Sinelnikov, R.; Iqbal, M.; Azulay, D.; Balberg, I.; Millo, O.; Rieger, B.; Veinot, J. G. C., "Grafting Poly(3-hexylthiophene) from Silicon Nanocrystal Surfaces: Synthesis and Properties of a Functional Hybrid Material with Direct Interfacial Contact", *Angew. Chem. Int. Ed.* **2016**, *55*, 7393–7397. I designed the project, performed the majority of the experiments and data analysis, as well as wrote the first draft of the manuscript. T. K. Purkait assisted with some experimental design, and material characterization (e.g., TEM, FT-IR) as well as manuscript composition. D. Azulay, I. Balberg, and Professor O. Millo at the Hebrew University of Jerusalem performed scanning tunneling microscopy and spectroscopy (STM and STS) measurements and wrote the associated section of the manuscript. M. Iqbal assisted with the synthesis of silicon nanocrystals. M. H. Mobarok, and I. M. D. Hoehlein (Technical University of Munich), supported with experimental design for Grignard reaction to generate polymer initiator sites on silicon

nanocrystals and contributed to the editing of the manuscript. R. Sinelnikov, helped with photoluminescence measurements. Professor B. Rieger at the Technical University of Munich contributed to the editing of the final draft of the manuscript. J. G. C. Veinot supervised the research and composed up to the final version of the manuscript.

A version of Chapter 4 has been published as Islam, M. A.; Mobarok, M. H.; Sinelnikov, R.; Purkait, T. K.; Veinot, J. G. C., "Phosphorus Pentachloride Initiated Functionalization of Silicon Nanocrystals", *Langmuir*, **2017**, *33*, 8766–8773. I designed the project with some assistance from M. H. Mobarok. I performed the majority of the experiments and data analyses and wrote the first draft of the manuscript. M. H. Mobarok assisted with NMR measurements and data analysis for the reaction of phosphorus pentachloride with hydride-terminated silicon nanocrystals and edited the manuscript throughout the composition and publication process. R. Sinelnikov performed photoluminescence measurements and lifetime analyses, as well as measurement of some TEM images. T. K. Purkait supported with data analysis and manuscript editing. J. G. C. Veinot supervised the research and composed up to the final version of the manuscript.

I dedicate this thesis to my family

Acknowledgment

First, I want to express my gratitude to the University of Alberta and Canada for giving the opportunity to fulfill my dream and my father's dream. I am from a rural area in Bangladesh. My father could not receive any formal education. My father told me that it was always his dream to see us highly educated and since he was unable to gain the opportunity to study, he wanted to reflect his talent in his children. The name my father gave me, Muhammad Amirul Islam, was inspired by the great achievement and honesty of his boss with the same name. My father used to give us an example of Dr. Muhammad Shahidullah and Dr. Kamal Hossain, and wanted us to be someone great like them. Now, I could fulfill his dream. I can remember the moment I came to the University of Alberta like it was yesterday. Everything seemed so big and rich that I felt unworthy of the opportunity presented to me by the University of Alberta. Then I realized: I am qualified, and that is why I am here. I would admit that it was not an easy journey for me. There were moments when I faced the situation to decide whether I would continue or quit. I kept my patience and I continued the program, and now I have finally completed the Ph. D. Thanks to my family, friends, supervisor, and supervisory committee members who helped me along the way to keep my patience.

At this point, I want to take the opportunity to acknowledge the people who were the trigger behind my successful completion of my Ph. D. Foremost, I want to express my gratitude to my supervisor Dr. Jonathan Veinot for his support throughout my Ph. D. program. I liked your approach to supervising the individuals. You gave me the complete freedom of my research. You have let me develop my skills for critical thinking, design, and execution of independent research. You challenged me a lot regarding the necessary skills to be a successful Ph. D. I do not know how much I could improve those skills, but I appreciate your patience and continuous drive for my

improvement. One observation that I would like to mention here about you is you were not only a supervisor but also like a father. A father wants the best of his son. If the son is not doing well, the father gets angry but does not kick out the son. You were exactly like a father to me. Another positive thing that I learned from you is to inspire people by praising them even for little positive results. This praise from a professor provides an enormous boost to a student since a professor is like a god of science to a student.

I would like to thank my examination committee members Dr. Jillian M. Buriak, Dr. James Harynuk, Dr. Arthur Mar, Dr. Steven H. Bergens, Dr. Eric Rivard, Michael J. Serpe and external committee member Dr. Mark T. Swihart from University of Buffalo, for their guidance and advice on my annual reports, candidacy exam and thesis. I want to thank Dr. Bernhard Rieger, Dr. Oded Millo, Prof Isaac Balberg, Dr. Doron Azulay, Dr. Ignaz M. D. Höehlein, for their excellent and friendly collaboration. I would like to thank Dr. William Torres Delgado and Dr. Anindya Swarnakar for their help with gel permeation chromatographic analysis of my synthesized P3HT and nickel catalyst synthesis. I want to thank Dr. Professor Michael J. Sailor and his group member Geoffrey Hollett at the University of California, San Diego for their collaboration on the project on amphiphilic photoluminescent SiNCs for bioimaging applications that I have developed; they performed the time-gated imaging of the SiNCs. I would also like to thank Dr. Christopher W. Cairo and his group member Md Amran Howlader for their collaboration with the study of the Prostate Cancer Cell uptake of amphiphilic SiNCs.

I would like to thank the present and past group members of Dr. Veinot group members. You were very fantastic and friendly. I did not feel lonely here after leaving my relatives back home since you were like my family members. I want to especially thank Dr. Tapas Purkait and Dr. Muhammad Iqbal who taught me the necessary techniques to start as a fresh graduate student and

helped me along the way by transferring necessary skills. Both of you were wonderful post-docs that anyone would be happy to have. I want to acknowledge Dr. Hosnay Mobarok for collaboration with me on many projects and helping me with my thesis. I would like to thank Regina Sinelnikov for collaboration with me on multiple projects. I want to thank Austin Toresdahl, Subha Jana, Angélique Faramus, Christopher Jay Robidillo, and Md Asjad Hossain for their collaboration with me on my bio-imaging project. I want to thank Dr. John Washington, Dr. Morteza Javadi Charani, Austin Toresdahl, Lydia Fialka, Mckenzie Oliver and Sarah Milliken for their support with editing my thesis.

I would like to thank graduate program assistant Anita Weiler for her administrative support. Every time I went to see her I came back with a happy face. I would like to thank Dr. Yoram Apelblat and Dr. Norman Gee for their close coordination during my teaching assistantship assignments.

I would like to thank the scientific research and support staff for all of their help: Wayne Moffat, Kai Cui, Gareth Lambkin, Mark Miskolzie, Nupur Dabral, Dimitre Karpuzov, Mike Xia, Jennifer Jones, Shihong Xu, Anqiang He, Greg Popowich, Randy Whittal, Jing Zheng, Katazhyna Haidukevich, Jeffery Kwasny, Ema Sretenovic, Brett Mason, Bernie Hippel, Laura Pham, Scott Stelck, Esther Moibi, Margaret Sisley, Matthew Sirtonski, Bonnie Gover without whom I could not continue my research, characterize the materials and prove my ideas experimentally. I would especially like to thank Kai Cui at NRC-CNRC for his assistance with electron microscopic analysis (HRTEM, STEM, HAADF, and EELS) of the SiN@P3HT hybrid material. I would like to thank Dr. Wayne Mofat and his team for their quick response to my request for analysis. I would like to thank Jing Zheng at mass spectrometry facility for her passion about her job. When I submitted a sample to her for characterization, she took it upon herself to make the analysis perfect.

I want to acknowledge the Alberta/Technical University of Munich International Graduate School for Hybrid Functional Materials (ATUMS) and its coordinator, Leah Veinot, for the professional development, research training, and funding supports.

I would like to recognize the Natural Science and Engineering Research Council of Canada (NSERC) Discovery Grant program and ATUMS training program supported by NSERC CREATE program for the continued generous funding support. I would also like to thank Alberta Innovates-Technology Futures (AITF) for a graduate student scholarship.

I would also like to thank my friends all around the world for giving me the experience of diverse culture.

In the end, I would like to thank my parents, wife, and siblings for their support throughout my life. Especially, I would like to mention about the support from my elder brother Md. Ariful Islam. Our father dreamt for us to be educated and honorable persons, but you paved the way to fulfill his dream.

Table of Contents

List of Figures

List of Tables

List of Symbols, Nomenclature, and Abbreviations

Å	Angstrom (10^{-10} m)
@	At
β	Beta
°C	Degree Celsius
δ	Delta
Δ	Delta (Heat)
ε	Dielectric constant
η	Optical efficiency
η_i	Internal quantum efficiency
λ_{exc}	Excitation wavelength in photoluminescence spectroscopy
λ_{max}	Wavelength maximum
μ	Micron
μL	Microliter
h	Planck's constant (6.626×10^{-34} J·s.)
N_A	Avogadro number (6.022×10^{23})
ν	Nu (Frequency)
%	Percent
Φ_{EET}	Combined efficiency of electron and energy transfer
τ	Excited state lifetime
τ_r	Lifetime for radiative recombination of the exciton

τ_{nr}	Lifetime for nonradiative recombination of the exciton
A	Absorbance
AIBN	Azobisisobutyronitrile
anti-EpCAM	Anti-epithelial cell adhesion molecule antibody
APTMS	(3-Aminopropyl)trimethoxysilane
AQY	Absolute quantum yield
a. u.	Arbitrary unit
BCP	Bathocuproine
B. E.	Binding energy
BF- STEM	Bright field scanning transmission electron microscopy
BHJ	Bulk heterojunction
bipy	Bipyridine
BP	Benzoyl peroxide
Br-HT	2-Bromo-3-hexylthiophene
Br-HT-I	2-Bromo-3-hexyl-5-iodothiophene
Br-SiNC(s)	Bromide-terminated silicon nanocrystal(s)
CB	Conduction band
CIGS	Copper indium gallium sulfide or selenide
ClMg-HT-Br	5-Chloromagnesio-2-bromo-3-hexylthiophene
Cl-SiNC(s)	Chloride-terminated silicon nanocrystal(s)
Cl-SiWF	Chloride-terminated silicon wafer
CP(s)	Conjugated polymer(s)

CTAB	Cetyltrimethylammonium bromide
CZTS	Copper zinc tin sulfide
d	Diameter
DBTJ	Double barrier tunnel junction
DCTB	2[(2E)-3-(4-tert-Butylphenyl)-2-methylpropy-2-enylidene]-malononitrile
Decyl-SiNC(s)	Decyl-terminated silicon nanocrystal(s)
DLS	Dynamic light scattering
DNT	2,4-Dinitrotoluene
Dodecyl-SiNC(s)	Dodecyl-terminated silicon nanocrystal(s)
DOS	Density of states
Dox	Doxorubicin
dppp	1,3-Bis(diphenylphosphino)propane
e	Elementary charge of the electron
e^-	Electron
EDC	1-Ethyl-3-(3-dimethylaminopropyl)carbodiimide
EDX	Energy-dispersive X-ray
EELS	Electron energy loss spectroscopy
E_g	Band gap
$E_{g,b}$	Band gap of bulk semiconductor material
EGDM	Ethylene glycol dimethacrylate
$E_{g,QD}$	Band gap of quantum dots

EL	Electroluminescence
EM	Electron microscopy
EpCAM	Epithelial cell adhesion molecule
EQE	External quantum efficiency
ET	Electron transfer
eV	Electron volt (unit of energy)
FET(s)	Field-effect transistor(s)
^{19}F NMR	Fluorine-19 nuclear magnetic resonance
FRET	Förster resonance energy transfer
F-SiNC(s)	Fluoride-terminated silicon nanocrystal(s)
FT-IR	Fourier transform infrared
fwhm	Full width at half maximum
GC-MS	Gas chromatography–mass spectrometry
GPC	Gel permeation chromatography
h	Hour
h^+	Electron vacancy or hole
HAADF	High annular angular dark field
HFM(s)	Hybrid functional material(s)
HH	Head-to-head
^{1}H NMR	Proton nuclear magnetic resonance
HOMO	Highest occupied molecular orbital
HO-SiNC(s)	Hydroxyl-terminated silicon nanocrystal(s)

HPLC	High-performance liquid chromatography
HRTEM	High-resolution transmission electron microscopy
HR-XPS	High-resolution X-ray photoelectron spectroscopy
HSQ	Hydrogen silsesquioxane
H-SiNC(s)	Hydride-terminated silicon nanocrystal(s)
H_xSiCl_y	Chlorosilanes
HT	Head-to-tail
-HT-Br	2-Bromo-3-hexyl-5-thienyl
Hz	Hertz
I	Integrated photoluminescence intensity
I_o	Initial photon intensity
IR	Infrared
I-SiNC(s)	Iodide-terminated silicon nanocrystal(s)
ITO	Indium tin oxide
K	Degrees Kelvin
kV	Kilovolt
LED(s)	Light-emitting diode(s)
LSC(s)	Luminescent solar concentrator(s)
LUMO	Lowest unoccupied molecular orbital
M	Molar mass
MALDI-TOF-MS	Matrix-assisted laser desorption ionization-time of flight-mass spectrometry

mg	Milligram
m_e	Effective mass of the electron
MEH-PPV	Poly[2-methoxy-5-(2′-ethylhexyl-oxy)1,4-phenylene-vinylene]
m_h	Effective mass of the hole
MMA	Methyl methacrylate
M_n	Number-average molecular weight
M_w	Weight-average molecular weight
m/z	Mass-to-charge ratio
N	Number
nA	Nanoampere
NALDI-MS	Nanostructure-assisted laser desorption/ionization mass spectrometry
NBS	N-Bromosuccinimide
NC(s)	Nanocrystal(s)
NIR	Near-infrared
nm	Nanometer
NP(s)	Nanoparticle(s)
ohm·cm	Ohms centimeter (unit of resistivity)
OLED(s)	Organic light-emitting diode(s)
PANI	Polyaniline
PC	Prostate cancer
PDI	Polydispersity index

PDMS	Polydimethylsiloxane
PDEVP	Poly (diethyl vinylphosphonate)
PEDOT:PSS	Poly (styrene sulfonate) doped poly(3,4-ethylenedioxythiophene)
PEG	Polyethylene glycol
PEGDM	Poly (ethylene glycol dimethacrylate)
Pentyl-SiNC(s)	Pentyl-terminated silicon nanocrystal(s)
PETN	Pentaerythritol tetranitrate
PFO	Poly (9,9-dioctylfluorene)
PL	Photoluminescence
PLMA	Poly (lauryl methacrylate)
ppm	Parts per million (unit of NMR chemical shift)
PPP	Poly (p-phenylene)
PPV	Poly (p-phenylene vinylene)
PS	Polystyrene
PS-SiNC(s)	Polystyrene functionalized silicon nanocrystal(s)
p-Si	Porous silicon
PTB7	Poly({4,8-bis[(2-ethylhexyl)oxy]benzo[1,2-*b*:4,5-b′]dithiophene-2,6-diyl}{3-fluoro-2-[(2-ethylhexyl)carbonyl]thieno[3,4-*b*]thiophenediyl})
PTFE	Polytetrafluoroethylene
P3HT	Poly (3-hexylthiophene)
QD(s)	Quantum dot(s)

QY	Quantum Yield
R	Radius of quantum dots
RDX	Cyclotrimethylenetrinitramine
rpm	Revolutions per minute
RROP	Radical ring-opening polymerization
R-SiNC(s)	Alkyl-terminated silicon nanocrystal(s)
RT	Room temperature
SEM	Scanning electron microscopy
SET	Single electron transfer
SI-GTP	Surface-initiated group transfer polymerization
SI-KCTP	Surface-initiated Kumada catalyst transfer polycondensation
SiNC(s)	Silicon nanocrystal(s)
SiNC@P3HT	Silicon nanocrystal@poly (3-hxylthiophene) core@shell
SiNC-g-PEGDM	Poly EGDM grafted SiNC
SiNC-g-PEGDM-g-PDEVP	Poly EGDM and poly (diethyl vinylphosphonate) grafted SiNC
SiNC-HT-Br	2-Bromo-3-hexyl-5-thienyl-capped silicon nanocrystal
SiNC-HT-Ni(bipy)-Br	Ni(bipy) catalyst immobilized silicon nanocrystal
SiNC-HT-Ni(dppp)-Br	Ni(dppp) catalyst immobilized silicon nanocrystal
SiNC/P3HT	Silicon nanocrystal and poly (3-hexylthiophene) blend
^{29}Si NMR	Silicon-29 nuclear magnetic resonance
SiO_x	Silicon-rich oxides
Si/SiO_2	Silicon nanocrystals embedded in silica matrix

≡Si-Cl	Silicon chloride species
≡Si$^{\bullet}$	Surface silicon radical
SMCC	Succinimidyl-*trans*-4-(N-maleimidylmethyl)cyclohexane-1-carboxylate
STEM	Scanning transmission electron microscopy
STM	Scanning tunneling microscopy
STS	Scanning tunneling spectroscopy
TEM	Transmission electron microscopy
TEOS	Tetraethyl orthosilicate
TGA	Thermogravimetric analysis
TNT	2,4,6-Trinitrotoluene
Tol-SiNC(s)	Toluene functionalized silicon nanocrystal(s)
TOPO	Trioctylphosphine oxides
Torr	Unit of pressure
TT	Tail-to-tail
UV	Ultraviolet
UV-Vis	Ultraviolet-visible
VB	Valence band
XPS	X-ray photoelectron spectroscopy
XRD	X-ray diffraction
X-SiNC(s)	Halide-terminated silicon nanocrystal(s)

Chapter 1:

Introduction

1.1 Quantum Dots

Quantum dots (QDs) are semiconductor nanoparticles (NPs) made up of a few hundred to several thousands of atoms.[1] They exhibit distinct size dependent optoelectronic properties upon reducing their size to be smaller than the exciton Bohr radius of the bulk semiconductor.[2,3] An exciton is defined as an electron (e^-) and an electron vacancy (hole, h^+) pair associated *via* Coulombic attraction.[4] The exciton Bohr radius is defined as the most probable distance between the bound electron-hole pair and is characteristic of semiconductors.[5]

Brus and coworkers[6–8] discovered QDs in the early 1980s. The unique properties of QDs have led to studies regarding applications in solar cells,[9–12] light-emitting diodes (LEDs),[2,13,14] lasers,[15–17] transistors,[18–20] catalysts,[21–23] bioimaging agents,[3,24–26] sensors,[3,27,28] and drug delivery agents.[29–31] Based on their composition QDs are broadly categorized as elemental or compound semiconductors. Elemental QDs are composed of silicon (Si)[32–35] or germanium (Ge) [36–39] whereas compound QDs are made up of a combination of group II–VI (*e.g.,* CdE, E = Se, S, Te,[40–43] and ZnE, E = O, S, Se, Te[44–46]), III–V (*e.g.,* InE, E = P, As, Sb,[47–51] and GaE, E = As, N[49,52]), IV–VI (*e.g.,* PbE, E = Se, S),[53–55] I-VI (*e.g.,* Ag_2Se),[56,57] II-V (*e.g.,* Zn_3N_2, Zn_3P_2, Cd_3P_2, Cd_3As_2)[58–61] or multiple group elements (*e.g.,* ternary CIS: $CuInS_2$,[62–64] $CuInSe_2$,[64,65] and quaternary CIZS: Cu-In-Zn-S, $CuInS_2$@ZnS,[63,66,67] CIGS: Cu–In–Ga–S,[68] Cu(In,Ga)Se_2,[64,69] or CZTS: Cu_2ZnSnS_4[70,71]).

The size-dependent optoelectronic properties of QDs have been investigated in multidisciplinary research areas which target promising optoelectronic applications.[1] One of the most studied optoelectronic properties of QDs is their size-dependent photoluminescence (PL). The band gap of QDs increases as size decreases. Therefore, the wavelength of emission decreases with a decrease in size of QDs and this results in the emission of radiation ranging from infrared to blue light.[72–76] Figure 1-1a shows an example of CdSe QDs and their size-dependent PL

emission colors that cover the visible spectrum.[5] The size-dependent PL of QDs is governed by quantum confinement; that is, the confinement of excitons into their discrete electronic energy states (Figure 1-1b).[74]

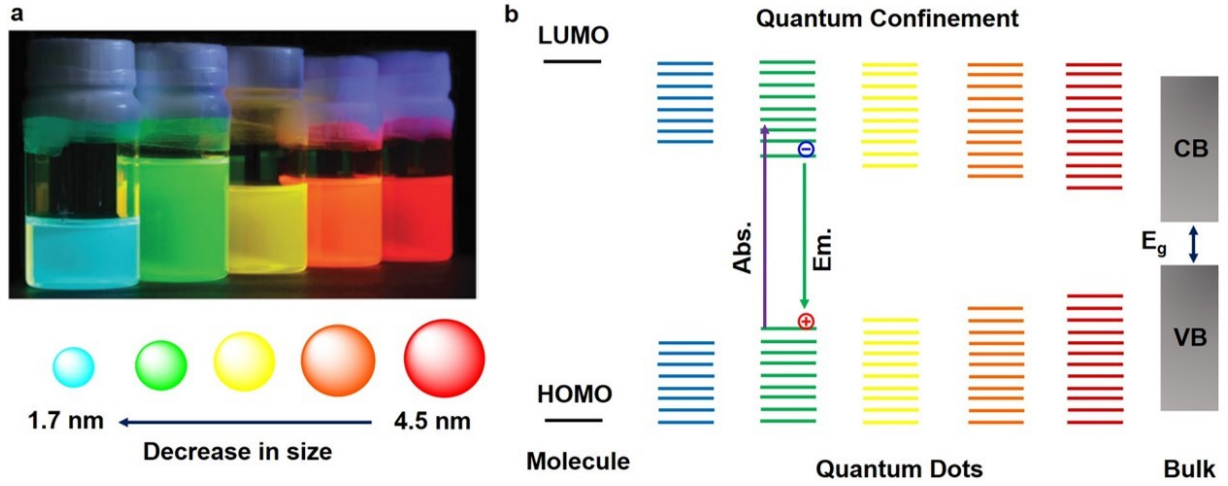

Figure 1-1. (a) Photographs showing the effect of CdSe QD size on their emission colors. Reproduced and adapted with permission from The Royal Society of Chemistry.[5] (b) an increase in the band gap of QDs with a decrease in their size due to quantum confinement of excitons in discrete electronic energy states; the density of energy states decreases in the transition from the bulk semiconductor to QDs and molecules.[4,74,77]

The low energy highest occupied molecular orbital (HOMO) and high energy lowest unoccupied molecular orbital (LUMO) are usually referred to as ground and excited electronic states, respectively (Figure 1-1b). The infinite number of these electronic states in bulk semiconductors results in continuous band structures that are termed valence band (VB) and conduction band (CB). (Figure 1-1b). The difference in energy between the VB and CB is known as the band gap (E_g). The density of these electronic states in QDs lies between the discrete molecular electronic states and the continuous bands of the bulk semiconductor.[3,77,78] Decreasing the size of QDs reduces the density of electronic states, which consequently increases the energy band gap (Figure 1-1b) and decreases the wavelength of PL emission.[3] PL emission from QDs occurs through a radiative recombination of photogenerated excitons (Figure 1-1b). These excitons

are generated upon absorption of sufficiently high energy photons which cause the transition of an electron from the VB to the CB of the QDs.[4,79]

The empirical formula that relates energy band gap of QDs with their sizes is shown in [Equation 1-1]:[79]

$$E_{g,QD} = E_{g,b} + \left(\frac{h^2}{8R^2}\right)\left(\frac{1}{m_e} + \frac{1}{m_h}\right) - \left(\frac{1.8e^2}{4\pi\varepsilon_0\varepsilon R}\right) \quad \ldots\ldots\ldots\ldots \quad (1-1)$$

where $E_{g,QD}$ and $E_{g,b}$ are the band gaps of the QDs and bulk semiconductor material, respectively, R is the radius of the QDs, m_e and m_h are the effective masses of the electron in the CB and hole in the VB, respectively, h is Planck's constant, e is the elementary charge of the electron, and ε is the dielectric constant of the bulk semiconductor. According to [Equation 1-1], the band gap of a QD is defined by both the band gap of the bulk semiconductor and the energy contribution from the confinement of an exciton within the QD.[80] The confinement of the exciton is insignificant for large NPs and band gap is close to that of the bulk semiconductor.[80] However, as the size of NPs approaches the exciton Bohr radius, the strong confinement increases the band gap significantly.[4,80]

The extremely small size of QDs leads to a significantly high surface-to-volume ratio.[81] In contrast to the core, the periodic arrangement of surface atoms in QDs is disturbed because of incomplete bonding, leaving dangling bonds on the surface that may create a secondary fast nonradiative relaxation path which reduces PL quantum yield (QY).[4,81] Passivation of the surface of QDs with organic ligands reduces the density of their surface dangling bonds and improves the PL QY. However, surface passivation with organic ligands is not effective since surface cationic and anionic components of QDs are not equally reactive to the same functional group of the ligand.[4,81]

The development of core@shell structures of QDs[82–85] provided substantial improvements in PL QY by circumventing the influence of undesirable surface dangling bonds and the environment.[4,81] In addition to passivation of surface dangling bonds, the core@shell structure enabled the tuning of PL color and enhancement of PL QY by manipulating the exciton confinement zone within the core and/or shell components. These core@shell structures are classified into three categories (Figure 1-2), depending on the core and shell composition and their corresponding band alignment.[81]

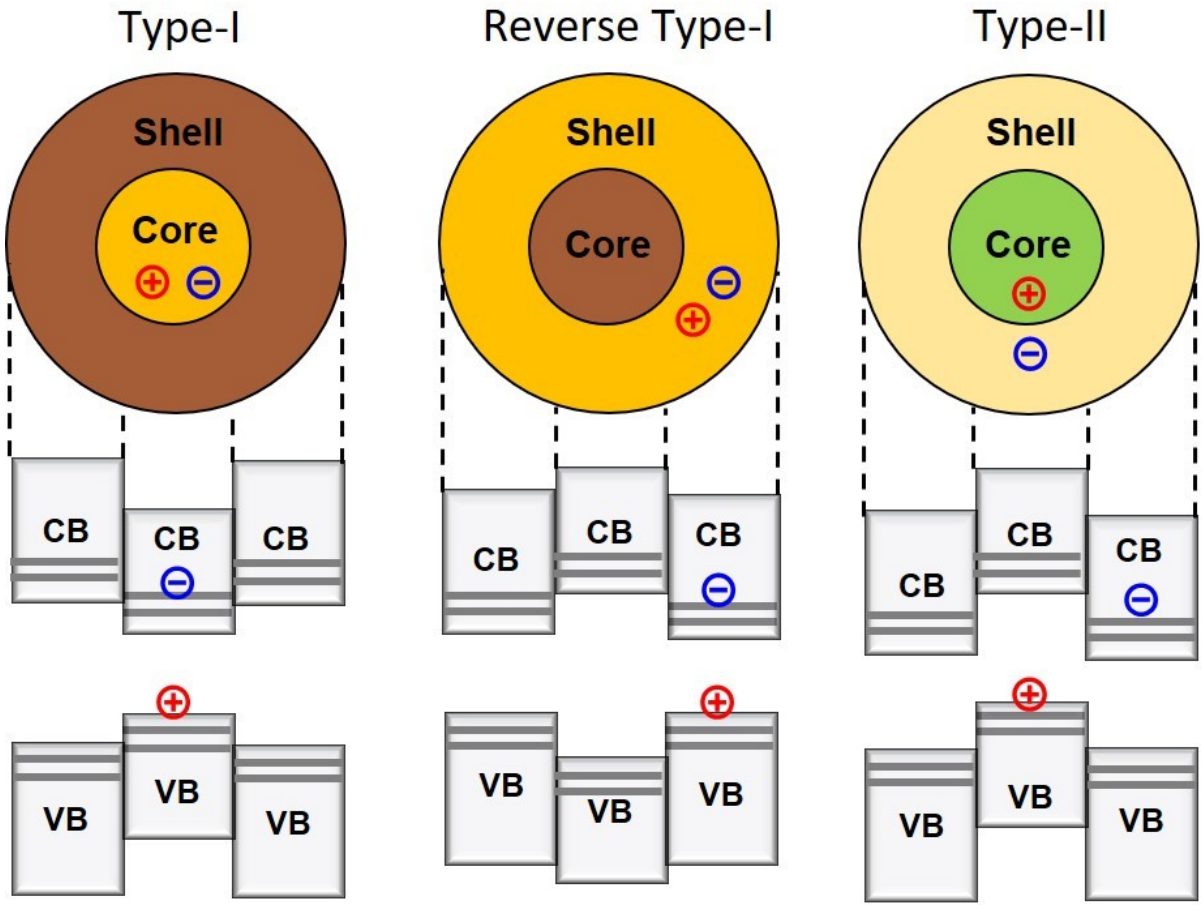

Figure 1-2. Schematic of the different types of band alignments in core@shell QDs (CB: conduction band, VB: valence band).[4,81,86]

In the Type-I structure (*e.g.,* CdSe@ZnS),[84] the electron and the hole are trapped in the core since it is coated with a wider band-gap semiconductor shell.[81] The band gap of the core determines emission color of this type of core@shell QD. In reverse Type-I (*e.g.,* ZnSe@CdSe),[87] the shell is composed of a low band-gap semiconductor allowing the delocalization of electron and hole in the shell and leading to the tunability of PL color from violet to red as a function of shell thickness.[81,86,87] In Type-II alignment (*e.g.,* CdSe@ZnTe or CdTe@CdSe),[88] there is an overlap between the VB and CB of the core/shell materials allowing the distribution the electron and hole into the core and shell.[4] This process leads to the electron and hole recombination through a lower energy route than the band gap of both the core and shell materials with a concomitant red-shift of PL color extending even to IR region.[4,81,88]

1.2 Silicon Nanocrystals

Although the synthesis, optoelectronic properties, and surface chemistry of compound QDs are well developed, the toxicity of heavy metals (*e.g.,* Pd, Cd, Hg, and As) and the inadequate reserves of some elements (*e.g.,* Ga, In, and Se) are significant barriers for their commercialization.[89–92] Silicon is earth abundant, non-toxic, and the workhorse material in electronic devices.[80,93] Since the discovery of photoluminescent porous silicon (*p*-Si) by Canham in the early 1990s,[94,95] many procedures have been developed to synthesize size-controlled silicon nanocrystals (SiNCs). SiNCs are usually prepared with hydrides, halides, oxides or hydroxides as reactive surface groups, allowing for many surface modification methods.[80,89] The unique size and surface related PL properties of SiNCs allowed for tunability of their PL emission colors and PL QY.

1.2.1 Synthesis of Silicon Nanocrystals

The protocols for synthesizing SiNCs are based on both top-down and bottom-up methods.[80,96] In top-down methods, bulk silicon is broken down into nanocrystals; in bottom-up methods, silicon-based precursors are decomposed or chemically oxidized/reduced to cause the nucleation and growth of SiNCs.

Top-down approaches include laser ablation,[97–100] electrochemical etching,[95,101–105] chemical etching,[106–111] and mechanochemical ball milling.[112,113]

Bottom-up approaches rely on reduction of silicon halides or alkoxides,[114–128] metathesis reactions of metal silicide (Zintl salt),[129–135] decomposition of silane precursors,[45,136–153] or the disproportionation of silicon-rich oxides.[154–163] Most of the top-down methods yield SiNCs with varied sizes and limited surface tailorability. Given that the Bohr exciton radius for Si is 4.9 nm,[164] it is important to synthesize size-tunable SiNCs to explore their size-dependent optoelectronic properties. Veinot *et al*.[157] have introduced a method for size-tunable synthesis of SiNCs via thermal disproportionation of hydrogen silsesquioxane (HSQ) (Scheme 1-1). In the initial report, the thermal processing of HSQ was studied over a temperature range of 500 to 1100 °C under reducing atmosphere of 4 % H_2 and 96 % Ar. The optimum annealing conditions were found to be 1100 °C for 1 h to synthesize luminescent SiNCs encapsulated in a SiO_2-like matrix. A post-synthetic HF-etching liberated highly luminescent H-SiNCs emitting PL over the range of green to NIR. The influence of temperature and time on the growth of nanocrystalline domain was studied in a follow-up report revealing the fact that an increase in temperature in the range from 1100 to 1400 °C changes the crystalline domain size and the corresponding emission colors.[158] SiNCs of tunable sizes in the range from ~3 - 9 nm could be synthesized simply by varying the

temperature. This size-tunability of SiNCs allowed for the exploration of their size-dependent PL covering red to IR regions.

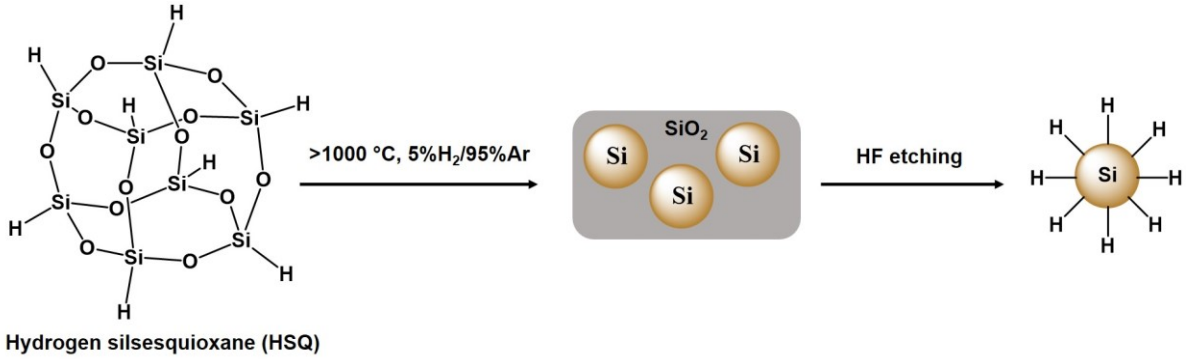

Scheme 1-1. Synthesis of SiNCs via thermal disproportionation of hydrogen silsesquioxane (HSQ).

1.2.2 Surface Modification of Silicon Nanocrystals

Surface modification of SiNCs is crucial for many reasons such as preventing oxidation, ensuring colloidal stability, applying readily available purification techniques, retaining band-gap PL, tuning PL color, enhancing PL QY, and tailoring surface chemistry for targeted applications. While surface modification of group II–VI, III–V and IV–VI QDs is achieved *via* the growth of another semiconductor shell and/or ligand exchange, the surface of SiNCs is modified through the formation of covalent bond between surface silicon and carbon or other heteroatoms (*e.g.,* O, N or S) of organic ligands.[80,89] Since ligands are directly attached to SiNCs, these types of modifications also provide tunability of their optoelectronic properties.[165] Surface modification of SiNCs is commonly achieved *via* the reaction of surface hydrides or halides with appropriate ligands or other multi-step processes.

1.2.2.1 Modification of Hydride-Terminated Silicon Nanocrystals

Hydrosilylation is the most widely applied modification method for hydride-terminated silicon surface where unsaturated ligands (*e.g.,* alkene, alkyne) are inserted between the Si-H bonds to form stable Si-C linkages.[166] The surface chemistry of bulk silicon has been developed

substantially after the pioneering work by Linford and Chidsey[167] that have led to the development of surface modification methods for *p*-Si and SiNCs.[80,89,101,166,168–178] Hydrosilylation of H-SiNCs can be achieved *via* thermal,[179–181] radical-initiated,[93,182,183] photochemical,[141,184] and catalytic processes.[128,185,186] Some of these important surface modification methods are summarized in Scheme 1-2 and will be discussed in the following sections.

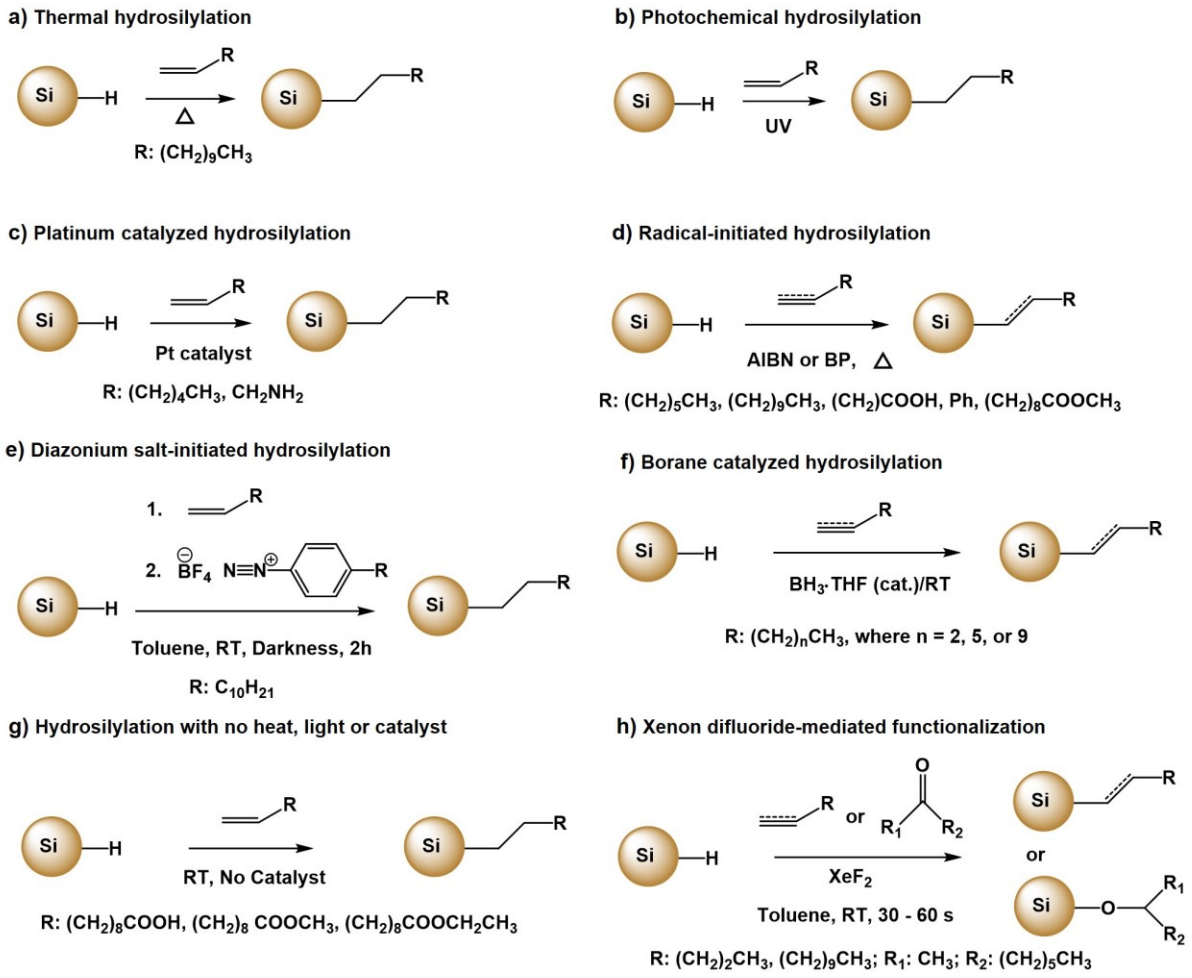

Scheme 1-2. Schematic of common hydrosilylation methods for H-SiNCs: a) thermal,[179] b) photochemical,[184] c) platinum catalyzed,[117,186] d) radical-initiated (AIBN 60 °C, BP 85 °C),[183] e) diazonium salt- initiated,[187] e) borane catalyzed,[188] g) ligand self-catalyzed,[189] and h) xenon difluoride-mediated.[93] For clarity, all surface groups the actual nature of surface hydrides and residual Si-H, Si-O, or Si-F species on passivated SiNCs are not shown.

Among the wide variety of hydrosilylation methods, thermal hydrosilylation (Scheme 1-2a) is the most straightforward for passivating H-SiNCs. It minimizes surface oxidation, provides high surface coverage and allows robust functional group tolerance.[190] Thermal hydrosilylation can be applied to functionalize SiNCs independent of particle size and shape, and it proceeds without a catalyst.[89] It is usually carried out in the neat alkene/alkyne in the temperature range of 100-190 °C.[179] Thermal hydrosilylation has been believed to provide an alkyl monolayer coverage.[167,191–193] However, this was shown to be unlikely by Yang *et al.*,[179] after convincing evidence of oligomerization of ligands that was detected *via* nanostructure-assisted laser desorption/ionization mass spectrometry (NALDI-MS) (Figure 1-3).

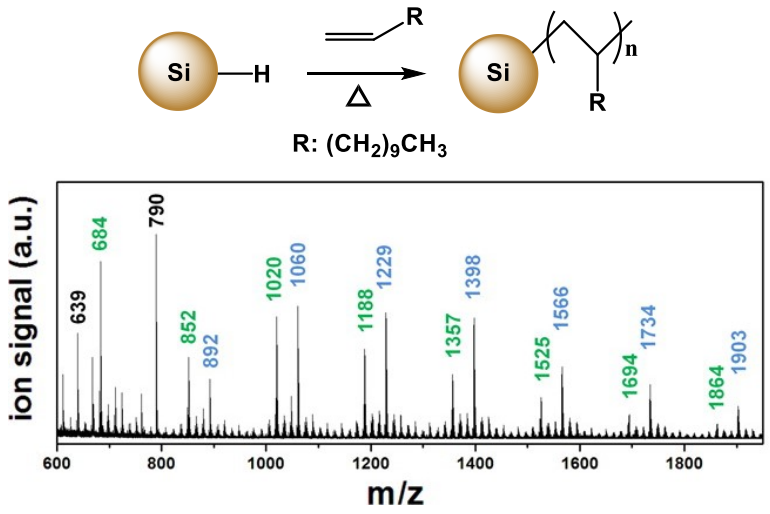

Figure 1-3. Depiction of alkyl oligomer functionalized SiNCs and representative NALDI-MS pattern of their surface oligomers. Mass spectrum reveals two patterns (colored numbers) with m/z peak separations of 168.3 corresponding to the molecular weight of dodecyl repeat unit. Reproduced and adapted with permission from Yang *et al.*[179] Copyright 2013, American Chemical Society.

Although oligomeric ligands can protect SiNCs against oxidation, the insulating nature of oligomeric alkyl chains hinders applications in optoelectronic devices (*e.g.,* solar cells and electroluminescence devices) that rely on interfacial charge transfer processes.[194] Moreover, thermal hydrosilylation is performed at elevated temperature and functionalization of SiNCs with

short chain is challenging.[183] Therefore, it is necessary to explore alternative hydrosilylation methods that proceed at low temperature, provide efficient monolayer coverage and are adaptable to short chain low boiling ligands. Photochemical hydrosilylation (Scheme 1-2b) can address many of these challenges; but it is limited by size-dependent reactivity. Larger nanocrystals (*e.g.,* $d \geq 6$ nm) are not effectively activated *via* photochemical means; the SiNC surface is poorly passivated and prone to oxidation (Scheme 1-2b).[184]

Chloroplatinic acid (H_2PtCl_6) catalyzed hydrosilylation of H-SiNCs was reported by Tilley and coworkers[186] and proceeds at room temperature (Scheme 1-2c). This catalytic route was also applied to prepare water-soluble amine-terminated SiNCs *via* hydrosilylation with allylamine.[117] However, amine termination is challenging due to the propensity of amine groups to react with H-SiNCs.[195] One significant drawback of this catalytic route is the metal contamination of SiNCs can compromise their optical properties.[89,183,190]

Yang *et al*.[183] carried out a low-temperature radical-initiated (*i.e.,* AIBN, 60 °C; BP 85 °C) hydrosilylation of H-SiNCs (Scheme 1-2d) which allowed for a wide range of functional group tolerance and provided surface coverage of as high as 64 %. Importantly, NALDI-MS analysis revealed no ligand oligomerization on SiNCs. However, radical-initiated hydrosilylation is slow (19 hours), and the functionalized SiNCs suffer from significant oxidation as evident from FT-IR and XPS analysis.

Given that the diazonium salts provided for rapid hydrosilylation on porous silicon,[196] and having observed that commercially available diazonium salts did not provide adequate surface passivation due to their solubility difference with H-SiNCs, Höhlein *et al*.[187] developed a series of organic-soluble diazonium salts and investigated their reactivity towards the hydrosilylation of several alkenes/alkynes on H-SiNCs (Scheme 1-2e). It was found that diazonium salts containing

electron-withdrawing groups (*e.g.,* 2,6-bromo-4-decyl-diazobenzene tetrafluoroborate) provide superior reactivity. However, this method also suffers from incomplete surface coverage leading to oxidation of SiNCs.

Purkait *et al*.[188] reported alkyl/alkenyl monolayer coverage on SiNCs including short-chain ligands such as pentene/pentyne (Scheme 1-2f). Borane-tetrahydrofuran complex (BH_3•THF) was used as a catalyst in this hydrosilylation method which, unlike transition metal catalyst, was readily removed during the purification process. No boron emission was detected in the XPS and EDX spectra of the functionalized SiNCs. Moreover, no borane resonance was observed in their ^{1}H NMR spectra. However, this method also leads significant oxidation of SiNCs.

The Korgel group[189] demonstrated a room-temperature hydrosilylation to acquire monolayer coverage of bifunctional ligands containing distal polar moieties (*e.g.,* esters, or carboxylic acids) (Scheme 1-2g). The reaction proceeds in the absence of any external trigger (*e.g.,* heat, light, or catalyst). The polar end groups of the bifunctional ligands are believed to self-catalyze the reaction by weakening surface Si-H bonds through coordination of nucleophilic carbonyl groups to the oxophilic silicon surface. However, the reaction is prolonged requiring about 12-120 hours to obtain colloidally stable SiNCs. Surface passivation is also inadequate leaving a significant portion of unreacted surface Si-H bonds that lead to oxidation of SiNCs.

Xenon difluoride (XeF_2)-mediated functionalization of SiNCs (Scheme 1-2 h) was reported by Mobarok *et al*.[93] The functionalization proceeds quickly at room temperature (30-60 s). This method facilitates size-independent reactivity with C=C, C≡C, and C=O bonds and enables the functionalization with the shortest possible unsaturated hydrocarbon (ethylene). This method also provides efficient surface passivation (40 - 60 %) with minimal surface oxidation. Significant enhancement of PL QY (40 - 70 %) was also observed and was attributed to XeF_2-mediated etching

of surface-related dark sites. Experiments based on this method also allowed for a clear mechanistic understanding of the SiNC surface chemistry.

However, the strong XeF_2 etchant reduces NC size considerably (15 - 20 %). This protocol also requires strict inert-atmosphere owing to the extreme air and moisture sensitivity of XeF_2. Post-functionalization purification was also performed under inert atmosphere since reactive residual Si-F bonds can provide sites for NC surface oxidation. These reactive Si-F bonds can limit the long-term stability of XeF_2-mediated surface-modified SiNCs against oxidation under ambient conditions and shortens the durability of their high PL QY. Phosphorus pentachloride (PCl_5)-initiated functionalization of SiNCs have been developed to address these limitations of XeF_2-mediated functionalization which will be discussed in experimental Chapter 4.

Despite the significant development of hydrosilylation of H-SiNCs, the reaction mechanism was unclear until a recent thorough mechanistic investigation by Neale group[197] using radical trapping process and subsequent analysis using a complementary suite of FT-IR and ^{1}H NMR spectroscopies. Thermal or photochemical hydrosilylation has long been believed to initiate *via* the surface silicon radicals (≡Si$^\bullet$) that are generated by homolytic cleavage of surface Si-H bonds. Reactive surface ≡Si$^\bullet$ attacks the unsaturated carbon-carbon double or triple bonds forming Si-C bonds while leaving β-carbon radicals. The β-carbon radical abstracts a hydrogen radical (H$^\bullet$) from a neighboring Si-H bond, regenerating surface ≡Si$^\bullet$ that propagates the reaction on SiNC surface (Scheme 1-3a).[166,184,197] Exciton mediated hydrosilylation was referred as an alternative pathway comparable to that for the bulk-silicon surface where an exciton is believed to attack the unsaturated bonds (Scheme 1-3b).[184] The mechanism of radical-initiated and thermal hydrosilylation is believed to be similar except a radical initiator creates the ≡Si$^\bullet$ by abstracting a H$^\bullet$ from NC surface Si-H bonds.[183]

Recently, thermal- and radical-initiated homolytic cleavage of Si-H bonds were shown to be an unlikely initiation step.[197] Rather, thermally-induced homolytic cleavage of ≡Si-SiH_3 bonds or abstraction of a silyl radical ($H_3Si^{\bullet}$) by a radical initiator was suggested as a source of surface ≡$Si^{\bullet}$ (Scheme 1-3a).[197] A comparison of deconvoluted Si-H_x stretching modes between H-SiNCs and SiNCs after functionalization revealed preferential disappearance of -SiH_3 frequency over =SiH_2 and ≡SiH frequencies. This analysis along with direct evidence of $H_3Si^{\bullet}$ formation, confirmed by radical trapping and subsequent FT-IR and ^{1}H NMR analysis of $H_3Si^{\bullet}$-trapped product, convincingly support the proposed mechanism.[197]

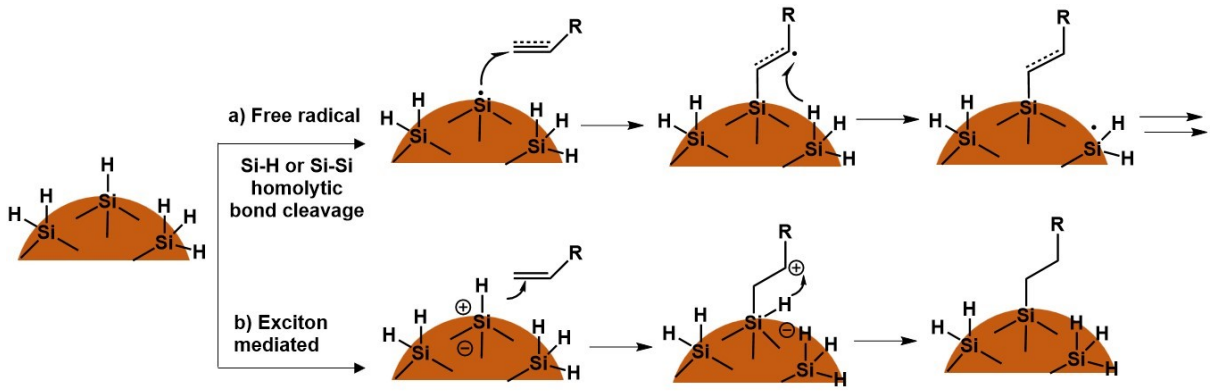

Scheme 1-3. A depiction of commonly proposed hydrosilylation mechanisms: a) radical mechanism in thermal, photo-initiated, radical-initiated, and XeF_2-mediated hydrosilylation, and b) exciton-mediated route in photo-initiated hydrosilylation.

Convincing evidence for the formation of surface ≡$Si^{\bullet}$ generation *via* Si−Si bond cleavage was provided by Mobarok *et al.*[93] in the study of XeF_2-mediated functionalization of SiNCs. According to this mechanism, fluorine radical generated from XeF_2 cleave the surface Si−Si bonds and instantaneously remove a significant portion of surface Si−H_x species in the form of hydrofluorosilane by-products (H_xSiF_y: H_3SiF, H_2SiF_2, and $HSiF_3$). These by-products were identified by ^{1}H, ^{19}F, and ^{29}Si NMR, as well as GC-MS. The "instantaneous" removal of

hydrofluorosilane by-products leaves the NC surface rich with transient radicals that presumably resemble the initiation and propagation steps proposed for other hydrosilylation methods.

Although hydrosilylation is the most common approach for the modification of H-SiNC surface, alternative methods for modifying SiNCs have been drawn from the bulk and porous silicon literature.[101,168,176,178,198–203] Sailor *et al*.[198] modified the hydride-terminated *p*-Si by reaction with organolithium reagents such as phenyllithium and lithium phenylacetylide while Kim and Laibinis[199] modified the hydride-terminated *p*-Si using the Grignard reagent (*e.g.,* decylmagnesium bromide). Recently, Höhlein *et al*.[204] adapted the organolithium reagent-based functionalization method to SiNC surfaces using several alkyl and aryl lithium reagents (Scheme 1-4). The reaction proceeds through the cleavage of Si-Si bonds into Si-alky/aryl and Si-Li bonds. Highly reactive Si-Li bonds were utilized to further functionalize the NC by reacting with bromoalkene and epoxide. Quenching Si-Li bonds with HCl resulted in surface Si-H bonds that were subsequently modified by hydrosilylation. However, Grignard reagents were not effective for SiNC surface modification.

Dasog *et al*.[165,195,205] explored the passivation of H-SiNCs with amines, carbon dioxide and trioctylphosphine oxides (Scheme 1-4).[165,195,205] Amine capping provides passivation through Si-N covalent bond formation while CO_2 forms acetal bonds. However, these bonds are not stable under ambient conditions. The modified SiNCs are not colloidally stable. On the other hand, trioctylphosphine oxides (TOPO) provide colloidal stability of oxidized SiNCs. The size-dependent PL of SiNCs was altered in all cases, regardless if the capping ligands are amines, carbon dioxide or trioctylphosphine oxides.

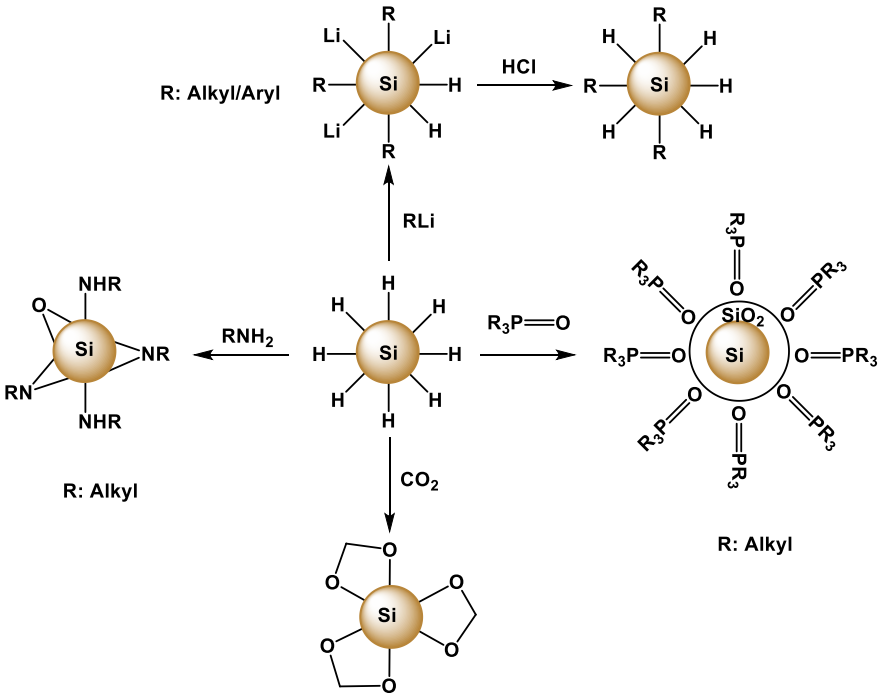

Scheme 1-4. Alternative surface modifications of H-SiNCs with organolithium, trialkylphosphine oxide, carbon dioxide and amines.[89]

1.2.2.2 Modification of Halide-Terminated Silicon Nanocrystals

Another important strategy of SiNC surface modification employed the diverse reactivity of surface Si-X (X = Cl, Br) bonds with ligands including, alcohols, amines, Grignard or organolithium reagents, silanols and lithium aluminum hydride (Scheme 1-5).[80,89] Most of the solution phase methods result in halide-terminated SiNC (X-SiNC) that are subsequently modified in-situ or during post-synthetic work up. One of the earliest examples of X-SiNC modification is the post-synthetic methoxy coating of Cl-SiNCs prepared by the metathesis reaction between KSi (Zintl salt) and $SiCl_4$.[129] Alkyl-capping of X-SiNCs was also achieved by using Grignard and organolithium reagents.[80,130–132,134,206] X-SiNCs also react with $LiAlH_4$, alkyl/aryl amines and silanols leading to the NC surface derivatization with Si-H, Si-NHR/Si-NHAr, and cross-linked siloxane, respectively.[80,117,128,186,207–209]

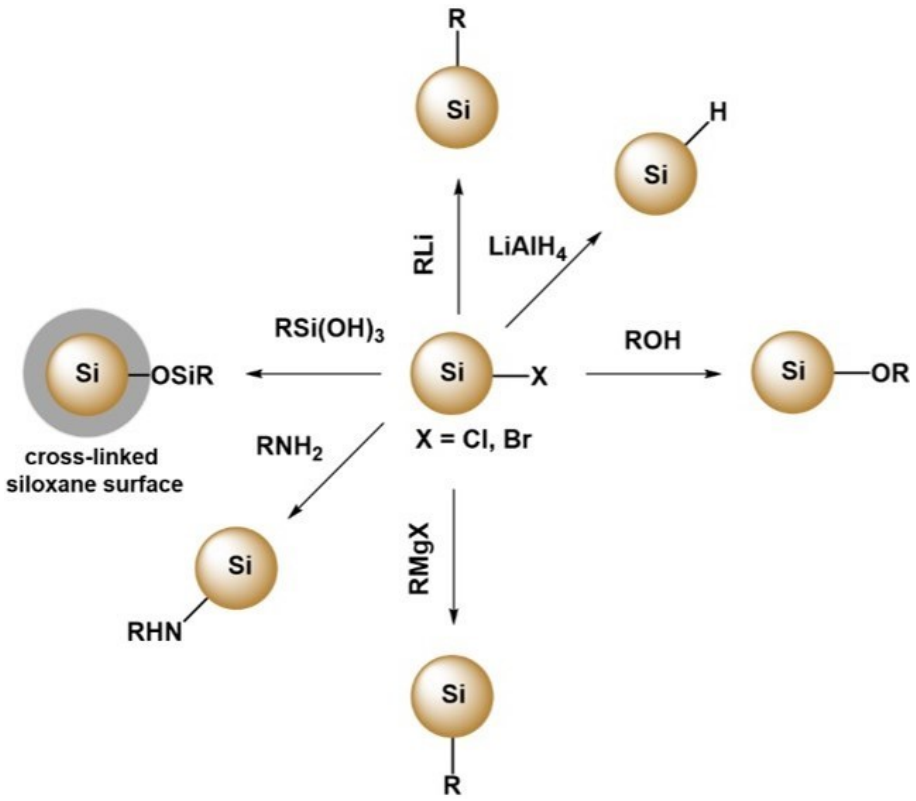

Scheme 1-5. Representative X-SiNC (X = Cl, or Br) surface modification *via* reaction of surface halides with nucleophiles.[80,175]

Aside from the modification of X-SiNCs formed *in-situ*, Lewis and coworkers[210] introduced a two-step chlorination/alkylation route for alkyl-capping on Si(111). High-temperature (80 - 100 °C) treatment of hydride-terminated Si (111) surface with phosphorus pentachloride (PCl_5) in the presence of a radical initiator (benzoyl peroxide) provided chloride surface termination. The reaction of surface Si-Cl bonds with alkyl magnesium halides or alkyl lithium reagents results in alkylation of the surface. Dasog *et al*.[165,211] applied this two-step strategy to modify Cl-SiNC surface with allyl-, alkyl-, and aryl amines. Importantly, chloride surface termination was achieved by simply treating H-SiNCs with PCl_5 at room temperature to 40 °C. This method allowed for the opportunity to isolate Cl-SiNCs and investigate their reactivity. However, the passivation of Cl-SiNCs in these methods is not effective rendering their surface oxidation.

Bell *et al.*[34] developed a similar two-step method involving N-bromosuccinimide (NBS)-mediated bromide surface termination of H-SiNCs followed by alkoxy or siloxane coating by treating them with alcohols or silanols, respectively (Scheme 1-6a). However, the SiNCs were poorly passivated that led to their oxidation.

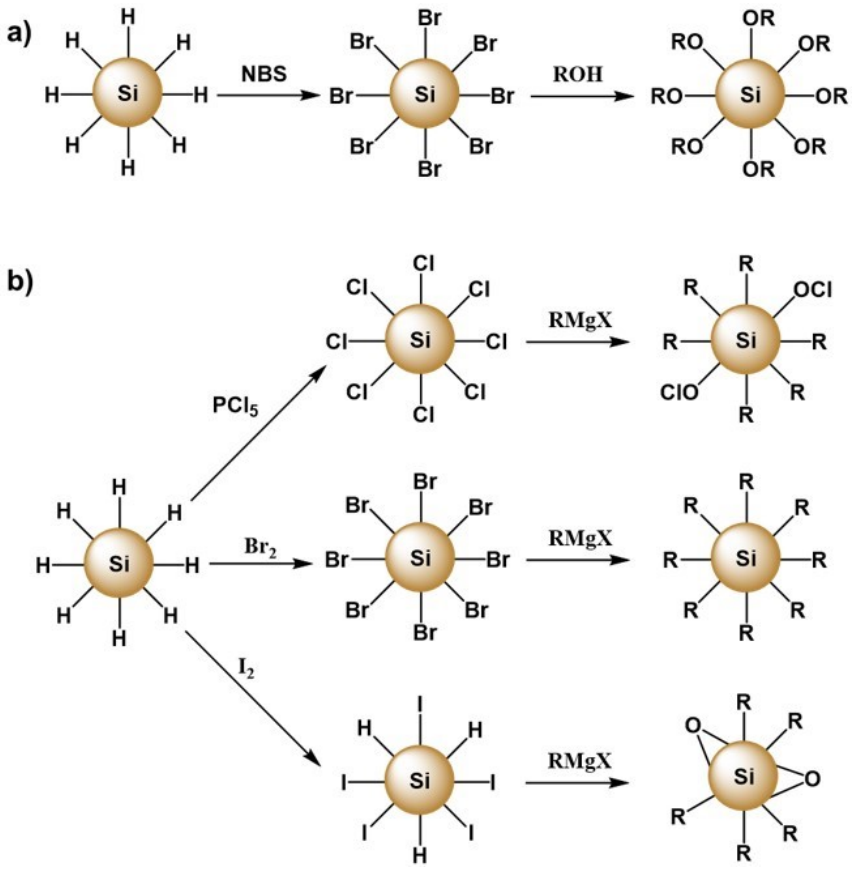

Scheme 1-6. Two-step surface modification of H-SiNCs: a) bromination using NBS followed by alkoxy and siloxane capping,[34] and b) halogenation with indicated halide sources followed by alkylation with Grignard reagents (RMgCl and RMgBr; R = Methyl, n-butyl, n-hexyl, and n-dodecyl).[212]

A recent investigation by Dasog *et al.*[212] extended the two-step modification method by using different halide sources (*e.g.,* PCl_5, Br_2, and I_2) (Scheme 1-6b). In this study, it was demonstrated that significant etching of SiNCs occur during halide (chloride or bromide) surface termination using PCl_5 or Br_2 while no detectable etching was observed during iodide termination using I_2. The halide-terminated SiNCs were then treated with Grignard reagents to prepare alkyl-

passivated SiNCs. In this approach, only Cl-SiNCs and Br-SiNCs undergo efficient reaction with Grignard reagents to produce effectively passivated and colloidally stable NCs while the equivalent SiNCs derived from I-SiNCs suffered significant oxidation and exhibited poor colloidal stability.

1.2.2.3 Multi-step Modifications of Hydride- and Halide-terminated Silicon Nanocrystals

Multi-step surface modification is advantageous to design multifunctional SiNCs. Multifunctional SiNCs can be achieved in one step *via* functionalization with a mixture of functional ligands or with a bifunctional ligand. However, difficulty arises when the functional groups of interest have competitive reactivity towards NC surface.[213] Moreover, due to heterogeneous nature of the reactions on surface, excess amounts of ligands are typically required to drive the reaction efficiently. Some molecules are just too expensive to use in large quantity.[80] Therefore, the coupling of functional ligands with the distal moieties of NC can be beneficial.[80] One of the earliest examples of multi-step modification is the methoxy capping of Cl-SiNCs, followed by controlled hydrolysis to prepare hydroxy-capped SiNCs (HO-SiNCs); finally, cross-linked siloxane coating was obtained by treating HO-SiNCs with chlorosilanes (Scheme 1-7a).[214] Swihart *et al*.[45] converted H-SiNCs (liberated from silica matrix by HF/HNO_3 etching) to HO-SiNCs *via* HNO_3 or piranha treatment; subsequent reaction HO-SiNCs with alkoxy silane resulted in their organosiloxane coating (Scheme 1-7b). So far, these multi-step modifications have been demonstrated only for a cross-linked siloxane coating that is not suitable for further chemical reactions on SiNCs surface-bonded ligands.

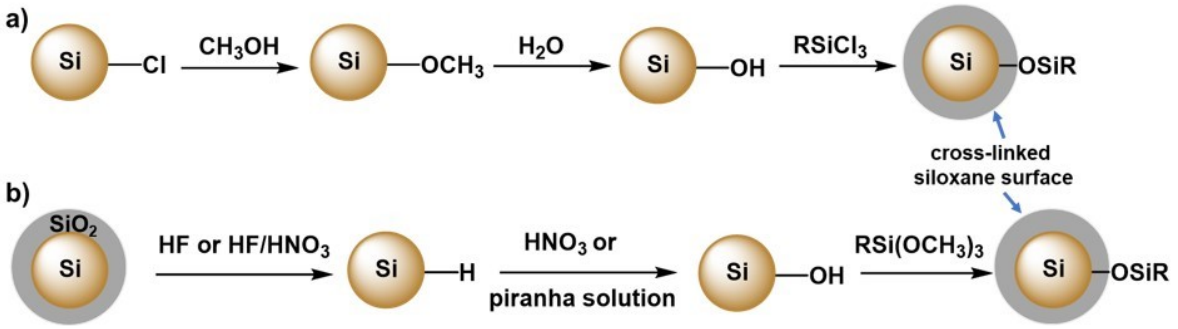

Scheme 1-7. Multi-step modification of SiNCs: a) cross-linked siloxane coating starting from Cl-SiNCs[214] and b) cross-linked siloxane coating *via* chemical oxidation of H-SiNCs to HO-SiNCs followed by silanization.[45]

Shiohara *et al.*[213] carried out chemical reactions using alkene terminal groups on the SiNC surface (Scheme 1-8a). In the first step, the pendant alkene moiety was obtained by hydrosilylation of H-SiNCs with 1,5-hexadiene. Epoxidation of the pendant alkene groups was carried out by the electrophilic addition of peracids. Finally, hydrolysis of the epoxide in the presence of a phase transfer catalyst (tetrabuthylammonium hydrogen sulfate) resulted in the distal diols moieties on SiNCs. Ruizendaal *et al.*[215] synthesized bifunctional SiNCs using the thiol-ene click reaction of thiol-containing molecules with distal alkene moieties (Scheme 1-8b). Cheng *et al.*[122] prepared series of hydrophilic and hydrophobic SiNCs by introducing functionalities such as $–NH_2$, –COOH, $–SO_3^-$, alkane, and alkene through thiol-ene click reactions.

Recently, Höhlein *et al.*[216] immobilized a reactive chlorosilane pendant group on SiNCs *via* diazonium salt-initiated hydrosilylation of H-SiNCs with chlorodimethyl(vinyl)silane. Subsequent nucleophilic substitution with alcohol, silanols, and organolithium reagents provided an additional passivation of the SiNCs (Scheme 1-8c).

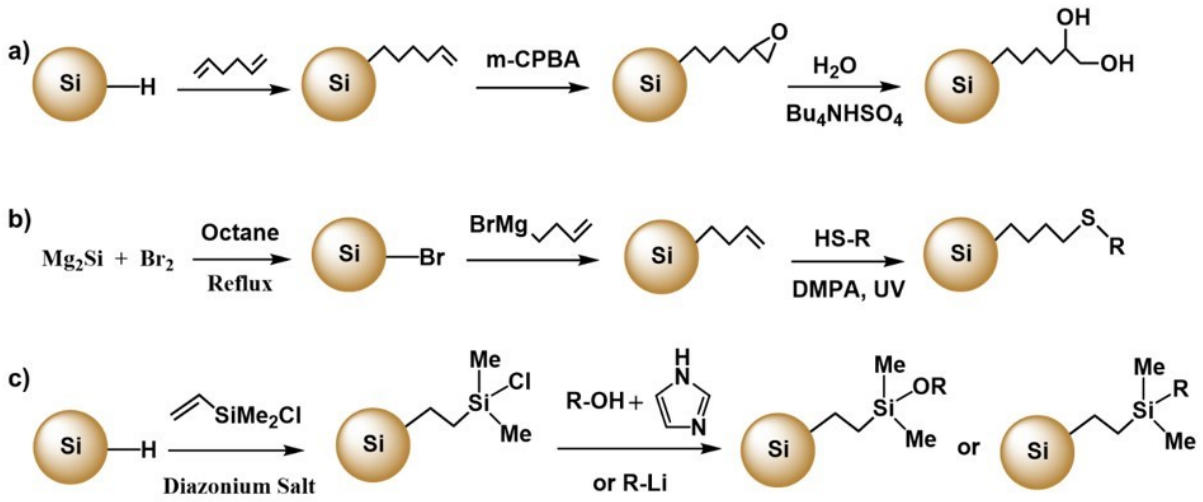

Scheme 1-8. Multi-step surface modification methods continued: a) epoxidation of surface alkene and hydrolysis to diols,[213] b) thiol-ene click reaction on surface alkene moieties,[215] and c) nucleophilic substitution of surface-bonded reactive chlorosilanes.[216]

1.2.3 Optical Properties of Silicon Nanocrystals

The size-dependent optical properties make SiNCs appealing for optoelectronic applications. Visible PL from *p*-Si was first observed by Canham,[94,95] and attributed to band-gap emission due to quantum confinement. However, unlike compound semiconductor materials, the indirect band gap of silicon limits its optical output. In a direct band-gap semiconductor, the VB maximum and the CB minimum are aligned vertically on the wave vector axis (Figure 1-4a).[217] They share the same crystal momentum; thus radiative recombination occurs very rapidly and efficiently *via* a dipole momentum allowed transition.[217] On the other hand, for an indirect band-gap semiconductor the CB minimum is not aligned on the same axis with the VB maximum (Figure 1-4b) prohibiting the direct radiative recombination[217] The transition can occur *via* the assistance of crystal lattice vibration (phonon) which conserves the crystal momentum.[96] As the phonon-assisted transition is a relatively slow process, the radiative recombination of the exciton has a significantly longer lifetime (τ_r), usually in the order of millisecond.[218] In contrast, the nonradiative recombination lifetime (τ_{nr}) for silicon is very short (few nanoseconds) which favours the

nonradiative recombination of the exciton.[218] Therefore, the internal quantum efficiency (η_i), defined as ratio of nonradiative lifetime over total lifetime ($\eta_i = \tau_{nr}/\tau_r+\tau_{nr}$), is very low (~$10^{-6}$) for bulk silicon semiconductor at room temperature.[217,218] Cooling bulk silicon near to 4 K allows a sharp emission line at 1060 nm to be observed.[219]

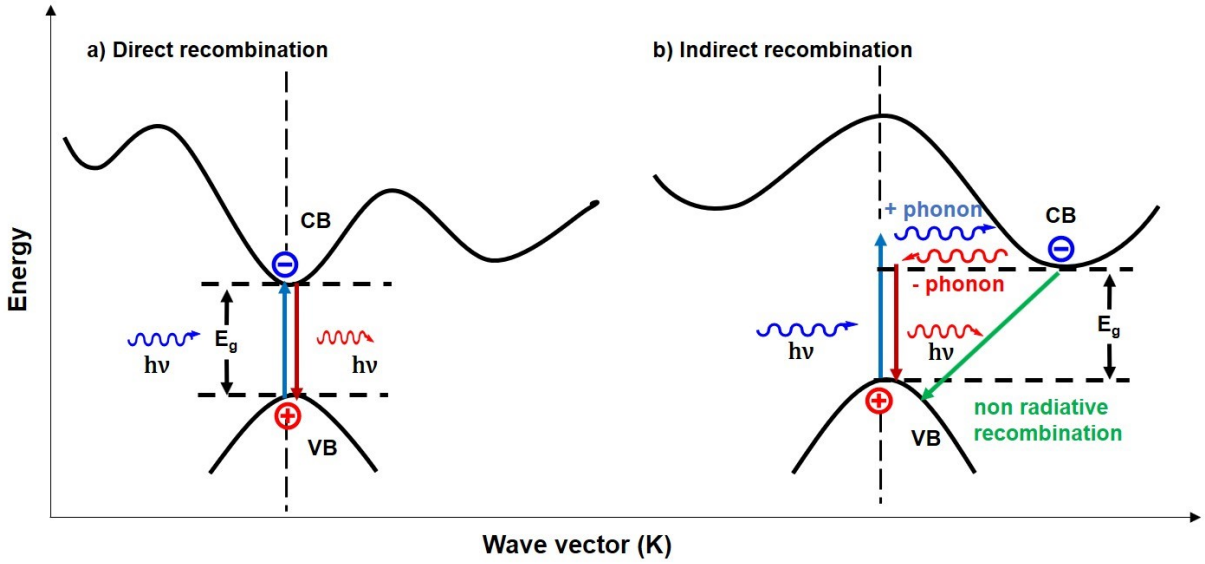

Figure 1-4. Simplified energy band diagram and electron-hole recombination process in a) direct and b) indirect band-gap semiconductors.[217,218]

For smaller SiNCs, there is an increased probability of the radiative recombination of the exciton. In accordance with the Heisenberg uncertainty principle, narrowing the probability of locations of an exciton in real space broadens their crystal momentum wave function (Figure 1-5).[96,218,220] Broadening of the wave function is negligible for larger NCs (Figure 1-5a)[96] but becomes significant when the exciton is three-dimensionally confined upon reduction of the NC size below the Bohr exciton radius (Figure 1-5b).[96,218,220] The broadening of the momentum wavefunction leads to an increasing probability of overlap between the CB and VB wave functions and radiative recombination of exciton becomes weakly dipole momentum allowed.[220]

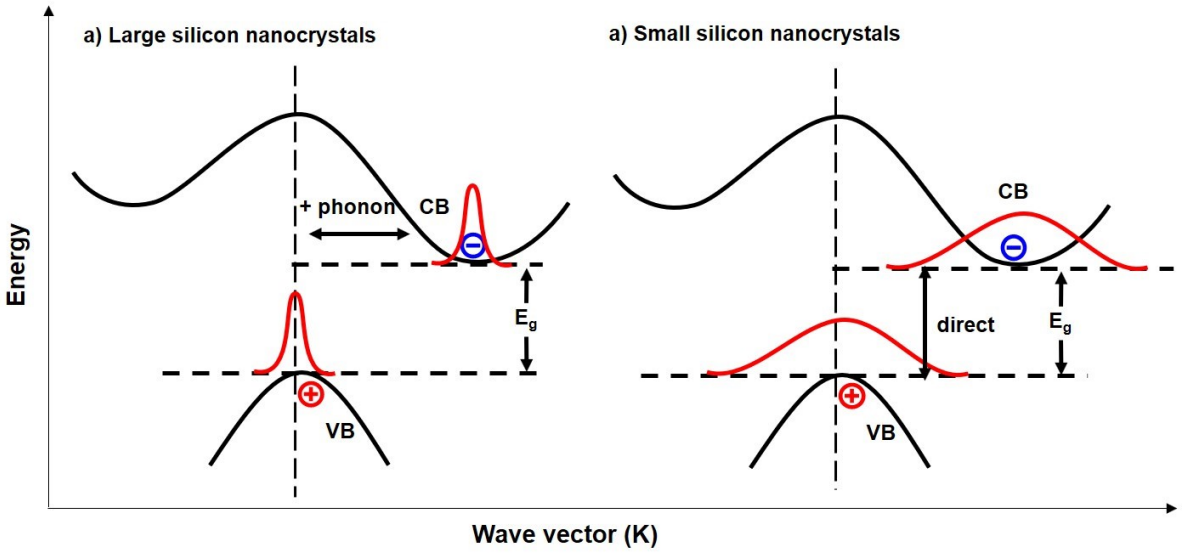

Figure 1-5. Simplified energy band diagram and exciton recombination process in a) large SiNCs with a low probability of momentum wavefunction overlap, causing reliance on phonon-assisted transition, and b) quantum-confined SiNCs with increased overlapping of momentum wave function exhibiting partially dipole momentum-allowed transition.[96]

The origin of PL in SiNCs is strongly debated[165,221–223] and two types of emission processes are readily considered: 1) band-gap emission, and 2) surface states-induced emission. According to the band-gap emission model proposed by Canham,[94,95] decreasing the NC size should increase band gap resulting in the blue shift of the emission wavelength. Indeed, full visible emission color was observed from SiNCs (Figure 1-6a) by reducing their size *via* plasma-induced and chemical (*e.g.,* HF/HNO_3) etching.[140,224,225] The band-gap emission model was experimentally supported by measuring the band gap *via* single-particle scanning tunneling spectroscopy (STS) and comparing to the corresponding PL peak emission wavelength.[226] Increase in the sizes of SiNCs results in the decrease of their band gap with an associated red-shift in their PL emission maximum (Figure 1-6b).

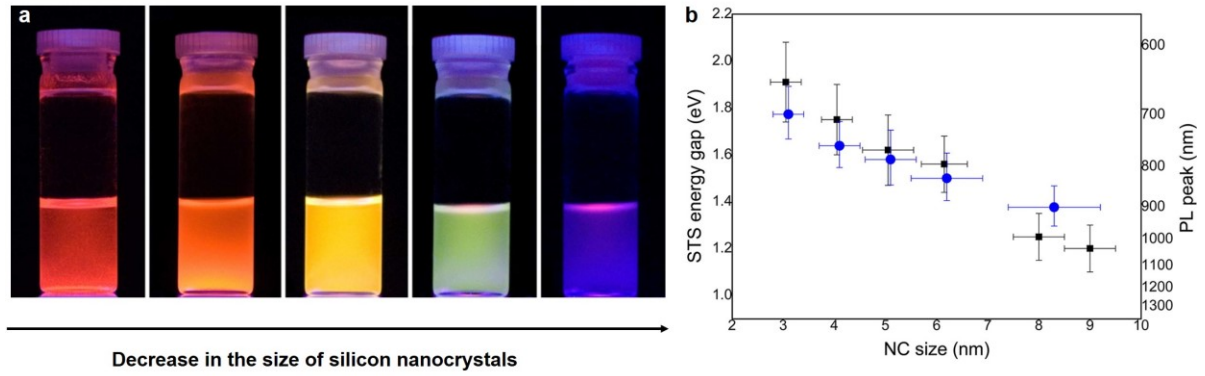

Figure 1-6. a) The shift in band-gap emission colors of SiNCs with a decrease in their size. Reproduced and adapted with permission from Pi *et al.*[224] Copyright 2008, IOP Publishing, b) comparison of SiNC band-gap (measured by STS) with their emission wavelength reveals size-dependent band-gap emission. Reproduced with permission from Wolf *et al.*[226] Copyright 2013, American Chemical Society.

If the band-gap emission is the origin of PL, the radiative decay time should be longer (*ca.* μs) due to indirect phonon assisted transition. The decay time should decrease, and PL QY should increase for smaller SiNCs since the transition becomes increasingly dipole allowed. Recently, our group reported the radiative decay time for SiNCs in the size range between 2.1 - 7.5 nm.[93] In all cases, microsecond decay times were observed and the lengths of decay decreased for smaller SiNCs (Figure 1-7). Hessel *et al.*[161] reported the relative PL QY for SiNCs in the size range of 2.7-11.8 nm. PL QY decreased from 8 % for 2.7 nm SiNCs to 0.4 % for 11.8 nm SiNCs. These experimental observations support indirect band-gap emission as the origin of PL in SiNCs. However, these experimental data were obtained for alky passivated SiNCs which have undergone surface modification.

Surface states (*e.g.,* traps, dangling bonds, and interface states) also play a significant role with respect to the PL properties of SiNCs.[165,221,227–229] Since SiNCs are obtained either as oxide-coated or passivated through covalent bonds with various ligands, there is a direct interaction between silicon core and surface species that can influence their PL color and PL QY.[80]

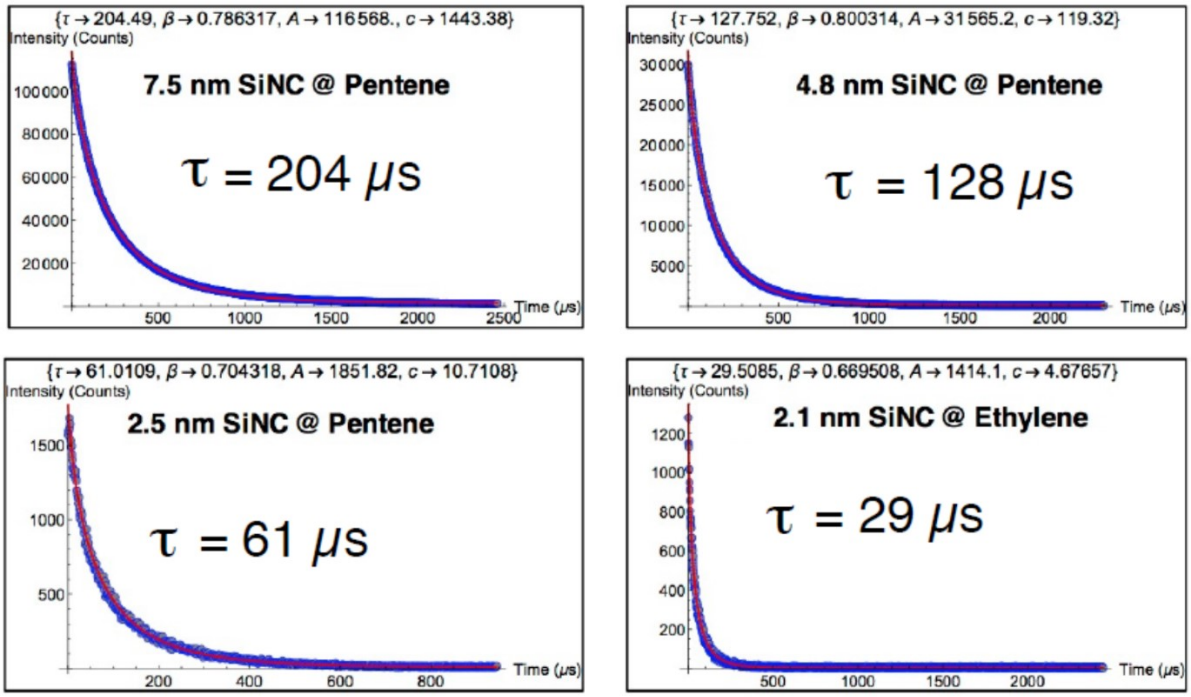

Figure 1-7. Microsecond decay times for PL of SiNCs that decreases with a decrease in their size; this demonstrates their indirect phonon-assisted band-gap emission. Reproduced with permission from Mobarok *et al.*[93] Copyright 2017, Wiley-VCH.

There are several models to explain the origin of PL arising from oxide coated SiNCs.[221,227–231] Koch *et al*.[227] proposed three types of exciton radiative recombination processes for oxide coated SiNCs: 1) recombination across the band gap, 2) band to surface states recombination and 3) recombination within the surface states.[227] Recombination across the band gap is defined by quantum confinement of exciton where the transition occurs in combination of a phonon-assisted and partially dipole momentum-allowed processes and PL lifetime is usually longer (microseconds) (Figure 1-8).[221,227,228] In band to surface states recombination process either electron or hole (e^-or h^+) moves to the surface states while the opposite remains in the core. Recombination of the e^-/h^+ pair results in radiation with nanosecond lifetime that is determined by the time required for capturing of the respective carrier in the surface states (Figure 1-8).[221,227,228] Recombination within the surface states is the process where both e^- and h^+ move to and are

captured into the surface states. The radiative recombination of this type is the slowest process since this requires tunneling or hopping of both charge carriers to the surface states (Figure 1-8).[221,227,228]

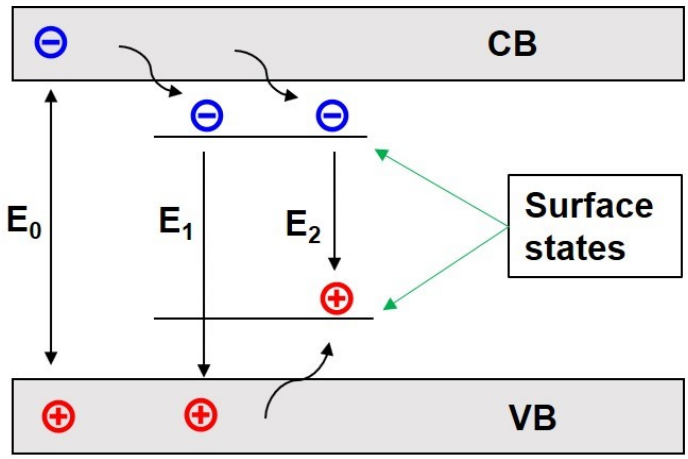

Figure 1-8. Diagram showing exciton recombination in oxide coated SiNCs: recombination across the band gap (E_0), band to surface state recombination (E_1), and recombination within surface states (E_2).[227]

For oxide-coated SiNCs the blue emission was ascribed to the recombination of exciton across the band-gap,[232] while the origin of yellow and green emission was attributed to the band to surface states recombination process.[227] However, the possibility of surface-related states, produced by Si-O bonds, as the origin of blue emission was not ruled out.[233] Recombination at the SiNCs and SiO_x interface, as well as recombination within the oxide defects, are also proposed to be the origin of blue PL.[222,233,234]

All the solution-based synthesis methods result in size-independent blue-emitting SiNCs.[35] Also, capping of SiNCs with certain ligands (*e.g.,* amines) results in size-independent blue PL.[195] The origin of this blue PL was attributed to the charge transfer process from surface oxynitride defects to the SiNC[195] based on nanosecond decay times and a solvatochromic effect on the emission wavelength.

The PL QY of SiNCs is relatively low since the exciton recombines with defects or surface states much faster than the phonon-assisted radiative pathway. However, organic ligand passivation of SiNC surface under strict inert atmosphere can provide improved PL QY.[147] Enhancement of PL QY can also be achieved through chemical modification of SiNC surface. Surface etching of SiNCs with XeF_2 has been shown to remove dark defects and the PL QY of the SiNCs was enhanced significantly (70 %) after subsequent ligand passivation in inert atmosphere.[93] Tethering a conjugated dye to the SiNC surface is an alternative strategy to enhance the PL QY. The dye absorbs light and transfers the photoenergy to the SiNCs through the process called Förster resonance energy transfer (FRET) (Figure 1-9).[235]

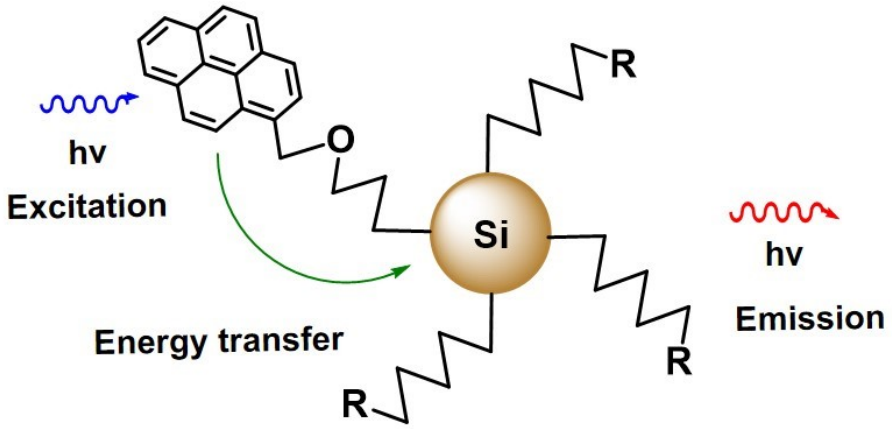

Figure 1-9. Energy transfer from a conjugated dye (pyrene) to SiNC enhancing its PL emission.[235]

1.2.4 Catalytic Properties of Silicon Nanocrystals

The criteria for a good photocatalyst is its ability to employ visible to near UV light, being abundant and non-toxic.[236] Many of these criteria can be met by using SiNCs based-photocatalysts. The size-dependent photocatalytic properties of SiNCs are essential for their potential catalytic applications in water splitting hydrogen production,[237] carbon dioxide reduction,[238] and other oxidation-reduction reactions.[236]

Recently, Wheeler *et al.*[239] reported that chloride surface termination generates Lewis acidic SiNC surface by lowering the energy of the LUMO of the surface Si-Cl bonds (Figure 1-10 left). The lowering of the LUMO facilitates the transfer of electron density from an electron-donor molecule to the electron-accepting surface through hypervalent interaction. This hypervalent interaction lengthens/weakens both the surface Si-Cl bonds and the donor molecule bonds (Figure 1-10 right). In this context, the Cl-SiNCs could be harnessed as a reactive species for catalytic applications; the reactivity of Cl-SiNCs for the synthesis of poly (3-hexylthiophene) (P3HT) have been investigated and will be discussed in the experimental chapter 2.

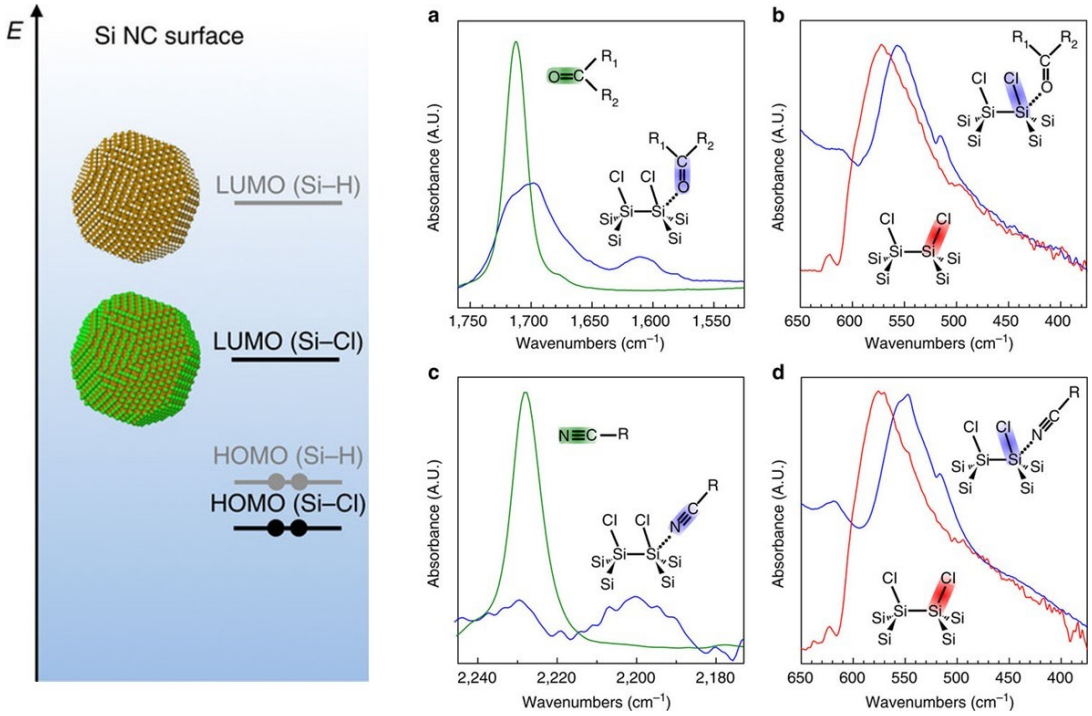

Figure 1-10. Effect of chloride surface group on the electronic and chemical properties of SiNCs: lowering of SiNC LUMO (right), and activation of the surface Si-Cl bonds as well as the bonds of the donor type molecules (left) as evident from the red-shift of the corresponding stretching modes. a) and b) represent the weakening of Si-Cl and C=O bonds upon interaction of ketone with Cl-SiNC; c) and d) show the weakening of Si-Cl and C≡N bonds due to the interaction of Cl-SiNCs with nitriles.[239]

1.2.5 Silicon Nanocrystals/Polymer Hybrid Functional Materials

Hybrid functional materials (HFMs) composed of inorganic nanomaterials and polymers are attractive because they can exhibit unique and tunable properties arising both from the individual components and the synergistic interactions between the nanomaterial and the polymer.[89,182,240,241] Especially, HFMs consisting of semiconducting nanoparticles and conjugated polymers offer the possibility of donor-acceptor interfacial energy transfer and charge transfer dynamics as well as enhanced charge carrier mobility. HFMs consisting of compound semiconductor NPs with polymers have been investigated for many prototype applications including solar cells,[242–244] light-emitting diodes,[245,246] photodetectors,[247] photocatalysis,[248] photothermal therapy,[249] bioimaging,[250] drug delivery,[251] and sensing.[252] However, significant developments in hybrid materials composed of SiNCs and polymers have not been achieved.

The most straightforward way to prepare HFMs is dispersing the NPs and polymer in a common solvent. Liu *et al*.[253] employed this blending process to prepare a SiNC/P3HT hybrid solar cell. Freshly HF etched H-SiNCs were mixed with P3HT in dichlorobenzene and spin coated onto indium tin oxide (ITO) substrates. However, agglomeration of the SiNCs resulted in nonuniformity of the film.

UV-blocking photoluminescent silicon nanocrystal/polydimethylsiloxane (SiNC/PDMS) HFMs were prepared by mixing hydride, or decyl-terminated SiNCs with vinyl-terminated PDMS (V-PDMS) followed by crosslinking of V-PDMS using Karstedt's catalyst (Figure 1-11a).[163] Both H-SiNC/PDMS and decyl-SiNC/PDMS HFMs were transparent to visible light; this is important for applications in transparent flexible electronics. The HFM of decyl-SiNC/PDMS was highly thermally stable, mechanically reinforceable, luminescent, and an effective UV-blocker (Figure 1-11b).

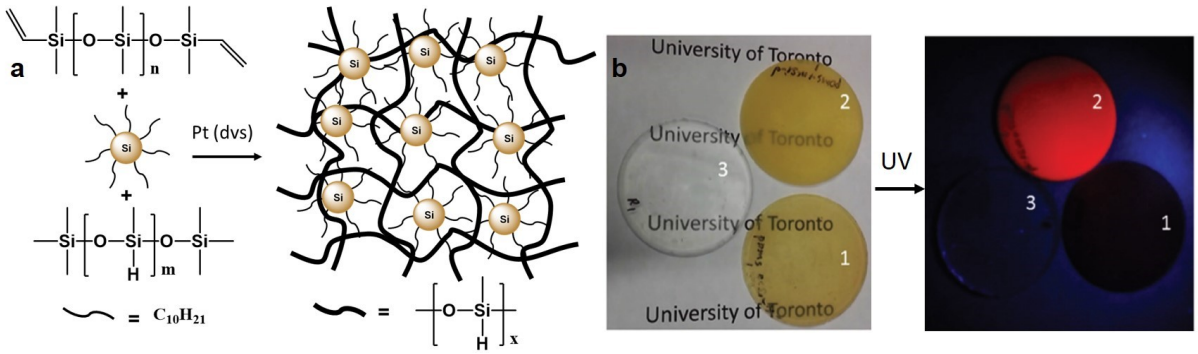

Figure 1-11. a) Preparation of decyl-SiNC/PDMS HFM, and b) photographs demonstrating the UV masking properties of the HFM (1: H-SiNC/PDMS, 2: decyl-SiNC/PDMS, 3: PDMS reference). Reproduced and adapted with permission from Chen *et al.*[163] Copyright 2017, WILEY-VCH.

Recently, Meinardi *et al.*[254] prepared SiNC and poly (lauryl methacrylate) (SiNC/PLMA) HFM. Dodecyl-SiNCs were mixed with lauryl methacrylate monomer, ethylene glycol dimethacrylate (EGDM) cross-linker and 2,2-Dimethoxy-1,2-diphenylethan-1-one (IRGACURE 651) photoinitiator; polymerization was carried under UV-irradiation (Figure 1-12a). SiNCs exhibit negligible overlap in their absorption and emission spectra.[254] This property is particularly beneficial for luminescent solar concentrators (LSCs) so that reabsorption of emitted light can be suppressed. On the other hand, transparent and flexible PLMA can act as a waveguide. An efficient LSC was fabricated by utilizing these properties in the HFM (Figure 1-12b).

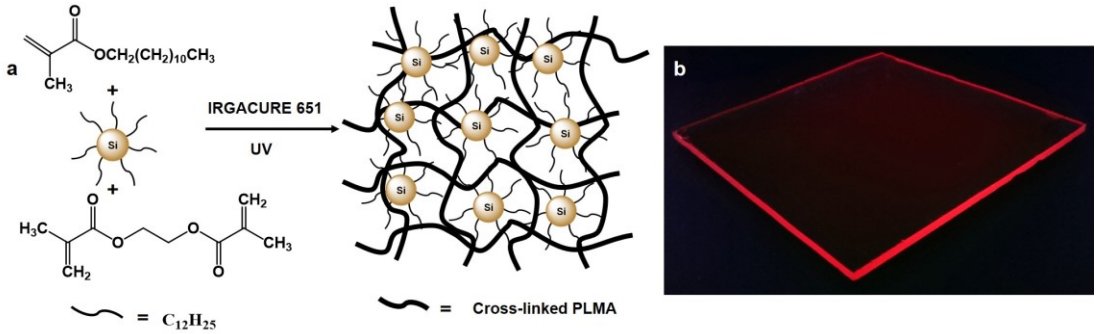

Figure 1-12. a) Preparation of cross-linked dodecyl-SiNC/PLMA HFM, and b) photographs of the HFM under UV-irradiation demonstrating the concentration of emitted light at the edge of the waveguide. Reproduced and adapted with permission from Meinardi *et al.*[254] Copyright 2017, Macmillan Publishers Limited.

Although physical blending is a simple method, it results in a noncovalent interaction between NCs and polymers. This non-robust nature of this interaction can be a challenge concerning colloidal stability.[89] The introduction of covalent bonds between NCs and polymers can minimize the concern of long-term colloidal stability. Also, a covalent bond can enhance interfacial contact between NCs and polymers.

Yang *et al*.[180] reported the synthesis of HFM composed of polystyrene functionalized SiNCs embedded in bulk polystyrene matrix (PS/PS-SiNC). The PS/PS-SiNC was prepared *via* thermal treatment of H-SiNCs with styrene (Figure 1-13a). The polymer chain initiation takes place in solution *via* thermal activation of styrene monomer forming benzylic radical which can attack other monomers in chain propagation steps or abstract hydrogen radical from H-SiNCs leaving a surface silicon radical (≡Si$^{\bullet}$). The surface ≡Si$^{\bullet}$ can add to a styrene monomer and initiate polymerization at the SiNC surface. Alternatively, solution grown polymeric or oligomeric radical species can attach to the surface ≡Si$^{\bullet}$ in a chain termination step. The resultant PS/PS-SiNC HFM was highly luminescent, solution processable, and mechanically stretchable such that highly luminescent micro and nanostructures could be prepared. A luminescent optical fiber was fabricated *via* simple dip-coating from a toluene solution of the HFM (Figure 1-13b). The hydrophobic polystyrene coating also provided resistance of SiNCs against basic etching environments (Figure 1-13c). The resistance against base facilitates the preparation of nanofibers of the HFM. Nanofibers were fabricated on aluminum oxide membrane template; potassium hydroxide (KOH)-induced etching of the template liberated the hybrid films (Figure 1-13d). SiNC/PS HFM has shown promise as a charge-trapping material in archetype metal-insulator-semiconductor device and thin-film field-effect transistor.[89,255]

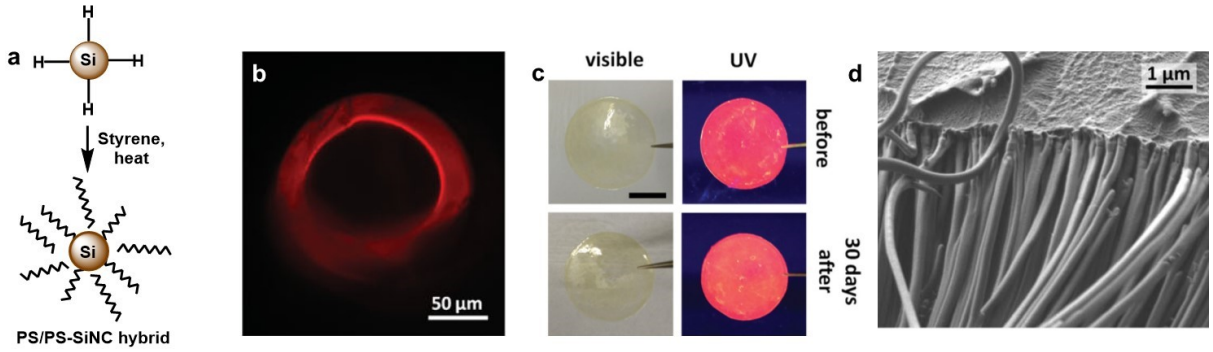

Figure 1-13. a) Synthesis of PS/PS-SiNC HFM, b) fluorescence microscope image of PS/PS-SiNC HFM coated optical fiber, c) long-term resistance of HFM film against basic NaOH, and d) SEM image of the nanofiber after removal of the template. Reproduced and adapted with permission from Yang *et al.*[180] Copyright 2013, WILEY-VCH.

Marinins *et al.*[256] prepared silicon nanocrystal/poly(methyl methacrylate) (SiNC/PMMA) HFM using both physical blending and covalent bonding approaches. In the blending process, dodecyl-SiNCs were mixed with methyl methacrylate (MMA) monomer and the polymer encapsulation was done by a radical initiated polymerization method (Figure 1-14a). In the latter approach, SiNC/PMMA was prepared directly by a radical-initiated hydrosilylation of H-SiNCs with MMA analogous to the polymerization outlined in the preparation of PS/PS-SiNCs HFMs (Figure 1-14b). Transparent, highly tunable luminescent SiNC/PMMA solid composite was obtained using both methods (Figure 1-14c). This HFM is targeted for potential applications in solid state lightings and displays.

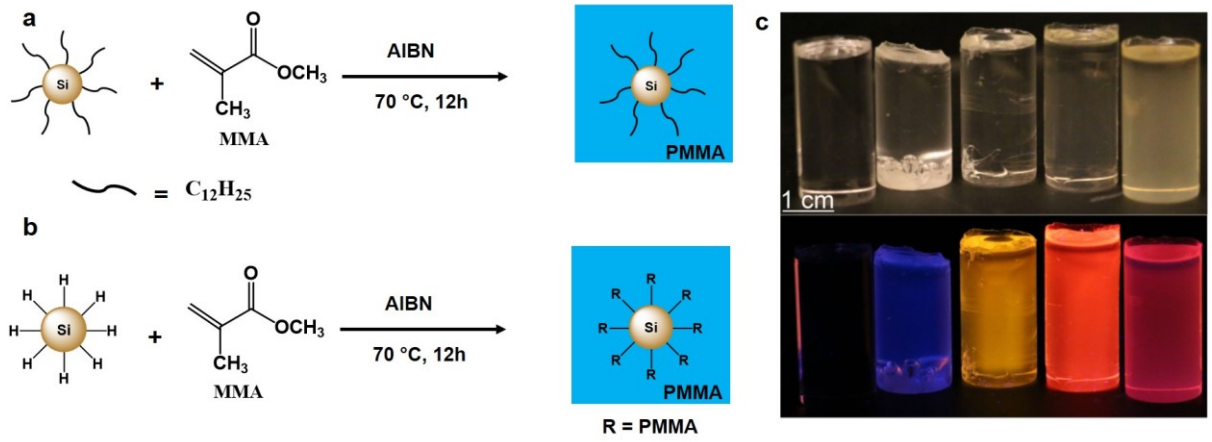

Figure 1-14. Preparation of SiNC/PMMA HFM through a) blending of dodecyl-SiNCs with MMA and *in-situ* polymerization, and b) covalent bonding *via* the radical-initiated hydrosilylation with MMA; c) photographs of the transparent HFM under ambient light (top) and UV irradiation (bottom) compared to PMMA reference (left most block). Reproduced and adapted with permission from Marinins *et al.*[256] Copyright 2016, American Chemical Society.

The polymer in most of the reported HFMs mainly serves as a template. Recently, Kehrle *et al.*[182] developed a new type of surface-initiated polymerization, named as surface-initiated group transfer polymerization (SI-GTP), to graft a thermoresponsive poly (diethyl vinylphosphonate) (PDEVP) from SiNC surface (Figure 1-15a). Photochemical hydrosilylation of H-SiNCs with ethylene glycol dimethacrylate (EGDM) yields poly EGDM grafted SiNCs (SiNCs-g-PEGDM) having pendant methyl acrylate binding sites. The group transfer catalyst (Cp_2YCH_2TMS) is covalently bonded to the surface binding sites through the formation of a metal-enolate complex. Finally, the diethyl vinylphosphonate (DEVP) monomer was added to prepare the thermoresponsive and photoluminescent (SiNCs-g-PEGDM-g-PDEVP) HFM. The as-prepared HFM is dispersible in water at room temperature and exhibits intense red PL under UV illumination (Figure 1-15b 1 and 2), while it precipitates upon heating the dispersion at 70 °C for several hours and then demonstrates a shift in PL color and intensity (Figure 1-15 b 2 and 3). The aggregation is driven by the transition of the thermoresponsive polymer from coils to globules.

The transition starts at 30 °C, as shown by the decrease in the hydrodynamic radius of the HFM *via* dynamic light scattering (DLS) analysis. Synergism of the thermoresponsive behavior of the polymer and PL of the SiNCs could potentially lead to the application of the HFM in sustained drug delivery and imaging as well as wound tissue detection and engineering.[257]

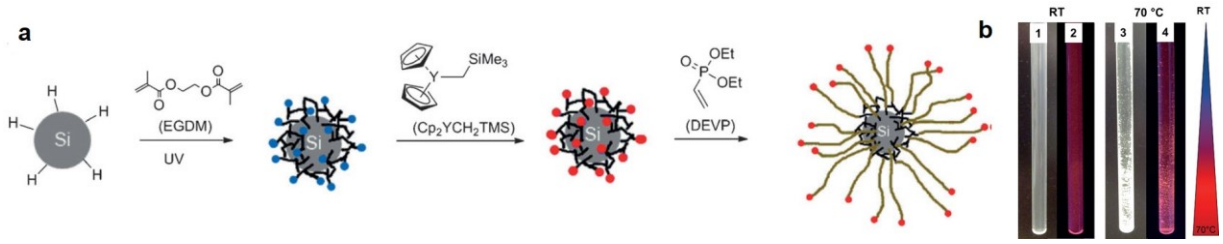

Figure 1-15. a) Schematic of SI-GTP-mediated synthesis of SiNC-g-PEGDM-g-PDEVP HFM, and b) photographs demonstrating the PL and thermoresponsive properties of the HFM; 1) and 2) show a dispersion of HFM in water at room temperature under ambient and UV light, respectively; 3) and 4) are the same dispersions after heating at 70 °C. Reproduced and adapted with permission from Kehrle *et al.*[182] Copyright 2014, WILEY-VCH.

The properties of the SiNC/non-conducting polymer HFMs are promising but do not enable electronic interactions. There are few examples of SiNC/conductive polymer HFMs, including polyaniline (PANI)[258–261] and poly(styrene sulfonate) doped poly(3,4-ethylenedioxythiophene) (PEDOT:PSS)[262] as the conductive polymers. Ruckenstein and coworkers[258] used surface-initiated polymerization to graft polyaniline from luminescent SiNCs (Scheme 1-9).[258] SiNCs were initially treated with piranha solution to prepare hydroxyl-terminated SiNCs (HO-SiNCs) which were then treated with (3-bromopropyl)trichlorosilane to generate a bromopropylsilane monolayer on the surface. Surface-bonded aniline monolayer was achieved by replacing bromine with aniline, which served as the surface-bonded initiator. The aniline-SiNCs initiators were treated with aniline monomer in the presence ammonium persulfate catalyst to graft polyaniline from the NC surface. The polyaniline coating provided improved PL stability of SiNCs against a series of acidic or basic solutions and organic solvents. Pellets prepared from SiNC@PANI HFM provided six times

higher electrical conductivity compared to that of SiNC alone. However, the conductivity of SiNC@PANI HFM was not compared with that of PANI alone. Therefore, the influence of SiNC on the conductivity of PANI is unclear. Nonetheless, the demonstration of enhanced conductivity by the marriage of conducting polymer and SiNC suggest that tailored HFM can be designed for various electronic applications.

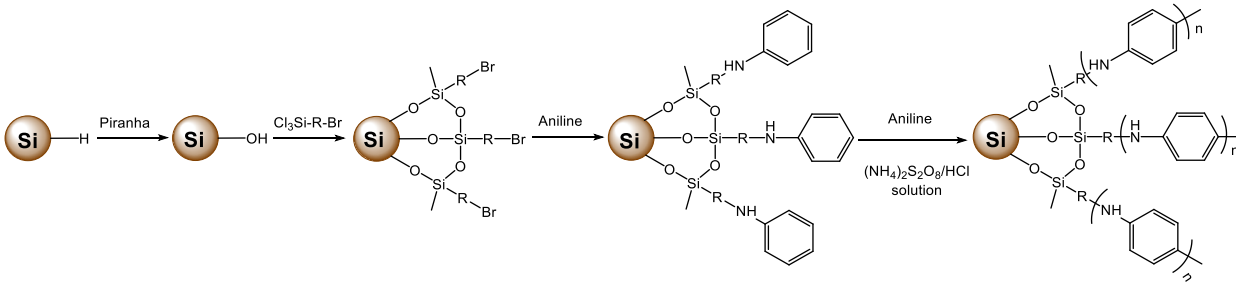

Scheme 1-9. Schematic for the surface-initiated polymerization of aniline to prepare SiNC@PANI HFM.[258]

Another important class of conductive polymer PEDOT:PSS was used by Mitra *et al*.[262] to prepare SiNC@PEDOT:PSS hybrid material *via* microplasma treatment of SiNCs with the polymer. The PEDOT coating provided long-term stability of the SiNCs against oxidation, as well as four-fold higher PL intensity of the SiNCs compared to the non-coated counterpart. It was found that this surface modification led to an improved electrical conductivity of the HFM which was attributed to enhanced interfacial exciton dissociation. This enhanced interfacial effect might be beneficial for applications including, photodetector and electroluminescence devices.

Poly (3-hexylthiophene) (P3HT) is a workhorse material for organic electronics and photovoltaic devices.[263] Numerous reports have appeared demonstrating the benefits of direct interfacial contact between compound semiconductor or metal oxide NPs with P3HT.[240,264–268] However, there is no precedence for direct grafting of P3HT onto or from SiNC surface.

Kiriy and coworkers[269] developed a surface-initiated Kumada catalyst transfer polycondensation (SI-KCTP) reaction to graft P3HT from poly (4-bromostyrene) substrate. Tetrakistriphenylphosphine-nickel $Ni(PPh_3)_4$ was the catalyst of choice. However, the polymer chain was very short. Sontag *et al*. [270] also found difficulty with the robustness of $Ni(PPh_3)_4$ complex for grafting polymer from other substrates. The SI-KCTP method was modified by Kiriy and coworkers[271] by applying a ligand exchange approach (Figure 1-16a) to graft P3HT from silica particles (SiO_2). Initially, the SiO_2 particles were coated with organosilica shell containing pendant phenylbromide groups. $Et_2Ni(bipy)$ catalyst was immobilized on the surface phenylbromide groups which was followed by exchanging the bipyridine (bipy) ligand with 1,3-bis(diphenylphosphino)propane (dppp). Finally, 5-chloromagnesio-2-bromo-3-hexylthiophene (ClMg-HT-Br) monomer was added to grow hairy P3HT from the surface. The modified SI-KCTP method provided a very high density of P3HT on the SiO_2 particles' surfaces (Figure 1-16b). The incorporation of P3HT on the surface of nanoparticles improves the light absorption owing to the broad absorption profile of the P3HT component (Figure 1-16c, d). The broad solar spectrum coverage originates from the surface-mediated effective planarization of the polymer backbone and interchain aggregation resulting in long-range π-electron delocalization. This property of surface grafted P3HT is promising for the solar cell applications.

Grafting P3HT from semiconductor SiNCs can provide a broad absorption profile as a sum of P3HT and SiNC constituents in addition to the surface alignment effect of P3HT. Moreover, direct interfacial contact between SiNC and P3HT will enhance the interfacial charge and/or energy transfer processes. These synergetic effects will provide an opportunity for fundamental studies and may facilitate potential applications in optoelectronic devices including LEDs, photodiodes, and transistors. In this context, grafting of P3HT from SiNC surfaces *via* SI-KCTP

method and the interfacial properties have been investigated and is described in the experimental chapter 3.

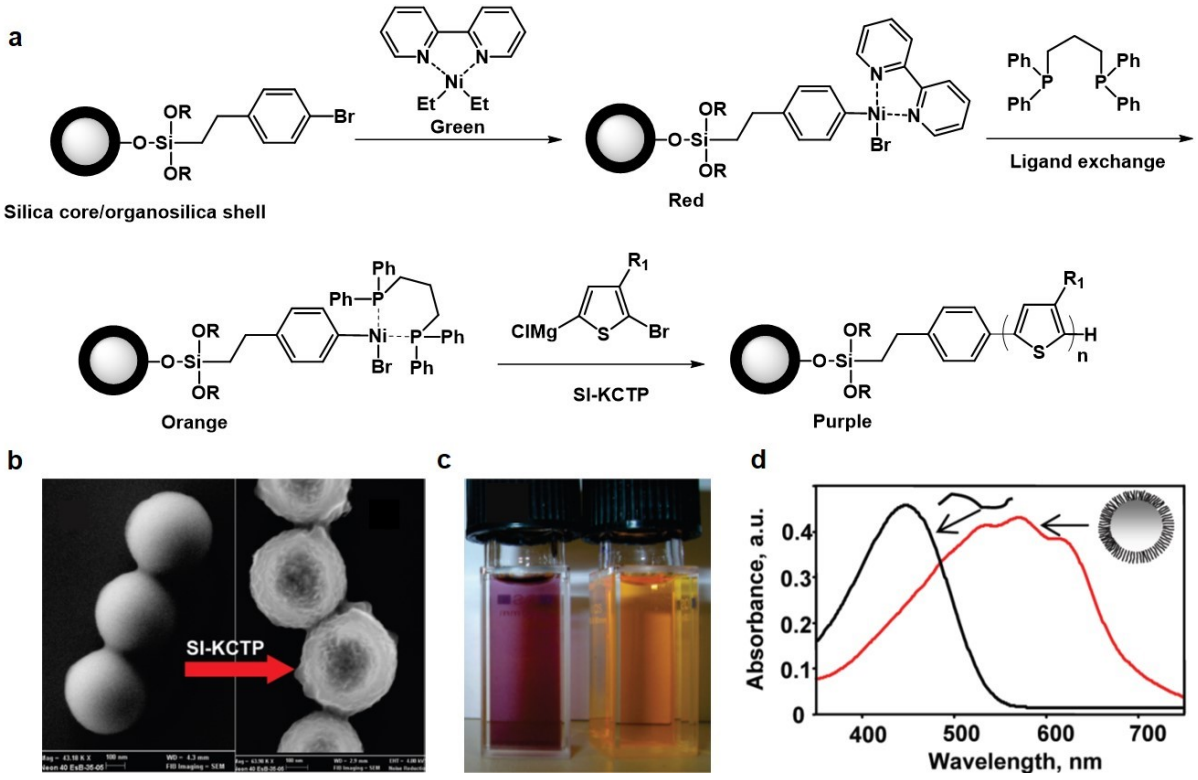

Figure 1-16. a) SI-KCTP-mediated grafting of P3HT from phenylbromide modified silica particles, b) SEM images of the silica particles before and after grafting of P3HT showing a thick polymer layer on particles, c) photographs and d) UV-Vis absorption spectra demonstrating a red shift in the absorption properties of the grafted P3HT compared to free P3HT. Reproduced and adapted with permission from Senkovskyy *et al.*[271] Copyright 2009, American Chemical Society.

1.2.6 Application of Silicon Nanocrystals and Silicon Nanocrystal/Polymer Hybrid Functional Materials

Over the last decades, the fundamental understanding regarding optoelectronic properties of SiNCs have matured quite significantly and the material is now considered as an alternative to compound QDs due to their non-toxic nature, abundance of silicon precursors, and potential for compatibility with existing silicon-based electronic platforms. As mentioned earlier, SiNCs have

been investigated for optoelectronic,[253,272–284] catalytic,[236–238,285,286] and biological applications.[287–292] The parallel development of conjugated polymers provided an opportunity to build a light weight, low cost, and flexible printed organic electronics and large area photovoltaics.[293–295] In many cases, the combination of inorganic NPs and conjugated polymers in a single platform led to unique synergistic property that is different from the individual components.[253,273,274,284,296] For the context of this thesis the following discussion will be focused on the optoelectronic and catalytic applications of SiNCs and SiNC/polymer HFMs.

1.2.6.1 Application in Light-Emitting Diodes

Size-dependent PL tunability and high PL QY of SiNCs are beneficial for applications in light-emitting diodes (LEDs). In the LED operation process, external electrons and holes are simultaneously injected into the CB and VB of a semiconductor material to form excitons which subsequently undergo radiative recombination and emit colors.[2] Cho *et al*.[272] fabricated the first SiNCs-based orange light-emitting electroluminescence (EL) device. However, EL efficiency was low having a maximum of 1.6% external quantum efficiency (EQE). EQE is defined as the ratio of number of photons emitted over the number of charges passing through the device.[272]

Cheng *et al*.[273] have shown that EL efficiency can be significantly improved by incorporating SiNC in the organic light-emitting diodes (OLEDs).[273] As an emissive layer, dodecyl-SiNCs were sandwiched between hole and electron transport layers; these layers are made from poly[2-methoxy-5-(2′-ethylhexyl-oxy)1,4-phenylene-vinylene] (MEH-PPV) and bathocuproine (BCP), respectively (Figure 1-17a). An EL efficiency of 8.6 % with a peak position at 800 nm was obtained from this inorganic-organic hybrid device by optimizing the layer compositions. Effective transport of the electrically generated charges to the SiNCs *via* polymer layers resulted in the enhancement of EL efficiency. Ozin and coworkers[274] used allylbenzene to

functionalize the SiNCs instead of the insulating dodecene ligands. Enhanced charge transport at the polymer/NC interfaces provided improved EL efficiency. Red/orange EL (Figure 1-17b) was observed from hybrid SiNC/organic LED with an EQE of 1.1%.

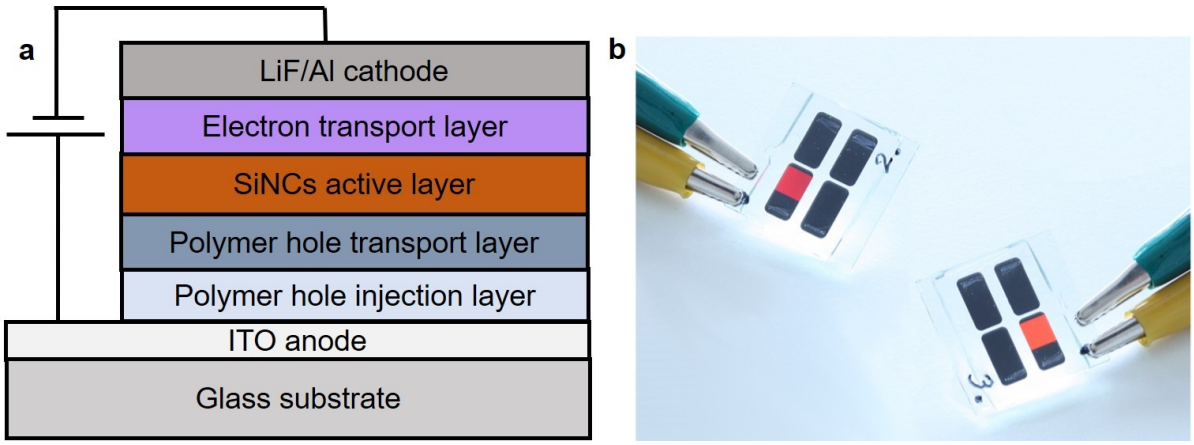

Figure 1-17. a) A simplified configuration of SiNC/polymer hybrid EL device,[89] b) red and orange electroluminescence from size-separated SiNCs in the hybrid device structure. Reproduced with permission from Maier-Flaig *et al.*[274] Copyright 2013, American Chemical Society.

Since long chain alkyl ligands are insulating and create a barrier for injection of electron or holes, functionalization SiNCs with short alkyl ligands may reduce this barrier. Moreover, grafting of conducting polymer on the NC surface may eliminate or at least reduce the barrier. Reports of improved EL from compound QD/polymer HFMs prepared by blending QDs with charge transporting polymers suggest that conjugated polymers grafted on SiNCs can act as an efficient charge transporting layer.[245,246]

1.2.6.2 Photovoltaic Applications

The current photovoltaic market is dominated by single crystalline silicon with a maximum power conversion efficiency of 26.3% (declared by the Japanese company, Kaneka Corporation) which is close to its theoretical maximum efficiency of 29%.[297] However, the cost of manufacturing crystalline silicon solar cell is still significantly high and is a significant bottle-neck

for silicon solar cell based energy production technology. Conjugated polymer-based bulk heterojunction (BHJ) solar cells were developed as a cost-effective alternative since they are prepared by solution-based techniques and can be processed as films using printing or coating techniques.[283,295] However, organic solar cells suffer from issues related to long-term stability and inefficient charge carrier mobility.[283] Colloidal SiNCs can share many of the advantages of organic solar cells such as low cost and solution processability; in addition, they can provide high charge carrier mobility.[283] Band-gap engineering of SiNCs provides the opportunity to harness the radiation from a wide range of the solar spectrum.[298] Quantum confinement can increase the absorption strength of SiNCs but induces a large barrier for efficient charge separation.[298] The simplest design of colloidal SiNCs only solar cell was reported by Kortshagen and coworkers (Figure 1-18a).[283] A Schottky junction solar cell was fabricated using a thin film of solution processable SiNCs sandwiched between the ITO anode and aluminum cathode. Unfortunately, power conversion efficiency was very low (0.02%) due to low optical absorption cross-section as well as increased density of surface defects in small SiNCs.[283] These issues could potentially be addressed by designing multijunction solar cells using SiNC/P3HT HFM which can effectively increase the absorption cross-section. The design of a multijunction solar cell may also provide enhanced interfacial charge separation dynamics.[298,299]

Kortshagen *et al*.[253] designed SiNC/P3HT hybrid solar cell where H-SiNCs were blended with P3HT and used as an active layer. A diagram of the hybrid solar cell and the corresponding band alignment is shown in Figure 1-18b. In this design, the first layer is a transparent ITO anode supported on a glass substrate; on top of the ITO layer is a hole conducting polymer (PEDOT:PSS) layer which is followed by a photoactive SiNC/P3HT layer to which an aluminum cathode is connected (Figure 1-18b left). Photogenerated excitons in P3HT (donor) move to the interface with

SiNCs (acceptor) and are dissociated by transferring the electrons into the CB of SiNCs which are collected at the aluminum cathode. On the other hand, the hole is transported by P3HT to PEDOT:PSS and collected at the ITO anode (Figure 1-18 right).

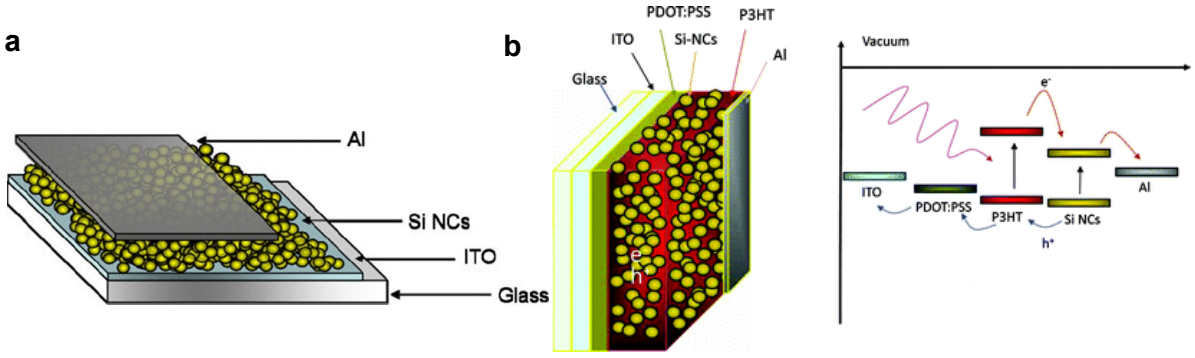

Figure 1-18. a) The configuration of a simple SiNC-only Shockley junction solar cell,[283] b) diagram of SiNC/P3HT HFM solar cell (left) and band-diagram demonstrating the operating mechanism of the HFM solar cell.Reproduced with permission from Liu et al.[253] Copyright 2009, American Chemical Society.

Although overall power conversion efficiency was not high (1.15%) due to SiNC aggregation-induced perturbation of the percolating network, a higher solar absorption in the UV region and a larger open circuit voltage compared to P3HT alone was observed. Solution processability of the SiNCs could be improved by octyl functionalization at the expense of generating an insulating barrier.[300] Therefore, SiNC@P3HT HFM prepared *via* direct grafting of P3HT can overcome the limitation of macroscopic phase separation between the donor and acceptor components. Moreover, the favorable band alignments and intimate interfacial contact between the donor and the acceptor may enhance the charge separation. Improvements of phase segregation and enhanced charge transport were indeed observed for covalently bonded NP/conjugated polymer HFM.[266,301–303] However, SiNC in the core of the hybrid can act as electron trap thus hindering their collection at the cathode.[304] Fortunately, these traps are shallow[304] and may be engineered by varying the band gaps of the NPs and conjugated polymers or incorporating another lower band-gap polymer. In 2014, Ding *et al.*[284] reported improvement in power

conversion efficiency (2.25%) by incorporating a lower bandgap polymer (PTB7) with SiNC/P3HT as an active layer. The improvement is attributed to better band alignments of PTB7 with SiNCs and an increased absorption in the longer wavelength region.

An alternative use of SiNCs is in selective emitter single crystalline silicon solar cells.[305] A selective emitter solar cell consists of a heavily doped front contact region to improve the ohmic contact with the electrodes. The remaining surface is lightly doped to reduce the charge recombination process which can give rise to enhanced short-circuit current and opened circuit voltage.[306] Innovalight corporation applied a SiNC ink as an n-type dopant to make ohmic contact between the electrode and silicon wafer, and this modification resulted in a 1% efficiency enhancement.[305]

SiNCs have a large Stokes shift between their absorption and emission spectra. Thus the probability of reabsorption of an emitted photon is reduced.[254] Blue to NIR emitting SiNCs with high PL QY has been developed which are essential for potential applications of SiNCs as luminescent solar concentrators (LSCs). Meinardi *et al*.[254] reported a SiNC and poly (lauryl methacrylate) (SiNC/PLMA) HFM-based LSC with an optical efficiency of η = 2.85%. This study opens the possibility of converting the urban buildings into energy generation units by incorporating the HFM as semi-transparent photovoltaic windows.[254]

1.2.6.3 Application in Photodetectors

Photodetectors have applications in biosensing,[307] optical storage,[308] image sensing,[309] communications,[310] and defence.[311] SiNCs-based photodetectors are promising because of their size-dependent spectral response, and high impact ionization rate.[279,280] Indeed, SiNCs have been shown to be highly photoconductive.[280,281] The quantum efficiency of photocurrent increases with the increase in NC size;[279] in smaller SiNCs quantum confinement reduces the dissociation of

photogenerated exciton resulting in limited photocurrent. Swihart[282] demonstrated that device performance could be enhanced by incorporating a charge separating layer (Figure 1-19a). In this device configuration, a film of PEDOT:PSS hole transporting (electron blocking) layer was spin coated on ITO coated glass substrate. A thin film of a solution processable SiNCs photoactive layer was spin coated on top of PEDOT:PSS layer; finally an aluminum layer was deposited on the SiNCs layer as back contact. As a postulate, a SiNC@P3HT core@shell hybrid photodetector may enhance the photocurrent generation *via* trap-induced hole injection.[304] The band alignment of P3HT and SiNC should facilitate the transfer of photogenerated electrons into the CB of the NC where the electrons can be trapped and accumulate negative charges (Figure 1-19b). This charging effect of the NC can result in band-bending in the hybrid film and significantly reduce the hole injection barrier under reverse bias condition.[304] Therefore, the photocurrent can be amplified under this reverse bias condition due to easy injection of a hole from the cathode (Figure 1-19c). In fact, the HFM of CdTeQD@P3HT[304] and ZnONP/P3HT[247] showed an impressive improvement in photodetection based on the trap-induced hole injection.

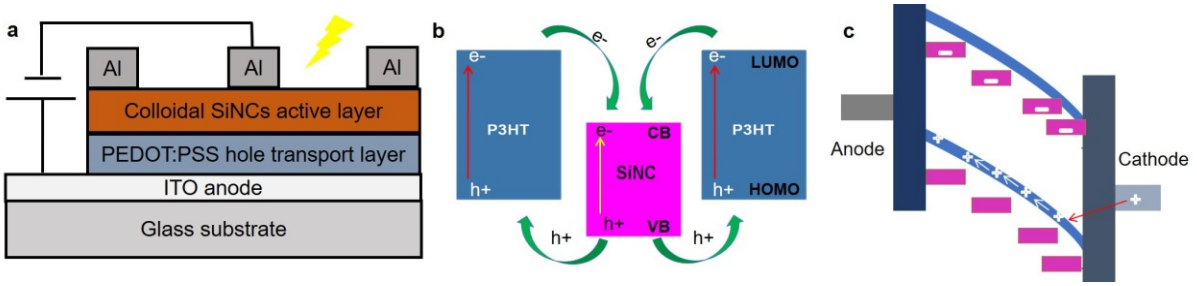

Figure 1-19. a) The configuration of a SiNC photodetector consisting of PEDOT:PSS hole transporting layer,[282] b) band alignment of P3HT and SiNCs in SiNC/P3HT HFM,[247,312] and c) band-banding and efficient hole injection from cathode under reverse bias conditions.[247]

1.2.6.4 Transistor Applications

The construction of most common field-effect transistors (FETs) relies on five main components: 1) source, 2) drain, 3) gate 4) gate dielectric and 5) semiconductor layer.[277,278]

Depending on the gate contact there are two types of FETs which are top-gate and bottom-gate contact FETs.[277] The first printed thin-film SiNCs FET was reported by Härting *et al*.[277] with a bottom gate contact design. SiNCs (70 nm) were used as the n-type channel which resulted in an effective carrier mobility in the range of 0.3 to 0.7 $cm^2\ V^{-1}\ s^{-1}$. The Kortshagen group[278] also used a bottom gate contact design (Figure 1-20 left) to evaluate the FET performance of smaller size silicon and germanium NCs (4-20 nm). Germanium nanocrystals have shown promising results with electron and hole mobilities as large as 0.02 and 0.006 $cm^2\ V^{-1}\ s^{-1}$) but SiNCs performance was very poor due to aggregation-induced poor film morphology. Kortshagen *et al*.[313] also studied the doping effect on the thin film SiNCs FET. Boron and phosphorus were electronically doped in the SiNCs thin film. When the dopant concentration was high, the FET did not exhibit gating behavior. In contrast, gating behavior was observed in case of low dopant concentration but with very low activation efficiency ($\sim 10^{-2}$-10^{-4}). Surface doping was also demonstrated to influence carrier concentration in SiNCs films. When Cl-SiNCs were used as a semiconducting channel, no gating behavior was observed (Figure 1-20 right side-a), but upon oxidation and subsequent hydride termination of SiNCs *via* HF etching, the H-SiNCs film exhibited charge mobility and gating behavior (Figure 1-20 right side-b). Chloride termination of SiNCs is believed to enhance their electron accepting nature; therefore, donation of electrons from the donor groups of the organic solvent increases electron concentration significantly at SiNCs surface, which destroys the gating behavior.

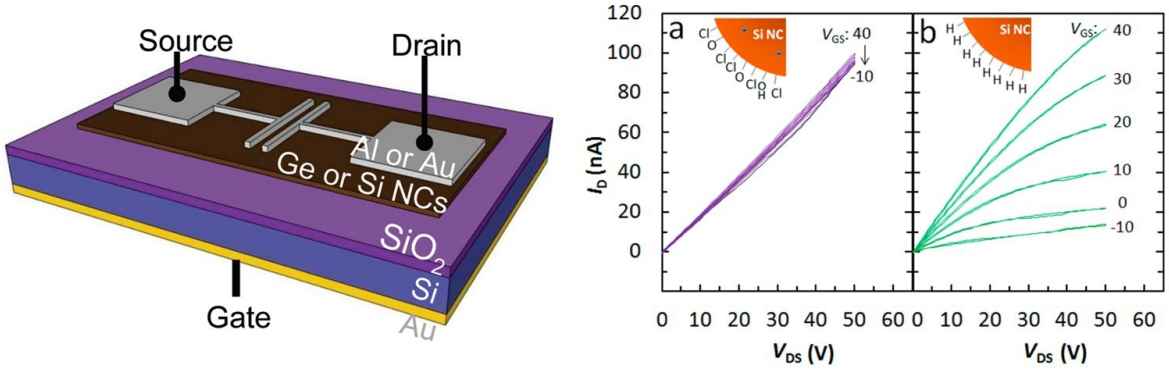

Figure 1-20. Configuration of a SiNC field-effect transistor (left side). Reproduced with permission from Holman et al.[278] Copyright 2010, American Chemical Society. Surface doping effect (right side figure): a) Cl-SiNC-based device shows constant current *vs.* voltage change signifying no gating behavior, b) current-voltage dependence could be observed for H-SiNCs, demonstrating their gating behavior. Reproduced with permission from Gresback *et al.*[313] Copyright 2014, American Chemical Society.

So far, SiNCs only transistors do not show significant promise while the performance of conjugated polymer-based organic FET[314] is limited by low charge carrier mobility of polymers.[315,316] FET fabricated from TiO_2NP/P3HT HFM demonstrated significantly higher hole mobility compared to pristine P3HT.[317] The enhancement was attributed to two possible reasons: 1) accumulation of hole in the P3HT phases resulting in their improved p-type behavior, and 2) higher degree of crystallization of P3HT on NP surface. Therefore, the design of a hybrid FET comprising SiNCs and conjugated polymers may offer these synergistic properties and is worth pursuing.

1.2.6.5 Chemical Sensing Applications

SiNCs are attractive for PL-based sensors due to their size-tunable photoluminescence properties and high PL QY. Sensing of analytes is based on three common mechanisms involving electron transfer (ET) between the NCs and analytes, Förster resonance energy transfer (FRET) from the analytes to the NCs, or fluctuation in photocurrent due to the interaction between the NCs and analytes.[318]

In the electron-transfer mechanism, photoexcited electrons from CB of NCs are transferred to the LUMO of analytes. Alternatively, HOMO electrons from analytes are transferred to VB of NCs and recombine with photogenerated holes on the VB of NCs. Both processes quench PL of NCs by preventing radiative recombination of the electron-hole pair.[318] Second sensing process involves the Förster mechanism in which non-radiative energy transfer occurs from the excited state of NCs to the ground state of the analytes or *vice-versa*.[318] The third sensing process involves photocurrent flow from NCs to an electrode surface and a change in photocurrent due to the interaction of NCs with analytes can be monitored.

Gonzalez *et al*.[275] developed a rapid, cost-effective, on-site sensing platform based on red luminescent dodecyl-SiNCs deposited on papers to detect nitro-groups containing explosives (Figure 1-21a). This paper-based sensor offered straightforward detection of nitroaromatic enabling the detection of 2,4-dinitrotoluene (DNT) as low as 18.2 ng level. This sensing process relies on electron transfer-mediated PL quenching of SiNCs. However, the dodecyl-SiNCs were prepared *via* thermal hydrosilylation that results in surface oligomerization. This can hinder electron transfer between the SiNC and analyte. Moreover, dodecyl-SiNCs prepared using this method exhibit low PL QY. Therefore, use of SiNCs functionalized with short chain ligands and exhibiting high PL QY may improve the detection efficiency. Ban *et al*.[276] utilized water dispersible amine-terminated blue emitting SiNCs for 2,4,6-trinitrotoluene (TNT) sensing in aqueous solution. According to the authors, the sensing mechanism is based on the quenching of SiNCs PL *via* the FRET process which was facilitated by TNT-amine complex formation on SiNCs surface (Figure 1-21b).

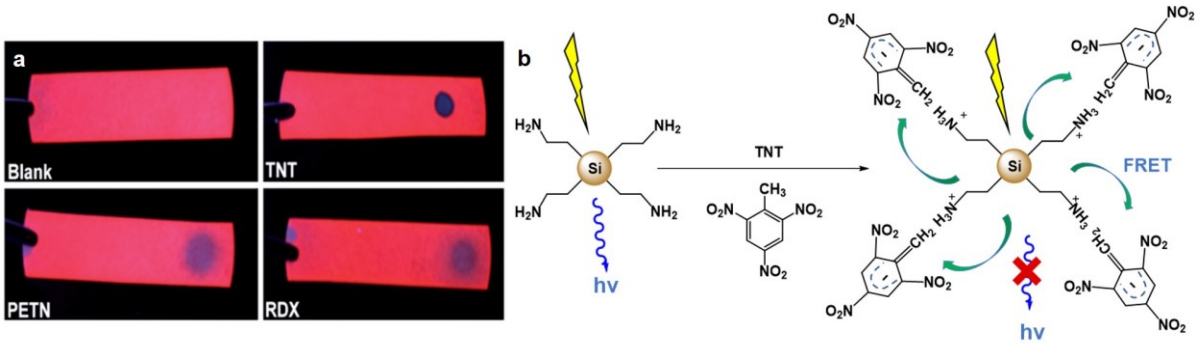

Figure 1-21. a) PL quenching of SiNCs on a paper-based sensor upon exposure to 2,4,6-trinitrotoluene (TNT), pentaerythritol tetranitrate (PETN), and cyclotrimethylenetrinitramine (RDX). Reproduced with permission from Gonzalez *et al.*[275] Copyright 2014, Royal Society of Chemistry. (b) TNT sensing through FRET-mediated quenching of SiNC PL.[276]

1.2.6.6 Catalytic Applications

As previously mentioned, SiNCs can utilize a broad range of the solar spectrum in the visible to near UV region; silicon is abundant and non-toxic. The combination of these advantages makes SiNC a reasonable candidate for photocatalytic applications.[236] Kang *et al.*[236] explored the size-dependent photocatalytic activity of SiNCs for oxidation-reduction reactions and dye degradation (Figure 1-22a). Smaller size SiNCs (1-2 nm) could efficiently catalyze the reduction of carbon dioxide (CO_2) under visible light resulting in the production of formaldehyde and formic acids. These SiNCs were also shown to degrade methyl red dye under visible light. However, larger size SiNCs (3-4 nm) were not effective for these reactions. Without any mechanistic study, the authors attributed this difference in reactivity to the variation in band gaps of SiNCs. Nevertheless, the larger SiNCs were demonstrated to catalyze the selective oxidation of benzene to phenol in the presence of hydrogen peroxide (H_2O_2). According to the authors, the decomposition of H_2O_2 on the pre-oxidized SiNC surface created reactive oxene species which resulted in oxidation of benzene to phenol. Iqbal *et al.*[319] studied the photocatalytic oxidation of methanol in the presence of SiNCs. The photocatalytic mechanism is shown in Figure 1-22b.

Under UV illumination an electron is promoted from the VB of SiNC to its CB which then migrates to the surface and reduces the oxygen (O_2) to superoxide radical species ($^{\bullet}O_2^-$). Consequently, the hole in the VB oxidizes methanol to α-hydroxymethyl radicals ($^{\bullet}CH_2OH$). These radical species react to form formaldehyde (HCHO). The photocatalytic efficiency was size-dependent. The CB of smaller SiNC is higher in energy than that of the larger SiNCs. Consequently, the higher energy electron in the CB of smaller SiNCs reduces O_2 more efficiently compared to larger counterparts. Surface states also play a significant role in the catalytic activity of SiNCs. The photogenerated electron (or hole) is required to migrate to the surface states where the reduction of O_2 or oxidation of CH_3OH takes place. Smaller SiNCs have a higher density of surface states leading to higher reactivity than the larger counterparts.

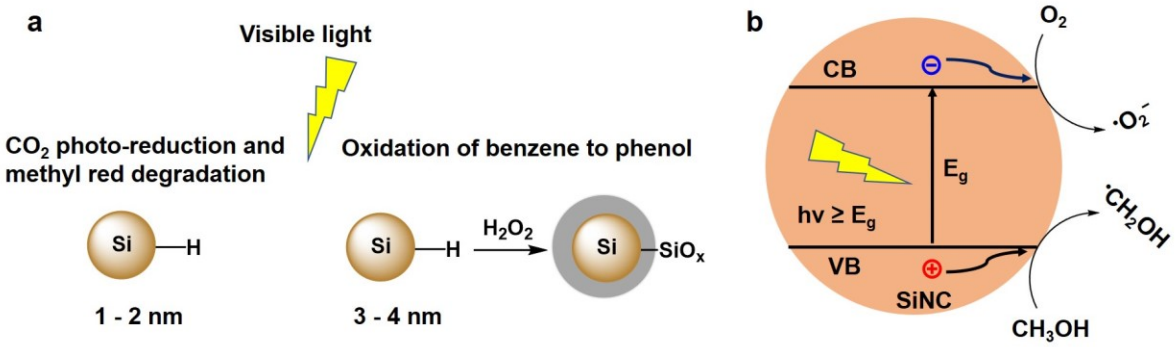

Figure 1-22. a) Photocatalytic reduction of CO_2 and degradation of methyl red using 1-2 nm SiNCs and oxidation of benzene using 3-4 nm SiNCs.[236] (b) mechanism of photocatalytic oxidation of methanol using SiNCs.[319]

Sun *et al*.[238] reported the reduction of carbon dioxide to carbon monoxide (CO) using 3.5 nm H-SiNCs as a catalyst. The surface on small SiNC is highly reactive that facilitates the abstraction of an oxygen atom from CO_2 converting it to CO.

1.2.7 Scope of this Thesis

As described earlier, SiNCs have been investigated for many potential applications including optoelectronics and catalysis. However, their success was not remarkable in many cases

due to the challenges related to SiNC surface modification. The overarching goal of this thesis is to explore surface chemistry of SiNCs to facilitate their relevant applications. Within this broad mandate, chapter 2 discusses how the Lewis acidic nature of Cl-SiNCs was explored to synthesize poly (3-hexylthiophene) (P3HT). Lewis acidic Cl-SiNCs were demonstrated to weaken bonds in electron-rich molecules through the hypervalent bond formation. In this context, it is reasonable to assume that Cl-SiNC can be a useful reactive platform to synthesize valuable materials from molecules that can be activated by the electron withdrawing effect of Cl-SiNCs. Grignard reagents are known to undergo oxidative homocoupling in the presence of Lewis acidic iron (III) catalysts. Therefore, the reactivity of Cl-SiNCs towards the activation and polymerization of a Grignard type thiophene monomer (5-chloromagnesio-2-bromo-3-hexylthiophene) was explored.

Phosphorus pentachloride (PCl_5) was used to prepare Cl-SiNCs from H-SiNCs. The effectiveness of this method was evaluated by a complementary set of characterization techniques. Afterward, the reactivity of Cl-SiNCs was investigated through the synthesis of P3HT from the Grignard monomer. The resulting P3HT was evaluated by MALDI-TOF mass spectrometry, ^1H NMR spectroscopy, gel permeation chromatography (GPC), and UV−vis and PL spectroscopies. After successful utilization of Cl-SiNCs for the synthesis of P3HT, the reactivity of other Cl-Si species, such as chloride-terminated silicon wafer (Cl-SiWF) and silicon tetrachloride ($SiCl_4$) was explored. A comparison of the reactivity of these Cl-Si species showed the superior reactivity of Cl-SiNCs over Cl-SiWF and $SiCl_4$.

As outlined previously, recent developments in SiNCs surface chemistry have also led to the development of hybrid functional materials (HFMs). HFMs comprising SiNCs and nonconjugated polymers have been studied considerably. Only a few examples of HFMs of SiNCs and conjugated polymers (prepared *via* blending) exist that show favorable optoelectronic

properties. Chapter 3 thus describes a novel method to prepare SiNC and P3HT HFM with direct interfacial contact to facilitate the potential applications of this HFM in optoelectronic devices. A surface-initiated Kumada catalyst transfer polycondensation (SI-KCTP) method was used to graft P3HT from the 2-bromo-3-hexyl-5-thienyl-capped SiNC initiator (SiNC-HT-Br). The SiNC@P3HT hybrid was evaluated *via* a comparison between SiNC-HT-Br and SiNC@P3HT. The core-shell structure and thermal stability of SiNC@P3HT were also investigated in detail. P3HT was degrafted from the surface to analyze its molecular weight and regioregularity. Finally, UV-Vis and PL properties of SiNC@P3HT were evaluated to gain an understanding of the impact of direct interfacial contact between SiNCs and P3HT.

To achieve improved optoelectronic performance, it is essential to modify SiNC surfaces in such a way so that the surface oxidation is prevented effectively without creating a highly insulating barrier while still provides high PL brightness. A recent investigation of XeF_2-mediated functionalization of SiNCs has shown significant improvement of these properties. However, as outlined previously, this method also has some limitations regarding the etching of SiNCs and its requirement of strict inert atmospheric manipulation. Like XeF_2, PCl_5 is a hypervalent compoundand has been used as a chlorinating agent in organic synthesis and silicon-based surface modifications. PCl_5 is a mild etchant compared to XeF_2 and can be handled under less stringent conditions. Chapter 4, therefore, discusses the PCl_5-initiated functionalization of SiNCs using several model species (alkenes/alkynes). PCl_5-induced etching of SiNCs produces chlorosilanes (*i.e.,* $HSiCl_3$, H_2SiCl_2, and H_3SiCl) as PCl_5 is converted to PCl_3. Observation of these by-products suggests radical-induced etching of SiNCs, leaving behind surface Si radicals (Si•) which are then utilized to functionalize H-SiNCs. The effectiveness of the method was evaluated in detail and

compared with existing methods. Finally, a mechanism was proposed based on an understanding of the reactivity and relevant spectroscopic analysis.

A summary of my research achievements during the period of my Ph. D. study and relevant future work is discussed in Chapter 5.

Chapter 2:

Chloride Surface Terminated Silicon Nanocrystal Mediated Synthesis of Poly(3-hexylthiophene)

A version of this Chapter has been published:

Islam, M. A.; Purkait, T. K.; Veinot, J. G. C. *J. Am. Chem. Soc.*, 2014, *136*, 15130–15133.

2.1 Introduction

Conjugated polymers hold substantial potential for applications in optoelectronic devices and flexible electronics, partly because of their low cost, favorable mechanical properties, structural tailorability, solution processability, and straightforward device fabrication.[320] Poly(3-alkylthiophenes) and their derivatives have been studied extensively as active materials in bulk-heterojunction solar cells, light-emitting diodes, organic thin-film transistors, and sensors.[320–323] In this context, it is reasonable to classify it as a workhorse material in organic electronics. Common synthetic methods employed to prepare poly- and oligothiophenes include electropolymerization,[324] transition-metal-catalyzed coupling,[325–331] and oxidative polymerization.[332,333] Electropolymerization usually provides insoluble products.[333] Metal-catalyzed oxidative polymerization typically employs Lewis acidic centers that induce a reaction. For example, ferric chloride ($FeCl_3$) is believed to initiate polymerization *via* single-electron oxidation of thiophene.[332] Other examples of Lewis acid-mediated processes employ $AlCl_3$ or BF_3 to decrease the aromaticity of the thiophene ring and lower its oxidation potential; this activation allows the preparation of high-quality films by subsequent electrooxidative polymerization.[334]

Despite allowing access to high-quality materials, metal-based catalysts can dramatically impact device performance. Even trace transition-metal impurities can limit the optoelectronic properties of these attractive materials.[335] It is also reasonable that transition-metal impurities can shorten device lifetimes by inducing degradation of the polymer. In this context, troublesome and costly purification steps are often essential. Clearly, a convenient metal-free synthesis of poly- and oligothiophenes and similar polymers would be extremely attractive, but few examples exist.[336]

Silicon tetrachloride is a weak Lewis acid that can form hypervalent species in the presence of Lewis bases.[337,338] Chloride-terminated silicon nanocrystals (Cl-SiNCs) can be prepared using

a variety of protocols.[124,165,208,239] Wheeler *et al.*[239] reported that Cl surface termination can lead to a Lewis acidic NC surface. It has been proposed that in these nanosystems electron density is drawn from surface atoms, which lowers the lowest unoccupied molecular orbital (LUMO). This process facilitates the transfer of electron density from donor molecules to the SiNC. This results in a weakening of surface Si−Cl bonds as well as lengthening/weakening of the donor molecule bonds through hypervalent bond formation. In this regard, Cl-SiNCs offer an attractive metal-free reactive species that could be exploited as a catalyst for the preparation of poly- and oligothiophene derivatives.

Given that single-electron transfer (SET) reactions are well known for Grignard reagents[339] and oxidative homocoupling of Grignard reagents is promoted by Lewis acidic iron(III) catalysts,[340] we chose to investigate the reactivity of 5-chloromagnesio-2-bromo-3-hexylthiophene (**1**) with Cl-SiNCs, Cl-terminated silicon wafers (Cl-SiWFs), and molecular chlorosilanes in the preparation of poly-3-hexylthiophene (P3HT). The general synthetic approach is summarized in Scheme 2-1, where SET from Grignard monomer **1** to the Cl- SiNC LUMO forms the radical cation followed by formation of thiophene radical which induces polymer formation.

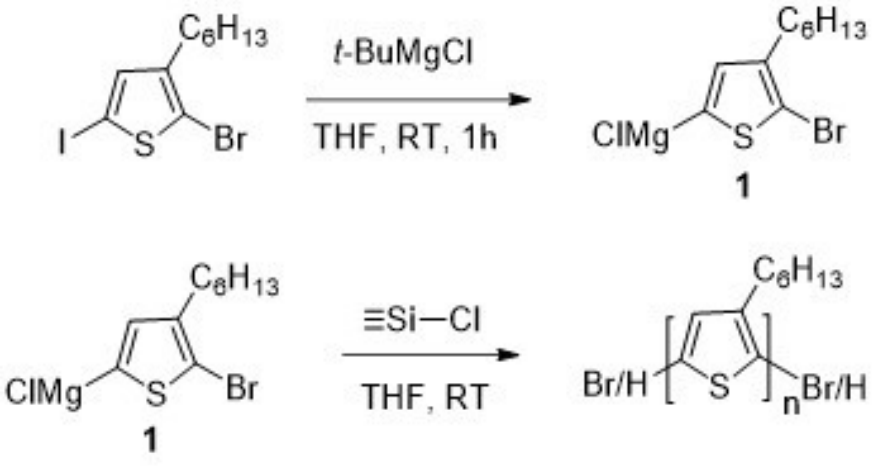

Scheme 2-1. Two-Step Synthesis of P3HT.

2.2 Experimental

2.2.1 Reagents and Materials

2-Bromo-3-hexyl-5-iodothiophene (Br-HT-I, > 97%, stabilized with a copper chip) from TCI America was eluted using hexane through 230-400 mesh silica gel (Sigma-Aldrich) immediately before use. THF and toluene (reagent grade) were freshly distilled over sodium benzophenone under Ar atmosphere. 1.0 M tert-butylmagnesium chloride (*t*-BuMgCl) solution in THF, phosphorus pentachloride (PCl_5, 95%), silicon tetrachloride ($SiCl_4$, 99%), hydrogen peroxide (30%) and deuterated chloroform ($CDCl_3$) were purchased from Sigma-Aldrich and used as received. Si (111) wafers (p-type, double side polished, resistivity ≥ 10000 ohm·cm) were purchased from University Wafer. Hydrogen silsesquioxane (HSQ, trade name Fox-17) was purchased from Dow Corning, and the solvent was removed to yield a white solid that was used directly. Hydrofluoric acid (48-50%) was purchased from Fisher Scientific and used as received. HPLC grade THF, 36.5-38% hydrochloric acid, anhydrous magnesium sulfate ($MgSO_4$), and 27% NH_4OH were purchased from Caledon and used as received. All other solvents were reagent grade, and deionized water was used throughout the experiments.

2.2.2 Synthesis of Chloride-Terminated Silicon Nanocrystals

Cl-SiNCs were prepared by using a slightly modified method reported by our group.[157,165,211] Briefly, HSQ was thermally processed in a Lindberg blue tube furnace at 1100 °C for 1 hour under flowing 5% H_2 and 95% Ar atmosphere. The resulting Si/SiO_2 composite was ground mechanically. Hydride terminated Si nanocrystals (H-SiNCs) were obtained *via* HF etching of the composite. In a typical experiment, 200 mg of Si/SiO_2 composite were etched in 9 mL of a 1:1:1 49% HF: water: ethanol solution for 1 hour and extracted into toluene and centrifuged at 3000 rpm for 10 minutes. The pellet was redispersed in dry toluene. The

centrifugation and redispersion cycle was repeated twice. This procedure results in the formation of about 3 nm H-SiNCs that were transferred with 10 mL freshly distilled toluene to a dry Schlenk flask containing 300 mg of PCl_5. The Schlenk flask was subjected to quick pump and purge cycles with Ar (1 minute, 3×). The H-SiNC dispersion was stirred for 1 hour at room temperature under Ar after which the solvent was removed *in vacuo*. Excess PCl_5 was removed upon raising the temperature to 70 °C for 20-30 minutes. After cooling to room temperature, the resulting Cl-SiNCs (d = 3 nm) were maintained in an Ar atmosphere until the addition of monomer **1**.

2.2.3 Chloride-Termination of Silicon Wafer (Cl-SiWF)

Typically p-type double side polished Si(111) wafers (resistivity ≥ 10000 ohm·cm) were cut into 1 × 1 cm^2 or 1 × 2 cm^2 pieces as appropriate. The wafer was cleaned and oxidized according to a modified literature procedure derived from that reported by O'Leary *et al.*[341] and Kern.[342] Briefly, the Si wafer was rinsed sequentially with water, methanol, acetone, methanol, and water to remove the organic contaminants from the Si wafer surface. After drying under N_2, the wafer was immersed in 30 mL of 1: 1: 5 27% NH_4OH: 30% H_2O_2: H_2O and heated at 80 °C for 10 minutes. After washing with deionized water, the wafer was etched in 9 mL of 1:1:1 49% HF: water: ethanol solution for 1 hour. Subsequently, the wafer was rinsed with dry toluene and transferred to a Schlenk flask containing 500 mg PCl_5 and 10 mL dry toluene. The solution was heated at 90 °C for 45 minutes after which the solvent and excess PCl_5 were removed as noted for the Cl-SiNCs above. The wafer was maintained in an Ar atmosphere until the monomer was added.

2.2.4 Polymerization Procedures

2.2.4.1 Cl-SiNC-Mediated Polymerization

Monomer **1** was prepared according to a modified literature procedure derived from that reported by Senkovskyy *et al.*[271] In a typical experiment 7.5 mmol of 2-bromo-3-hexyl-5-

iodothiophene (Br-HT-I) was placed in an argon charged round bottom flask equipped with a rubber septum. Freshly distilled THF (70 mL) and 8 mmol *t*-BuMgCl (8 mL of 1.0 M solution in THF) were added to the round bottom flask *via* syringe. The solution was stirred using a magnetic stir bar for 1 hour at room temperature and transferred *via* cannula to a Schlenk flask containing *ca*. 15 mg Cl-SiNCs. The color of the monomer solution immediately changed to red. The solution was stirred at room temperature for 6 hours. The reaction mixture was purified, and the polymer was isolated as noted in section 2.2.4.7 below. The amount of isolated polymer was 912 mg, and the yield was calculated to be 73% (Appendix A).

2.2.4.2 Reaction of Cl-SiNCs in the Absence of Light

Monomer **1** was prepared upon reaction of 0.5 mmol of Br-HT-I in 7.0 mL freshly distilled THF with 0.55 mmol *t*-BuMgCl (0.55 mL of 1.0 M solution in THF). The solution was stirred in an argon atmosphere using a magnetic stir bar for 1 hour at room temperature and transferred *via* cannula to a Schlenk flask charged with *ca*. 8 mg of d = 3.2 nm Cl-SiNCs. After stirring in an argon atmosphere for 6 hours at room temperature in subdued light, the reaction mixture was red. The reaction mixture was purified, and the polymer was isolated as noted in section 2.2.4.7 below. The amount of purified and isolated polymer was 47.5 mg and the yield was calculated to be 57% (Appendix A).

2.2.4.3 Reaction of Monomer 1 in the Absence of Cl-SiNCs

Monomer **1** was prepared upon reaction of 0.5 mmol of Br-HT-I in 7.0 mL freshly distilled THF with 0.55 mmol of 1.0 M *t*-BuMgCl. The solution was stirred in an argon atmosphere using a magnetic stir bar in ambient light. Aliquots of the reaction mixture were withdrawn at 1 hour (*i.e.,* monomer **1** isolated for characterization), 7 hours, and 25 hours intervals and neutralized with 5M HCl. After stirring for 25 hours no color change was observed. The thiophene species were

extracted into $CHCl_3$ and washed with water. The $CHCl_3$ extracts were dried with anhydrous $MgSO_4$ and gravity filtered. The reaction products were evaluated as control samples as outlined below (Section 2.2.5.8).

2.2.4.4 Cl-SiWF-Mediated Polymerization

Monomer **1** was prepared upon reaction of 3.75 mmol of Br-HT-I in 50 mL freshly distilled THF with 4 mmol *t*-BuMgCl (4 mL 1.0 M solution in THF). The solution was stirred in an argon atmosphere using a magnetic stir bar for 1 hour at room temperature and transferred *via* cannula to a Schlenk flask charged with a 1×2 cm^2 Cl-SiWF. The expected appearance of a red solution was not noted after 1 hour. After 6 hours, only a light red solution was noted. Hence the mixture was stirred for 24 hours at room temperature under argon to yield a red solution. The reaction mixture was purified and the polymer was isolated as noted in section 2.2.4.7 below. The amount of isolated polymer was 410 mg and the yield was calculated to be 66% (Appendix A).

2.2.4.5 $SiCl_4$-Mediated Polymerization

Monomer **1** was prepared upon reaction of 3.75 mmol of Br-HT-I in 50 mL freshly distilled THF with 4 mmol *t*-BuMgCl (4 mL 1.0 M solution in THF). Following stirring in an argon atmosphere using a magnetic stir bar for 1 hour at room temperature 0.094 mmol of $SiCl_4$ (2.5 mol% of Br-HT-I) was added. The mixture was stirred for a total of 24 hours at room temperature under argon to yield the desired red solution. The reaction mixture was purified and the polymer was isolated as noted in section 2.2.4.7 below. The amount of isolated polymer was 461 mg and the yield was calculated to be 74% (Appendix A).

2.2.4.6 Comparison of Cl-SiNC, Cl-SiWF, and $SiCl_4$ Reactivity

Three identical solutions of monomer **1** were prepared upon reaction of 0.5 mmol of Br-HT-I in 7.0 mL freshly distilled THF with 0.55 mmol *t*-BuMgCl (0.55 mL of 1.0 M solution in

THF). The polymerization reactions were performed as noted above using *ca*. 8 mg of 3 nm Cl-SiNCs, 1×1 cm^2 Cl-SiWF, or 0.05 mmol $SiCl_4$. The reaction mixtures were stirred in an argon atmosphere for 6 hours in ambient light at room temperature. The crude product mixture was purified and the polymer was isolated as noted in section 2.2.4.7 below. Polymers were evaluated using gel permeation chromatography (Table 2-1). Yield data are provided in Table 2-1.

2.2.4.7 General Polymer Isolation and Purification Procedure

Following polymerization reaction, the red THF solution was quenched upon addition of an excess 5 M aqueous HCl (*ca*. 20 mL). The crude product mixture was subsequently extracted into $CHCl_3$ (*ca*. 30 mL). The resulting red $CHCl_3$ extract was washed with water (3×30 mL) and subsequently passed through silica gel *via* gravity filtration. The solvent was evaporated using rotary evaporator to yield a red solid that was dissolved in a minimum amount of $CHCl_3$. A red precipitate of pure product was obtained upon addition of excess methanol. The resulting precipitate was collected by vacuum filtration and dried *in vacuo*.

2.2.5 Materials Characterization

2.2.5.1 Transmission Electron Microscopy

Bright-field TEM images were obtained using a JEOL 2011TEM with LaB_6 electron gun using accelerating voltage of 200 kV. TEM samples were prepared by depositing a drop of dilute Cl-SiNCs suspension in toluene onto a holey carbon coated copper grid (electron microscopy sciences) and the solvent was evaporated. The NC size was averaged for more than 200 particles using Image J software (version 1.45). The histogram for NC size distribution was plotted using OriginLab software.

2.2.5.2 Fourier Transform Infrared Spectroscopy

Samples of H-SiNCs and Cl-SiNCs were prepared in a nitrogen filled glovebox as a thin film on a KBr plate placed in an airtight sample holder. FT-IR spectra were recorded using a Nicolet Nexus 760 FT-IR spectrometer by placing the sample into a nitrogen-purged sample chamber (32 scans).

2.2.5.3 X-ray Photoelectron Spectroscopy

Cl-SiNCs were deposited from a toluene dispersion onto a copper wafer in a glovebox and maintained within an airtight XPS sample holder and immediately transferred to a Kratos AXIS 165 instrument. The base pressure in the sample analytical chamber was lower than 1×10^{-9} Torr. Monochromatic Al Kα source with an energy hν = 1486.6 eV was used at 210 W. Survey spectra were collected with analyzer pass energy of 160 eV and a step of 0.3 eV. For high-resolution spectra, the pass energy was 20 eV and the step was 0.1 eV with dwell time of 200 ms. CasaXPS (VAMAS) software was used to process and fit the XPS data. All the spectra were calibrated with respect to C 1s emission (284.8 eV). The extrinsic loss structure was removed by using a Shirley type background. High-resolution Si 2p XP spectra were fitted by creating sufficient number of Gaussian-Lorentzian curves. The position constraint was increased for each curve by 0.6 or 1 eV to account for spin-orbit splitting or to evaluate different oxidation states. The area constraints for Si $2p_{1/2}$ components were multiplied by 0.5 to account for the ratio of population of Si $2p_{1/2}$ sates over Si $2p_{3/2}$ states. The full width at half maximum (fwhm) was maintained the same for both the Si $2p_{1/2}$ and Si $2p_{3/2}$ states by multiplying the fwhm constraints for the former by 1. The fwhm was maintained below 1.2 eV. A spin-orbit splitting energy of 1.6 eV and an area ratio of 0.5 were used for the fitting of Cl $2p_{1/2}$ and Cl $2p_{3/2}$ components.

2.2.5.4 UV-Vis and Photoluminescence Spectroscopy

UV-Vis and PL spectra of a dichloromethane solution of Cl-SiNCs were acquired using a Varian Cary 400 Scan UV-Vis spectrophotometer (instrument version: 8.01, beam mode: double, resolution: 1 nm) and Varian Cary Eclipse fluorescence spectrophotometer (λ_{exc} = 300 nm; excitation, and emission slits widths: 5; photomultiplier tube voltage: medium), respectively. UV-Vis data of P3HT solution or film were also obtained using the same UV-Vis spectrophotometer and instrument setup. Typically, 0.05 or 0.01 mg/mL solution of P3HT was prepared in $CHCl_3$ for solution phase UV-Vis spectra. Solid film sample was prepared upon drop-casting the $CHCl_3$ solution onto a quartz plate. The UV-Vis spectrum of the solution and solid film were recorded using a double and a single-front beam mode, respectively. PL spectra (λ_{exc} = 350 nm; photomultiplier tube voltage: medium) were recorded for 0.05 or 0.0033 mg/mL solution of P3HT in $CHCl_3$ and solid film of P3HT drop cast onto quartz plates from $CHCl_3$ solution. Both the excitation and emission slits widths were 5 for solution phase and 20 for solid phase PL measurements.

2.2.5.5 Matrix Assisted Laser Desorption Ionization-Time of Flight-Mass Spectrometry

MALDI-TOF-MS were acquired using an UltraflexXtremeTM MALDI-TOF/TOF (Bruker Daltonics, Billerica, MA, USA) mass spectrometer in positive MS mode. 2[(2E)-3-(4-tert-Butylphenyl)-2-methylpropy-2-enylidene]-malononitrile (DCTB) was used as matrix. A matrix solution was prepared in dichloromethane with a concentration of 10 mg/mL. The polymer sample in question was dissolved in a minimal volume of $CHCl_3$ and mixed with an equal volume of the DCTB solution. 0.8 μL of the polymer/matrix solution was then spotted onto a stainless steel MALDI target for analysis.

2.2.5.6 Nuclear Magnetic Resonance Spectroscopy

^{1}H NMR of P3HT in $CDCl_3$ was obtained using a Varian Unity Inova Console 500 MHz NMR spectrometer using tetramethylsilane (^{1}H, $^{13}C\{^{1}H\}$) as an external reference. The NMR data were processed and plotted using ACD/NMR processor academic edition and OriginLab software, respectively.

2.2.5.7 Gel Permeation Chromatography

GPC measurements were performed using GPC 270 max instrument equipped with a autosampler (Viscotek VE 2001 plus), three μ-Styragel columns, and a refractive index detector (Viscotek VE 3580). Measurements were performed at room temperature with THF eluent and flow rate of 0.5 mL/min. P3HT samples were prepared at concentrations of 1.0-3.0 mg/mL in HPLC grade THF. Polystyrene standards (Viscotek-PolyCAL^{TM}-PS 99 K) were used to calibrate the columns and evaluated for comparison.

2.2.5.8 Control Sample Characterization

Upon neutralization with 5M HCl, monomer **1** was hydrolysed to 2-bromo-3-hexylthiophene (Br-HT). The GC-MS analysis was performed using an Agilent GCD G1800A GC-MS and DB-5MS (25m × 0.25mm × 0.25 micrometer film thickness) column and a helium carrier gas. GC-MS analysis revealed the presence of 73% of hydrolysed product (Br-HT) of monomer **1** and 27% of Br-TH-I starting material (calculated based upon the relative peak area percentage). Aliquots withdrawn at 7 and 25 hours were analyzed by MALDI-TOF and negligible polymers or oligomers were detected.

2.3 Results and Discussion

2.3.1 Synthesis of Cl-SiNCs

Cl-SiNCs were prepared *via* PCl_5-induced chlorination of H-SiNCs obtained from a well-established method involving thermal treatment of commercial hydrogen silsesquioxane.[157,165] The average diameter of the Cl-SiNCs (3.2 ± 0.7 nm) was determined using TEM (Figure 2-1a). The chloride surface termination of SiNCs is evidenced by the evolution of the FT-IR spectra (Figure 2-1b). The Si-H absorption at 2068 cm^{-1} characteristic of H-SiNCs is replaced by a characteristic Si-Cl absorption at 565 cm^{-1}. X-ray photoelectron spectroscopy showed Si 2p and Cl 2p emissions (Figure 2-1c-e) further supporting the chloride surface termination. The UV-Vis spectrum of Cl-SiNCs in dichloromethane (Figure 2-1f) shows a featureless absorption characteristic of SiNCs.[116] The Cl-SiNCs photoluminesce in the blue region of the visible spectrum with an emission maximum at 465 nm (Figure 2-1f). It was reported that the partial air oxidation induces blue PL from chloride-terminated SiNCs.[212]

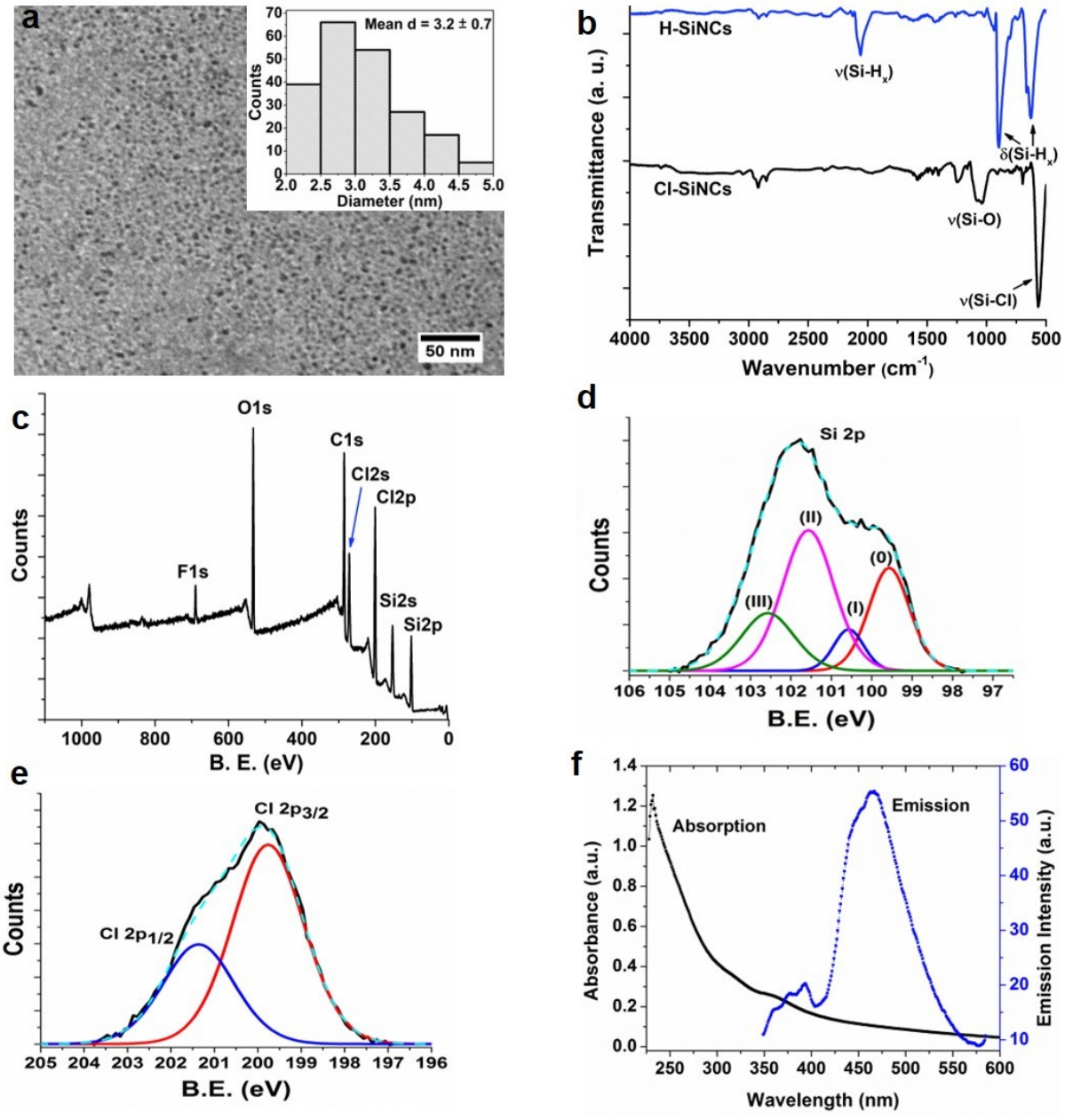

Figure 2-1. (a) Bright-field TEM image of Cl-SiNCs (inset: particle size distribution); (b) FT-IR spectra of H-SiNCs (blue trace) and Cl-SiNCs (black trace); (c) Survey XP spectrum of Cl-SiNCs; (d) Si 2p and (e) Cl 2p regions of the high-resolution XP spectra of Cl-SiNCs; (f) UV-Vis absorption spectra (black trace) and photoluminescence spectra (blue trace, excitation 300 nm) of dichloromethane solutions of Cl-SiNCs.

2.3.2 Cl-SiNCs-Mediated Synthesis of P3HT

A modified literature procedure derived from that reported by Senkovskyy *et al*.[271] was employed to obtain **1** from the Grignard metathesis reaction of 7.5 mmol of 2-bromo-3-hexyl-5-iodothiophene (Br-HT-I) with 8 mmol of tert-butylmagnesium chloride in 70 mL of dry tetrahydrofuran (THF). Following preparation, the THF solution of 1 was transferred directly to a Schlenk flask charged with *ca*. 15 mg of Cl-SiNCs, and the mixture was stirred at room temperature for 6 hours under argon followed by quenching upon addition of 20 mL of 5 M aqueous HCl. The crude product mixture was extracted into $CHCl_3$ (*ca*. 30 mL). The resulting red solution was washed with water (3 × 30 mL), passed through silica gel, and concentrated to dryness under vacuum to yield a red solid. This solid was dissolved in a minimum volume of $CHCl_3$, and a red precipitate was obtained upon addition of excess methanol. The pure solid product was collected by vacuum filtration, dried *in vacuo*, and evaluated using MALDI-TOF mass spectrometry, ^{1}H NMR spectroscopy, gel-permeation chromatography, and UV−vis and photoluminescence spectroscopy.

The formation of P3HT was first evaluated by MALDI-TOF analysis (Figure 2-2a). The spectrum reveals two overlapping patterns with peak separations of m/z 166 corresponding to the molecular weight of the hexylthiophene repeat unit. Mass peaks at m/z 1652.7 and 1574.8 arise from hexylthiophene oligomers consisting of nine repeat units with Br/Br and H/Br end capping, respectively. High-resolution isotope patterns are provided in Figure 2-2.

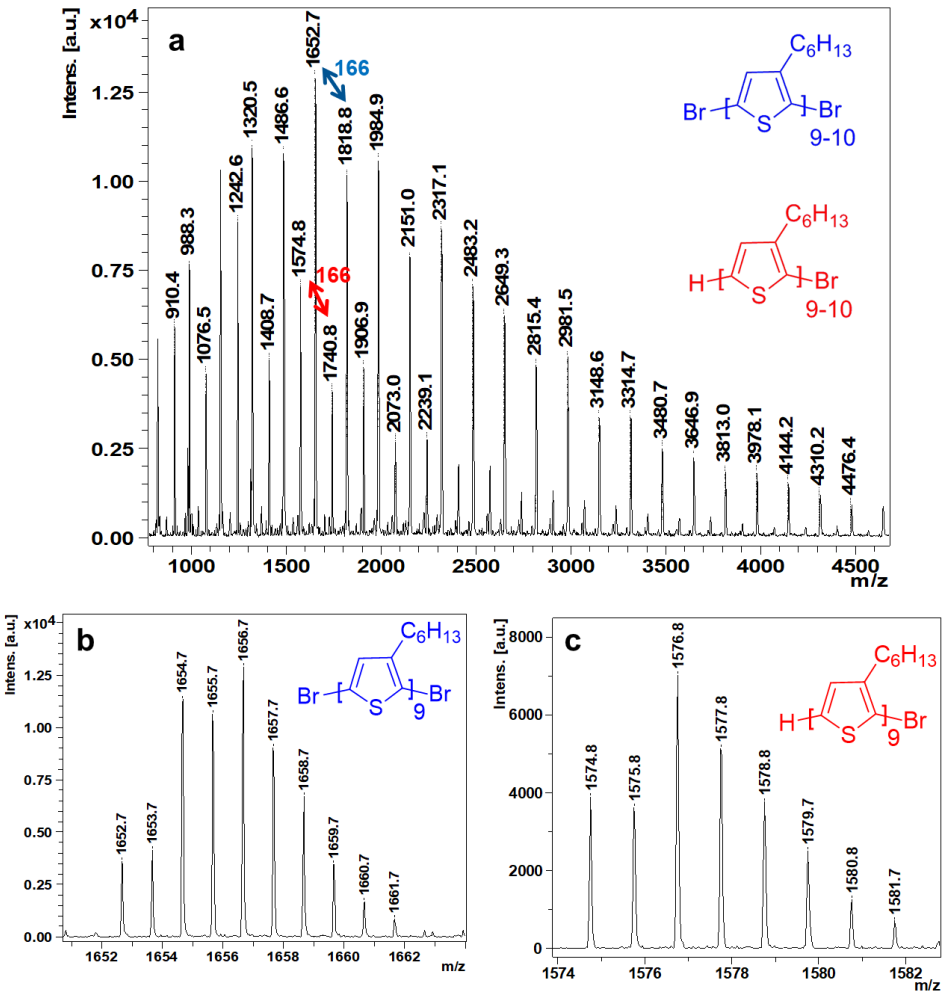

Figure 2-2. (a) MALDI-TOF mass spectrum of P3HT obtained from a 6 hours reaction of **1** in the presence of Cl-SiNCs; blue and red arrows represent the m/z differences (166) between the hexylthiophene oligomers consisting of 9 and 10 repeating units with Br/Br and H/Br end capping, respectively. Isotope patterns of the hexylthiophene oligomers with 9 repeating units; (b) Br/Br and (c) H/Br end groups.

^{1}H NMR analysis (Figure 2-3) of the product showed broad signals consistent with P3HT. The signal centered at *ca*. 6.98 ppm is readily attributed to the aromatic proton on the thiophene ring.[329] Consistent with previous assignments, protons on the pendant hexyl groups appear as broadened complex multiplets: α-methylene protons appear at 2.80 and 2.58 ppm; β-and other methylene protons at 1.69, 1.43, 1.34, 1.26 ppm; and terminal methyl group protons at 0.9 ppm.[329] The regioregularity of P3HT can be readily evaluated on the basis of the integration of the α-

methylene proton signals (Figure 2-3, right inset). From this analysis we conclude that the present polymer is a mixture of *ca*. 68% regioregular head-to-tail (HT) and 32% regiorandom head-to-head (HH) and tail-to-tail (TT) coupling (Appendix B). The expanded ^{1}H NMR spectrum in the aromatic region is also indicative of four different types of couplings (Figure 2-3, left inset): HT−HT (6.98 ppm), TT−HT (7.00 ppm), HT−HH (7.02 ppm), and TT−HH (7.05 ppm).[329]

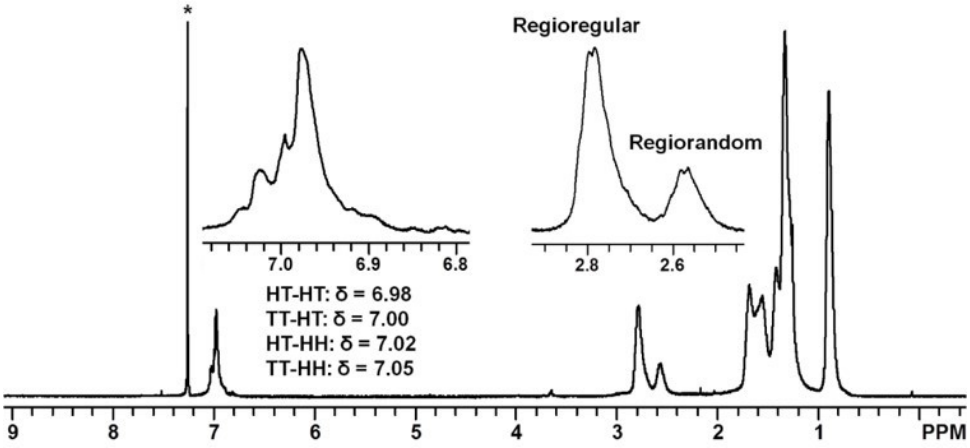

Figure 2-3. ^{1}H NMR spectra of P3HT in $CDCl_3$ obtained after a 6 h reaction of 1 in the presence of Cl-SiNCs (* indicates a residual NMR solvent peak).

GPC analysis of the P3HT product provided a number-average molecular weight (M_n) of *ca*. 4k, a weight-average molecular weight (M_w) of *ca*. 10k, and a polydispersity index (PDI) of *ca*. 2.5. The polymer molecular weight obtained from this reaction is low relative to those for standard metal-based Lewis acid-mediated P3HT polymerizations (*i.e.,* M_w = 20−40 k), but this is not unexpected given the relatively weak Lewis acidity of Cl-SiNCs. The present PDI is typical for oxidative polymerization methods.[333]

Evaluation of the optical properties of the present P3HT is crucial if these materials are to find future applications in optoelectronic devices.[333,343,344] UV−vis spectroscopy was performed on chloroform solutions of P3HT and thin solid films drop-cast from this solution onto quartz wafers. The solution-phase spectrum (Figure 2-4a, dotted trace) shows a characteristic broad

absorption at λ_{max} = 431 nm; a slight red-shift to λ_{max} = 451 nm is noted for the cast films (Figure 2-4a, solid trace). This red-shift has been previously attributed to the increased conjugation resulting from interchain interactions of P3HT in solid films due to π–π stacking.[333,344,345] In addition, the absorption bandwidth is broader for the films, tailing out to *ca*. 650 nm.

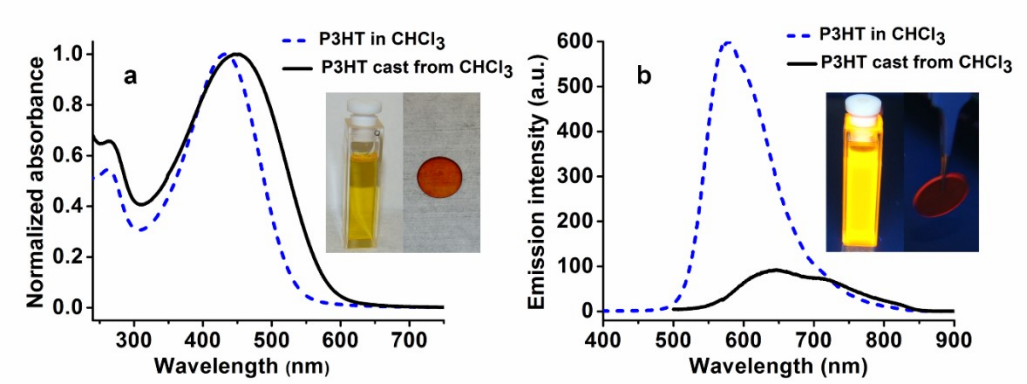

Figure 2-4. (a) UV−vis absorption and (b) PL emission spectra upon excitation at 350 nm for P3HT obtained from a 6 h reaction with Cl-SiNCs, recorded on a 0.05 mg/mL solution in $CHCl_3$ (dotted trace) and a solid film (solid trace). Insets show the P3HT solution in $CHCl_3$ and the solid film under ambient light and UV excitation, respectively.

Another characteristic P3HT property is its photoluminescence. PL spectra of the present P3HT are shown in Figure 2-4b. The spectrum obtained from a $CHCl_3$ solution affords a featureless emission with a maximum at 570 nm tailing out to 800 nm (dotted trace). The PL maximum shifts to longer wavelengths for the solid film deposited from $CHCl_3$ solution, showing a peak emission at 647 nm and two shoulder features at 725 and 823 nm (solid trace). The appearance of the low energy shoulder features has previously been attributed to polaron formation in solid films.[346]

To support our hypothesis that the polymerization reaction arises as a consequence of the Lewis acidity of the Cl-SiNCs and to eliminate possible contributions from monomer photooxidation, we performed identical reactions in the presence and absence of light. The two reactions afforded equivalent products. The M_n, M_w, PDI and yield of the polymer obtained from

Cl-SiNCs in the presence of light were 3.8k, 6.8k, 1.8 and 79 % (Appendix A), respectively, while the dark reaction provided polymer with M_n, M_w, PDI and yield of 4.5k, 7.3k, 1.6 and 57 % (Appendix A), respectively. Furthermore, an additional control reaction was performed under ambient light in the absence of Cl-SiNCs. GC-MS analysis revealed the presence of 73% of hydrolysed product (Br-HT) of monomer **1** and 27% of Br-TH-I starting material (calculated based upon the relative peak area percentage). Aliquots withdrawn at 7 and 25 hours were analyzed by MALDI-TOF and negligible polymers or oligomers were detected. (Figure 2-5).

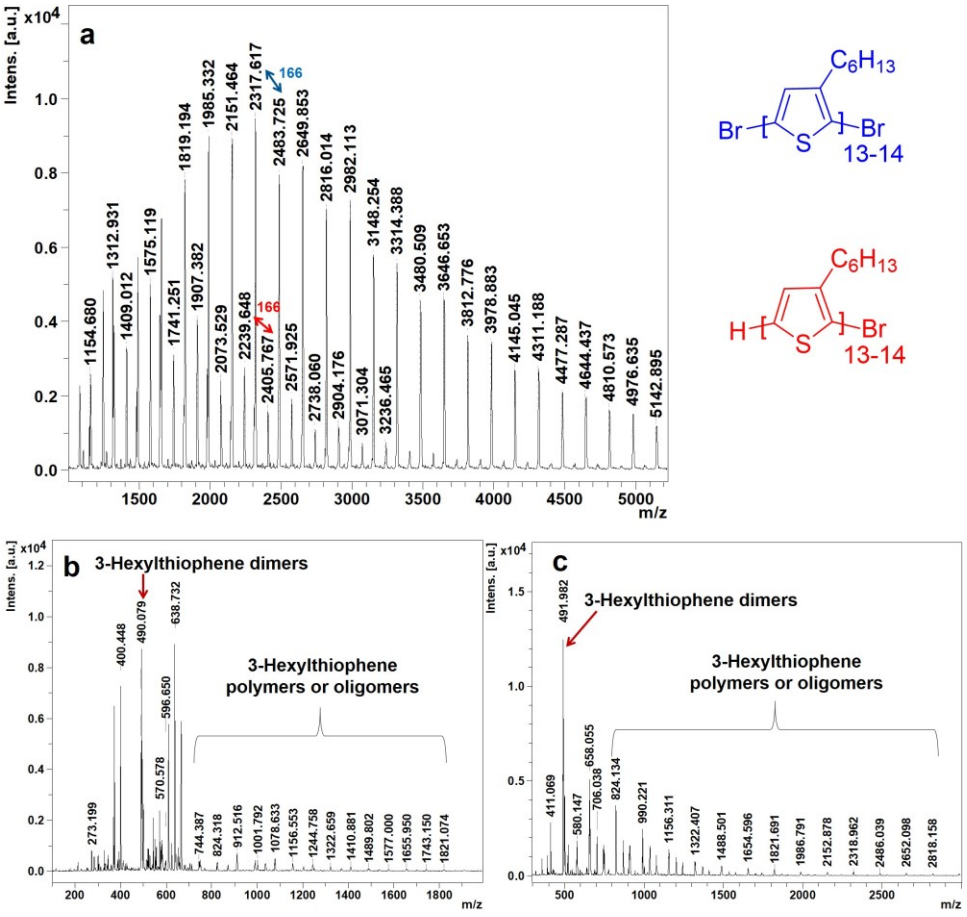

Figure 2-5. MALDI-TOF of a) P3HT obtained upon reaction of monomer **1** with Cl-SiNCs after 6 hours at room temperature in the absence of light; b) and c) products obtained from stirring monomer **1** for 7 and 25 hours in ambient light when no Cl-SiNCs were present. Note: Only 3-hexylthiophene dimers and trace quantities of polymers or oligomers were detected.

2.3.3 Cl-SiWF and $SiCl_4$-Mediated Synthesis of P3HT

Having established that the reaction of **1** with Cl-SiNCs provides P3HT under the presented conditions, we endeavored to evaluate other Si-Cl-containing species for similar reactivity. In this context, we performed equivalent reactions with Cl-SiWF [p-type Si(111) wafers; double side polished; 1×2 cm^2] and $SiCl_4$. Qualitative inspection of the color of the reaction mixture suggested negligible polymer formation after 6 hours. Extending the reaction time to 24 hours afforded a red solution. MALDI-TOF analysis of the isolated products revealed that the reaction catalyzed by Cl-SiWFs afforded H/Br- and Br/Brterminated P3HT with the number of repeat units ranging from 6 to 22 (Figure 2-6a). The M_n, M_w, and PDI of the polymer obtained from Cl-SiWFs were 4.0k, 9.5k, and 2.4, respectively. Polymerization of **1** induced by $SiCl_4$ provided P3HT with H/H-terminated P3HT as a major product, as evidenced by MALDI-TOF analysis (Figure 2-6b). GPC evaluation provided M_n, M_w, and PDI of 3.9k, 8.4k, and 2.1, respectively.

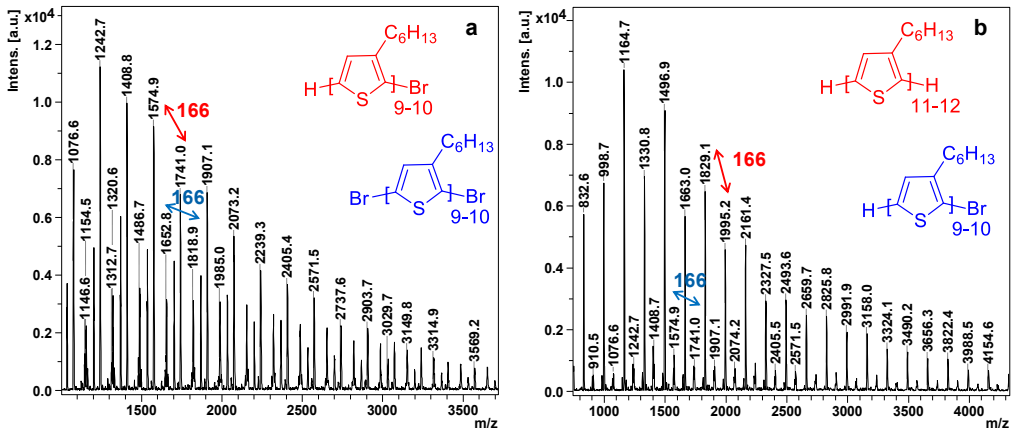

Figure 2-6. MALDI-TOF of P3HT synthesized using a) Cl-SiWF, and b) $SiCl_4$ after stirring for 24 hours.

Similar to the observations made for polymers prepared using Cl-SiNCs, ^1H NMR analysis (Figure 2-7a,b) revealed the polymers obtained from the reactions of **1** with Cl-SiWFs and $SiCl_4$ to be 64 % and 62 % regioregular (HT), respectively (Appendix B). The optical properties of the

polymers obtained from these reactions are equivalent to those of the P3HT obtained from Cl-SiNCs (Figure 2-7c,d).

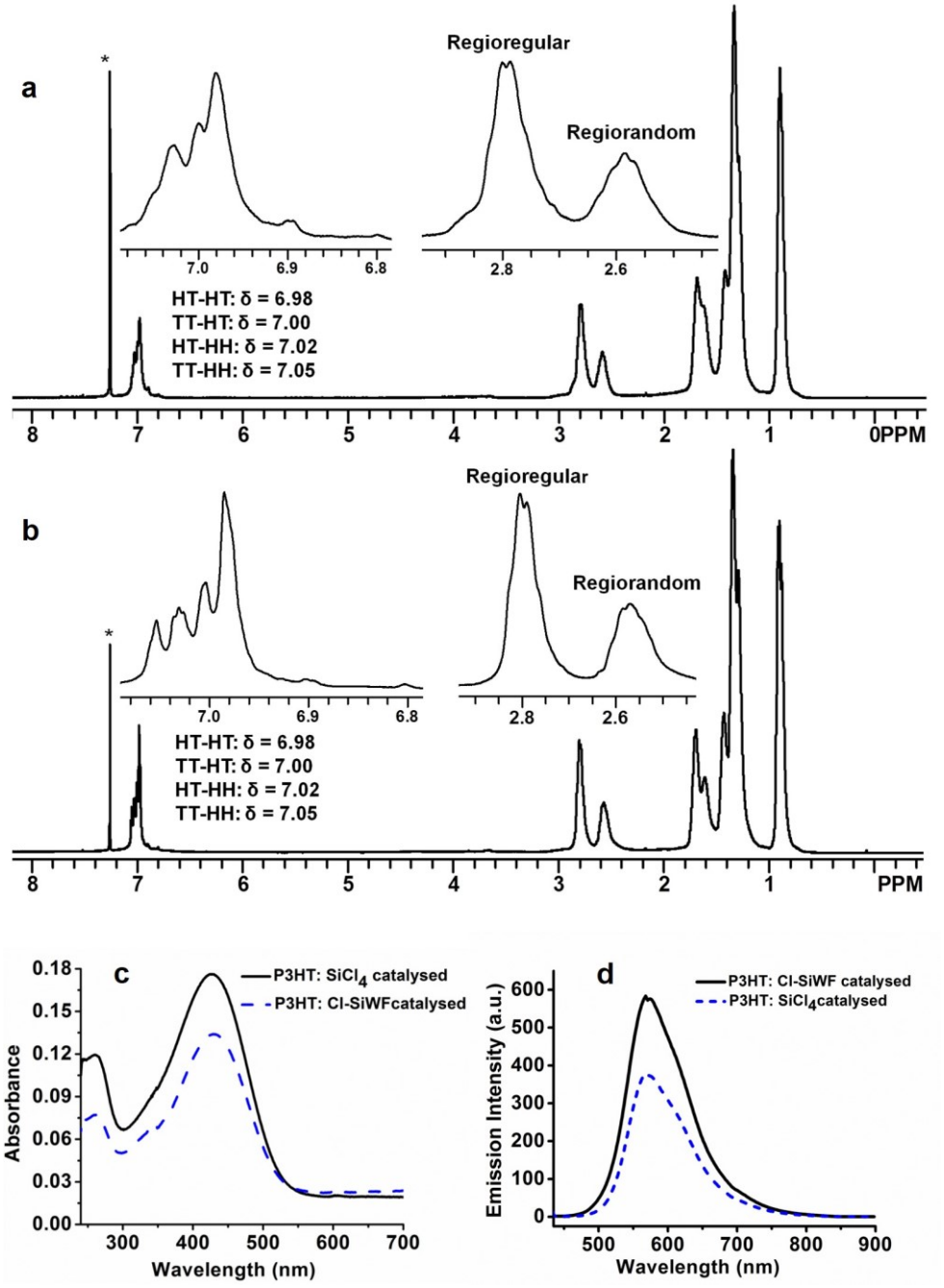

Figure 2-7. ^{1}H NMR spectra of P3HT in $CDCl_3$ prepared using a) Cl-SiWF and b) $SiCl_4$ for 24 hours reaction at room temperature. Optical properties of these P3HT; c) UV-Vis spectra (0.01 mg/mL P3HT solution in $CHCl_3$) d) Photoluminescence spectra (0.0033 mg/mL P3HT solution in $CHCl_3$; excitation wavelength 350 nm).

2.3.4 Comparison of the Reactivity of Cl-SiNC, Cl-SiWF, and $SiCl_4$.

To obtain a more direct comparison of the catalytic efficiencies of Si-Cl containing species, we performed reactions using each catalyst under identical conditions. The present comparison of catalytic performance cannot be viewed as strictly quantitative because knowing the exact number of catalytic sites for Cl-SiNCs and Cl-SiWFs is impossible. Still, we believe that this comparison provides valuable insight into the origin of our observations. The results are summarized in Table 2-1. Reactions with all three catalysts produced polymer, and the M_n, M_w, and yield were highest for the product of the reaction involving Cl-SiNCs. These data are consistent with the qualitatively slower reactions noted for the Cl-SiWF and $SiCl_4$ catalysts and indicate that the high surface area and surface Lewis acidity of the Cl-SiNCs play important roles in the observed reactivity.

Table 2-1. P3HT M_n, M_w, and PDIs obtained for indicated catalysts.

Catalyst	M_n (Da)	M_w (Da)	PDI = M_w/M_n	%Yield
Cl-SiNCs	3756	6788	1.8	79
Cl-SiWF	2530	4991	2.0	19
$SiCl_4$	2696	6076	2.3	32

2.3.5 Proposed Mechanism

The oxidative polymerization 3-hexylthiophenes by strong Lewis acidic $FeCl_3$ is believed to initiate *via* single-electron transfer from thiophene ring resulting in cationic thiophene radical. Polymerization proceeds through the radical formed by H^+ abstraction from cationic thiophene radical by the Cl^- ion.[332] The ≡Si-Cl species used in this study is also Lewis acidic. Therefore, polymerization of monomer **1** (Scheme 2-2) is foreseen to initiate *via* single-electron transfer from **1** to ≡Si-Cl anti-bonding orbital yielding the radical cation **2** and ≡Si-Cl]$^{\bullet-}$ radical anion. The abstraction of $MgCl^+$ from **2** by the Cl^- ion from ≡Si-Cl]$^{\bullet-}$ forms thiophene radical **3** and ≡Si$^{\bullet}$

radical. Thiophene radical **3** reacts with a neutral monomer forming radical **4**. The ≡Si• radical abstracts Br• from **4** completing a coupling cycle.

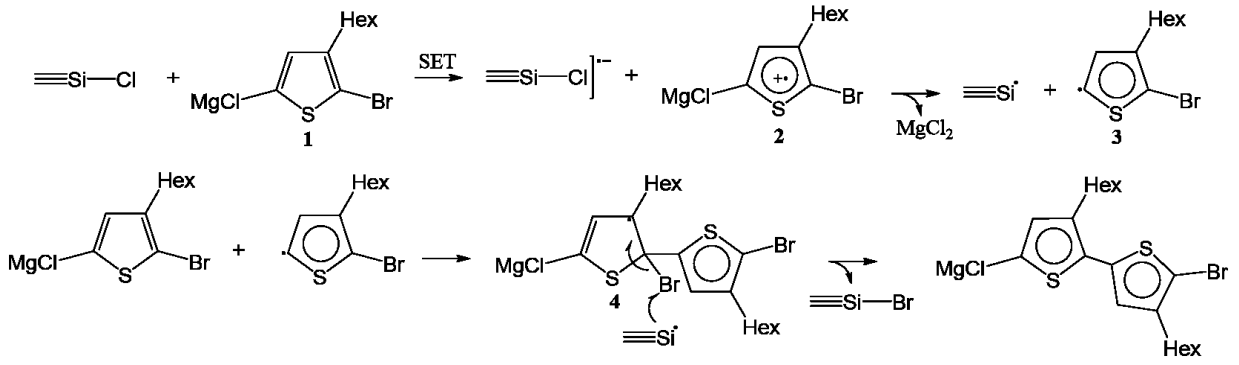

Scheme 2-2. Proposed radical mechanism for the synthesis of P3HT by chlorinated silicon based species.

2.4 Conclusion

In conclusion, three silicon-based metal-free catalysts were employed to prepare P3HT. These catalysts have various attractive features, including reasonable reaction times and straightforward separation from the target products. The presented syntheses of the workhorse conjugated polymer P3HT indicate that abundant silicon-based catalysts offer alternative approaches for the preparation of functional materials free from costly and potentially harmful transition metals.

Chapter 3:

Grafting Poly(3-hexylthiophene) from Silicon Nanocrystal Surfaces: Synthesis and Properties of a Functional Hybrid Material with Direct Interfacial Contact

A version of this Chapter has been published:

Islam, M. A.; Purkait, T. K.; Mobarok, M. H.; Höehlein, I. M. D.; Sinelnikov, R.; Iqbal, M.; Azulay, D.; Balberg, I.; Millo, O.; Rieger, B.; Veinot, J. G. C. *Angew. Chem. Int. Ed.* **2016**, *55*, 7393–7397.

Reproduced with permission from WILEY-VCH.

3.1 Introduction

The properties of semiconductor nanoparticles (or quantum dots) can be readily designed to address the needs for a multitude of applications.[347–350] This exquisite tunability is achieved by tailoring nanoparticle size, shape, and surface chemistry.[348,349,351] Similarly, the properties of conjugated polymers may also be tuned and complement those of quantum dots.[240,268,352] Hybrid functional materials (HFMs) combining nanomaterials and polymers can exhibit unique and tunable properties that may not otherwise be observed in the individual components.[89,182,240,241] In particular HFMs made up of compound semiconductor (for example, CdSe) nanoparticles and conjugated polymers have shown promise as functional materials in solar cells,[243,253] light-emitting diodes,[245,246] photodetectors,[247] photocatalysis,[248] and photothermal therapy.[249]

While HFMs based upon metal chalcogenide and metal oxide nanoparticles with conjugated polymers have received much attention, similar materials involving SiNCs remain relatively unexplored. Silicon is abundant, environmentally benign, and is widely used in electronic devices.[80,226,353] More importantly, state-of-the-art methods for preparing SiNCs now afford tangible quantities of well-defined materials, the band gap of which may be tuned in the range of *ca.* 1.1-2.1 eV.[226,236] Furthermore, advanced procedures for tailoring NC surface functionalities now provide convenient approaches for designing their electronic[226] and optical properties.[354] Clearly, SiNCs are an attractive component on which HFMs may be formed. A few examples of physical blends made up of SiNCs with conjugated polymers have appeared.[253,300,312,355] However, to our knowledge, no reports of direct grafting of conjugated polymers onto or from the surfaces of well-defined SiNCs have appeared.

In this chapter, we report a new method that effectively interfaces conjugated polymers with SiNCs. P3HT was directly grafted from SiNC surface utilizing a variation of surface-initiated

Kumada catalyst transfer polycondensation.[271] Subsequently, the photophysical properties of the resulting SiNC@P3HT hybrid were evaluated to ascertain the impact of directly attaching P3HT to SiNCs.

3.2 Experimental

3.2.1 Reagents and Materials

Nickel(II)acetylacetonate ($Ni(acac)_2$, 95 %), 2,2′-bipyridyl (bipy, ≥ 99 %) and 1,3-bis(diphenylphosphino)propane (dppp, 97 %), 1,3-dichlorobenzene (DCB), chloroform ($CHCl_3$) and deuterated chloroform ($CDCl_3$) were purchased from Sigma-Aldrich and used as received. Diethylaluminum ethoxide ($(C_2H_5)_2AlOC_2H_5$, 25 % w/w in hexane) was purchased from Alfa Aesar and used as received. Hydrogen silsesquioxane (HSQ, trade name Fox-17) was purchased from Dow Corning and the solvent was removed to yield a white solid that was used directly. Hydrofluoric acid (HF, 48-50 %) was purchased from Fisher Scientific and used as received. 2-Bromo-3-hexyl-5-iodothiophene (Br-HT-I, > 97 %, stabilized with a copper chip) from TCI America was passed through 230-400 mesh silica gel (Sigma-Aldrich) immediately prior to use. 2.0 M tert-butylmagnesium chloride (*t*-BuMgCl) solution in THF was purchased from TCI America and used as received. THF, ether, toluene and hexane solvents were collected from Pure-Solv purification systems prior to use. Concentrated hydrochloric acid (HCl) was purchased from Caledon and used as received. All other solvents were reagent grade and deionized water was used throughout the experiments.

3.2.2 Synthesis of Diethyldipyridylnickel ($Et_2Ni(bipy)$)

$Et_2Ni(bipy)$ was synthesized according to modified literature procedure.[356] In a nitrogen purged glovebox 2 g of $Ni(acac)_2$ and 3 g of bipy were suspended in diethyl ether in a Schlenk flask and kept for 1 h in the glovebox freezer set at -20 °C. After cooling, 6 g of diethylaluminum

ethoxide (24 mL of 25 % w/w in hexane solution) was slowly added into the flask. The mixture was warmed to 25 °C and stirred until the complete dissolution of all the reagents and was then left to stand at 25 °C in order to obtain dark green precipitate. The precipitate was recrystallized from diethyl ether to obtain dark green crystals. Finally, the crystals were washed with diethyl ether followed by hexane.

3.2.3 Synthesis of Hydride-Terminated Silicon Nanocrystals

H-SiNCs were prepared using a method reported by our group.[157] Briefly, HSQ was thermally processed in a Lindberg blue tube furnace at 1100 °C for 1 hour under flowing 5 % H_2 and 95 % Ar atmosphere. The resulting Si/SiO_2 composite was further annealed at 1400 °C for 1 hour under flowing Ar atmosphere then mechanically ground. H-SiNCs were obtained *via* HF etching of the composite. In a typical experiment, 400 mg of Si/SiO_2 composite were etched in 18 mL of a 1:1:1 49 % HF: water: ethanol solution for 1 h, extracted into toluene, and then centrifuged at 3000 rpm for 10 minutes. The pellet was redispersed in dry toluene and type 4Å molecular sieves were added to remove moisture. A redispersion-centrifugation was done using dry THF. This procedure results in the formation of *ca.* 11 nm H-SiNCs. The resulting H-SiNCs were transferred with 5 mL freshly distilled THF to a Schlenk flask and the system was subjected to freeze-pump-thaw cycles (3×). The flask was kept into the nitrogen purged glovebox until use.

3.2.4 Preparation of 2-Bromo-3-hexyl-5-thienyl-Terminated SiNC

5-Chloromagnesio-2-bromo-3-hexylthiopehene (**1**) was prepared using a modified literature procedure.[271] In a nitrogen filled glovebox, 1.86 g (5 mmol) of 2-bromo-3-hexyl-5-iodothiophene (Br-HT-I) was placed in a round bottom flask equipped with a magnetic stirring bar. Dry THF (3 mL) and 4 mmol *t*-BuMgCl (2 mL of 2.0 M solution in THF) was added to the round bottom flask. The solution was stirred for 1 h at 25 °C and transferred *via* glass pipette to a

Schlenk flask containing H-SiNCs dispersed in 5 mL THF. The mixture was stirred at 25 °C for 24 hours to obtain 2-bromo-3-hexyl-5-thienyl-terminated SiNC (SiNC-HT-Br). Note that the reaction mixture was purified in different ways whether for characterizations or subsequent further reaction steps involving P3HT grafting. For the characterization, the reaction mixture was subjected to several purification cycles by centrifuging from 30 mL methanolic hydrochloric acid (25:1 methanol: 36.5-38 % HCl, used to neutralize the Grignard reagents) and from a solution of 15 mL THF and 25 mL hexane (10,000 rpm, 20 minutes, 3×). For grafting P3HT, the reaction mixture was transferred into screw capped PTFE centrifuge tubes in the glove box and 30 mL hexane was added to it and was centrifuged at 12,000 rpm for 20 minutes. The resulting pellet was further purified by 2 more redispersion centrifugation cycles from 15 mL THF and 25 mL hexane at 12,000 rpm for 20 minutes. Note that aqueous HCl based purification was avoided since the next catalyst immobilization step requires extremely air and moisture free condition.

3.2.5 Generating SI-KCTP Initiating Sites on SiNC-HT-Br

Purified SiNC-HT-Br prepared as above was redispersed in 5 mL dry THF and transferred to Schlenk flask. Then 5 mg of $Et_2Ni(bipy)$ was added to the dispersion in 100 µL portions from a 10 mg/mL solution in THF. Each new portion was added after the consumption of the previous addition estimated from the color change from green for $Et_2Ni(bipy)$ to dark red brown for SiNC-HT-Ni(bipy)-Br. After stirring for total of 2 h, ligand exchange was performed by adding 20 mg of dppp and stirring overnight. The suspension color changed to orange-brown during overnight stirring. Residual catalyst and ligands were removed by centrifugation cycles from 40 mL THF and CH_2Cl_2 at 4000 rpm for 15 minutes (3×). The initiator particles were redispersed in 5 mL dry THF and transferred to the Schlenk flask.

3.2.6 Polymerization Procedures

In a nitrogen filled glovebox, 1.86 g (5 mmol) of 2-bromo-3-hexyl-5-iodothiophene was placed in a round bottom flask equipped with a magnetic stirring bar. Dry THF (45 mL) and 4.5 mmol *t*-BuMgCl (2.25 mL of 2.0 M solution in THF) was added and the solution was stirred for 1 h at 25 °C. The solution was transferred *via* glass pipette to a Schlenk flask containing SiNC-HT-Ni(dppp)-Br dispersed in 5 mL THF. The solution was stirred overnight at 25 °C to obtain P3HT grafted SiNC (SiNC@P3HT). The reaction mixture was subjected sequentially to 5 M HCl, water, methanol (2 × 50 mL of each), THF and DCB (3 × 50 mL). In each step the solid grafted SiNC (SiNC@P3HT) was separated by centrifugation at 10000 rpm.

3.2.7 Degrafting P3HT from SiNCs

The P3HT was degrafted from the SiNC surface by etching SiNC@P3HT in 50 mL solution of 3:1:1 THF: 49 % HF: water for 5 days. The degrafted P3HT was extracted into $CHCl_3$. A portion of the $CHCl_3$ was directly used for mass spectrometric analysis; for ^1H NMR the $CHCl_3$ solution was dried and P3HT redesolved in $CDCl_3$.

3.2.8 Synthesis of Pentyl Functionalized SiNC

Pentyl functionalized SiNCs were prepared according to our previous report.[188] 200 mg of Si/SiO_2 composite were etched in 9 mL of a 1:1:1 49 % HF: water: ethanol solution by stirring for 1 h. The resulting H-SiNCs were extracted from the etching mixture upon addition of toluene and isolated upon centrifugation at 3000 rpm for 10 minutes. The H-SiNCs were redispersed into toluene that had been pre-dried over molecular sieves S4 (4Å) and isolated by centrifugation. Finally, H-SiNCs were redispersed in dry toluene (5 mL) and transferred to a Schlenk flask. The nanocrystal suspension was degassed by three freeze-pump-thaw cycles using an Ar charged double manifold Schlenk line. Degassed pentene (*ca.* 20 mmol) was added to the 5 mL of degassed H-SiNC suspension. The BH_3•THF solution (*ca.* 2.5 mol% of pentene, 0.5 mL, 1 M solution in

THF) was added slowly to the solution with stirring using a syringe at 0 °C under Ar. The reaction mixture was allowed to warm to 25 °C and was stirred for 12 hours. To purify the functionalized SiNCs, the solution (*ca.* 7-10 mL) was transferred to a 50 mL PTFE centrifuge tube and a methanol (*ca.* 35 mL) antisolvent was added. The mixture was subsequently centrifuged at 14,000 rpm for 30 minutes. The supernatant was decanted and discarded. The pellet was redispersed in 3 mL toluene with sonication. An additional *ca.* 35 mL of methanol was added to the pellet, the mixture was sonicated and finally it was centrifuged at 14,000 rpm for 30 minutes. The process was repeated one more time and finally the solid SiNCs were dispersed in dry THF.

3.2.9 Characterization

3.2.9.1 Electron Microscopy

Brightfield TEM images were obtained using a JEOL 2011TEM with LaB_6 electron gun using accelerating voltage of 200 kV. The TEM core-shell image was obtained with JEM-2100 TEM operating at 120 kV. TEM samples were prepared by depositing a drop of dilute SiNC-HT-Br or SiNC@P3HT suspension in toluene onto a holey carbon coated copper grid and the solvent was removed under vacuum. The NC size was averaged for more than 200 particles using Image J software (version 1.45). The bright field scanning transmission electron microscopy (BF- STEM) is performed on a Hitachi-S5500 STEM, operating at 30 kV. High-resolution (HR) TEM and high annular angular dark field (HAADF) imaging and electron energy loss spectroscopic (EELS) mapping were carried on a JEOL-2200FS TEM-STEM with an accelerating voltage of 200 kV. The HAADF and EELS were recorded simultaneously under STEM mode with a nominal beam size of 0.5 nm. Digital Micrograph (Gatan Inc.) was employed for data collection and processing. The standard procedure of pre-edge background subtraction, and integration on the corresponding edges was used to generate the elemental maps.[357] Specifically, we collected the spectra and

worked on the silicon L, carbon K and sulfur L core-loss edges to represent the qualitative elemental distribution around single nanoparticle. The HRTEM images were processed using Gatan Digital Micrograph software (Version 2.02.800.0).

3.2.9.2 Fourier Transform Infrared Spectroscopy

Samples of SiNC-HT-Br or SiNC@P3HT were prepared as a thin film on a silicon wafer by drop casting from THF. FT-IR spectra were recorded using a Thermo Nicolet Continuum FT-IR microscope.

3.2.9.3 X-ray Photoelectron Spectroscopy

SiNC-HT-Br or SiNC@P3HT sample were deposited from THF dispersion onto a copper wafer and immediately transferred to a Kratos AXIS 165 instrument. The base pressure in the sample analytical chamber was lower than 1×10^{-9} Torr. Monochromatic Al Kα source with an energy $h\nu = 1486.6$ eV was used at 210 W. Survey spectra were collected with analyzer pass energy of 160 eV and a step of 0.3 eV. For high-resolution spectra, the pass energy was 20 eV and the step was 0.1 eV with a dwell time of 200 ms. XPS data were calibrated and fitted as described in experimental chapter 2.

3.2.9.4 Thermogravimetric Analysis

SiNC-HT-Br or SiNC@P3HT samples were prepared as solid residue and transferred to a platinum pan. Weight loss was monitored in the temperature range of 25 to 800 °C at a temperature increment rate of 10 °C/min under N_2 atmosphere using Perkin Elmer Pyris 1 TGA.

3.2.9.5 Matrix Assisted Laser Desorption Ionization-Time of Flight-Mass Spectrometry

MALDI-TOF-MS were acquired using an UltraflexXtremeTM MALDI-TOF/TOF (Bruker Daltonics, Billerica, MA, USA) mass spectrometer in positive MS mode. 2[(2E)-3-(4-tert-

Butylphenyl)-2-methylpropy-2-enylidene]-malononitrile (DCTB) was used as matrix. A matrix solution was prepared in dichloromethane with a concentration of 10 mg/mL. The polymer (P3HT) sample detached from SiNC was dissolved in a minimal volume of $CHCl_3$ and mixed with an equal volume of the DCTB solution. 0.8 μL of the polymer/matrix solution was then spotted onto a stainless steel MALDI target for analysis.acquired using an UltraflexXtremeTM MALDI-TOF/TOF (Bruker Daltonics, Billerica, MA, USA) mass spectrometer in positive MS mode.

3.2.9.6 Nuclear Magnetic Resonance Spectroscopy

^1H NMR of P3HT in $CDCl_3$ was obtained using a Varian Unity Inova Console 500 MHz NMR spectrometer. Tetramethylsilane (^1H, $^{13}C\{^1H\}$) was used as an external reference. NMR data were processed using ACD/NMR Processor Academic Edition and the processed data were plotted using an OriginLab software.

3.2.9.7 UV-Vis and PL Spectroscopy

UV-Vis spectroscopic data were obtained using an Agilent Hewlett Packard 8453 UV-Vis spectrophotometer. The solutions of P3HT, pentyl-SiNC, pentyl-SiNC/P3HT and SiNC@P3HT in THF were prepared in such a way that the concentration of SiNC (*ca.* 12.6 μg/mL) and P3HT (*ca.* 6.6 μg/mL) are the same in all samples. Briefly, stock solutions of 1 mg/mL of P3HT, pentyl-SiNC and SiNC@P3HT in THF were prepared and diluted with THF to obtain the final concentrations. For the physical mixture of pentyl-SiNC and P3HT, 630 μL of 1 mg/mL pentyl-SiNC and 330 μL of 1 mg/mL P3HT stock solutions were mixed and diluted with THF to obtain the desired concentration. The absorption spectra of the corresponding solutions were recorded and integrated PL (Varian Eclipse fluorescence spectrophotometer) intensity of P3HT, pentyl-SiNC/P3HT and SiNC@P3HT were measured at an excitation wavelength of 450 nm (excitation and emission slit widths: 5, photomultiplier voltage: medium).

3.2.9.8 Scanning Tunneling Microscopy and Spectroscopy

For STM measurements, NCs were spin cast from a toluene solution onto atomically flat flame-annealed Au(111) substrates. All measurements were performed at room temperature, using Pt-Ir tips. Tunneling current-voltage (I-V) characteristics were acquired after positioning the STM tip above individual NCs, realizing a double barrier tunnel junction (DBTJ) configuration[358] and momentarily disabling the feedback loop. In general, care was taken to retract the tip as far as possible from the NC, so the applied tip-substrate voltage would fall mainly on the tip-NC junction rather than on the NC-substrate junction whose properties (capacitance and tunneling resistance) are determined by the layer of organic capping ligands that cannot be modified during the STM measurement. This protocol reduces the voltage division induced broadening effects, and thus the measured gaps and level separations in general better correspond to the real SC gaps, although broadening on the order of 10-15% is still expected.[358,359] The dI/dV-V tunneling spectra, proportional to the local tunneling density of states (DOS), were numerically derived from the measured I-V curves. We have acquired the topographic images with a set sample-bias, Vs, of 1.8 V and set current Is = 0.2 nA. This bias value ensures tunneling to states well above the conduction band edge, where the DOS is rather large. Thus the measured SiNC height corresponds well to the real height. The tunneling spectra (on the NCs) were measured with lower set bias, of Vs ≅ 0.8 V, and Is ≅ 0.1 nA. These Vs values still ensure tunneling above the band edge (before disconnecting the feedback loop), yet being sensitive to the details of the DOS around the band edge. Is was reduced as much as possible, to the lowest value that still allowed acquisition of smooth tunneling spectra, in order to retract the tip as much as possible from the NC (thus reducing the voltage division factor).

3.3 Results and Discussion

3.3.1 Generating SI-KCTP Initiating Sites on SiNCs

To achieve our goal of covalently interfacing SiNCs with P3HT, it was necessary to generate surface-bonded initiator sites. This was achieved by introducing an aromatic halide to the NC surface (Scheme 3-1). The moiety of choice for the present preparation was 2-bromo-3-hexyl-5-thienyl because it is expected to limit interfacial effects. Amongst the various strategies available for modifying SiNC surface chemistry,[80,89] reaction of hydride (that is, Si-H) surfaces with Grignard reagents was chosen because it allows for direct bonding of the thiophene ring to SiNC (Scheme 3-1).[199,204] Accordingly, hydride-terminated SiNCs (H-SiNCs) were prepared using a well-established procedure developed in our laboratories[157] and subsequently treated with 5-chloromagnesio-2-bromo-3-hexylthiophene (1) to obtain 2-bromo-3-hexyl-5-thienyl (-HT-Br)-terminated SiNC (SiNC-HT-Br) (Scheme 3-1).

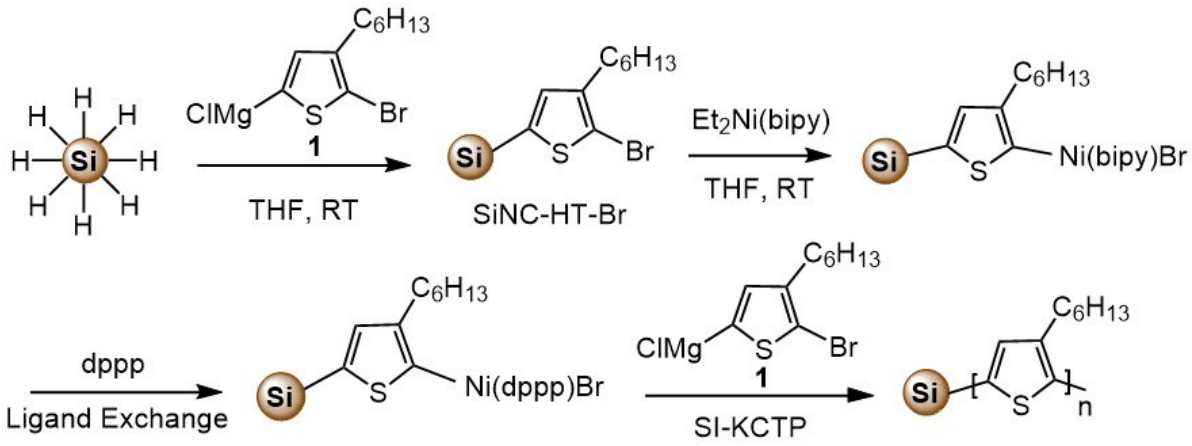

Scheme 3-1. Preparation of SiNC@P3HT hybrid material.

Transmission electron microscopy afforded an average diameter of 11.1 ± 1.1 nm for SiNC-HT-Br (Figure 3-1a). Effective introduction of the -HT-Br functionality onto the SiNC surface was evidenced by the appearance of characteristic C-H stretching (2850–2950 cm^{-1}) and C-H bending (1400–1465 cm^{-1}) in the FT-IR spectrum (Figure 3-1b) that arise from the hexyl

chain. High-resolution X-ray photoelectron spectroscopy (HR-XPS; Figure 3-1c–e) further supports functionalization, showing Si 2p, S 2s, and Br 3d emissions.

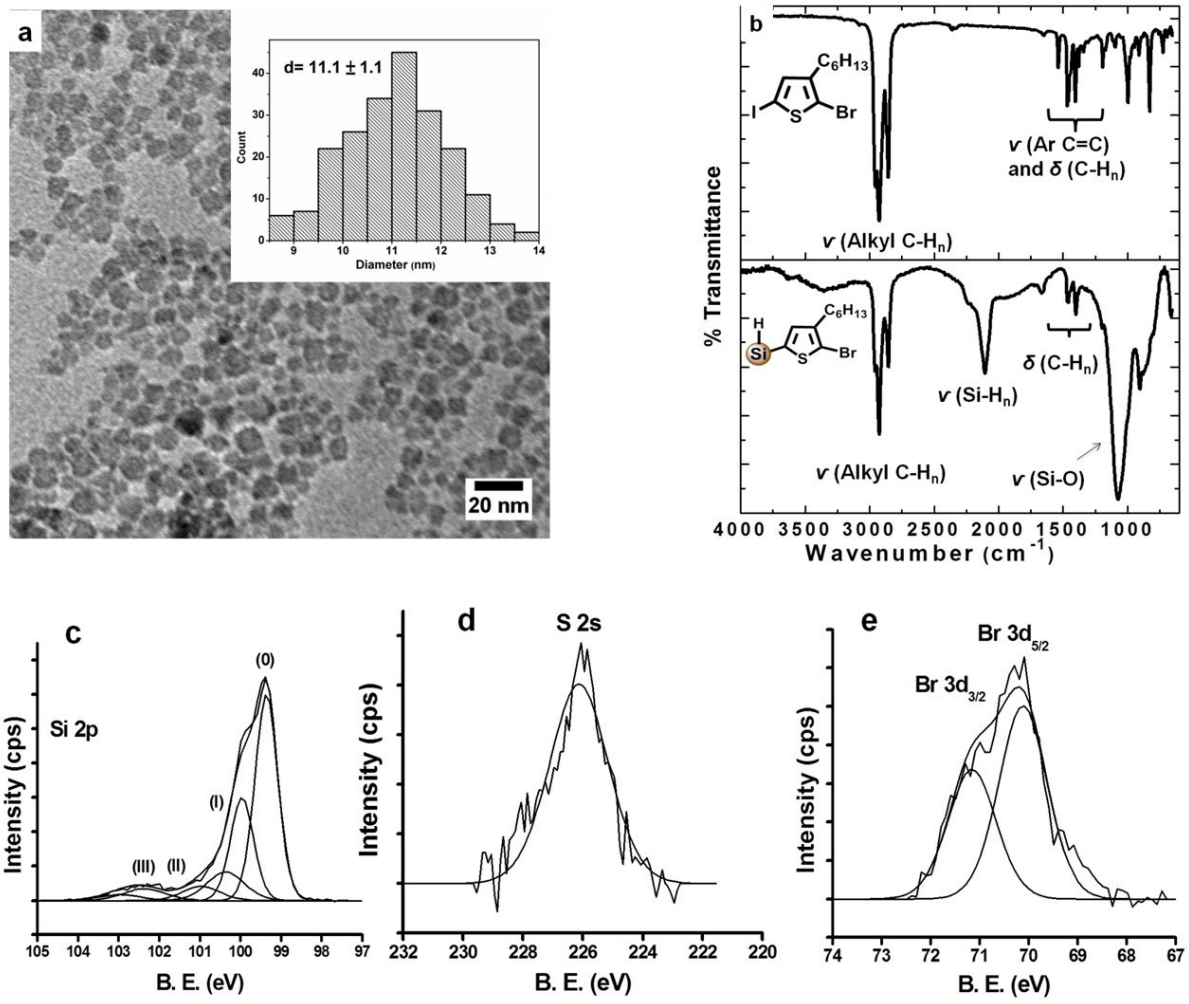

Figure 3-1. a) Bright-field TEM image of SiNC-HT-Br (Inset: particle size distribution showing an average diameter of 11.1 ± 1.1 nm). b) FT-IR spectra of I-HT-Br (top) and SiNC-HT-Br (bottom). c) Si 2p, d) S 2s, and e) Br 3d regions of the high-resolution XP spectra of SiNC-HT-Br.

3.3.2 Grafting P3HT from SiNC-HT-Br

Having introduced reactive -HT-Br moieties to the surface of SiNCs, P3HTwas grafted from the particles as outlined in Scheme 3-1. $Et_2Ni(bipy)$ catalysts were immobilized onto the aromatic bromide termini followed by ligand exchange of bipyridine (bipy) with 1,3-Bis(diphenylphosphino)propane (dppp) to yield an orange dispersion of SiNC-HT-Ni(dppp)-Br.

SI-KCTP was subsequently performed by adding monomer **1** to the SiNC-HT-Ni(dppp)-Br followed by stirring for 12 h at 25 °C under a dry nitrogen atmosphere. The resulting SiNC@P3HT hybrid was isolated and purified as described in the provided experimental procedure (Section 3.2.6).

The FT-IR spectrum (Figure 3-2a) of the SiNC@P3HT hybrid exhibits features at 3060, 2850–2950, and 1360–1600 cm^{-1} that we assign to aromatic C-H stretch, aliphatic C-H stretch, and C=C stretch/C-H bending absorptions, respectively. Figure 3-2b,c shows the Si 2p and S 2s regions of the XP spectrum of the SiNC@P3HT hybrid; consistent with surface grafting of P3HT. We note an approximate 8-fold increase in the ratio of S over Si compared to SiNC-HT-Br.

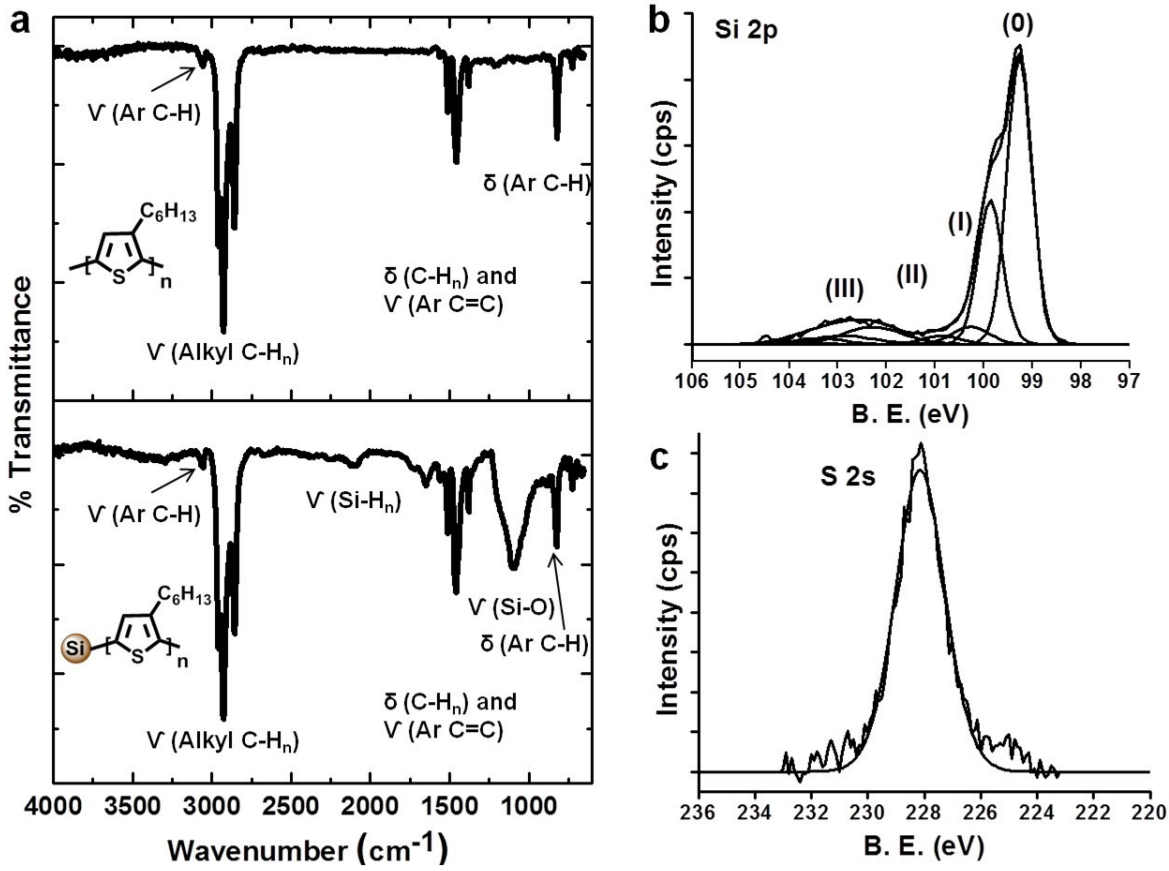

Figure 3-2. (a) FT-IR spectra of P3HT (top) and SiNC@P3HT (bottom). b) Si 2p and c) S 2s regions of the high-resolution XP spectrum of SiNC@P3HT.

A complementary suite of electron microscopy techniques and associated spectroscopic methods provide valuable insight into the core–shell structure of the present hybrid. Bright field TEM analysis of SiNC@P3HT (Figure 3-3a,b) shows an increase in particle diameter by about 4 nm compared to the parent SiNC-HT-Br that is attributed to the shell of P3HT.

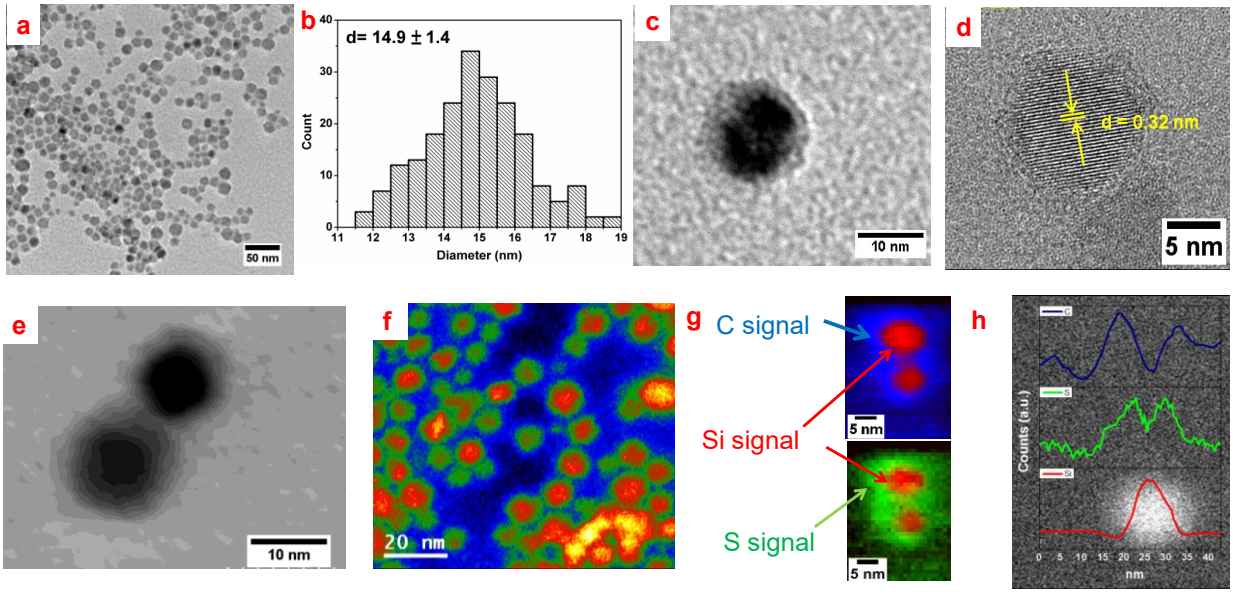

Figure 3-3. Electron microscopy imaging and elemental analyses of SiNC@P3HT: a) Bright-field TEM image, b) particle size distribution histogram of SiNC@P3HT obtained from bright-field TEM image showing an average diameter of 14.9 ± 1.4 nm, c) low-resolution TEM image of SiNC@P3HT core–shell, d) high-resolution TEM image of SiNC@P3HT, e) STEM bright field and f) HAADF images showing core–shell structures, g) EELS mapping of two neighboring SiNC@P3HT particles and h) EELS line scan of a single SiNC@P3HT particle showing core-shell composition.

A representative high magnification bright-field TEM image of a SiNC@P3HT particle (Figure 3-3c) shows expected contrast resulting from a core–shell structure. HR-TEM evaluation of SiNC@P3HT (Figure 3-3d) shows lattice fringes separated by 0.32 nm indicative of Si (111) lattice planes[104] confirming the crystalline Si core remained intact throughout the modification procedure. Furthermore, “hairy” features are apparent in the HR-TEM surrounding the SiNC core consistent with a P3HT coating. Scanning transmission electron microscopy (STEM) and high

annular angular dark field (HAADF) images clearly show core–shell structures (Figure 3-3e,f). Electron energy loss spectroscopy (EELS) mapping of two particles (Figure 3-3 g) exhibits a Si rich core while the shell is rich in carbon and sulfur. Moreover, an EELS line scan spectrum (Figure 3-3h) of a representative single particle indicates the intensities of sulfur and carbon signals are substantially higher at particle edges while the composition of the core is dominated by silicon.

Thermogravimetric analysis (TGA) performed under continuous nitrogen flow was employed to estimate the amount of P3HT on the SiNC@P3HT; it also provided an evaluation of SiNC@P3HT thermal stability. The SiNC@P3HT hybrid was stable up to 400 °C in nitrogen; a weight loss of approximately 23 % was observed between 400-600 °C (Figure 3-4a). This is the typical temperature range reported for pristine P3HT thermal decomposition.[267] Considering the 70 % weight loss for pristine P3HT after decomposition at 600 °C,[267] the 23 % weight loss for SiNC@P3HT hybrid corresponds to an estimated value of *ca.* 33 % P3HT in the hybrid.

To gain insight into the molecular weight and regioregularity of the grafted P3HT, the P3HT was degrafted from the SiNC surface upon etching with a 3:1:1 THF/49 % HF/water solution for 5 days; the resulting free P3HT was evaluated using mass spectrometry and ^{1}HNMR spectroscopic analysis. Matrix-assisted laser desorption ionization-time-of-flight (MALDI-TOF) mass spectrum (Figure 3-4b) reveals two overlapping patterns for the degrafted P3HT with peak separations of m/z 166 corresponding to the molecular weight of the hexylthiophene repeat unit. ^{1}HNMR reveals 100% regioregular head-to-tail (HT) coupling of hexylthiophene repeat units at the sensitivity of the NMR technique (Figure 3-4c).

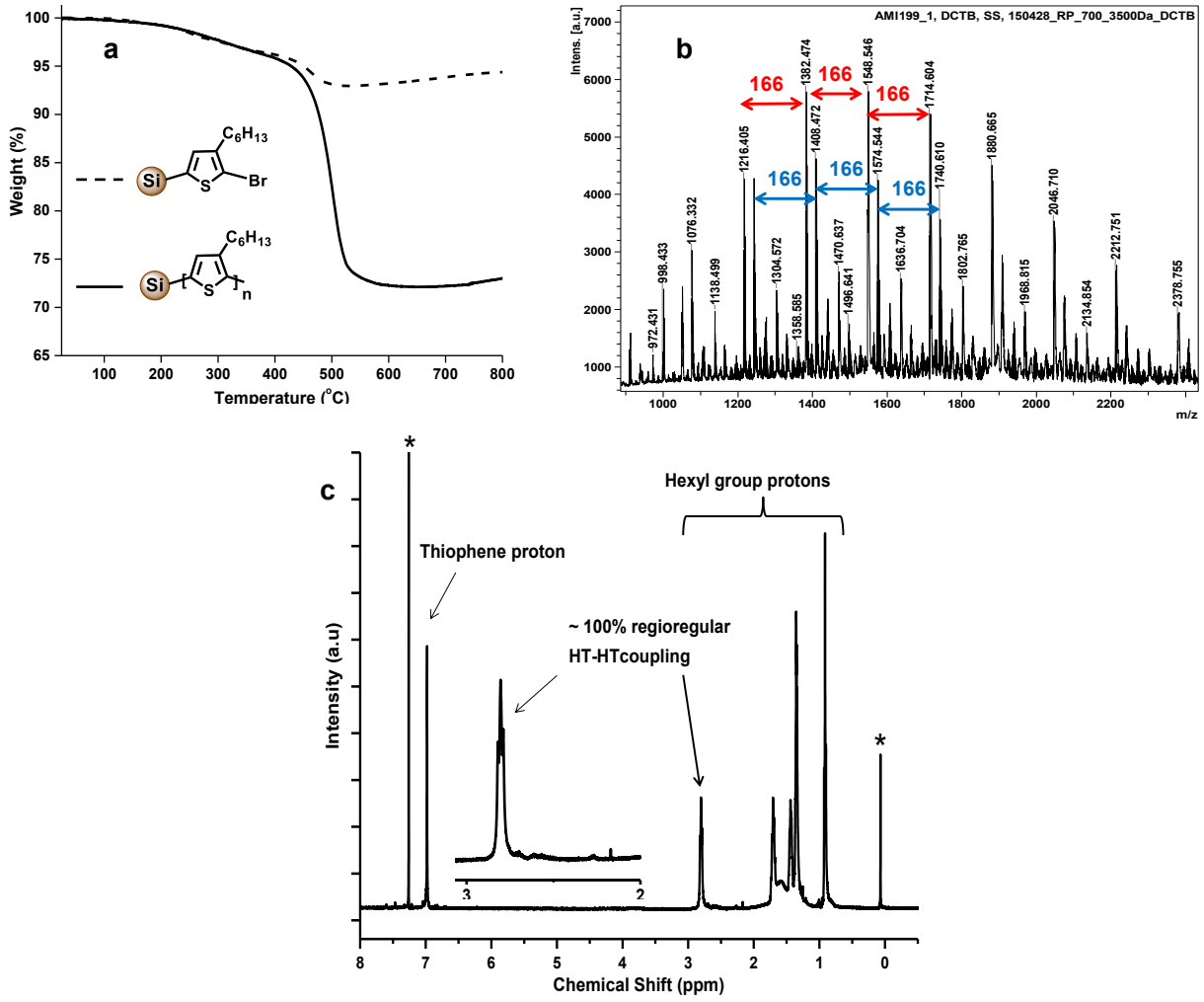

Figure 3-4. (a) TGA traces of SiNC-HT-Br (dotted trace) and SiNC@P3HT hybrid materials (solid trace), (b) MALDI-TOF mass spectrum of P3HT degrafted from SiNC@P3HT, (c) ^{1}H NMR spectrum of degrafted P3HT in $CDCl_3$ (* indicates a residual solvent and grease peak).

After confirming successful grafting of P3HT on SiNCs, the interfacial properties of the hybrid were investigated with UV/Vis absorption and photoluminescence (PL) spectroscopy. The spectra of the SiNC@P3HT hybrid were compared to those of pentyl-capped SiNC (pentyl-SiNCs), degrafted P3HT, and a physical mixture of pentyl-SiNC and P3HT (pentyl-SiNC/P3HT). The physical mixture was produced by combining pentyl- SiNCs obtained from borane-catalyzed hydrosilylation of pentene on H-SiNCs (see: Section 3.2.8 and Figure 3-5)[188] with degrafted P3HT. Unlike the present hybrid, the P3HT is not covalently bonded to the SiNCs in the blend and the

surface alkyl groups are expected to passivate the SiNC surface.[360] All solutions used for the presented spectroscopic studies were prepared using THF and the concentrations of SiNCs and/or P3HT were maintained the same.

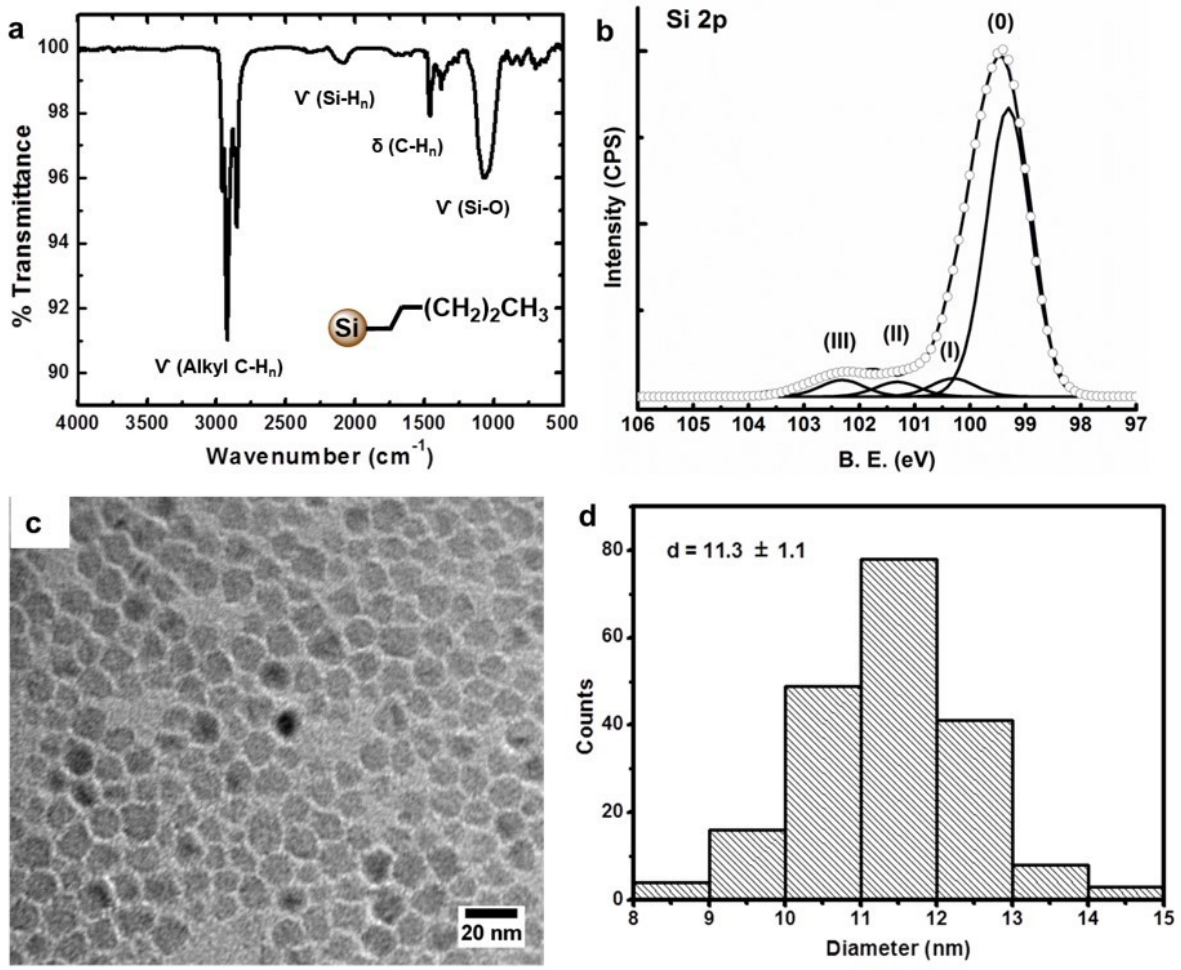

Figure 3-5. Characterization of pentyl-SiNCs. (a) FT-IR spectrum, (b) Si 2p egion of the high-resolution XP spectrum, (c) Bright-field TEM image and (d) Particle size distribution histogram showing average diameter of 11.3 ± 1.1 nm.

Qualitatively, solutions of pentyl-SiNC, P3HT, and pentyl-SiNC/P3HT appeared orange, while the solution of the SiNC@P3HT hybrid was red (Figure 3-6a). The UV/Vis absorption spectra of THF solutions of pentyl-SiNC, P3HT, pentyl-SiNC/P3HT, and SiNC@P3HT are shown in Figure 3-6b. The absorption spectrum of a solution of pentyl-SiNCs is featureless, while that of

P3HT exhibits a broad absorption from 300 to 550 nm (λ_{max} = 450 nm). The pentyl-SiNC/P3HT physical mixture displays a spectrum consistent with the straightforward sum of the absorption features of the SiNCs and P3HT components; this supports our proposal that negligible electronic interaction between P3HT and SiNCs surfaces exists. In contrast, the absorption spectrum obtained from the covalently bonded SiNC@P3HT hybrid shows a broad absorption (λ_{max} = 450 nm) attributed to the sum of hybrid constituents and new shoulders featured at 518, 555, and 620 nm.

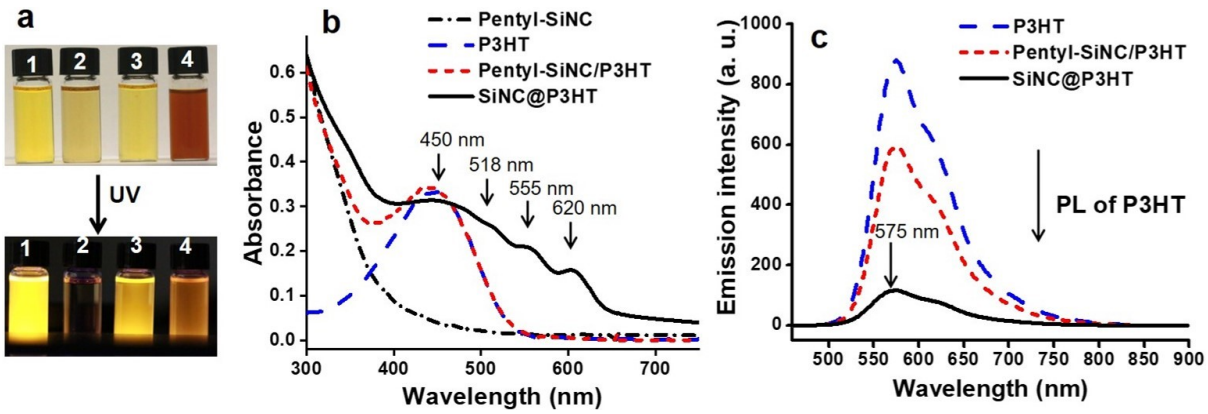

Figure 3-6. Photophysical properties of SiNC@P3HT. (a) Photographs of the dispersions of 1) P3HT, 2) pentyl-SiNC, 3) pentyl-SiNC/P3HT and 4) SiNC@P3HT in THF under ambient light (top) and the photoluminescence of the respective dispersions (bottom). (b) UV-Vis spectrum of a THF dispersion of all four types materials. (b) Emission spectra of P3HT, pentyl-SiNC/P3HT and SiNC@P3HT hybrid in THF (excitation wavelength 450 nm).

Consistent with the MALDI-TOF analysis of polymer obtained from the degrafting of SiNC@P3HT, the maximum absorption at 450 nm indicates the presence of low-molecular-weight P3HT.[361] The shoulders at 518, 555, and 620 nm only appeared in the spectrum of the covalently bonded hybrid. Similar features have been attributed to efficient delocalization of electrons through conjugated backbone planarization with the additional requirement of inter-chain aggregation of P3HT on the surface.[271]

Photoluminescence (PL) studies were used to evaluate the interfacial electronic communication between the P3HT and SiNCs (Figure 3-6c). The integrated PL intensity obtained

from the covalently bonded SiNC@P3HT hybrid shows an approximate 7-fold quenching of P3HT-based emission when compared to that of degrafted P3HT. In contrast, and highlighting the impact of the covalent surface linkage in the hybrid, only a 1.5-fold quenching of the P3HT-based PL was observed for the analogous physical mixture of degrafted P3HT and pentyl-SiNCs. Boon *et al.*[267] have postulated that similar observations for TiO_2@P3HT hybrids resulted from conjugated surface linkages facilitating efficient charge transfer at the donor-acceptor interface.

The combined energy and electron transfer efficiency may be determined for the present SiNC@P3HT hybrid using Equation (3-1):[362]

$$\Phi_{EET} = 1 - \frac{A_{P3HT}(\lambda_{exc})}{A_{Hybrid}(\lambda_{exc}) - A_{NC}(\lambda_{exc})} \times \frac{I_{Hybrid}}{I_{P3HT}} \quad \ldots\ldots\ldots (3-1)$$

where Φ_{EET} is the combined efficiency of electron and energy transfer, $A_{P3HT}(\lambda_{exc})$ is the absorption of degrafted P3HTat the excitation wavelength λ_{exc} and $A_{Hybrid}(\lambda_{exc})$ - $A_{NC}(\lambda_{exc})$ is the absorption of P3HT in the hybrid; I_{Hybrid} and I_{P3HT} are integrated PL intensity of P3HT with and without SiNCs, respectively. From these analyses, Φ_{EET} was found to be 83 % for the SiNC@P3HT hybrid and 24 % for pentyl-SiNC/P3HT physical mixture (*i.e.,* blend).

To gain further insight into the electronic properties of the SiNC@P3HT hybrids, we performed scanning tunneling microscopy and spectroscopy (STM and STS) measurements. Here, we position the STM tip over a single particle and acquire tunneling dI/dV−V spectra, which are proportional to the local density of states (DOS; details are given in the experimental section 3.2.9.8). The band-gap values extracted from these spectra (Figure 3-7) are about 1.4 eV, which is somewhat larger than the gap of bulk Si. This apparent band-gap widening is due to a combination of the (rather weak) quantum confinement and the voltage division between the two tunnel

junctions involved in the measurement (Figure 3-7).[358] Importantly, an in-gap spectral structure emerged in the DOS close to the valence-band (VB) edge, which is absent in spectra measured of alkyl functionalized SiNCs of the same size (11.2 ± 1.2 nm). This in-gap state can be associated with the HOMO level of P3HT, which is consistent with suggested models for Si-P3HT junctions.[363] The LUMO level should reside well within the conduction band of the SiNCs, where the DOS is relatively large, and therefore cannot be detected in our measurements.

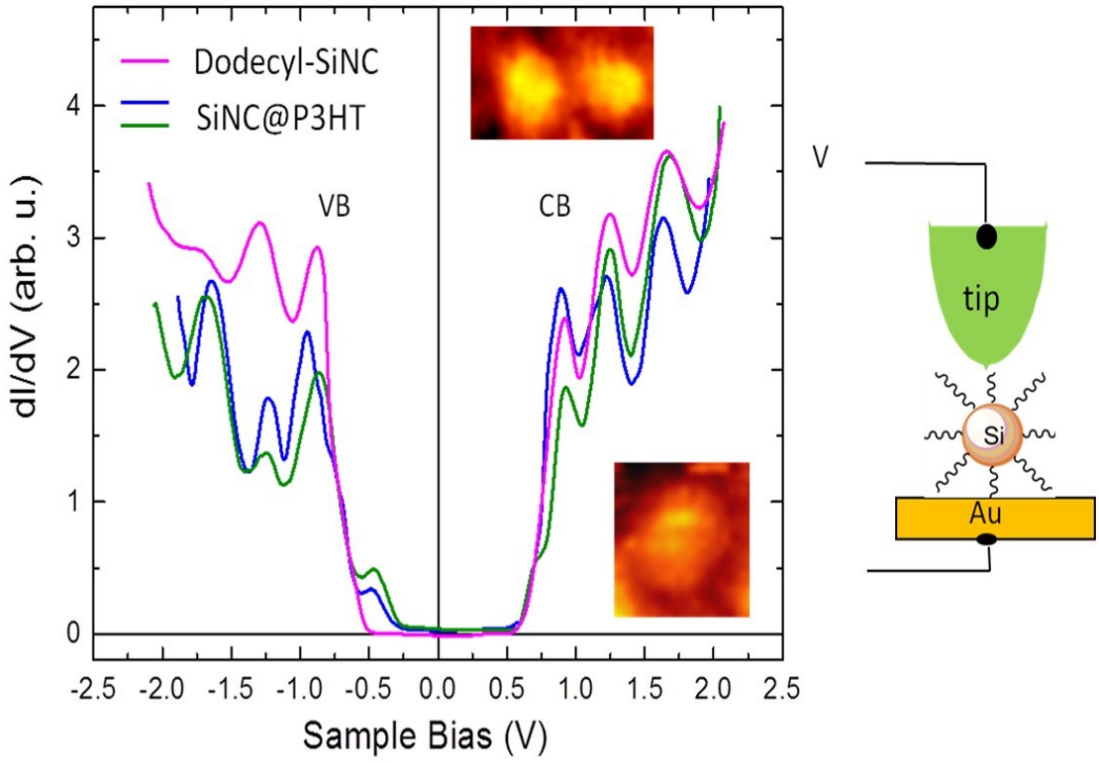

Figure 3-7. Tunneling dI/dV–V spectra measured at room temperature on SiNC@P3HT (green and blue curves), showing pronounced in-gap structure near the valence-band (VB) edge, which is absent in the spectrum acquired from a SiNC functionalized with dodecane (magenta curve). These states are attributed to the HOMO level of P3HT. The lower inset shows a topographic image of the NC on which the blue spectrum was measured, while the magenta curve was measured on the right NC shown in the upper topographic image. The double-barrier tunnel junction measurement configuration is shown to the right.

3.4 Conclusion

In conclusion, a covalently bonded SiNC@P3HT hybrid was successfully prepared by applying surface-initiated Kumada catalyst transfer polycondensation. The resulting hybrid exhibits physical and optical properties that differ substantially from those of a physical mixture of SiNCs and P3HT. The direct linkage of SiNC to P3HT through a conjugated covalent bond gives rise to new features in the absorption and tunneling spectra, along with enhanced interfacial electronic communication.

Chapter 4:

Phosphorus Pentachloride Initiated Functionalization of Silicon Nanocrystals

A version of this chapter has been published:

Islam, M. A.; Mobarok, M. H.; Sinelnikov, R.; Purkait, T. K.; Veinot, J. G. C. *Langmuir*, **2017**, *33*, 8766–8773.

4.1 Introduction

Silicon is abundant, environmentally benign and ubiquitous in electronic devices.[80,226,353] Recent progress in preparing SiNCs means tangible quantities of well-defined materials are available and the band gap of these systems may be tuned in the range of *ca*. 1.1–2.1 eV.[226,236] Tailoring SiNC surface chemistry also provides a convenient approach for designing their electronic[226] and optical properties.[354] These developments facilitated demonstrations of many prototype applications including photovoltaics,[253] light-emitting diodes,[364] batteries,[365] bioimaging,[366] drug delivery,[367] and catalysts.[350]

The formation of robust Si-C bonds by exploiting hydrosilylation reactions of surface Si-H moieties allows incorporation of surface-bonded organic layers that minimize the impact of oxidation and allow solution processability.[166–169,198,368] These surface reactions are often promoted using radical initiators.[167,197] In this vein, we recently demonstrated XeF_2 mediated reactions of hydride-terminated SiNCs can generate radical-rich surfaces that undergo rapid reactions with alkenes, alkynes, and ketones.[93] It is reasonable that other reagents that produce silicon surface radicals could afford similar effective surface modification protocols.

Chlorine plasmas have long been used to etch silicon surfaces; plasma activated molecular and atomic chlorine react with silicon surfaces forming a chlorinated layer.[369–372] Laser-induced chlorine radicals ($Cl^{\bullet}$) also etch silicon surfaces.[373] Phosphorus pentachloride (PCl_5) is a hypervalent compound like XeF_2 which generates $Cl^{\bullet}$ radicals and has been shown as a $Cl^{\bullet}$ radical source in organic synthesis.[374,375] It is also used as a chlorinating agent to obtain chloride-terminated Si surfaces.[376] These surfaces have been treated with Grignard or alkyl lithium reagent to obtain alkyl-passivated SiNCs.[210] As described in chapter 2, we have used PCl_5 as a chlorinating agent to prepare chloride-terminated SiNCs which were used to mediate the synthesis of P3HT.[350]

Of important note here, etching of bulk and nanocrystalline Si surfaces has been reported for PCl_5 mediated chlorination.[212,377–379]

Drawing on the established reactivity of XeF_2 with SiNCs,[93] we hypothesized that surface radicals formed during PCl_5 induced etching could initiate/mediate functionalization. Since PCl_5 is more moisture resistant, less stringent manipulations and handling protocols than those used for XeF_2 reactions will be required.

In this chapter, we report rapid room temperature functionalization of H-SiNCs with alkenes and alkynes *via* PCl_5 activated reactions. We also elucidate a reasonable reaction mechanism by monitoring key byproducts using multinuclear NMR spectroscopy. The functionalized SiNCs obtained from this procedure possess minimal surface oxidation and exhibit size-dependent red photoluminescence with exceptionally high quantum yields (QY ~ 62 ± 6 %).

4.2 Experimental

4.2.1 Reagents and Materials

Hydrogen silsesquioxane (HSQ, trade name Fox-17) was purchased from Dow Corning and the solvent was removed to yield a white solid that was used directly. Hydrofluoric acid (48 – 50 %) was purchased from Fisher Scientific and used as received. 1-pentene (≥ 98.5 %, sure sealed), 1-dodecene (95 %), methyl-10-undecenoate (96 %), 1-dodecyne (98 %) and phosphorus pentachloride (95 %) were purchased from Sigma-Aldrich and used as received. All solvents were reagent grade and used as received. Toluene was collected from a Pure-Solv purification system immediately prior to use.

4.2.2 Synthesis of Hydride-Terminated Silicon Nanocrystals

H-SiNCs were prepared using a well-established literature procedure.[157] Briefly, HSQ was thermally annealed in a Lindberg blue tube furnace at 1100 °C for 1 hour in a flowing 5 % H_2/95 % Ar atmosphere. The resulting SiNC/SiO_2 composite was mechanically ground using an agate mortar and pestle to yield a fine powder. The powder was shaken for *ca.* 8 h with d = 3 mm borosilicate glass beads using a wrist action shaker. The powder was suspended in 95 % ethanol, and collected by vacuum filtration with Millipore 0.45 μm PVDF hydrophilic membrane filter. H-SiNCs were obtained *via* HF etching of the ground composite (**Caution**! HF is dangerous and must be handled with extreme care and in accordance with local regulations). Typically, 200 mg of SiNC/SiO_2 composite was transferred to Teflon beaker; 3 mL Ethanol and 3 mL water were added under stirring. Afterword, 3 mL of 49 % HF aqueous solution was added to the suspension followed by stirring for 1 hour. The resulting cloudy yellow reaction mixture containing H-SiNCs was extracted using three 10 mL portions of toluene and H-SiNCs were isolated by centrifugation at 3000 rpm for 10 min. The H-SiNCs were redispersed into toluene and activated molecular sieves S4 (4Å) were added. The suspension was mixed thoroughly with the molecular sieves using a glass pipette to remove residual moisture, transferred to another test tube and isolated by centrifugation at 3000 rpm for 10 minutes (2×). This procedure provides *ca.* 20 mg of d~3 nm H-SiNCs that were suspended in dry toluene (7 mL) and transferred to a dry Schlenk flask for further modification. Larger (d~7 nm) H-SiNCs were obtained upon further annealing of the original SiNC/SiO_2 composite at 1300 °C for 1 hour under flowing Ar atmosphere followed by HF etching as outlined above.

4.2.3 PCl_5 Induced Etching of H-SiNCs

The 3 nm H-SiNCs (*ca.* 20 mg) isolated from the alcoholic HF mixture noted above were isolated and redispersed in benzene (5 mL). The benzene suspension of H-SiNCs was subsequently freeze-dried for ~ 12 hours providing yellow/brown H-SiNCs as a free-flowing powder. The powder was redispersed in 0.7 mL dichloromethane-d_2 (CD_2Cl_2) and transferred to a Teflon sealed J. Young NMR tube in a nitrogen-filled glovebox. Approximately 50 mg (0.23 mmol) of PCl_5 was added to the dispersion, and the NMR tube was sealed immediately. After 12 hours reaction with occasional agitation, the reaction mixture was evaluated using ^{1}H and ^{31}P NMR spectroscopy.

4.2.4 PCl_5-Initiated Functionalization of H-SiNCs with Toluene

A dry toluene (10 mL) dispersion of H-SiNCs (*ca.* 20 mg) was degassed by three freeze-pump-thaw cycles and warmed to room temperature. Subsequently, 20 mg of PCl_5 (0.1 mmol) was added, and the reaction was stirred for 30 minutes. The resulting turbid suspension was transferred to a 50 mL PTFE centrifuge tube in a nitrogen filled glovebox, and toluene functionalized SiNCs (Tol-SiNCs) were separated by centrifugation at 5000 rpm for 20 minutes. The supernatant was transferred to a separatory funnel; 20 mL of deionized water was added, shaken, and the aqueous layer was discarded. The toluene supernatant portion was analyzed by GC-MS to identify reaction by-products. The Tol-SiNCs were redispersed in toluene (50 mL) and separated by centrifugation at 12000 rpm for 20 minutes (2×). The purified Tol-SiNCs were analyzed by Fourier transform infrared (FT-IR) spectroscopy and X-ray photoelectron spectroscopy (XPS).

4.2.5 PCl_5-Initiated Functionalization of H-SiNCs with Alkenes and Alkynes

In a typical reaction, excess (*i.e., ca*. 3 mL) ligand of choice (*i.e.,* 12.8 mmol 1-dodecene, 13.8 mmol 1-dodecyne, 12.8 mmol methyl 10-undecenoate) was added to a dry toluene dispersion of H-SiNCs (7 mL; *ca.* 20 mg) in an oven-dried Schlenk flask. The nanocrystal dispersions were

subjected to three freeze-pump-thaw cycles using an Ar charged double manifold Schlenk line. After warming to room temperature 20 mg of PCl_5 (0.1 mmol) was added under flowing Ar and the dispersions were stirred for 2 hours at room temperature under Ar. The reaction mixtures became transparent within 30 - 60 minutes.

For hydrosilylation reactions involving 1-pentene, a slightly modified procedure was employed. First, the dry toluene (15 mL) dispersion of *ca.* 20 mg H-SiNCs was subjected to three freeze-pump-thaw cycles followed by warming to room temperature. Subsequently, 1-pentene (4 mL; 36 mmol) and 30 mg of PCl_5 (0.14 mmol) were added consecutively, and the reaction was stirred for 2 hours.

After the reaction mixture clarified, methanol (20 mL) was added to the Schlenk flask followed by stirring for 10 minutes. The resulting turbid suspension was transferred to a 50 mL PTFE centrifuge tube and ethanol (20 mL) was added. The alkyl functionalized SiNCs (R-SiNCs) were separated by centrifugation at 12000 rpm for 20 minutes. The R-SiNCs were redispersed in toluene (10 mL) with sonication, and methanol (20 mL) and ethanol (20 mL) were added to induce precipitation. The solid was isolated by centrifugation (12,000 rpm, 20 minutes). (Note: The anti-solvent of choice for methyl 10-undecenoate functionalized SiNCs was 10 mL methanol, 5 mL ethanol, and 25 mL hexane). This purification procedure was repeated twice. The purified R-SiNCs were dispersed in 5 mL dry toluene and activated molecular sieves S4 (4Å) were added. The suspension was mixed thoroughly with the molecular sieves using a glass pipette to remove residual moisture, transferred to a screw-capped glass vial and stored under ambient conditions prior to characterization.

4.2.6 Characterization

4.2.6.1 Fourier Transform Infrared Spectroscopy

SiNC samples were prepared as a thin film on a silicon wafer by drop casting from toluene. FT-IR spectra were recorded using a Thermo Nicolet Continuum FT-IR microscope. The silicon wafer with H-SiNCs film was maintained under inert atmosphere prior to acquiring spectra. The same silicon wafer was used for background subtraction in FT-IR data processing. FT-IR data were plotted using an OriginLab software. For the deconvolution of Si-H_x modes, the % transmittance data were converted to absorbance using the relationship A = 2- log (%T). The plots were fitted using Gaussian peak function described in the OriginLab tutorial for multiple peak fit.

4.2.6.2 Gas Chromatography-Mass Spectrometry

GC-MS analysis was performed using an Agilent GCD G1800A GC-MS and DB-5MS (25 m × 0.25 mm × 0.25-micron film thickness) column and helium carrier gas. The GC parameters for the presented study are: injection volume 1 µL, split ratio 50:1, gas flow rate 1 mL/min, initial temperature 50 °C, initial time 2.00 min, temperature increment rate 10 °C/min, final temperature: 280 °C, injection temperature: 280 °C, final time: 10.00 min.

4.2.6.3 Thermogravimetric Analysis

R-SiNCs samples were prepared as solid residue and transferred to a platinum pan. Weight loss was monitored in the temperature range of 35 to 700 °C at a temperature increment rate of 10 °C/min under Ar atmosphere using Mettler Toledo TGA/DSC 1 Star System. Surface coverage was evaluated from TGA plots assuming that the mass loss resulted from the loss of grafted organic surface groups. The number of surface groups per NC and surface coverage were estimated for compact icosahedral d = 3.5 nm SiNCs consisting of 1100 Si atoms of which 300 reside at the surface.[380] The surface coverage from TGA weight loss was calculated as follows:

$$\%\, Surface\ coverage = \frac{\%\, Experimental\ weight\ loss}{\%\, Theoritical\ weight\ loss} \times 100 \ldots\ldots\ldots (4-1)$$

$$\%\, Theoritical\ weight\ loss = \frac{Ligands\ theoretical\ weight}{Ligands\ and\ SiNCs\ theoretical\ weight} \times 100 \ldots\ldots (4-2)$$

$$SiNCs\ theoretical\ weight\ = \frac{N\ (Si)\ \times\ M\ (Si)}{N_A} \ldots\ldots\ldots (4-3)$$

$$Ligands\ theoretical\ weight = \frac{N\ (L)\ \times\ M\ (L)}{N_A} \ldots\ldots\ldots (4-4)$$

Where, $N\ (Si) =$ Total number of silicon atoms per nanocrystal

$N\ (L) =$ Total number of ligands per nanocrystal surafce

$M\ (Si) =$ Molar mass of Si

$M\ (L) =$ Molar mass of lignad

$N_A =$ Avogadro number

Substituting equation (4-3) and (4-4) into equation (4-2) and simplifying results in equation (4-5)

$$\%\, Theoretical\ weight\ loss = \frac{N\ (L)\ \cdot\ M\ (L)}{N\ (L)\ \cdot\ M\ (L) + N\ (Si)\ \cdot M\ (Si)} \times\ 100 \ldots\ldots\ldots (4-5)$$

4.2.6.4 Nuclear Magnetic Resonance Spectroscopy

^{1}H NMR and ^{31}P NMR spectra of the H-SiNC/PCl_5 reaction mixtures in CD_2Cl_2 were obtained consecutively using an Agilent/Varian 400 MHz NMR spectrometer. The purified R-SiNCs obtained from a specific reaction were dried by solvent evaporation. About 0.8 mL $CDCl_3$ was added to R-SiNCs and transferred to the NMR tubes. ^{1}H NMR spectra of purified R-SiNCs in $CDCl_3$ were obtained using a Varian Unity Inova Console 500 MHz NMR spectrometer.

4.2.6.5 X-ray Photoelectron Spectroscopy

R-SiNCs samples were deposited from toluene dispersions onto a copper foil. After drying, the foil was transferred to a Kratos AXIS 165 instrument. An air sensitive transfer system was used to transfer the Tol-SiNCs. The base pressure in the sample chamber was lower than 1×10^{-9} Torr. A monochromatic Al Kα source operating at 210 W with an energy hν = 1486.6 eV was used. Survey spectra were collected with an analyzer pass energy of 160 eV and step of 0.3 eV. For high-resolution spectra, the pass energy was 20 eV, and the step was 0.1 eV with a dwell time of 200 ms. The XPS data were processed and fit using CasaXPS (VAMAS) software. The process for XPS data fitting is the same as described in chapter 2.

4.2.6.6 Electron Microscopy

Bright-field transmission electron microscopy (TEM) images were acquired using a JEOL 2011 TEM with LaB_6 filament operating at an accelerating voltage of 200 kV. TEM samples were prepared by depositing a droplet of a dilute toluene suspension of functionalized SiNC onto a holey carbon-coated copper grid placed on a filter paper. The excess solvent was drawn into the filter paper, and the grid was dried in a vacuum chamber (0.1 mTorr) for at least 24 hours prior to data collection. The NC size was obtained by evaluating 300 particles using Image J software (version 1.45). High-resolution (HR) TEM images were obtained using a Hitachi-9500 electron microscope with an accelerating voltage of 300 kV. The HRTEM images were processed using Gatan Digital Micrograph software (Version 2.02.800.0).

4.2.6.7 Powder X-ray Diffraction

XRD data were collected using an Intel Multi-Purpose Diffractometer equipped with a CPS 120 curved position-sensitive X-ray detector and a Cu Kα (8.047 S5 KeV energy) source. A concentrated toluene dispersion of functionalized SiNCs (20 mg/mL) was deposited onto a Si (111) wafer substrate.

4.2.6.8 UV-Vis and PL Spectroscopy

Toluene dispersions of R-SiNCs were prepared such that their absorbance at 290 nm was ~ 1 for all samples. The UV-Vis absorption spectra of the various dispersions were recorded using Hewlett Packard 8453 UV-Vis spectrophotometer. An argon ion laser with 351 nm emission wavelength was used to excite SiNCs suspended in toluene. The resulting photoluminescence was collected by an optic fiber, passed through a 400 nm long-pass filter to eliminate scattered light from the excitation source and fed into an Ocean Optics USB2000 spectrometer. The spectral response was calibrated by a black-body radiator (Ocean Optics LS1).

Qualitative evaluation of sample brightness was achieved by preparing toluene suspensions of equal concentrations (as indicated by their absorbance at 350 nm) of dodecyl-SiNCs (functionalized using thermal and PCl_5 initiated methods). Emission spectra of the corresponding dispersions were recorded as noted above.

4.2.6.9 Photoluminescence Lifetime

PL lifetimes were acquired upon illuminating a quartz cuvette containing a toluene solution of the R-SiNCs in question using a modulated argon ion laser (351 nm, ~20 mW). The laser was modulated by an acousto-optic modulator operating at 200 Hz. Emission from the SiQDs was channeled into a photomultiplier (Hamamatsu H7422P-50) connected to a photon counting card (PMS-400A). Lifetime decay data was fit to a stretched exponential function in Mathematica (Version 10) given by $I(t) = I_o [\exp(-(t/\tau)\beta)] + C$, where I_o is the initial photon intensity, τ is the effective lifetime, and β is a stretching parameter that can vary between 0 and 1 (smaller values indicate broader lifetime distributions).[381]

4.2.6.10 PL Quantum Yield Measurements

The R-SiNCs were suspended in toluene and diluted such that the solution absorbance was below 0.1 at 445 nm. Absolute photoluminescent QYs were measured using a HORIBA K-Sphere Petite integrating sphere (diameter: 3.2 inches), equipped with a xenon lamp (185 – 850 nm) with a wavelength-selecting monochromator for the excitation. All measurements were carried out using a 445 nm excitation wavelength. Spectra of the sample suspension and the reference (*i.e.,* toluene) were corrected for system response, and the reference response was subtracted from the sample (*i.e.,* used as a background). The absolute quantum yield was determined by taking the appropriate ratio of excitation and emission peak areas and applying the following equation:[382]

$$\phi = \frac{\#\ Emitted\ photons}{\#\ Absorbed\ photons} = \frac{\int I_{em(\lambda)}^{sam} - I_{em(\lambda)}^{ref} d\lambda}{\int I_{ex(\lambda)}^{sam} - I_{ex\,(\lambda)}^{ref} d\lambda} \ldots\ldots\ldots (4-6)$$

where,

$I_{em(\lambda)}^{sam} =$ intensity of emitted light from the SiNCs sample

$I_{em(\lambda)}^{ref} =$ intensity of background emission measured with reference cuvette

$I_{ex(\lambda)}^{sam} =$ excitation light intensity measured with SiNCs sample

$I_{ex(\lambda)}^{ref} =$ excitation light intensity measured with reference cuvette.

4.3 Results and Discussion

To evaluate the reactivity of PCl_5 toward H-SiNCs, PCl_5 was added to a dispersion of H-SiNCs in CD_2Cl_2 in sealed J-Young NMR tube. The reaction by-products were analyzed by ^1H and ^{31}P NMR spectroscopy. The ^{31}P NMR spectrum (Figure 4-1a) displays two prominent singlets at δ –80.9 ppm and δ 219.5 ppm, which are assigned to PCl_5 and PCl_3, respectively.[383] The ^1H NMR spectrum (Figure 4-1b) shows a set of singlet resonances (centered at δ 6.17 ppm, $^1JSi,H$ =

370.25 Hz; δ 5.48 ppm, ^{1}JSi,H = 286.17 Hz; δ 4.63 ppm, ^{1}JSi,H = 241.64 Hz), which are attributed to dissolved $HSiCl_3$, H_2SiCl_2, and H_3SiCl, respectively.[384]

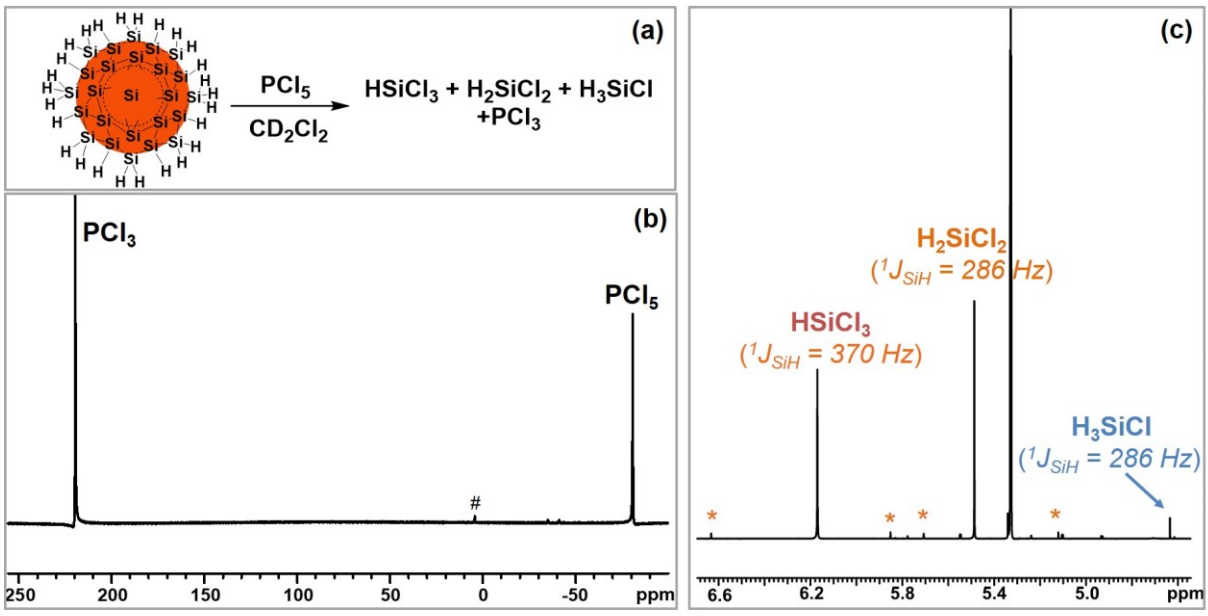

Figure 4-1. a) A schematic representation of the reaction of H-SiNCs with PCl_5. b) ^{31}P NMR and c) ^{1}H NMR spectra of the reaction mixture of H-SiNCs with PCl_5 in CD_2Cl_2. # denotes $POCl_3$ arising from PCl_5 hydrolysis and * indicates ^{29}Si satellites.

In the context that PCl_5 etches Si surfaces, the production of chlorosilanes (*i.e.,* $HSiCl_3$, H_2SiCl_2 and H_3SiCl) is not unexpected given the FT-IR spectrum of H-SiNCs shows three Si-H stretching modes at 2085, 2100, and 2137 cm^{-1} (Figure 4-2a).[197] These observations are consistent with PCl_5 removing the outermost atoms of H-SiNC surface and suggests the formation of transient surface radicals during etching. Based upon the peak areas of the ^{1}H resonances the relative distribution of the chlorosilanes ($HSiCl_3$: H_2SiCl_2 : H_3SiCl) is 0.69:0.30:0.01 For comparison, the relative SiNC surface concentrations of Si-H_x species can be obtained by deconvoluting the overlapping peaks in the Si-H_x stretching region of the FT-IR spectrum (Figure 4-2a).[197] Consistent with the present ^{1}H NMR analysis, ≡SiH (75.0 %) is the dominant surface species followed by =SiH_2 (17.4 %) and –SiH_3 (7.6 %). Despite the agreement between the chlorosilane product

distribution and the relative concentration of surface silicon hydride species, this data should be considered in the context that PCl_5 can remove more than the just the surface atoms.

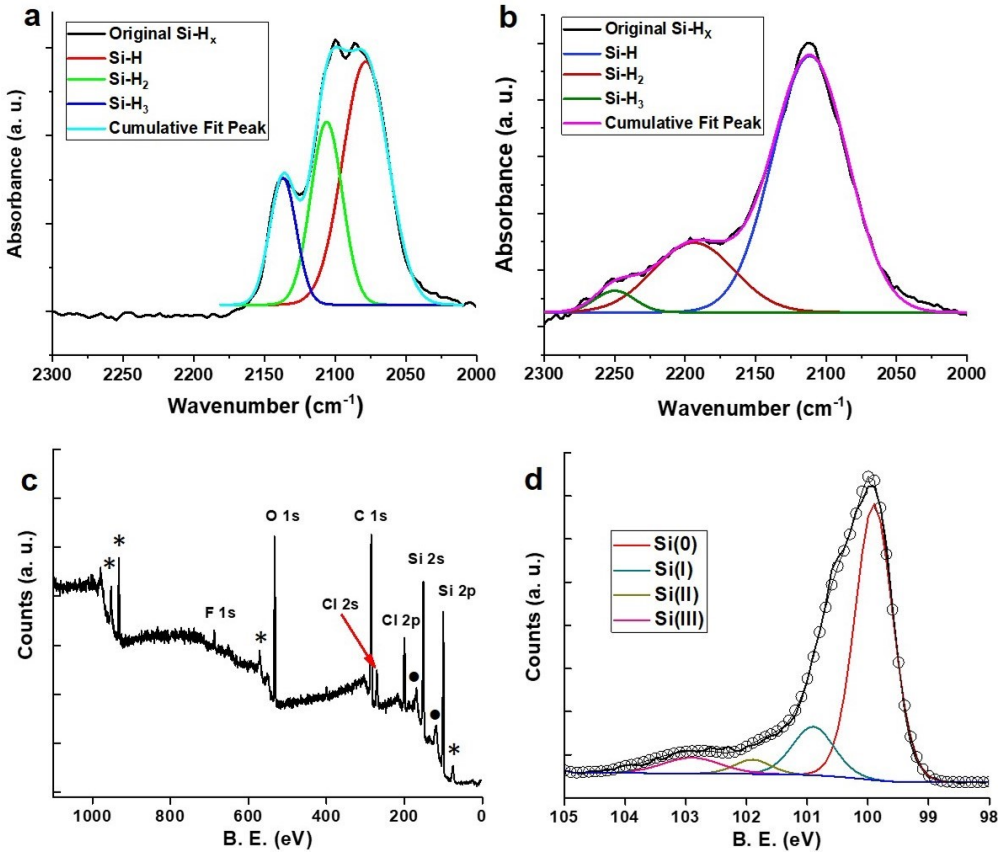

Figure 4-2. Deconvoluted ν(Si-H_x) regions of the FT-IR spectrum of d~3.4 nm SiNCs (a) freshly etched/freeze-dried H-SiNCs, (b) after reaction with PCl_5 in toluene showing substantial reduction of peak intensity of $=SiH_2$ and $–SiH_3$ compared to ≡SiH (Note: A shift to higher energy is noted in the Si-H region in the IR spectra upon reaction with PCl_5. This shift to high energy is tentatively attributed to the influence of electron withdrawing nature of surface chloride- and oxide-based species; peak broadening may be originating from the varition in the extent of chlorination and oxidation of the surface silicon atoms on different regions). (c) Survey (d) high-resolution (Si2p emission) XP spectra of d~3.4 nm H-SiNCs after reaction with PCl_5 in toluene; residual fluorine is from HF etching. • represents the Si satellite peaks, * denotes the Cu emissions from the substrate.

Activation and direct bonding of the toluene aromatic ring with H-SiNCs was observed upon XeF_2 treatment in absence any other reactive substrates.[93] In this context, we investigated possible reactions between H-SiNCs treated with PCl_5 and toluene. A survey XP spectrum of the

resulting product (Figure 4-2c) confirms the presence chlorine (7.70 %) and oxygen (11.41 %) in addition to silicon (43.25 %) and carbon (37.65 %). Surface oxidation is expected given the limited ability of surface bonded toluene to passivate/protect the underlying SiNC surface (Figure 4-2d). The Si-H_x stretching region of the FT-IR spectrum (Figure 4-2b) of the PCl_5 treated particles shows the presence of ν(Si–H_x) features suggesting that all of the surface atoms are not eliminated upon reaction for a given time with a given amount of PCl_5. The stretching modes ≡SiH, =SiH_2 and –SiH_3 are shifted to higher energy at 2112, 2192, and 2250 cm^{-1} presumably due to the electron withdrawing surface chloride and/or oxide. Interestingly, the relative intensity of =SiH_2 stretching mode is significantly diminished while the –SiH_3 stretching mode is almost disappeared compared to ≡SiH. This suggests that silyl radical $^{\bullet}SiH_3$ abstraction by the $Cl^{\bullet}$ is favoured.[197] In addition, (Figure 4-3b) prominent features associated with ν(C-H_x) vibrational (2950 - 2850 cm^{-1}) and bending (~1450 cm^{-1}) modes are present that may be attributed to the cycloaddition of the toluene aromatic ring to the PCl_5 etched SiNC surface diradical [93] followed by hydrosilylation of the remaining unsaturated double bonds and possibly the benzyl radical generated by $H^{\bullet}$ radical abstraction from toluene by $Cl^{\bullet}$. These processes would lead to the loss of toluene aromaticity and formation of surface-bonded methylcyclohexyl type species. The formation of benzyl chloride, ortho-benzyltoluene and para-benzyltoluene are evaluated using GC-MS (Appendix C). The observation of these products suggests that the $Cl^{\bullet}$ or transient surface $\equiv Si^{\bullet}$ radical abstract $H^{\bullet}$ from methyl group of toluene resulting in benzyl radical $C_6H_5CH_2^{\bullet}$, which can yield the observed products by radical attack. Alternatively, the (C-H_x) vibrational and bending modes may be arising from the surface alkyl groups originating from the functionalization of SiNCs with unsaturated hydrocarbon impurities in the reaction system. No conclusion can be made about the activation and functionalization with toluene just from the FTIR data.

With observations suggesting the formation of transient surface radical in hand, we set out to explore PCl_5 induced reactivity of several alkenes and alkynes with H-SiNCs (Scheme 4-1). In a typical functionalization procedure, solid PCl_5 was added to a cloudy mixture of H-SiNCs and ligand of choice in toluene. After 30 minutes of PCl_5 addition, the reaction mixture became transparent: an observation that has previously been considered an indication of the formation of sterically stabilized colloidal suspensions.[93] To investigate the scope of this protocol we evaluated a series of reagents bearing carbon-carbon (*e.g.,* alkenes, alkynes) multiple bonds. We also found the reaction proceeded with SiNCs with diameters of 3.4 and 7.0 nm to yield transparent colloids within *ca.* 30 minutes.

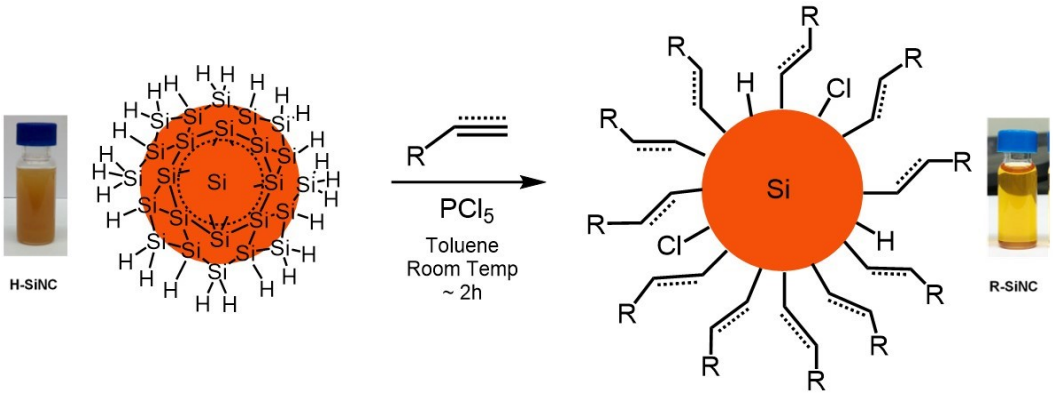

Scheme 4-1. PCl_5 initiated functionalization of H-SiNCs with alkenes/alkynes.

Fourier transform-infrared spectroscopy (FT-IR) was used to gain insight into the apparent SiNC surface functionalization. After PCl_5-mediated surface modification, all spectra (Figure 4-3c-f) display prominent ν(C-H_x) vibrational (2950 - 2850 cm^{-1}) and bending (~1450 cm^{-1}) modes associated with alkyl groups as well as additional characteristic spectral features specific to the surface bonded moiety. For example, 1-dodecyne treated SiNCs exhibit (Figure 4-3e) ν(=CH) and ν(C=C) vibration at 3010 and 1645 cm^{-1}, consistent with hydrosilylation of C≡C bonds and formation of 'Si–C=C(H)–R' surface species. Similarly, ν(C=O) and ν(C-O) stretching modes appear at *ca.* 1700 and 1200 cm^{-1} respectively, for SiNCs modified with methyl-10-undecenoate

(Figure 4-3f). In addition, the spectra of all functionalized SiNCs show a broadened ν(Si–H_x) feature that is of diminished intensity compared to the starting H-SiNCs.

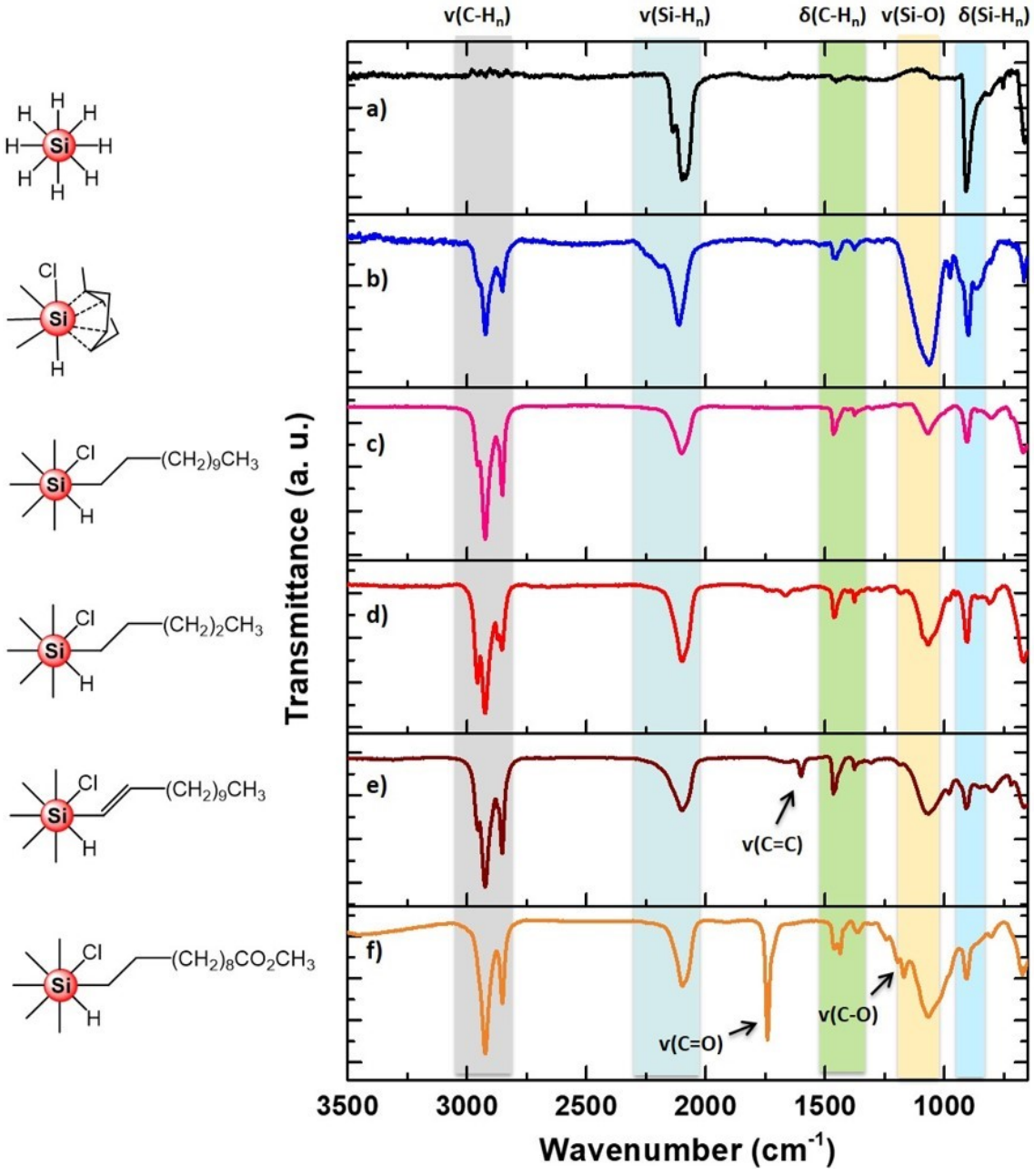

Figure 4-3. FT-IR spectra of 3.4 nm H-SiNCs (a) before and after functionalized with the following reagents in the presence of PCl_5: (b) toluene (c) 1-dodecene, (d) 1-pentene, (e) 1-dodecyne, (f) methyl-10-undecenoate.

Equivalent observations are noted in the FT-IR (Figure 4-4) spectra of d = 7.0 nm SiNCs functionalized with equivalent ligands.

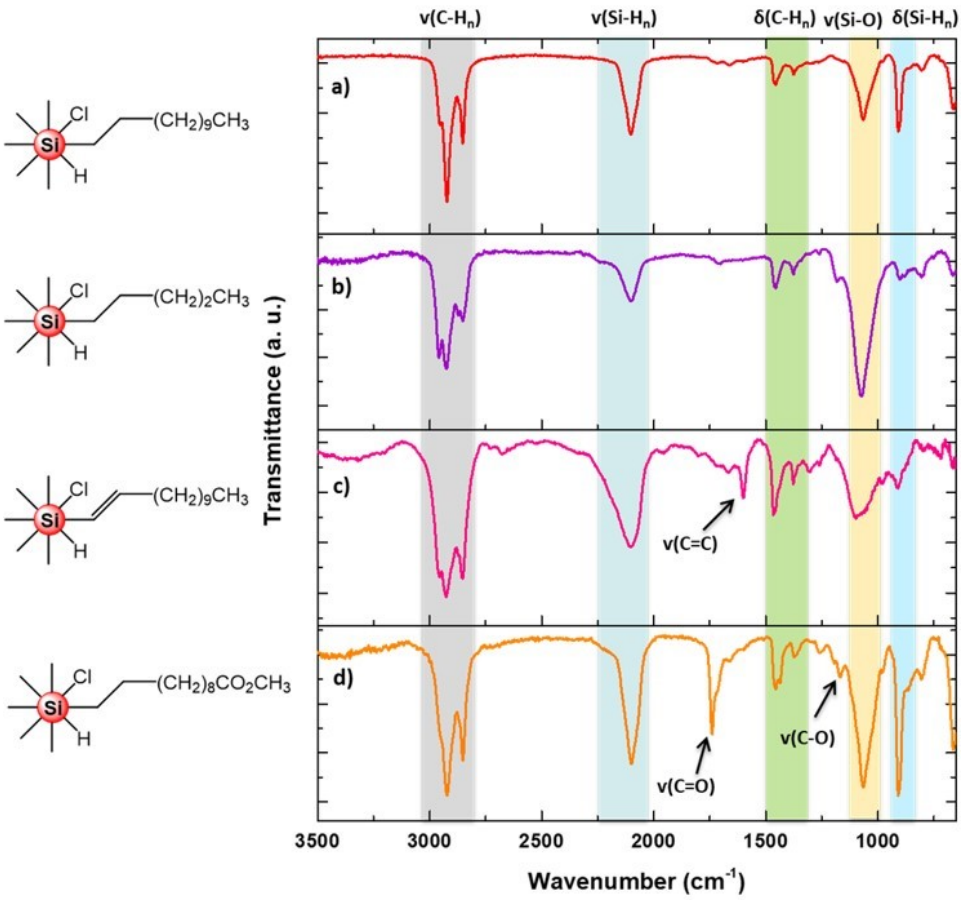

Figure 4-4. FT-IR spectra of 7 nm SiNCs after functionalization with the following reagents in the presence of PCl_5: (a) 1-dodecene, (b) 1-pentene, (c) 1-dodecyne, (d) methyl-10-undecenoate.

^{1}H NMR spectroscopy provides information regarding the proton environments on surface ligands and more conclusive identification of SiNC surface modification. The ^{1}H NMR spectrum of SiNCs functionalized with 1-dodecene in $CDCl_3$ (Figure 4-5a) is representative of those obtained in the present study. It shows resonances from terminal methyl protons at ~0.9 ppm and methylene chain protons in the range of ~1.1 to 1.6 ppm. Broadening of ^{1}H NMR resonance peaks of the functionalized SiNCs has previously been attributed to long relaxation times resulting from slow rotation of surface bonded ligands on SiNCs.[188] As expected, the ^{1}H NMR spectrum of dodecyne-functionalized SiNCs acquired in $CDCl_3$ (Figure 4-5b) shows resonances associated with terminal methyl protons at 0.9 ppm and methylene protons in the range of 1.1−1.6 ppm as a

broad peak. Features arising from vinylic protons on the nanoparticle surfaces usually appear between ~5 and 6 ppm; however, they were not observed in the present ^{1}H NMR, as these protons were closely associated with the nanocrystal surface.[188] The ^{1}H NMR spectrum of methyl 10-undecenoate functionalized SiNCs acquired in $CDCl_3$ (Figure 4-5c) clearly showed resonances from terminal methyl ester protons (marked as 'a') with a chemical shift at 3.65 ppm and methylene proton bonded to C=O (marked as 'b') with a with a chemical shift at 2.31 ppm as well as the methylene protons (marked as 'c') with chemical shifts in the range of 1.1−1.6 ppm.

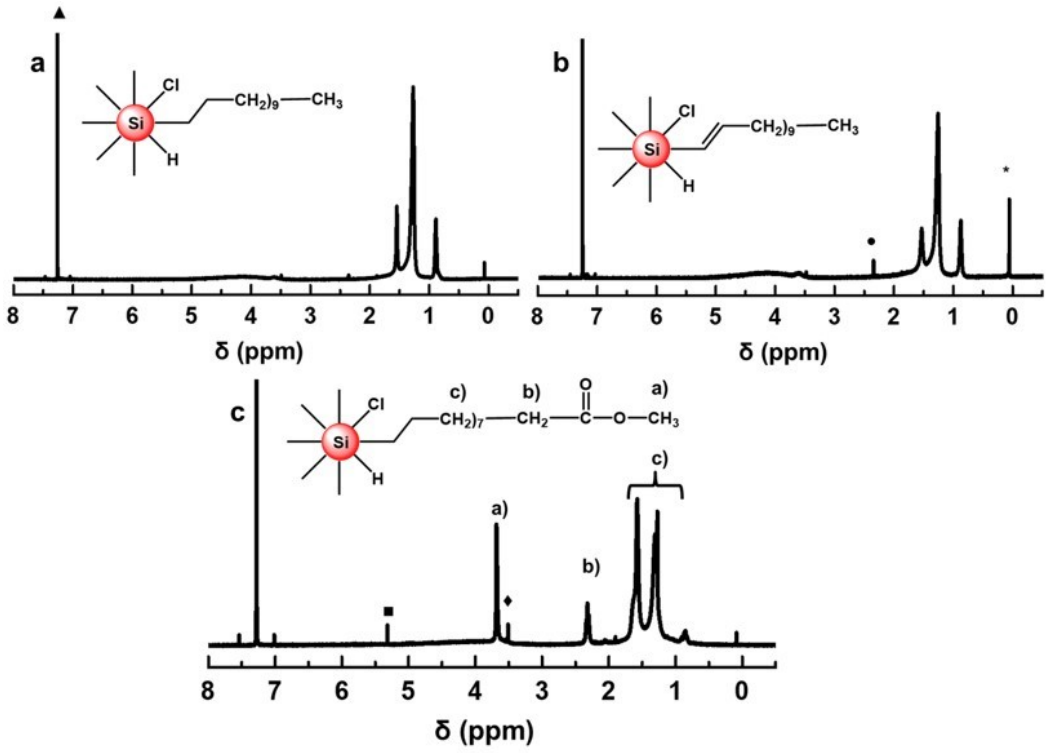

Figure 4-5. ^{1}H NMR spectra of ~3.4 nm SiNCs functionalized with: 1-dodecene (a), 1-dodecyne (b) and methyl-10-undecenoate (c) in $CDCl_3$. ▲$CHCl_3$ from NMR solvents; ● toluene, ♦ methanol, ■ dichloromethane solvents from work up and * silicon grease.

XPS was used to evaluate the NC composition, as well as the oxidation state of the constituent elements. In all cases, the R-SiNCs obtained from PCl_5 mediated reactions contain silicon, carbon, oxygen, and chlorine (Figure 4-6 a-d).

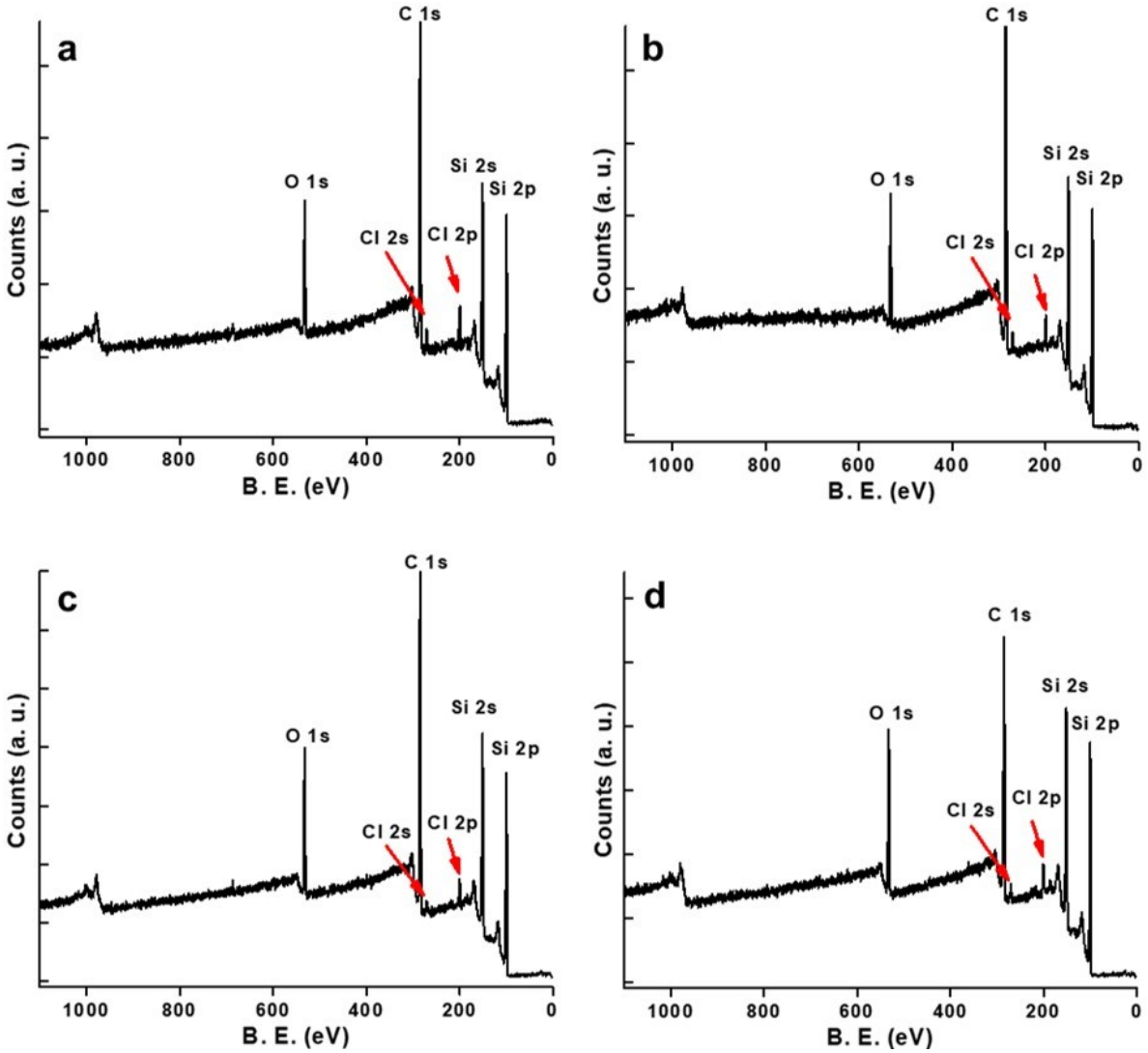

Figure 4-6. Survey XP spectra of 3.4 nm SiNCs obtained from PCl_5 mediated functionalization with: (a) 1-dodecene (Si 38.8 %, C 51.7 %, O 6.7 %, Cl 2.8 %), (b) 1-pentene (Si 34.7 %, C 57.6 %, O 5.8 %, Cl 1.9 %), (c) 1-dodecyne (Si 39.9 %, C 50.6 %, O 7.5 %, Cl 1.9 %), (d) methyl-10-undecenoate (Si 43.8 %, C 44.6 %, O 9.5 %, Cl 2.1 %).

Figures 4-7 a-d show Si 2p emissions of 3.4 nm SiNCs after functionalization. Minimal oxidation is observed and in all cases Si(0) is the dominant component of the Si-based spectral feature. Consistent with pendant ester groups, the XP spectrum of methyl 10-undecenoate functionalized SiNCs (Figure 4-7e) display prominent C=O (289.2 eV) and C–O components

(286.4 eV) in C 1s emission. Some surface chlorination is observed for all functionalized SiNCs (atomic concentration 4.8-7.2 % *vs.* silicon) (Figure 4-7f).

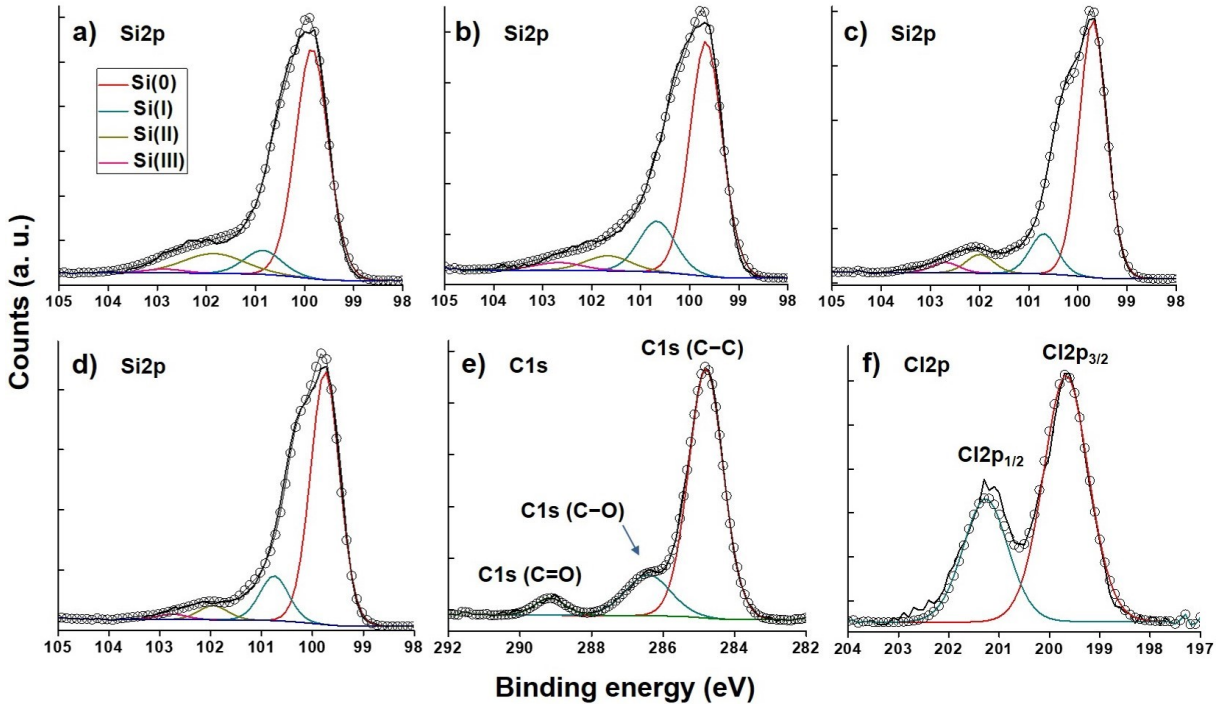

Figure 4-7. Representative high-resolution XP spectra of ~3.4 nm SiNCs functionalized with (a) 1-dodecene, (b) 1-pentene, (c) 1-dodecyne, (d) methyl-10-undecenoate; e) and f) are the C 1s and Cl 2p high-resolution spectra of methyl-10-undecenoate and 1-dodecene functionalized SiNCs, respectively.

Larger (d = 7.0 nm) R-SiNCs functionalized with the same ligands show similar characteristic XP features (Figure 4-8 and 4-9).

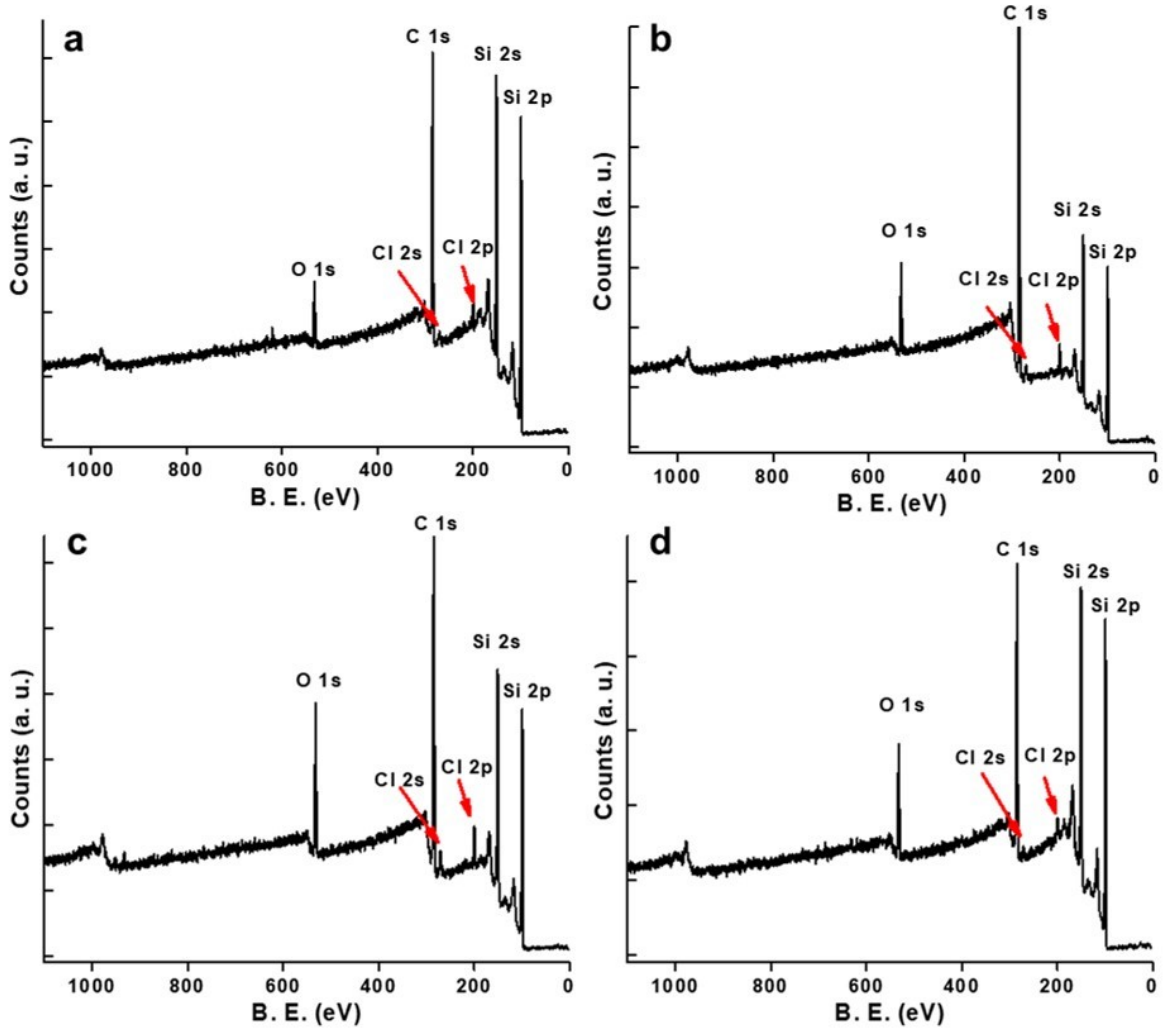

Figure 4-8. Survey XP spectra of 7.0 nm SiNCs obtained from PCl5 mediated functionalization with: (a) 1-dodecene (Si 52.5 %, C 42.8 %, O 3.2 %, Cl 1. 5 %), (b) 1-pentene (Si 28.1 %, C 66.1 %, O 4.1 %, Cl 1.6 %), (c) 1-dodecyne (Si 38.3 %, C 52.6 %, O 6.4 %, Cl 2.7 %), (d) methyl-10-undecenoate (Si 51.6 %, C 41.3 %, O 6.2 %, Cl 1.0 %).

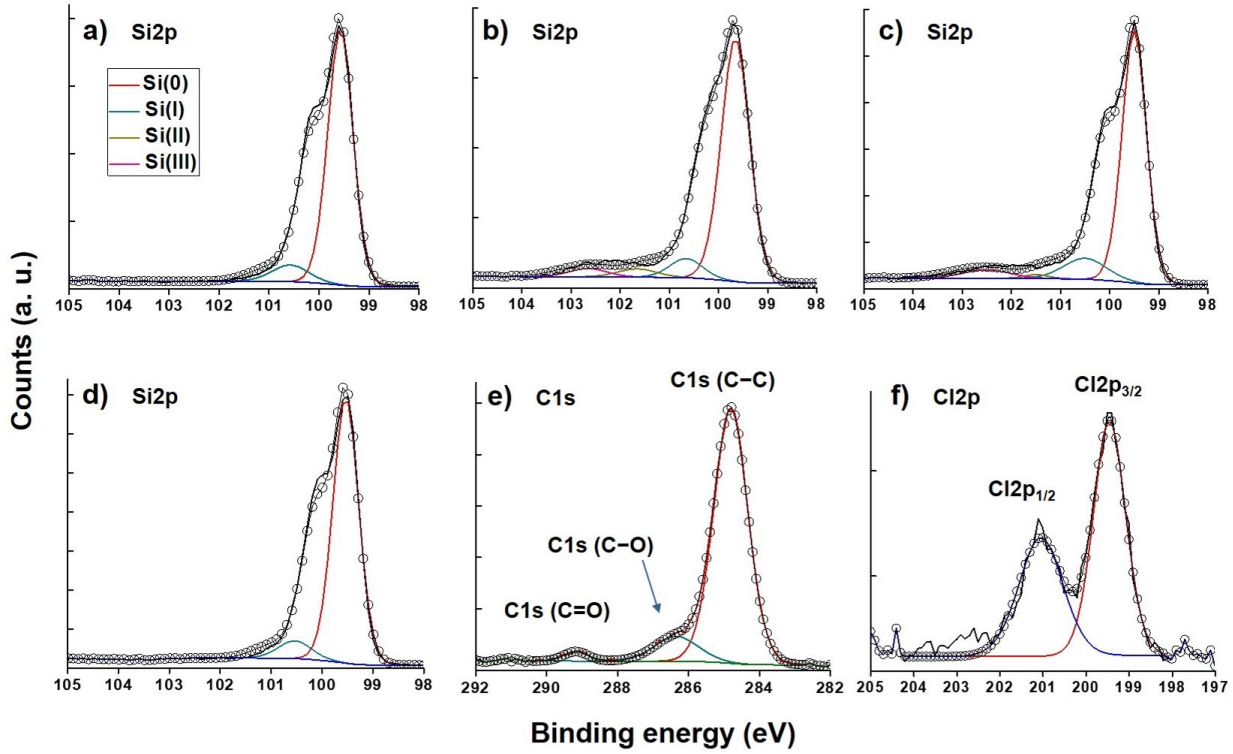

Figure 4-9. Representative high-resolution XP spectra of 7.0 nm SiNCs functionalized with (a) 1-dodecene, (b) 1-pentene, (c) 1-dodecyne, (d) methyl-10-undecenoate; e) and f) are the C 1s and Cl 2p high-resolution spectra of methyl-10-undecenoate and 1-dodecene functionalized SiNCs, respectively.

An estimate of the degree of surface coverage was obtained from thermogravimetric analysis (TGA), which lay in the range of 27 − 82 % (Figure 4-10 and Table 4-1). The surface coverage for dodecyl-SiNCs was also compared with that obtained through thermal hydrosilylation. Thermal hydrosilylation provides significantly higher surface coverage, presumably the result of previously identified surface oligomerization.[179]

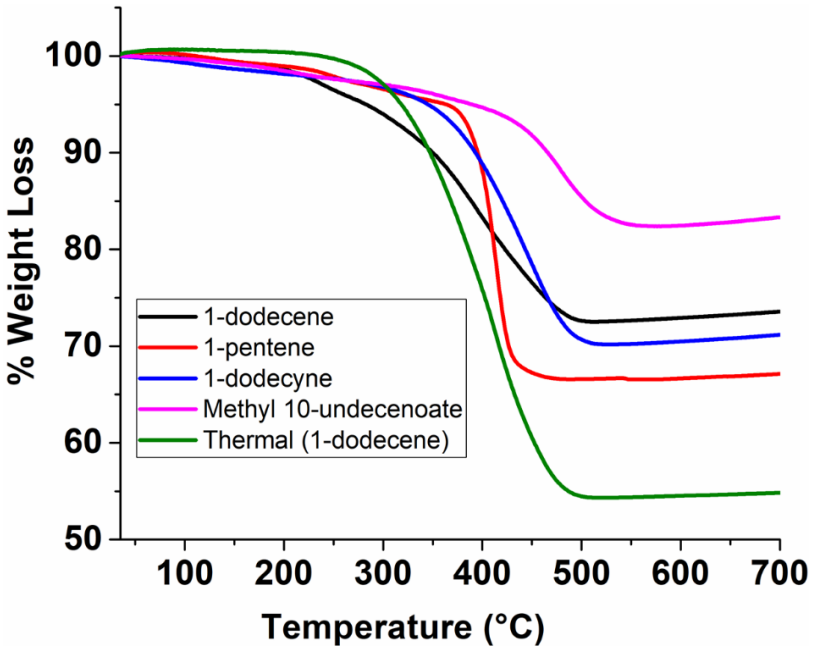

Figure 4-10. TGA weight loss plot for 3.4 nm SiNC after PCl_5 initiated functionalization with 1-dodecene, 1-pentene, 1-dodecyne, and methyl 10-undecenoate and thermal hydrosilylation with 1-dodecene.

Table 4-1. Surface coverage metrics of 3.4 nm SiNCs functionalized with different ligands, determined by using TGA analysis.

Ligands	Theoretical Weight Loss (%)*	Experimental Weight loss (%)	% Surface Coverage
1-dodecene	62.2	27.5	44.2
1-pentene	40.9	33.7	82.4
1-dodecyne	61.9	29.7	48.0
Methyl 10-undecenoate	65.9	17.6	26.7
Thermal (1-dodecene)	62.2	45.9	73.8

The average sizes of the dodecyl functionalized SiNCs were evaluated by transmission electron microscopy (Figures 4-11a–h). No statistically significant difference is noted for SiNC sizes obtained from PCl_5 functionalization (d = 3.4 ± 0.4 nm and 7.0 ± 1.2 nm) when compared to that obtained for analogous thermally initiated hydrosilylation (d = 3.7 ± 0.4 nm and 7.1 ± 1.3 nm). This is in stark contrast to previous observations for XeF_2-mediated functionalization, which always accompanied by 15-20 % reduction of particle size[93] and is attributed to the milder nature

of the PCl_5 etchant. Confirming the nanocrystalline core of the present SiNCs is maintained throughout functionalization, XRD (Figure 4-11i) and HRTEM (Figure 4-11a,c insets) show broadened reflections and lattice fringes characteristic of crystalline silicon.

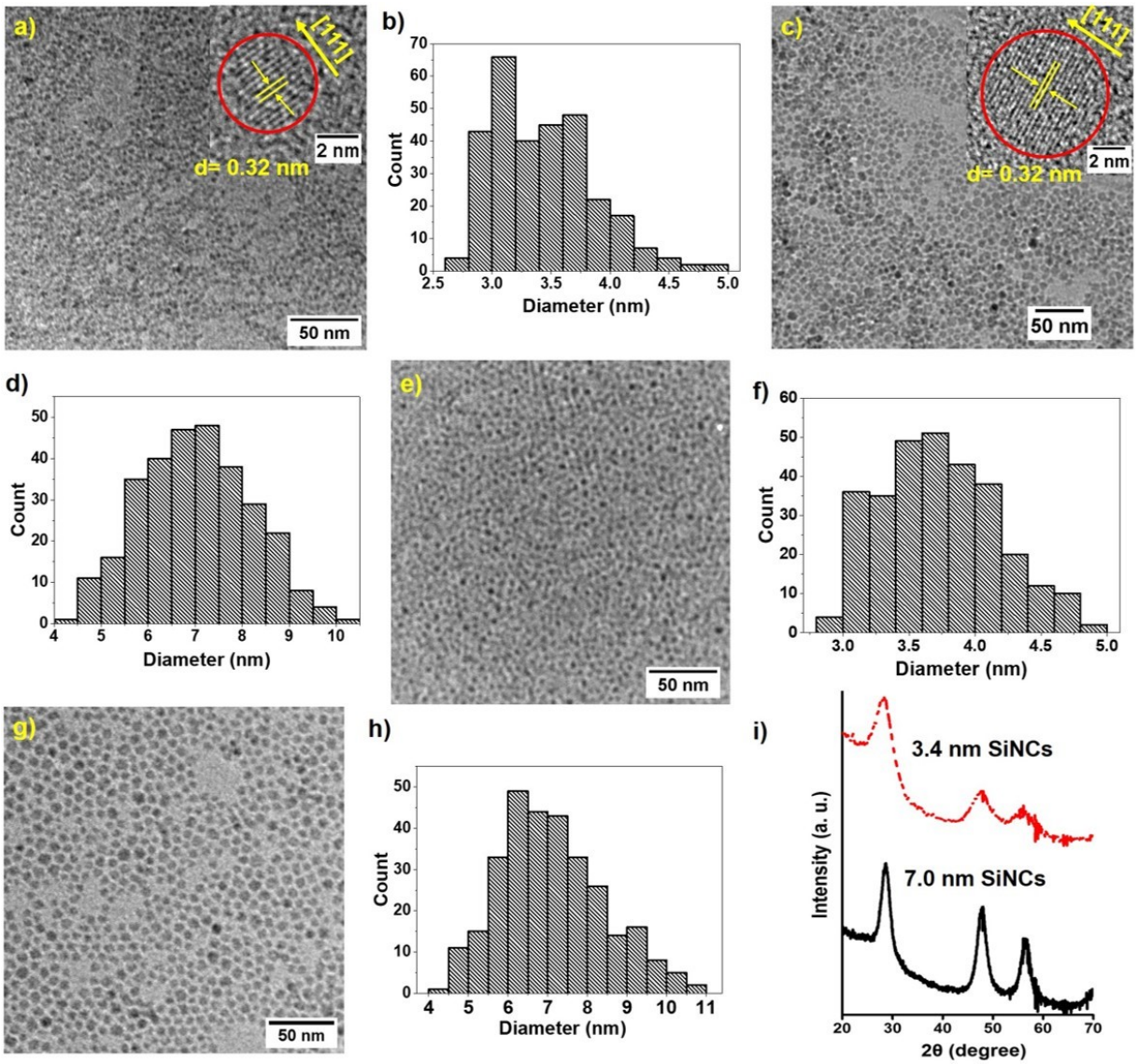

Figure 4-11. Representative TEM, HRTEM (insets) and size distribution analysis of d = 3.4 ± 0.4 nm (a, b) and 7.0 ± 1.2 nm dodecyl-SiNCs (c, d) obtained by PCl_5 initiated functionalization. (e, f) and (g, h) are the TEM images and size distribution analysis of d = 3.7 ± 0.4 nm and 7.1 ± 1.3 nm dodecyl-SiNCs obtained by thermal hydrosilylation. (i) XRD patterns of 3.4 and 7.0 nm dodecyl-SiNCs from PCl_5 initiated functionalization.

Toluene dispersions of SiNCs functionalized with all four ligands investigated here are transparent and exhibit featureless absorption spectra consistent with other reports of functionalized SiNCs (Figure 4-12a,b).[93] Upon functionalization with saturated alkyl groups (*e.g.,* 1-dodecene, 1-pentene, methyl-10-undecenoate) the PL maximum is size-dependent (Figure 4-12c,d).

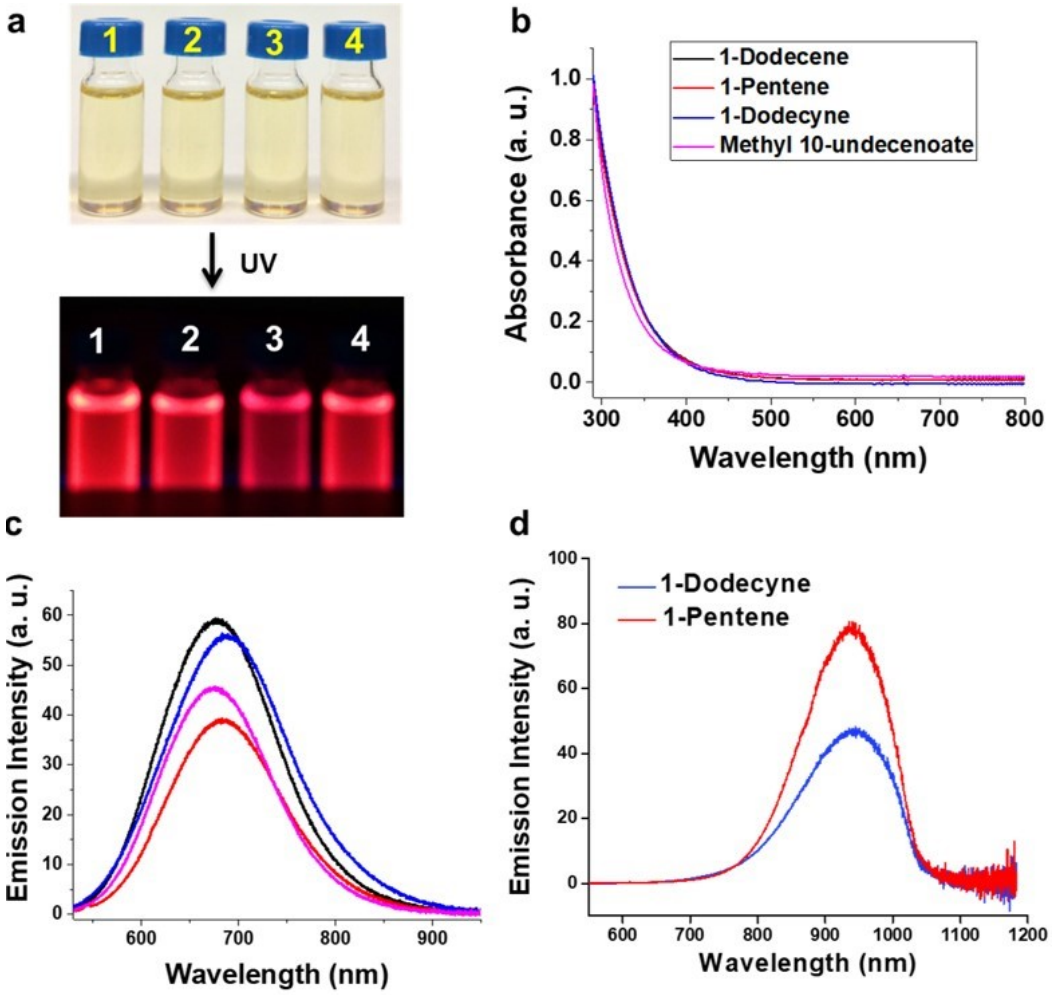

Figure 4-12. Optical properties of 3.4 nm SiNCs functionalized with indicated ligands in the presence of PCl_5 initiator. (a) A photograph of toluene dispersions of SiNCs functionalized with 1) 1-dodecene, 2) 1-penetene, 3) 1-dodecyne, 4) methyl 10-undecenoate (under ambient and 365 nm illumination, (b) UV-Vis absorption and (c), (d) PL emission spectra of the 3.4 nm and 7.0 nm SiNCs functionalized with the indicated ligands (351 nm excitation wavelength).

Previously it has been observed that the presence of surface chlorine-based species (*e.g.,* oxychlorides) leads to blue PL arising from surface states.[212] Surprisingly, in the present case we observe size-dependent PL despite the presence of residual chlorine suggesting the identity of the chlorine-based species is important to the PL response. Furthermore, in all cases, microsecond excited-state lifetimes were observed, consistent with PL originating from indirect band gap transitions (Figure 4-13). The origin of this different behavior is the subject of ongoing study.

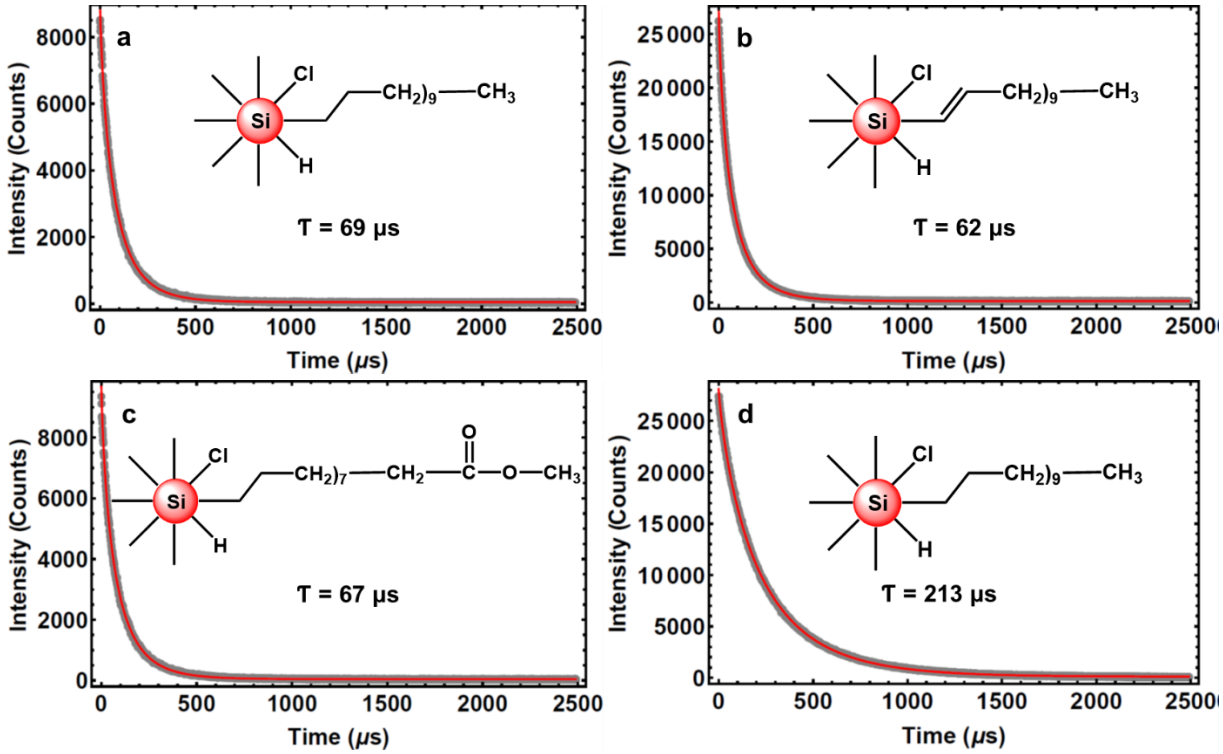

Figure 4-13. Photoluminescence lifetime decay of 3.4 nm (a-c) and 7 nm (d) SiNC after functionalization with indicated ligands. The grey circles are the raw data and the red line is the stretched-exponential fitting from which we obtained the lifetime.

The PL response of SiNCs is an attractive, and potentially useful material property. For comparison, the PL of dodecyl-SiNC obtained with PCl_5 initiated functionalization was compared with conventional thermal hydrosilylated dodecyl-SiNC. Toluene solutions of dodecyl-SiNCs (thermal and PCl_5 initiated methods) were prepared with identical concentrations confirmed using

UV-Vis spectroscopy (Figure 4-14a). The integrated PL intensity of the solution containing dodecyl-SiNCs obtained from the PCl_5 initiated reaction was about 3 times that of the solution containing dodecyl-SiNCs prepared using standard thermal hydrosilylation (Figure 4-14b). The absolute PL quantum yield (QY) of 3 replicate dodecyl-SiNCs samples functionalized with each method on different days was also measured at 445 nm excitation. The dodecyl-SiNC prepared using PCl_5 initiated functionalization exhibited a QY = 62 ± 7% while the equivalent NCs modified using thermally induced hydrosilylation exhibited only 24 ± 3%. Currently, we attribute the improved in PL brightness and QY exhibited by the present SiNCs functionalized using PCl_5 initiation to the removal of dark surface defects during the PCl_5 mediated surface etching.[385] However, DFT calculations have suggested that low surface concentrations of Cl can also play a role and cannot be ruled out at this time.[386]

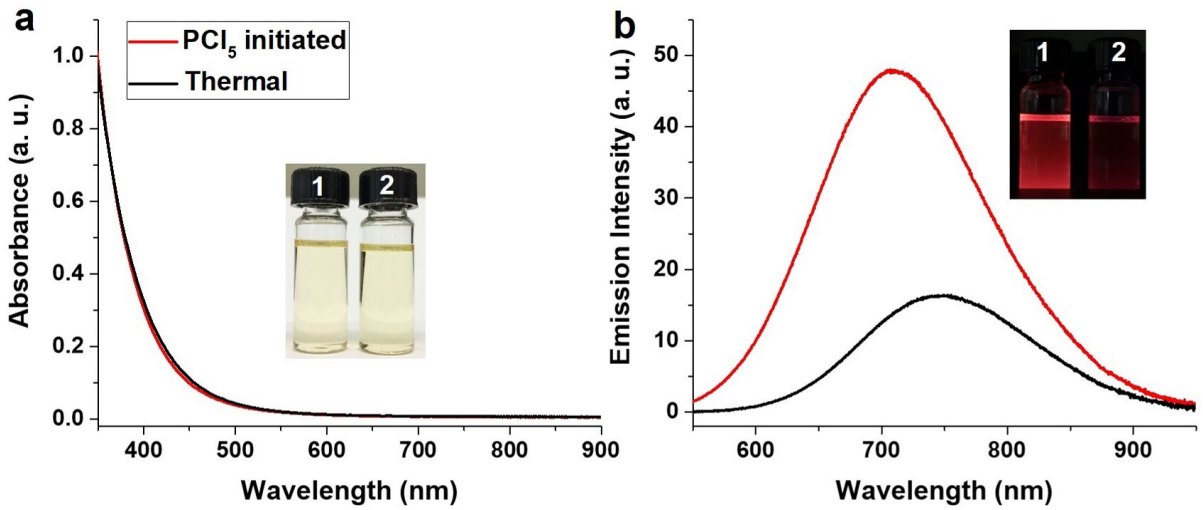

Figure 4-14. a) UV-Vis and b) photoluminescence (351 nm excitation wavelength) properties of dodecyl-SiNC (d = 3.4 nm) obtained *via* PCl_5 initiated (red trace) and thermal hydrosilylation (black trace). Insets show photographs of the dodecyl-SiNCs solutions in toluene obtained with 1) PCl_5 initiated functionalization and 2) thermal hydrosilylation.

In order to evaluate the long-term colloidal stability, resistance to surface oxidation and retention of PL quantum yield, these properties of the dodecyl-SiNCs (PCl_5 functionalization) were

re-investigated after two months. No obvious precipitation/agglomeration of the dodecyl-SiNCs from the toluene dispersion was observed (Figure 4-15a inset). The PL of the respective solution under UV illumination was bright red (Figure 4-15a inset) which suggest that the PL is also stable for the tested period. However, XPS analysis indicates a decrease in Cl concentration of ~1 % and a corresponding increase in oxidation (~6 %; Figure 4-6a and 4-15a). We also evaluated the PL AQY of the sample and found it was unchanged (58 % *vs.* 62 ± 6 %). This demonstrates that despite minor compositional changes seen in XPS analysis the favorable properties of R-SiNCs obtained using PCl_5 remained after at least two months under ambient conditions.

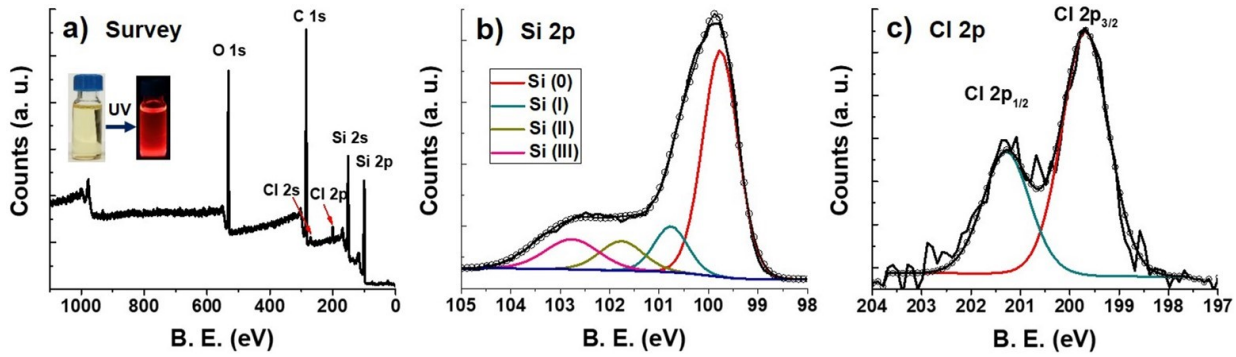

Figure 4-15. Evaluation of long-term colloidal stability, retention of PL and resistance to surface oxidation of 3.4 nm dodecyl-SiNCs obtained by PCl_5 initiated functionalization and dispersed in toluene; (a) Photos of dodecyl-SiNCs under ambient light and UV demonstrating the colloidal and PL stability; the survey spectrum shows the presence of Si (35.4 %), C (50.2 %), O (12.7 %) and Cl (1.7 %), (b) and (c) are the Si 2p and Cl 2p high-resolution XP spectra of same NCs.

PCl_5 is a Lewis acid and chlorine radical source. In this context, it is reasonable that the present surface modification could proceed *via* a Lewis acid or a $Cl^{\bullet}$ radical mediated reaction mechanisms. While the possibility of a Lewis acid mediated reactivity cannot be entirely ruled out, from the presented spectroscopic analysis (UV-Vis, ^{1}H NMR, and ^{31}P NMR) it is reasonable to conclude the observed functionalization mechanism proceeds *via* $Cl^{\bullet}$ radicals (Scheme 4-2). Chlorosilane by-products ($HSiCl_3$, H_2SiCl_2, and H_3SiCl) are formed *via* Si–Si bond cleavage on

H-SiNC surfaces. During the elimination of chlorosilanes, surface ≡Si• radicals are formed that subsequently drive the functionalization on the surface by attacking C–C multiple bonds to form surface–bonded alkyl groups with radical on the β-carbon. Finally, the reaction propagates on the NC surface by regenerating surface ≡Si• *via* the abstraction of neighboring hydrides.

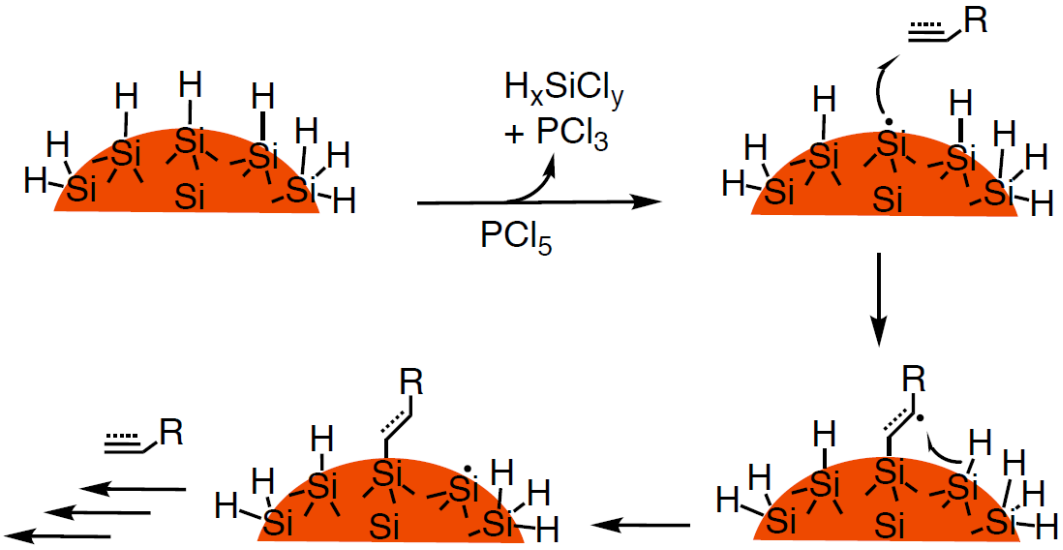

Scheme 4-2. Proposed mechanism for PCl_5 initiated functionalization of H-SiNC with alkenes/alkynes.

4.4 Conclusion

We have successfully demonstrated that PCl_5 is an effective radical initiator for surface reactions on hydride-terminated silicon nanocrystals and can induce functionalization with alkenes and alkynes at room temperature while maintaining morphology and crystallinity. The observation of chlorosilanes (H_xSiCl_y) in NMR investigations upon treating H-SiNCs with PCl_5 suggests facile cleavage of surface Si-Si bonds by Cl• leading to the generation of transient surface ≡Si• radicals. These reactive sites subsequently drive the functionalization reactions with C=C and C≡C bonds. This approach minimizes surface oxidation on functionalized SiNCs and retains the size-dependent photoluminescence properties even in the presence chlorine-based species on NC surfaces. The

SiNCs functionalized by the presented method exhibited PL that was approximately 3 times as bright as their thermally hydrosilylated counterparts; this was also manifested in a doubling of the absolute PL quantum yield. These excellent photoluminescence properties are expected to pave the way for utilizing these non-toxic nanomaterials in various applications including bioimaging and light-emitting devices.

Chapter 5:

Conclusions

and

Future Work

5.1 Conclusion

Quantum dots (QDs) have been investigated for more than three decades in a wide range of research fields driven by their size dependent optoelectronic properties.[89] The discovery of QDs in the early 1980s[6–8] has since garnered enormous interest in their synthesis, surface modification and fundamental photophysical properties[80] and has led to the high-quality QDs with fine-tuned sizes, compositions, and photoluminescence (PL) properties.[3,4,81,349,387] The development of these high-quality QDs has prompted investigations into their applications in photonics,[387] photocatalysis,[388] and biomedicine.[389] However, many QDs contain toxic heavy metals such as lead, cadmium, and mercurywhichhinders their incorporation in consumer products.[89,390,391] Alternatively, gallium, indium and selenium may be used in the preparation of safer QDs, although, their low natural abundance hinders the development of technology requiring large-scale fabrication (*e.g.*, solar cells and light-emitting diodes).[89,298,390]

On the other hand, silicon is non-toxic, abundant and forms the foundation of the modern semiconductor industry..[80,89] Since Canham's [94,95] observation of PL from porous silicon, the synthesis of silicon nanocrystals (SiNCs) exhibiting size-dependent and/or surface-mediated optoelectronic properties has received substantial attention.[80,89,165,298] The development of size-tuned SiNCs spurred investigation into a plethora of potential applications such as solar cells,[253,283] light emitting diodes,[272–274] photodetectors,[279,282] transistor,[277,278] sensors,[275,276] catalysts,[236–238] diagnostic tools,[142,288] and drug delivery agents.[290,292] However, in many of the aforementioned applications a common limitor factor was the inadequacy of appropriate surface chemistry of the SiNCs.

Most of the solution and gas phase synthetic methods provide *in-situ* hydrocarbon passivated SiNCs which limits further surface manipulations.[37,80,175,298] In addition, another

drawback of these methods is limited size tunability of the resulting nanocrystals; the insulating nature of the surface hydrocarbon ligands and limited size-tunability are not compatible with photonic applications. Fortunately, some synthetic methods, for example, laser pyrolysis of silane (SiH_4)[140] and thermal disproportionation of silicon-rich oxides[157] yield isolable hydride terminated SiNC (H−SiNCs); this permits investigations into their surface reactivity. Though, it should be noted that surface modifications of H-SiNCs have largely been subjected to hydrosilylation resulting in hydrocarbon chain passivation.[89]

Dasog *et al*.[165,211] in our group demonstrated the synthesis of chloride-terminated SiNCs (Cl-SiNCs) *via* a bulk Si (111) surface modification method; a two-step chloride-termination followed by alkylation.[210] This method provided the opportunity to isolate and investigate the surface reactivity of Cl−SiNCs. Meanwhile, Wheeler *et al*.[239] demonstrated the Lewis acidic nature of the Cl−SiNC surface, a property that weakens the surface Si-Cl bonds upon interaction with electron-rich molecular bonds *via* hypervalent bond formation. This observed bond activation may lead to catalytic applications of Cl-SiNCs in the syntheses of functional materials.

Solution processable poly(3-hexylthiophene) (P3HT), an important semiconducting material in organic electronics, is commonly synthesized using transition metal catalysts.[263] However, metal-based impurities may compromise the optoelectronic properties of P3HT.[335] Alternatively, conjugated polymers have been synthesized *via* Lewis acidic iron(III)chloride-mediated oxidative homocoupling of Grignard reagents.[247] In this context, the Lewis acidic nature of Cl−SiNCs has been investigated in the synthesis of P3HT *via* oxidative coupling of the representative Grignard monomer 5-chloromagnesio-2-bromo-3-hexylthiophene. Details regarding synthesis, characterization and reactivity were described in experimental chapter 2. This project provided an opportunity to evaluate the reactivity of Cl-SiNCs as a metal-free catalyst for

room temperature synthesis of P3HT. The as-prepared P3HT exhibits moderate molecular weight and regioregularity and is suitable for film processing. The PL of P3HT in solution was very bright but is markedly quenched when processed into a solid film, indicating suppressed recombination of the photogenerated electron and hole (exciton). This behavior is desired for thin-film solar cell applications of P3HT whereby exciton dissociation is necessary for electricity production. The MALDI-TOF analysis revealed that P3HT contains H/Br or Br/Br end groups. These end groups allow the as-prepared P3HT to be used as a macroinitiator for the synthesis of block copolymers.

A comparison of reactivity of three Si−Cl-containing species, Cl-SiNCs, Cl-SiWF (chloride-terminated silicon wafer), and $SiCl_4$ revealed the superior reactivity of Cl-SiNCs in the synthesis of P3HT. Overall, this study led to the exploration of abundant silicon-based catalysts for metal-free synthesis of functional materials. Further possibilities for utilizing Cl-SiNCs reactivity will be discussed in the future work sections.

As mentioned earlier, the limited success of SiNCs in photonic applications (e.g., solar cell, LED and photodetector) is in part, due to issues related to surface manipulation. While SiNC only devices of these types showed limited efficiencies,[272,279,283] incorporation of SiNCs into organic-inorganic hybrid devices consisting of both electron- and hole- transporting organic layers provided improved efficiencies.[253,273,274,282,284] However, these hybrid devices were constructed either (i) using layer by layer deposition of thin films of the respective organic and inorganic components or (ii) by blending these components in a common solvent. Covalent attachment of the conjugated polymer P3HT to semiconductor nanoparticles (e.g., CdS,[302] CdSe,[266,268,301,303] CdTe,[304] TiO_2,[267] ZnO[392]) provided favourable conditions for photonic device applications. This improvement is attributed to the synergistic effect of the organic and inorganic components on the

properties of the hybrid functional materials (HFMs) (e.g., homogeneous film morphology, surface-induced alignment of polymer and enhanced interfacial electronic interaction).

In this regard, a method has been developed to graft P3HT from SiNCs using surface-initiated Kumada catalyst transfer polycondensation (SI-KCTP)[271] which facilitated direct interfacial contact between these two components (experimental chapter 3). As this method requires surface-bonded aromatic halide initiator sites, 2-bromo-3-hexyl-5-thienyl (-HT-Br) moieties on the SiNC surface were utilized as initiator sites to allow for interfacial matching with the grafted P3HT. This was achieved by reacting H-SiNCs with the Grignard monomer 5-chloromagnesio-2-bromo-3-hexylthiophene (ClMg-HT-Br). This Grignard form of the monomer was chosen to allow direct covalent bonding of the thiophene ring with SiNCs. After generation of the initiator sites on SiNCs (denoted as SiNC-HT-Br), diethyldipyridylnickel ($Et_2Ni(bipy)$) catalysts were immobilized on the aromatic bromide moieties to generate a red-brown dispersion of SiNC-HT-Ni(bipy)-Br. This was followed by ligand exchange of bipy with 1,3 -bis(diphenylphosphino)propane (dppp) which resulted in an orange dispersion of SiNC-HT-Ni(dppp)-Br. Finally, P3HT was grafted from SiNC-HT-Ni(dppp)-Br by the addition of ClMg-HT-Br resulting in a purple color dispersion of SiNC@P3HT HFMs.

The grafting of the P3HT was evaluated by a complementary suite of characterization techniques. The Fourier transform infrared (FT-IR) spectrum of SiNC@P3HT exhibited an aromatic C-H stretching band at 3060 cm^{-1} that was not observed for SiNC-HT-Br. Using X-ray photoelectron spectroscopy (XPS) the estimated ratio of sulfur over silicon was 8-fold higher for SiNC@P3HT than for SiNC-HT-Br. Particle size distribution analysis *via* transmission electron microscopy (TEM) showed an increase in SiNC@P3HT size by about 4 nm compared to SiNC-HT-Br. Bright-field scanning transmission electron microscopy (BF-STEM) and high annular

angular dark field (HAADF) imaging showed core-shell structures for SiNC@P3HT. All of these evaluations were consistent with the presence of P3HT on SiNCs. However, these spectroscopic techniques cannot confirm that the corresponding signals are coming from surface bonded P3HT and the microscopic imaging techniques do not provide information about core-shell chemical identity. Therefore, electron energy loss spectroscopic (EELS) mapping was performed on individual particles and this analysis showed that the core is SiNC and the shell is P3HT.

UV-Vis absorption and PL spectroscopic analyses were performed to evaluate the impact of direct interfacial contact between SiNC and P3HT. The SiNC@P3HT HFM exhibit a broad absorption spectrum which resembles the sum of the SiNC and P3HT absorption spectra. However, additional shoulders at the longer wavelengths were also observed and are attributed to the efficient π-electron delocalization in P3HT as facilitated by their inter-chain alignment on the NC surface.

P3HT-based PL quenching experiments were performed to provide insight into the interfacial electron and/or energy transfer processes. Blending pentyl-capped SiNCs with P3HT resulted in 1.5-fold quenching of P3HT-based PL whereas 7-fold quenching was observed for P3HT grafted on SiNCs. The enhanced quenching of PL demonstrates efficient electron and/or energy transfer at the donor-acceptor interface of SiNC@P3HT. Finally, scanning tunneling microscopy and spectroscopy (STM and STS) measurements suggested the presence of a n/p junction between SiNC and P3HT which is consistent with interfacial electronic communication.

The direct interfacial contact in SiNC@P3HT may lead to use as an active material in hybrid LEDs, photodetectors, and p-channel transistors. In the literature, there is precedent for using SiNC@P3HT HFMs as a material in the previously mentioned devices; there have been reports of improved efficiencies using HFMs of many semiconductor nanoparticles with

conjugated polymers.[245,304,317] Moreover, this method can also be applied to graft P3HT directly from silicon nanowire and nanohole arrays to fabricate hybrid heterojunction solar cells.[393]

To improve the efficiency of SiNCs emission-based devices (*e.g.*, LEDs, and sensors) it is necessary to develop NC surface modification methods that effectively passivate the surface defects and protect against oxidation without creating a highly insulating barrier. Such modification may improve the PL quantum yield (PL QY) of SiNCs and facilitate the charge transfer processes necessary for these applications. Most of the SiNC surface modification methods result in long insulating hydrocarbon chain passivation or inefficient surface passivation leading to oxidation. Therefore, phosphorus pentachloride (PCl_5)-initiated functionalization of H-SiNCs has been developed (experimental Chapter 4) which provides improved passivation of SiNC against oxidation without creating a large oligomeric alkyl chain insulating barrier.

Initially, the reactivity of PCl_5 with H-SiNCs was been examined. The observation of chlorosilanes (H_xSiCl_{4-x}, x = 1, 2, 3) and PCl_3 by-products *via in-situ* ^{1}H NMR and ^{31}P NMR suggests that the PCl_5 treatment of SiNCs leads to etching of the nanocrystal surface *via* Si–Si bond cleavage, producing reactive surface silicon radicals (≡Si•). The surface radicals subsequently initiate hydrosilylation with alkenes/alkynes to produce the alkyl/alkenyl- passivated SiNCs. The reaction proceeds at room temperature and thus, is compatible with functionalization requiring short chain volatile ligands (*e.g.*, pentene). Moreover, PCl_5-induced etching and subsequent functionalization reduce the surface traps leading to significantly brighter PL. In fact, the PL was approximately three times as bright as that observed for the corresponding thermally hydrosilylated SiNCs. Also, the absolute PL QY also more than double of that which was seen for the thermally hydrosilylated species. The colloidal stability, oxidation resistance, and high PL QY of the as-functionalized SiNCs did not considerably change over two months. The properties

derived from this functionalization protocol are expected to provide a way to efficiently modify the surface for targeted applications such as LEDs, sensors, and bioimaging agents.

5.2 Future Work

5.2.1 Chloride- and Fluoride-Surface Terminated Silicon Nanocrystals Mediated Synthesis of Commodity Chemicals and Functional Materials.

Weakly Lewis acidic $SiCl_4$ have been widely used in organic synthesis. Some examples, to name a few include the addition of allylic organometallic reagents to carbonyl compounds (Scheme 5-1a),[394] aldol additions of silyl enol ethers to aldehyde (Scheme 5-1b),[395] aldol additions of silyl ketene acetals to aldehyde (Scheme 5-1c),[396] and ring opening of epoxides (Scheme 5-1d).[338] These reactions are facilitated *via* Lewis basic activation of $SiCl_4$ through hypervalent bond formation.[397] Recently, Wheeler *et al.*[239] demonstrated that Lewis acidic sites of Cl-SiNCs can also form hypervalent bonds with many aldehydes, ketones, and nitriles containing electron rich moieties. This hypervalent interaction results in the weakening of both the Si-Cl bonds, as well as the carbonyl or nitrile bonds of the interacting molecules. Our investigations have shown that the Cl-SiNC mediated synthesis of P3HT provides superior reactivity to Cl-SiWF and $SiCl_4$. In this context, Cl-SiNCs could provide an effective platform to promote various organic reactions including the examples provided in Scheme 1. Fluoride-terminated SiNCs (F-SiNCs) may also provide a highly Lewis acidic NC surface. Note that F-SiNCs may be synthesized by reacting H-SiNCs with XeF_2.[93] Both Cl-SiNCs and F-SiNCs are expected to be easily separated from organic products and consequently can be regenerated. Moreover, steric effects on the SiNC may be exploited for applications related to asymmetric catalysis.

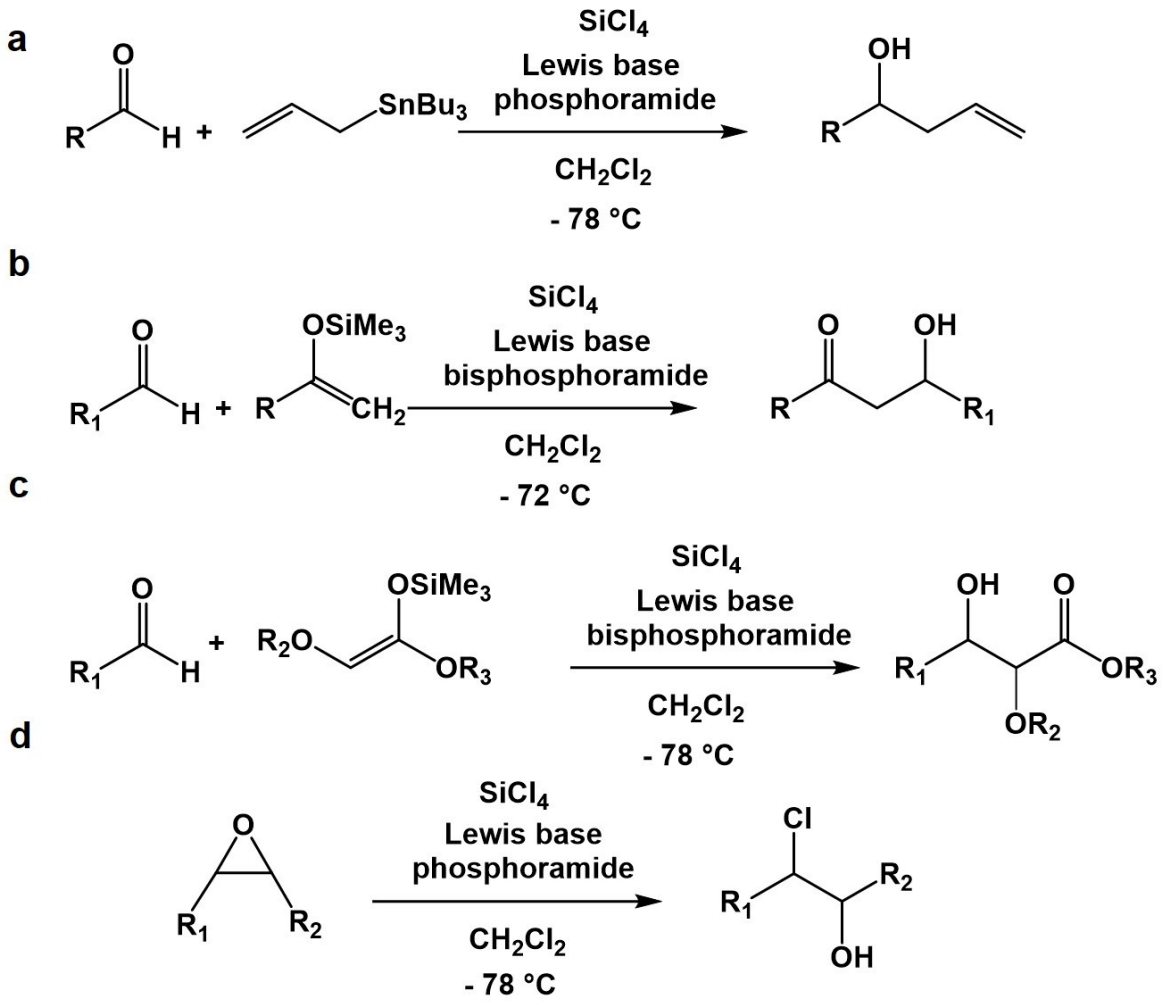

Scheme 5-1. Lewis acidic $SiCl_4$ as a promoter in organic synthesis.

We performed the ring-opening polymerization of propylene oxide by reaction with F-SiNCs prepared *in-situ via* the reaction between H-SiNCs and XeF_2 (Scheme 5-2a) The formation of poly(propylene oxide) was evaluated by MALDI-TOF analysis. This ring-opening reaction exemplifies a simple one-pot room temperature synthesis of SiNC/polymer hybrid materials from very useful cyclic monomers such as ether, thioether lactone, thiolactone, and siloxanes (Scheme 5-2b).[398] The mechanism of this ring-opening polymerization is unclear and requires further analysis; it might be cationic or anionic ring-opening[398] polymerization caused by the polarity of

surface Si-F bonds or possibly radical ring-opening polymerization[399] mediated by SiNC surface silicon radical generated *via* XeF_2-mediated etching.

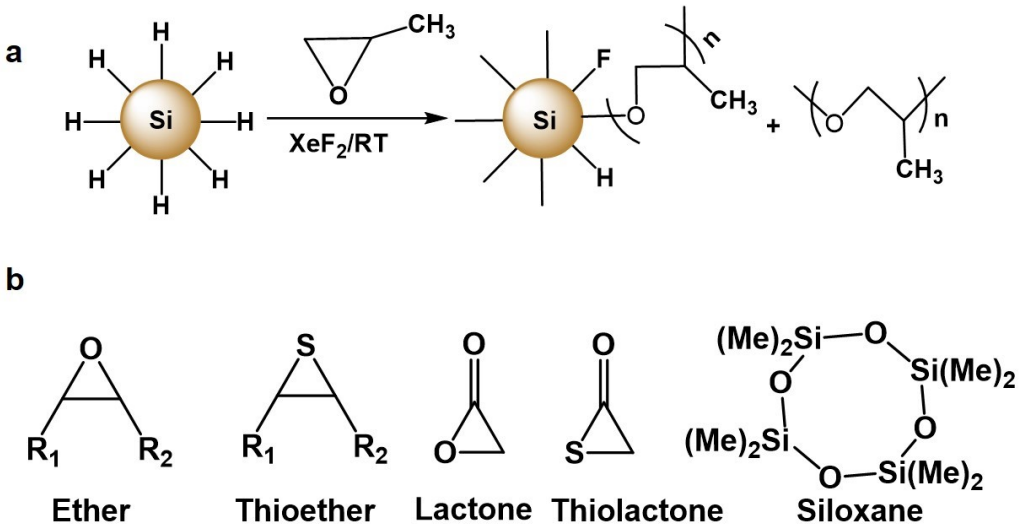

Scheme 5-2. a) Ring-opening polymerization of propylene oxide *via* F-SiNCs, and b) representative examples of potential cyclic monomers for ring-opening polymerization.

In the presence of a suitable catalyst organo silyl hydrides can convert carbon dioxide (CO_2) to carboxylic acids (RCOOH), alcohols (RCH_2OH), aldehydes (RCHO), and methane (CH_4).[400] Oxide coated SiNCs were also demonstrated as being effective photocatalysts for the reduction of CO_2 to formic acid (HCOOH) and formaldehyde (HCHO).[236] The oxide coated SiNCs-mediated reduction is thought to be driven by photogenerated electrons.[236] In contrast, H-SiNCs were reported to convert CO_2 to carbon monoxide (CO) in the absence of a catalyst or light.[238] The molecular silane-mediated reduction is believed to proceed through the formation of an intermediate such as $SiOCH_2OSi$ or SiOCHO,[400] while the insertion of O to the H-SiNC surface was proposed to convert the CO_2 to CO.[238] The variations in reactivity of SiNCs due to different surface species suggest that Cl-SiNCs and F-SiNCs could lead to new reaction routes involving CO_2. Moreover, the high oxophilicity and ability for hypervalent bond formation make these NCs superior candidates for CO_2 activation. An additional advantage of using Cl-SiNCs and F-SiNCs

is that these species might be regenerated in-situ *via* the simultaneous addition of PCl_5 and XeF_2, respectively.

5.2.2 Grafting High Band-Gap Conjugated Polymers from Silicon Nanocrystals Surfaces.

Core-shell HFMs consisting of a low band-gap semiconductor nanoparticle (NP) core and a high band-gap conjugated polymer (CP) shell can facilitate the confinement of electron and hole pairs into the core while allowing charge and/or energy transfer from the shell.[245,362,401] The CP shell can also facilitate charge injection from an external source to the NP core.[245,304,317] These properties can influence performance in the following devices: LEDs, photodetectors, and transistors. Poly (p-phenylene) (PPP), poly (p-phenylene vinylene) (PPV), and poly (9,9-dioctylfluorene) (PFO) are high band-gap polymers (2.8, 2.4, and 3.10 eV, respectively) [402,403] which have been grafted on various NP surfaces.[401,404,405] Grafting PPV onto CdSe QDs was shown to provide enhanced interfacial energy transfer that resulted in increased PL QY of the QDs.[401] This phenomenon is important for nanoparticle-based LEDs and we envision that grafting these high band-gap CPs on band-gap tunable SiNCs will provide an opportunity to manipulate their interfacial communication and facilitate their use in targeted optoelectronic devices. The methodology to graft these CPs on other NP surfaces can be adapted to SiNCs as shown in Scheme 5-3.

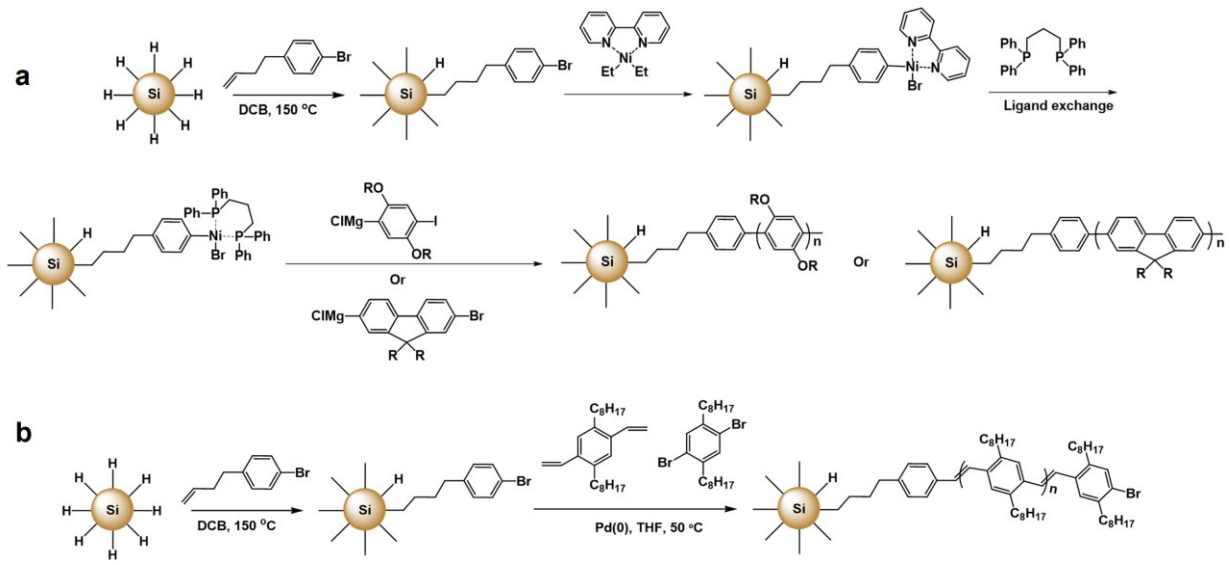

Scheme 5-3. a) Grafting PPP and PFO from SiNCs surface *via* SI-KCTP, b) Pd catalyzed surface grafting of PPV on SiNCs.

5.2.3 Silicon Nanocrystals Surface Radical Mediated Ring-Opening Polymerization.

Radical ring-opening polymerization (RROP) can be utilized to prepare the following polymers with industrial applications: polyethylene oxide, polypropylene oxide, polyketones, poly-ε-caprolactone, polytetrahydrofuran and polydimethylsiloxane.[398,406–408] RROP provides opportunities to introduce functional groups such as ethers, esters, amides, carbonates, sulfides, alcohols, halides, cyanide, and aliphatic/aromatic ligands into the targeted polymer.[406] Radical ring-opening can proceed *via* a direct attack on the heteroatoms of strained cyclic monomers[399,408] (Scheme 5-4a) or *via* attack on an allyl/vinyl substituted cyclic monomers (Scheme 5-4b,c).[406,407,409] Recently, we demonstrated that PCl_5 and XeF_2-mediated etching of H-SiNCs generate reactive surface silicon radicals (≡Si•). This provides an opportunity to graft a wide range of polymers (Scheme 5-2b and Scheme 5-4c) on SiNCs. In particular, RROP *via* allyl/vinyl substituted rings (Scheme 5-4c) may enable the grafting of polymers containing a variety of functional groups. The surface grafted polymers may be detached *via* further SiNCs etching using

XeF_2. In the case of XeF_2-mediated etching, the surface radicals are created so rapidly that hydrosilylation with unsaturated bonds proceeds instantaneously while PCl_5-mediated etching and the corresponding hydrosilylation proceeds at a moderate rate. The different SiNC surface reactivity created by these two different methods is expected to provide an opportunity to manipulate the polymerization time and polymer molecular weights.

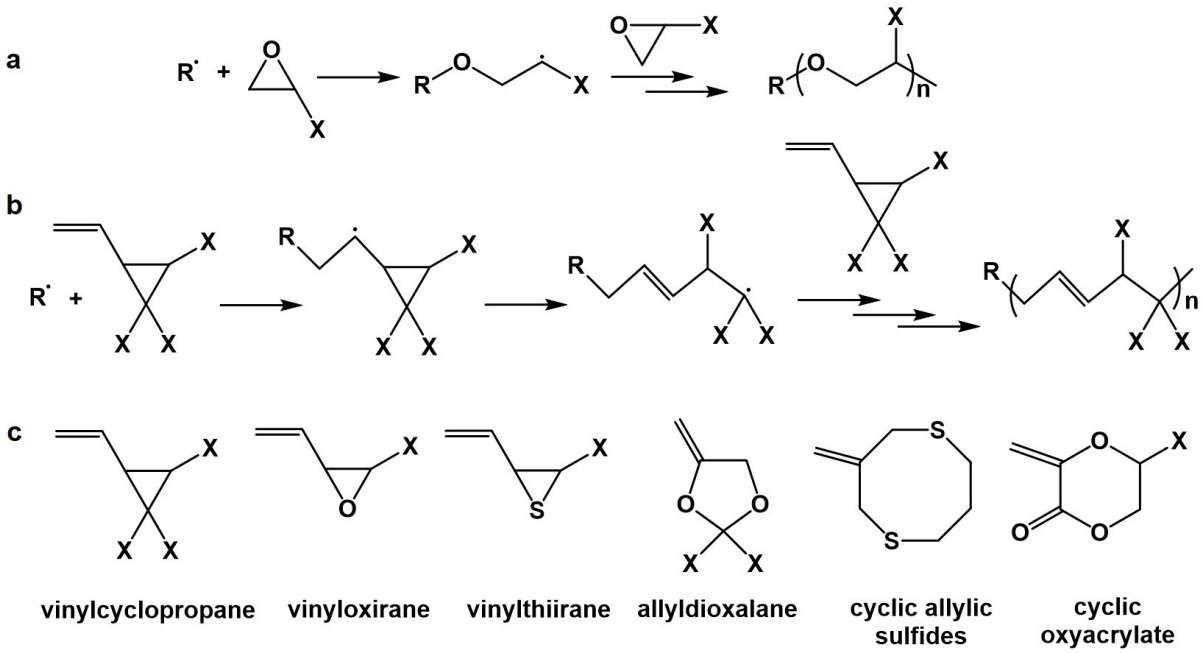

Scheme 5-4. Radical ring-opening of a) strain ring cyclic ether *via* a radical attack on heteroatoms[399,408] and b) vinyl substituted cyclic ring where initiation occurs *via* radical attack on the vinyl group; [406,407,409] c) representative substituted rings that undergoes radical ring-opening polymerization.[406,407,409]

5.2.4 Development of Amphiphilic Photoluminescent Silicon Nanocrystals for Bioimaging Applications.

Quantum dots are attractive for luminescence-based bio-imaging, bio-sensing, and drug delivery due to their size-dependent PL, high PL QY, long-term photostability, and robustness to bioconjugation.[410,411] However, the commonly used QD CdSe is toxic and so severely limits its *in-*

vivo applications. The nontoxic nature of SiNCs makes them ideal for bioapplications.[411] Recent developments in SiNCs synthetic methods are offering size and surface controlled PL QY. Moreover, progress in SiNC surface chemistry provides an opportunity to develop SiNC based diagnostic and theragnostic tools.[89,410,411]

Amphiphilic nanoparticles (NPs) are of great interest for cellular imaging, drug delivery and therapy since the amphiphilic nature of the NPs allows their passage through the lipid bilayer membrane barrier surrounding all types of cells.[412,413] Sudeep *et al*.[119] developed amphiphilic SiNCs *via* hydrosilylation of H-SiNCs with undecenyl-terminated polyethylene glycol. Despite the many advantages associated with these amphiphilic SiNCs, removal of excess CTAB surfactant is not straightforward and residual CTAB is known to exhibit severe cytotoxicity.[414] Moreover, the SiNCs emit blue light which overlaps spectrally with cell autofluorescence. In this context, we have developed a simple one-step thermal hydrosilylation method to prepare amphiphilic SiNCs that exhibit favorable properties for bioimaging such as amphiphilic colloidal stability, bright red PL, retention of PL properties in biological pH, and bio-conjugable surface moieties (−$COOCH_3$ and −OH groups) (Figure 5-1).

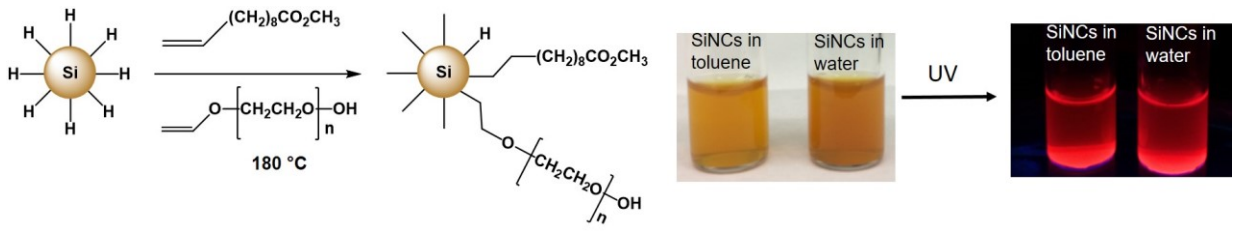

Figure 5-1. Scheme for the one-step synthesis of amphiphilic SiNCs. Photographs demonstrate the dispersibility of amphiphilic SiNCs in toluene and water and the corresponding PL under UV illumination.

The as-prepared amphiphilic SiNCs were thoroughly characterized using FT-IR, XPS, UV-Vis, PL, TEM, DLS and TGA analysis techniques. *In-vitro* cell viability and internalization were evaluated by treating human prostate cancer (PC-3) cell lines with amphiphilic SiNCs (Figure 5-

2a). No cytotoxicity was observed within a 2 h incubation period. Confocal microscope images show internalization of SiNCs into the PC-3 cells as evaluated *via* PL signal originating from SiNCs. However, cell autofluorescence is also observed from untreated cells. As SiNCs exhibit microsecond lifetimes which are much longer than that of cell autofluorescence the interference from cell autofluorescence can be overcome using time-gated PL imaging.[415] Continuous and time-gated images of SiNCs were acquired and compared to those obtained for a model dye (Rhodamine B) exhibiting nanosecond fluorescence lifetime. Both the dye and the SiNC emit under continuous wave imaging whereas PL observed only from SiNC after 1μs of time-gating (Figure 5-2b, c).

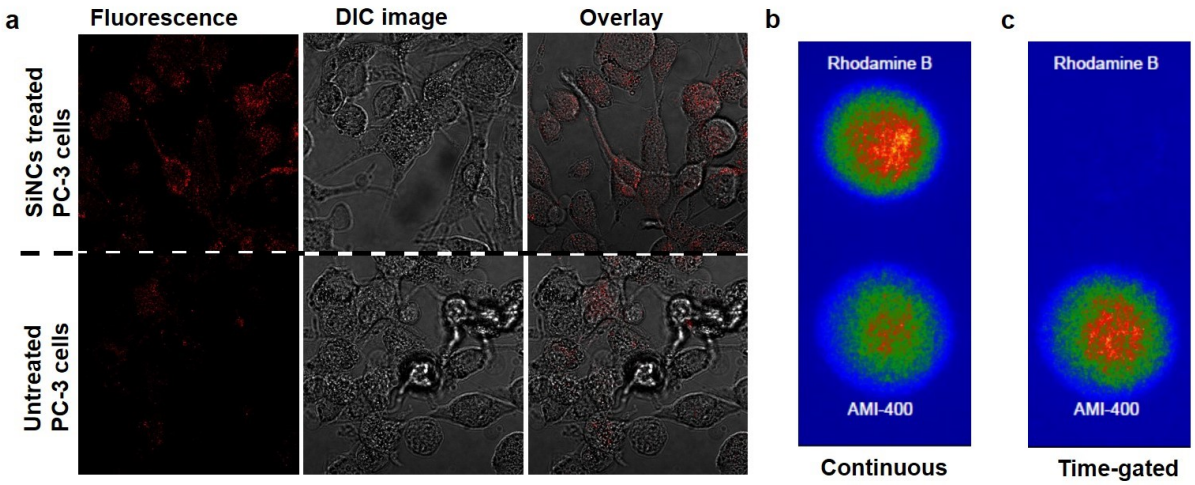

Figure 5-2. a) Confocal microscopic evaluation of internalization of amphiphilic SiNC in human prostate cancer (PC-3) cells; fluorescence signals of Rhodamine B model dye and amphiphilic SiNC under b) continuous wave and c) time-gated imaging (excitation wavelength 375nm).

The time-gated imaging technique utilized under *in-vivo* by injecting the Rhodamine B and the SiNC into the subcutaneous space on a chicken wing (Figure 5-3). The cell autofluorescence was overpowered by very bright fluorescence from the dye under steady illumination and the PL from the SiNCs was extremely difficult to discern due to interference from cell autofluorescence. However, upon using 1μs time-gating only PL from the NCs was observed and demonstrate their potential for *in-vivo* imaging applications. Future work involves further characterization of these

SiNCs such as measurement of PL QY, optimization of cell imaging conditions, and an evaluation of a potential application in sentinel lymph node mapping.

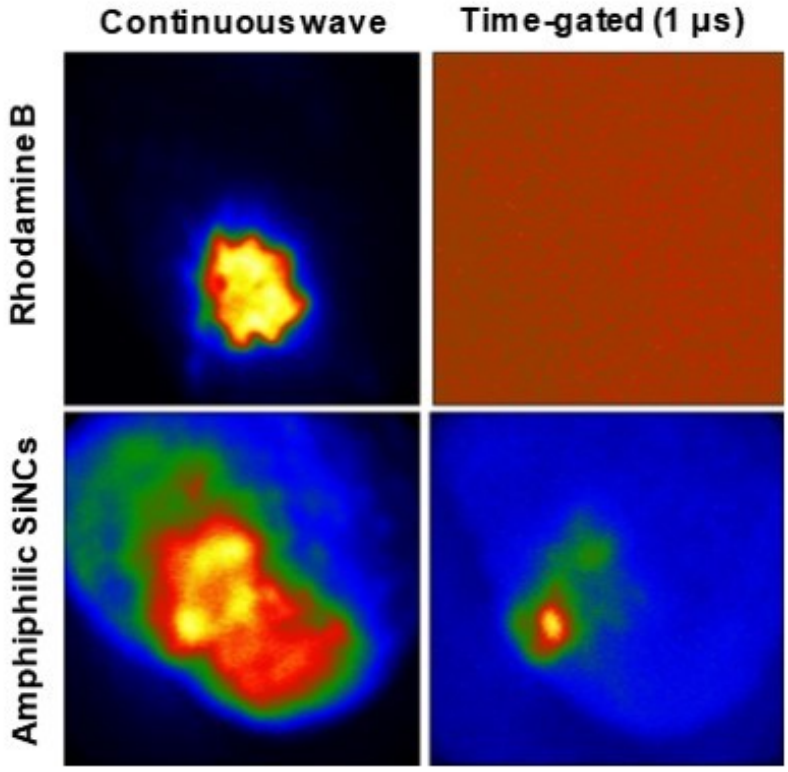

Figure 5-3. Steady state and time-gated images of Rhodamine B dye and amphiphilic SiNCs injected into the subcutaneous space on a chicken wing.

5.2.5 Development of Multifunctional Photoluminescent Silicon Nanocrystals for Immunofluorescent Cell Imaging Applications.

Specific cell labeling and imaging with SiNCs requires functional modification of the SiNCs with proteins,[287,416,417] carbohydrates,[418] peptides[142,415,419,420] or antibodies.[90,126,288,289] Despite the promising demonstration of bioconjugated SiNCs in cell imaging significant limitations exist in many of the reported approaches. For example, micelle stability in the biological settings[142,287] cyan color emission of SiNCs,[126,288] both colloidal and photostability SiNCs, and complicated synthesis methods[90,289] are all limiting factors.

To facilitate SiNCs-based immunofluorescence cell imaging, we have initiated the development of bright red-emitting amphiphilic SiNCs bearing bio-conjugable surface moieties such as biotin and carboxylic acid groups (−COOH) (Figure 5-4a, b). The success of carboxyl termination was evaluated *via* EDC coupling with amine-terminated Fe_2O_3 nanoparticles (Figure 5-4c-1a,b) while the biotin functionalization was verified with streptavidin conjugated Fe_2O_3 particles (Figure 5-4c-2a,b). The carboxylic acid-terminated SiNCs were coupled with streptavidin and anti-epithelial cell adhesion molecule (anti-EpCAM) antibody *via* EDC coupling.

Although this method is promising for the development of multifunctional SiNCs, the acrylate functional groups of the polyethylene glycol (PEG 5000 MW) presumably lead to oligomerization/polymerization in the solution as well as on the surface. This contributes to the difficulty of separating the PEG functionalized SiNCs from bulk PEG. Therefore, the coupling reactions probably occur preferentially with the functional groups of the bulk PEG. To overcome this limitation, hydrosilylation of H-SiNCs with a mixture of allyloxy (polyethylene oxide) methyl ether (9-12 repeating unit) and 10-undecenoic acid was carried out to obtain water dispersible carboxylic acid-terminated SiNCs. These particles are easier to purify than the acrylate analogues. Future work involves coupling streptavidin and antibodies with these carboxylic acid-terminated SiNCs, and optimization of SiNCs size according to the need for *in-vitro* immunofluorescent cell imaging. After optimizing the *in-vitro* imaging conditions, these NCs will be evaluated for *in-vivo* cancer cell imaging.

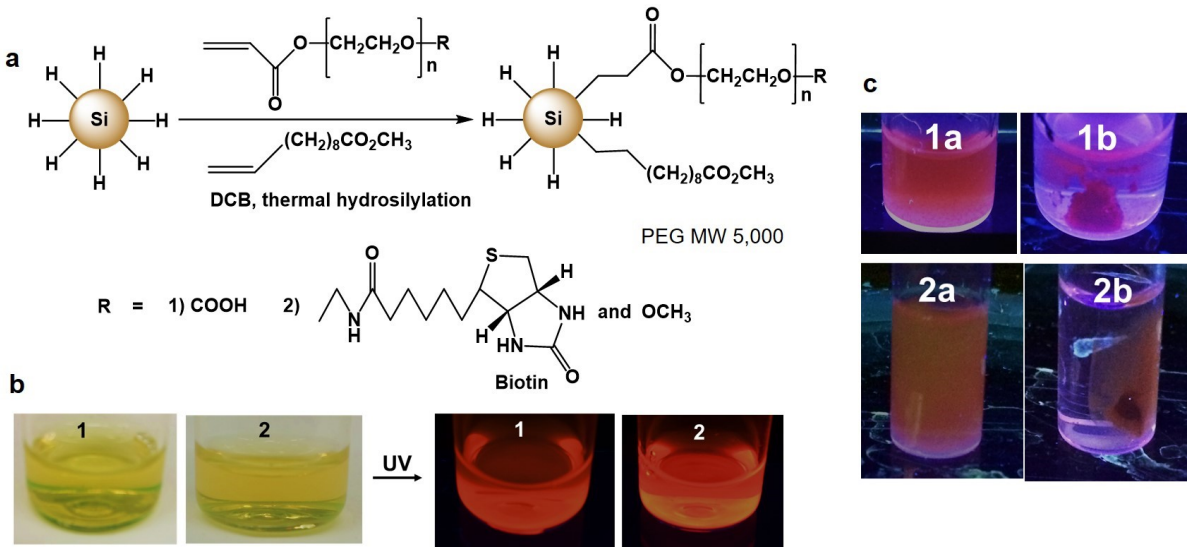

Figure 5-4. a) Scheme for the synthesis of biotin and carboxylic acid-terminated SiNCs; b) photographs demonstrate their dispersibility in water and the corresponding PL under UV illumination, c) Evaluating the presence of functional groups on SiNCs *via* Fe_2O_3 magnetic particles coupling: 1 a and b for carboxylic acid groups, 2 a and b for biotin groups.

5.2.6 Development of Multifunctional Photoluminescent Silicon Nanocrystals for Simultaneous Imaging and Drug Delivery Applications.

Recently, SiNCs have emerged as promising materials for simultaneous imaging and treatment of tumors.[291,421] A drug is loaded onto the SiNCs which first carries the drug to the tumor. The drug is then released upon tumoral stimuli such as a more acidic environment within the tumor.[422] The delivery of the drug and the progress of treatment can be monitored by SiNCs PL based imaging. Photoluminescent SiNCs based multifunctional drug carriers have been developed by several groups[290–292] but the methods suffer from preferential drug release in bodily fluid pH (7.4),[290] blue photoluminescence of SiNCs,[291,292] and weak hydrophobic[291] or nonspecific H-bonding[292] interaction-based drug loading.

We have demonstrated successful doxorubicin (Dox: a model cancer drug) coupling with red emitting SiNCs through a 3-step reaction sequence: (i) hydrosilylation of H-SiNCs with methyl

10-undecenoate, (ii) conversion of pendant ester groups to hydrazide groups, and finally (iii) formation of pH cleavable hydrazone linkages with Dox (Figure 5-5). The presence of pendant ester groups on SiNCs is most evident from the prominent ν(C=O) vibrational (1740 cm^{-1}) mode. The prominent ν(C=O) vibrational mode at 1740 cm^{-1} shifts to 1650 cm^{-1} along with the evolution of a ν(N-H) vibrational mode at 3300 cm^{-1} after reaction with hydrazine. This indicates successful conversion of the ester to a hydrazide. Figure 5-5 shows the intense red color dispersion of Dox-coupled SiNCs in water; the red color is characteristic of Dox. Under UV illumination the Dox coupled SiNCs exhibit red to NIR PL.

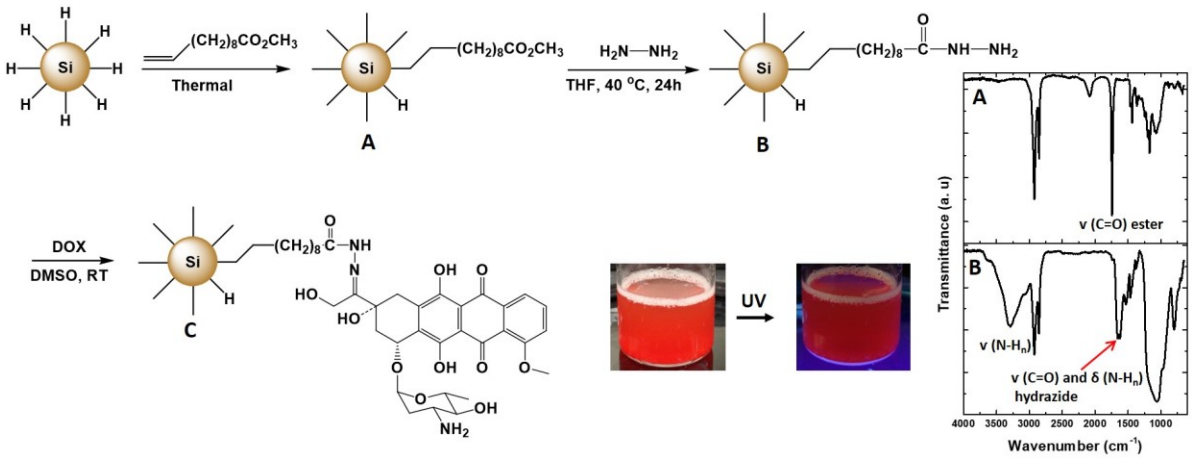

Figure 5-5. Scheme of the 3 steps method for coupling Dox with SiNCs through an acidic pH cleavable hydrazone bond. FT-IR reveals the efficient conversion of ester groups to hydrazide groups. Photographs show the Dox coupled SiNCs under ambient light and UV irradiation.

This species contains a covalently bonded but pH cleavable hydrazone linkage between SiNCs and Dox and gives rise to red emission. This combination of properties makes this platform appealing for sequential cancer diagnosis and therapy. However, further improvement is required to achieve high water dispersibility and to couple antibodies for immunofluorescent cell imaging. In this context, we have prepared multifunctional SiNCs bearing -COOH and -COOR pendant groups. The -COOH groups were used to couple SiNCs to a heterobifunctional PEG (H_2N-PEG-

SH) with the intent to improve water solubility; conjugation to an antibody through a combination of carbodiimide and maleimide chemistry using succinimidyl-*trans*-4-(N-maleimidylmethyl)cyclohexane-1-carboxylate (SMCC) as a cross-linker would be the subsequent step. Although significant work would be required to optimize the conditions (e.g., tuning the NCs surface passivation, PL, colloidal stability, and bioconjugation) for imaging, and drug delivery the potential benefits outweigh the effort that would be required.

5.3 Potential future impact of SiNCs

SiNCs have been explored for many potential applications as described in the previous chapters. However, many studies aimed at applications have been focused on improving the performance of existing technologies. For example, the focus of SiNC-based transistor research has been to enhance the speed and reduce transistor size. However, these types of improvements are reaching a fundamental limit.[423] In contrast, the development of organic and polymer semiconductors like the presented HFMs could have significant and game changing impact in flexible, stretchable and wearable large area electronics (e.g., displays, artificial skin, smart textiles, and even smart robots).[424–432] For example a robot could be made sensitive to pressure, temperature, light, motion, sound, humidity, oxygen and other chemicals by integrating appropriate sensing elements that employ advanced materials such as HFMs.[425,430,432,433] To do so, advanced responsive materials must be developed that would facilitate the development of appropriate device components. Colloidal SiNCs offer attractive properties that can be incorporated into HFMs for flexible electronics. The present research points toward the vast potential for SiNCs and associated HFMs laying the groundwork for the development of smart/responsive systems based upon an abundant, biologically compatible exquisitely tuneable material.

References

(1) Alivisatos, A. P. *Science (80-.).* **1996**, *271*, 933–937.

(2) Shirasaki, Y.; Supran, G. J.; Bawendi, M. G.; Bulović, V. *Nat. Photonics* **2013**, *7*, 13–23.

(3) Wegner, K. D.; Hildebrandt, N. *Chem. Soc. Rev.* **2015**, *44*, 4792–4834.

(4) Smith, A. M.; Nie, S. *Acc. Chem. Res.* **2009**, *43*, 190–200.

(5) de Mello Donega, C. *Chem. Soc. Rev.* **2011**, *40*, 1512–1546.

(6) Rossetti, R.; Brus, L. *J. Phys. Chem.* **1982**, *86*, 4470–4472.

(7) Rossetti, R.; Nakahara, S.; Brus, L. E. *J. Chem. Phys.* **1983**, *79*, 1086–1088.

(8) Brus, L. E. *J. Chem. Phys.* **1984**, *80*, 4403–4409.

(9) Chuang, C.-H. M.; Brown, P. R.; Bulović, V.; Bawendi, M. G. *Nat. Mater.* **2014**, *13*, 796–801.

(10) Kamat, P. V. *J. Phys. Chem. C* **2008**, *112*, 18737–18753.

(11) Carey, G. H.; Abdelhady, A. L.; Ning, Z.; Thon, S. M.; Bakr, O. M.; Sargent, E. H. *Chem. Rev.* **2015**, *115*, 12732–12763.

(12) Wang, R.; Shang, Y.; Kanjanaboos, P.; Zhou, W.; Ning, Z.; Sargent, E. H. *Energy Environ. Sci.* **2016**, *9*, 1130–1143.

(13) Coe, S.; Woo, W.-K.; Bawendi, M.; Bulović, V. *Nature* **2002**, *420*, 800–803.

(14) Rogach, A. L.; Gaponik, N.; Lupton, J. M.; Bertoni, C.; Gallardo, D. E.; Dunn, S.; Li Pira, N.; Paderi, M.; Repetto, P.; Romanov, S. G. *Angew. Chemie Int. Ed.* **2008**, *47*, 6538–6549.

(15) Klimov, V. I.; Mikhailovsky, A. A.; Xu, S.; Malko, A.; Hollingsworth, J. A.; Leatherdale, C. A.; Eisler, H.-J.; Bawendi, M. G. *Science (80-.).* **2000**, *290*, 314–317.

(16) Huffaker, D. L.; Park, G.; Zou, Z.; Shchekin, O. B.; Deppe, D. G. *Appl. Phys. Lett.* **1998**, *73*, 2564–2566.

(17) Bimberg, D.; Grundmann, M.; Heinrichsdorff, F.; Ledentsov, N. N.; Ustinov, V. M.; Zhukov, A. E.; Kovsh, A. R.; Maximov, M. V; Shernyakov, Y. M.; Volovik, B. V. *Thin Solid Films* **2000**, *367*, 235–249.

(18) Del Alamo, J. A. *Nature* **2011**, *479*, 317–323.

(19) Talapin, D. V; Murray, C. B. *Science (80-.).* **2005**, *310*, 86–89.

(20) Hetsch, F.; Zhao, N.; Kershaw, S. V; Rogach, A. L. *Mater. Today* **2013**, *16*, 312–325.

(21) Wang, X.; Sun, G.; Li, N.; Chen, P. *Chem. Soc. Rev.* **2016**, *45*, 2239–2262.

(22) Macdonald, T. J.; Nann, T. *Nanomaterials* **2011**, *1*, 79–88.

(23) Sun, W.-T.; Yu, Y.; Pan, H.-Y.; Gao, X.-F.; Chen, Q.; Peng, L.-M. *J. Am. Chem. Soc.* **2008**, *130*, 1124–1125.

(24) Bruchez, M.; Moronne, M.; Gin, P.; Weiss, S.; Alivisatos, A. P. *Science (80-.).* **1998**, *281*, 2013–2016.

(25) Michalet, X.; Pinaud, F. F.; Bentolila, L. A.; Tsay, J. M.; Doose, S.; Li, J. J.; Sundaresan, G.; Wu, A. M.; Gambhir, S. S.; Weiss, S. *Science (80-.).* **2005**, *307*, 538–544.

(26) Liu, S.-L.; Wang, Z.-G.; Zhang, Z.-L.; Pang, D.-W. *Chem. Soc. Rev.* **2016**, *45*, 1211–1224.

(27) Medintz, I. L.; Uyeda, H. T.; Goldman, E. R.; Mattoussi, H. *Nat. Mater.* **2005**, *4*, 435–446.

(28) Freeman, R.; Willner, I. *Chem. Soc. Rev.* **2012**, *41*, 4067–4085.

(29) Bagalkot, V.; Zhang, L.; Levy-Nissenbaum, E.; Jon, S.; Kantoff, P. W.; Langer, R.; Farokhzad, O. C. *Nano Lett.* **2007**, *7*, 3065–3070.

(30) Xie, J.; Lee, S.; Chen, X. *Adv. Drug Deliv. Rev.* **2010**, *62*, 1064–1079.

(31) Elzoghby, A. O.; Hemasa, A. L.; Freag, M. S. *J. Control. Release* **2016**, *243*, 303–322.

(32) Wilson, W. L.; Szajowski, P. F.; Brus, L. E. *Science (80-.).* **1993**, *262*, 1242–1244.

(33) Delley, B.; Steigmeier, E. F. *Phys. Rev. B* **1993**, *47*, 1397–1400.

(34) Bell, J. P.; Cloud, J. E.; Cheng, J.; Ngo, C.; Kodambaka, S.; Sellinger, A.; Williams, S. K. R.; Yang, Y. *RSC Adv.* **2014**, *4*, 51105–51110.

(35) McVey, B. F. P.; Tilley, R. D. *Acc. Chem. Res.* **2014**, *47*, 3045–3051.

(36) Lee, D. C.; Pietryga, J. M.; Robel, I.; Werder, D. J.; Schaller, R. D.; Klimov, V. I. *J. Am.*

Chem. Soc. **2009**, *131*, 3436–3437.

(37) McVey, B. F. P.; Prabakar, S.; Gooding, J. J.; Tilley, R. D. *Chempluschem* **2017**, *82*, 60–73.

(38) Lu, X.; Ziegler, K. J.; Ghezelbash, A.; Johnston, K. P.; Korgel, B. A. *Nano Lett.* **2004**, *4*, 969–974.

(39) Taylor, B. R.; Kauzlarich, S. M.; Delgado, G. R.; Lee, H. W. H. *Chem. Mater.* **1999**, *11*, 2493–2500.

(40) Murray, Cb.; Norris, D. J.; Bawendi, M. G. *J. Am. Chem. Soc.* **1993**, *115*, 8706–8715.

(41) Peng, X.; Wilson, T. E.; Alivisatos, A. P.; Schultz, P. G. *Angew. Chemie Int. Ed. English* **1997**, *36*, 145–147.

(42) Manna, L.; Scher, E. C.; Alivisatos, A. P. *J. Am. Chem. Soc.* **2000**, *122*, 12700–12706.

(43) Yen, B. K. H.; Stott, N. E.; Jensen, K. F.; Bawendi, M. G. *Adv. Mater.* **2003**, *15*, 1858–1862.

(44) Shim, M.; Guyot-Sionnest, P. *J. Am. Chem. Soc.* **2001**, *123*, 11651–11654.

(45) Li, X.; He, Y.; Swihart, M. T. *Langmuir* **2004**, *20*, 4720–4727.

(46) Jun, Y.; Choi, C.-S.; Cheon, J. *Chem. Commun.* **2001**, 101–102.

(47) Battaglia, D.; Peng, X. *Nano Lett.* **2002**, *2*, 1027–1030.

(48) Xie, R.; Battaglia, D.; Peng, X. *J. Am. Chem. Soc.* **2007**, *129*, 15432–15433.

(49) Marzin, J.-Y.; Gérard, J.-M.; Izraël, A.; Barrier, D.; Bastard, G. *Phys. Rev. Lett.* **1994**, *73*, 716.

(50) Zimmer, J. P.; Kim, S.-W.; Ohnishi, S.; Tanaka, E.; Frangioni, J. V; Bawendi, M. G. *J. Am. Chem. Soc.* **2006**, *128*, 2526–2527.

(51) Liu, W.; Chang, A. Y.; Schaller, R. D.; Talapin, D. V. *J. Am. Chem. Soc.* **2012**, *134*, 20258–20261.

(52) Mićić, O. I.; Ahrenkiel, S. P.; Bertram, D.; Nozik, A. J. *Appl. Phys. Lett.* **1999**, *75*, 478–

480.

(53) Steckel, J. S.; Coe-Sullivan, S.; Bulović, V.; Bawendi, M. G. *Adv. Mater.* **2003**, *15*, 1862–1866.

(54) Murray, C. B.; Sun, S.; Gaschler, W.; Doyle, H.; Betley, T. A.; Kagan, C. R. *IBM J. Res. Dev.* **2001**, *45*, 47–56.

(55) Ellingson, R. J.; Beard, M. C.; Johnson, J. C.; Yu, P.; Micic, O. I.; Nozik, A. J.; Shabaev, A.; Efros, A. L. *Nano Lett.* **2005**, *5*, 865–871.

(56) Sahu, A.; Khare, A.; Deng, D. D.; Norris, D. J. *Chem. Commun.* **2012**, *48*, 5458–5460.

(57) Dong, B.; Li, C.; Chen, G.; Zhang, Y.; Zhang, Y.; Deng, M.; Wang, Q. *Chem. Mater.* **2013**, *25*, 2503–2509.

(58) Miao, S.; Hickey, S. G.; Rellinghaus, B.; Waurisch, C.; Eychmüller, A. *J. Am. Chem. Soc.* **2010**, *132*, 5613–5615.

(59) Luber, E. J.; Mobarok, M. H.; Buriak, J. M. *ACS Nano* **2013**, *7*, 8136–8146.

(60) Taylor, P. N.; Schreuder, M. A.; Smeeton, T. M.; Grundy, A. J. D.; Dimmock, J. A. R.; Hooper, S. E.; Heffernan, J.; Kauer, M. *J. Mater. Chem. C* **2014**, *2*, 4379–4382.

(61) Harris, D. K.; Allen, P. M.; Han, H.-S.; Walker, B. J.; Lee, J.; Bawendi, M. G. *J. Am. Chem. Soc.* **2011**, *133*, 4676–4679.

(62) Kolny-Olesiak, J.; Weller, H. *ACS Appl. Mater. Interfaces* **2013**, *5*, 12221–12237.

(63) Akkerman, Q. A.; Genovese, A.; George, C.; Prato, M.; Moreels, I.; Casu, A.; Marras, S.; Curcio, A.; Scarpellini, A.; Pellegrino, T.; Manna, L.; Lesnyak, V. *ACS Nano* **2015**, *9*, 521–531.

(64) Panthani, M. G.; Akhavan, V.; Goodfellow, B.; Schmidtke, J. P.; Dunn, L.; Dodabalapur, A.; Barbara, P. F.; Korgel, B. A. *J. Am. Chem. Soc.* **2008**, *130*, 16770–16777.

(65) Aldakov, D.; Lefrancois, A.; Reiss, P. *J. Mater. Chem. C* **2013**, *1*, 3756–3776.

(66) Zang, H.; Li, H.; Makarov, N. S.; Velizhanin, K. A.; Wu, K.; Park, Y.-S.; Klimov, V. I. *Nano Lett.* **2017**, *17*, 1787–1795.

(67) Chuang, P.-H.; Lin, C. C.; Liu, R.-S. *ACS Appl. Mater. Interfaces* **2014**, *6*, 15379–15387.

(68) Song, W.-S.; Kim, J.-H.; Lee, J.-H.; Lee, H.-S.; Do, Y. R.; Yang, H. *J. Mater. Chem.* **2012**, *22*, 21901–21908.

(69) Liao, Y.; Brossard, M.; Hsieh, D.; Lin, T.; Charlton, M. D. B.; Cheng, S.; Chen, C.; Shen, J.; Cheng, L.; Hsieh, T. *Adv. Energy Mater.* **2015**, *5*, 1401280.

(70) Karimi, M.; Eshraghi, M. J.; Jahangir, V. *Mater. Lett.* **2016**, *171*, 100–103.

(71) Bai, B.; Kou, D.; Zhou, W.; Zhou, Z.; Tian, Q.; Meng, Y.; Wu, S. *J. Power Sources* **2016**, *318*, 35–40.

(72) Yang, Z.; Voznyy, O.; Liu, M.; Yuan, M.; Ip, A. H.; Ahmed, O. S.; Levina, L.; Kinge, S.; Hoogland, S.; Sargent, E. H. *ACS Nano* **2015**, *9*, 12327–12333.

(73) Bansal, A. K.; Antolini, F.; Zhang, S.; Stroea, L.; Ortolani, L.; Lanzi, M.; Serra, E.; Allard, S.; Scherf, U.; Samuel, I. D. W. *J. Phys. Chem. C* **2016**, *120*, 1871–1880.

(74) Algar, W. R.; Susumu, K.; Delehanty, J. B.; Medintz, I. L. *Anal. Chem.* **2011**, *83*, 8826–8837.

(75) Jeong, K. S.; Guyot-Sionnest, P. *ACS Nano* **2016**, *10*, 2225–2231.

(76) Lim, S. J.; Zahid, M. U.; Le, P.; Ma, L.; Entenberg, D.; Harney, A. S.; Condeelis, J.; Smith, A. M. *Nat. Commun.* **2015**, *6*, 8210.

(77) Alivisatos, A. P. *J. Phys. Chem.* **1996**, *100*, 13226–13239.

(78) O'Farrell, N.; Houlton, A.; Horrocks, B. R. *Int. J. Nanomedicine* **2006**, *1*, 451–472.

(79) Mansur, H. S. *Wiley Interdiscip. Rev. Nanomedicine Nanobiotechnology* **2010**, *2*, 113–129.

(80) Cheng, X.; Lowe, S. B.; Reece, P. J.; Gooding, J. J. *Chem. Soc. Rev.* **2014**, *43*, 2680–2700.

(81) Reiss, P.; Protiere, M.; Li, L. *small* **2009**, *5*, 154–168.

(82) Spanhel, L.; Haase, M.; Weller, H.; Henglein, A. *J. Am. Chem. Soc.* **1987**, *109*, 5649–5655.

(83) Hines, M. A.; Guyot-Sionnest, P. *J. Phys. Chem.* **1996**, *100*, 468–471.

(84) Dabbousi, B. O.; Rodriguez-Viejo, J.; Mikulec, F. V; Heine, J. R.; Mattoussi, H.; Ober, R.;

Jensen, K. F.; Bawendi, M. G. *J. Phys. Chem. B* **1997**, *101*, 9463–9475.

(85) Peng, X.; Schlamp, M. C.; Kadavanich, A. V; Alivisatos, A. P. *J. Am. Chem. Soc.* **1997**, *119*, 7019–7029.

(86) Vasudevan, D.; Gaddam, R. R.; Trinchi, A.; Cole, I. *J. Alloys Compd.* **2015**, *636*, 395–404.

(87) Zhong, X.; Xie, R.; Zhang, Y.; Basché, T.; Knoll, W. *Chem. Mater.* **2005**, *17*, 4038–4042.

(88) Kim, S.; Fisher, B.; Eisler, H.-J.; Bawendi, M. *J. Am. Chem. Soc.* **2003**, *125*, 11466–11467.

(89) Dasog, M.; Kehrle, J.; Rieger, B.; Veinot, J. G. C. *Angew. Chemie Int. Ed.* **2016**, *55*, 2322–2339.

(90) He, Y.; Zhong, Y.; Peng, F.; Wei, X.; Su, Y.; Lu, Y.; Su, S.; Gu, W.; Liao, L.; Lee, S.-T. *J. Am. Chem. Soc.* **2011**, *133*, 14192–14195.

(91) He, Y.; Kang, Z.; Li, Q.; Tsang, C. H. A.; Fan, C.; Lee, S. *Angew. Chemie* **2009**, *121*, 134–138.

(92) Zhong, Y.; Song, B.; Peng, F.; Wu, Y.; Wu, S.; Su, Y.; He, Y. *Chem. Commun.* **2016**, *52*, 13444–13447.

(93) Mobarok, M. H.; Purkait, T. K.; Islam, M. A.; Miskolzie, M.; Veinot, J. G. C. *Angew. Chem. Int. Ed.* **2017**, *56*, 6073 –6077.

(94) Canham, L. T. *Appl. Phys. Lett.* **1990**, *57*, 1046–1048.

(95) Cullis, A. G.; Canham, L. T. *Nature* **1991**, *353*, 335–338.

(96) Ghosh, B.; Shirahata, N. *Sci. Technol. Adv. Mater.* **2014**, *15*, 14207.

(97) Okada, R.; Iijima, S. *Appl. Phys. Lett.* **1991**, *58*, 1662–1663.

(98) Werwa, E.; Seraphin, A. A.; Chiu, L. A.; Zhou, C.; Kolenbrander, K. D. *Appl. Phys. Lett.* **1994**, *64*, 1821–1823.

(99) Umezu, I.; Minami, H.; Senoo, H.; Sugimura, A. In *Journal of Physics: Conference Series*; IOP Publishing, 2007; Vol. 59, pp 392–395.

(100) Shirahata, N.; Linford, M. R.; Furumi, S.; Pei, L.; Sakka, Y.; Gates, R. J.; Asplund, M. C.

Chem. Commun. **2009**, No. 31, 4684–4686.

(101) Anglin, E. J.; Cheng, L.; Freeman, W. R.; Sailor, M. J. *Adv. Drug Deliv. Rev.* **2008**, *60*, 1266–1277.

(102) Heinrich, J. L.; Curtis, C. L.; Credo, G. M.; Kavanagh, K. L.; Sailor, M. J. *Science (80-.).* **1992**, *255*, 66–68.

(103) Bley, R. A.; Kauzlarich, S. M.; Davis, J. E.; Lee, H. W. H. *Chem. Mater.* **1996**, *8*, 1881–1888.

(104) Kang, Z.; Tsang, C. H. A.; Zhang, Z.; Zhang, M.; Wong, N.; Zapien, J. A.; Shan, Y.; Lee, S.-T. *J. Am. Chem. Soc.* **2007**, *129*, 5326–5327.

(105) Behray, M.; Webster, C. A.; Pereira, S.; Ghosh, P.; Krishnamurthy, S.; Al-Jamal, W. T.; Chao, Y. *ACS Appl. Mater. Interfaces* **2016**, *8*, 8908–8917.

(106) Robbins, H.; Schwartz, B. *J. Electrochem. Soc.* **1959**, *106*, 505–508.

(107) Archer, R. J. *J. Phys. Chem. Solids* **1960**, *14*, 104–110.

(108) Turner, D. R. *J. Electrochem. Soc.* **1960**, *107*, 810–816.

(109) Kelly, M. T.; Chun, J. K. M.; Bocarsly, A. B. *Appl. Phys. Lett.* **1994**, *64*, 1693–1695.

(110) de Vasconcelos, E. A.; Da Silva, E. F.; Dos Santos, B.; De Azevedo, W. M.; Freire, J. A. K. *Phys. status solidi* **2005**, *202*, 1539–1542.

(111) Sato, K.; Tsuji, H.; Hirakuri, K.; Fukata, N.; Yamauchi, Y. *Chem. Commun.* **2009**, No. 25, 3759–3761.

(112) Heintz, A. S.; Fink, M. J.; Mitchell, B. S. *Adv. Mater.* **2007**, *19*, 3984–3988.

(113) Chaudhary, A.-L.; Sheppard, D. A.; Paskevicius, M.; Saunders, M.; Buckley, C. E. *RSC Adv.* **2014**, *4*, 21979–21983.

(114) Heath, J. R. *Science (80-.).* **1992**, *258*, 1131–1133.

(115) Arul Dhas, N.; Raj, C. P.; Gedanken, A. *Chem. Mater.* **1998**, *10*, 3278–3281.

(116) Wilcoxon, J. P., Samara., G. A. *Appl. Phys. Lett.* **1999**, *74*, 3164–3166.

(117) Warner, J. H.; Hoshino, A.; Yamamoto, K.; Tilley, R. *Angew. Chem., Int. Ed* **2005**, *44*, 4550–4554.

(118) Shiohara, A.; Prabakar, S.; Faramus, A.; Hsu, C.-Y.; Lai, P.-S.; Northcote, P. T.; Tilley, R. D. *Nanoscale* **2011**, *3*, 3364–3370.

(119) Sudeep, P. K.; Page, Z.; Emrick, T. *Chem. Commun.* **2008**, No. 46, 6126–6127.

(120) Linehan, K.; Doyle, H. *Small* **2014**, *10*, 584–590.

(121) Wang, J.; Sun, S.; Peng, F.; Cao, L.; Sun, L. *Chem. Commun.* **2011**, *47*, 4941–4943.

(122) Cheng, X.; Gondosiswanto, R.; Ciampi, S.; Reece, P. J.; Gooding, J. J. *Chem. Commun.* **2012**, *48*, 11874–11876.

(123) Rosso-Vasic, M.; Spruijt, E.; van Lagen, B.; De Cola, L.; Zuilhof, H. *Small* **2008**, *4*, 1835–1841.

(124) Baldwin, R. K.; Pettigrew, K. A.; Ratai, E.; Augustine, M. P.; Kauzlarich, S. M. *Chem. Commun.* **2002**, 1822–1823.

(125) Lin, N.; Han, Y.; Wang, L.; Zhou, J.; Zhou, J.; Zhu, Y.; Qian, Y. *Angew. Chemie Int. Ed.* **2015**, *54*, 3822–3825.

(126) Zhong, Y.; Peng, F.; Bao, F.; Wang, S.; Ji, X.; Yang, L.; Su, Y.; Lee, S.-T.; He, Y. *J. Am. Chem. Soc.* **2013**, *135*, 8350–8356.

(127) Shavel, A.; Guerrini, L.; Alvarez-Puebla, R. A. *Nanoscale* **2017**, *9*, 8157–8163.

(128) Tilley, R. D.; Yamamoto, K. *Adv. Mater.* **2006**, *18*, 2053–2056.

(129) Bley, R. A.; Kauzlarich, S. M. *J. Am. Chem. Soc.* **1996**, *118*, 12461–12462.

(130) Yang, C.-S.; Bley, R. A.; Kauzlarich, S. M.; Lee, H. W. H.; Delgado, G. R. *J. Am. Chem. Soc.* **1999**, *121*, 5191–5195.

(131) Mayeri, D.; Phillips, B. L.; Augustine, M. P.; Kauzlarich, S. M. *Chem. Mater.* **2001**, *13*, 765–770.

(132) Pettigrew, K. A.; Liu, Q.; Power, P. P.; Kauzlarich, S. M. *Chem. Mater.* **2003**, *15*, 4005–

4011.

(133) Neiner, D.; Chiu, H. W.; Kauzlarich, S. M. *J. Am. Chem. Soc.* **2006**, *128*, 11016–11017.

(134) Atkins, T. M.; Cassidy, M. C.; Lee, M.; Ganguly, S.; Marcus, C. M.; Kauzlarich, S. M. *ACS Nano* **2013**, *7*, 1609–1617.

(135) Wang, L.; Lin, N.; Zhou, J.; Zhu, Y.; Qian, Y. *Chem. Commun.* **2015**, *51*, 2345–2348.

(136) Cannon, W. R.; Danforth, S. C.; Flint, J. H.; Haggerty, J. S.; Marra, R. A. *J. Am. Ceram. Soc.* **1982**, *65*, 324–330.

(137) Cannon, W. R.; Danforth, S. C.; Haggerty, J. S.; Marra, R. A. *J. Am. Ceram. Soc.* **1982**, *65*, 330–335.

(138) Huisken, F.; Kohn, B.; Paillard, V. *Appl. Phys. Lett.* **1999**, *74*, 3776–3778.

(139) Ledoux, G.; Gong, J.; Huisken, F.; Guillois, O.; Reynaud, C. *Appl. Phys. Lett.* **2002**, *80*, 4834–4836.

(140) Li, X.; He, Y.; Talukdar, S. S.; Swihart, M. T. *Langmuir* **2003**, *19*, 8490–8496.

(141) Hua, F.; Swihart, M. T.; Ruckenstein, E. *Langmuir* **2005**, *21*, 6054–6062.

(142) Erogbogbo, F.; Yong, K.-T.; Roy, I.; Hu, R.; Law, W.-C.; Zhao, W.; Ding, H.; Wu, F.; Kumar, R.; Swihart, M. T. *ACS Nano* **2010**, *5*, 413–423.

(143) Liu, J.; Erogbogbo, F.; Yong, K.-T.; Ye, L.; Liu, J.; Hu, R.; Chen, H.; Hu, Y.; Yang, Y.; Yang, J. *ACS Nano* **2013**, *7*, 7303–7310.

(144) Kortshagen, U. *J. Phys. D. Appl. Phys.* **2009**, *42*, 113001.

(145) Otobe, M.; Kanai, T.; Ifuku, T.; Yajima, H.; Oda, S. *J. Non. Cryst. Solids* **1996**, *198*, 875–878.

(146) Mangolini, L.; Thimsen, E.; Kortshagen, U. *Nano Lett.* **2005**, *5*, 655–659.

(147) Jurbergs, D.; Rogojina, E.; Mangolini, L.; Kortshagen, U. *Appl. Phys. Lett.* **2006**, *88*, 233116.

(148) Viera, G.; Mikikian, M.; Bertran, E.; Cabarrocas, P. R. i; Boufendi, L. *J. Appl. Phys.* **2002**,

92, 4684–4694.

(149) Sankaran, R. M.; Holunga, D.; Flagan, R. C.; Giapis, K. P. *Nano Lett.* **2005**, *5*, 537–541.

(150) Mangolini, L.; Kortshagen, U. *Adv. Mater.* **2007**, *19*, 2513–2519.

(151) Kramer, N. J.; Aydil, E. S.; Kortshagen, U. R. *J. Phys. D. Appl. Phys.* **2015**, *48*, 35205.

(152) Holmes, J. D.; Ziegler, K. J.; Doty, R. C.; Pell, L. E.; Johnston, K. P.; Korgel, B. A. *J. Am. Chem. Soc.* **2001**, *123*, 3743–3748.

(153) English, D. S.; Pell, L. E.; Yu, Z.; Barbara, P. F.; Korgel, B. A. *Nano Lett.* **2002**, *2*, 681–685.

(154) Nesheva, D.; Raptis, C.; Perakis, A.; Bineva, I.; Aneva, Z.; Levi, Z.; Alexandrova, S.; Hofmeister, H. *J. Appl. Phys.* **2002**, *92*, 4678–4683.

(155) Liu, S.; Sato, S.; Kimura, K. *Langmuir* **2005**, *21*, 6324–6329.

(156) Sun, W.; Qian, C.; Cui, X. S.; Wang, L.; Wei, M.; Casillas, G.; Helmy, A. S.; Ozin, G. A. *Nanoscale* **2016**, *8*, 3678–3684.

(157) Hessel, C. M.; Henderson, E. J.; Veinot, J. G. C. *Chem. Mater.* **2006**, *18*, 6139–6146.

(158) Hessel, C. M.; Henderson, E. J.; Veinot, J. G. C. *J. Phys. Chem. C* **2007**, *111*, 6956–6961.

(159) Yang, Z.; Dobbie, A. R.; Cui, K.; Veinot, J. G. C. *J. Am. Chem. Soc.* **2012**, *134*, 13958–13961.

(160) Mastronardi, M. L.; Hennrich, F.; Henderson, E. J.; Maier-Flaig, F.; Blum, C.; Reichenbach, J.; Lemmer, U.; Kübel, C.; Wang, D.; Kappes, M. M. *J. Am. Chem. Soc.* **2011**, *133*, 11928–11931.

(161) Hessel, C. M.; Reid, D.; Panthani, M. G.; Rasch, M. R.; Goodfellow, B. W.; Wei, J.; Fujii, H.; Akhavan, V.; Korgel, B. A. *Chem. Mater.* **2011**, *24*, 393–401.

(162) Yu, Y.; Lu, X.; Guillaussier, A.; Voggu, V. R.; Pineros, W.; de la Mata, M.; Arbiol, J.; Smilgies, D.-M.; Truskett, T. M.; Korgel, B. A. *Nano Lett.* **2016**, *16*, 7814–7821.

(163) Chen, D.; Sun, W.; Qian, C.; Wong, A. P. Y.; Reyes, L. M.; Ozin, G. A. *Adv. Opt. Mater.*

2017, *5*, 1700237.

(164) Beard, M. C.; Knutsen, K. P.; Yu, P.; Luther, J. M.; Song, Q.; Metzger, W. K.; Ellingson, R. J.; Nozik, A. J. *Nano Lett.* **2007**, *7*, 2506–2512.

(165) Dasog, M.; De los Reyes, G. B.; Titova, L. V; Hegmann, F. A.; Veinot, J. G. C. *ACS Nano* **2014**, *8*, 9636–9648.

(166) Buriak, J. M. *Chem. Mater.* **2013**, *26*, 763–772.

(167) Linford, M. R.; Fenter, P.; Eisenberger, P. M.; Chidsey, C. E. *J. Am. Chem. Soc.* **1995**, *117*, 3145–3155.

(168) Buriak, J. M. *Chem. Rev.* **2002**, *102*, 1271–1308.

(169) Buriak, J. M.; Allen, M. J. *J. Am. Chem. Soc.* **1998**, *120*, 1339–1340.

(170) Buriak, J. M.; Stewart, M. P.; Geders, T. W.; Allen, M. J.; Choi, H. C.; Smith, J.; Raftery, D.; Canham, L. T. *J. Am. Chem. Soc.* **1999**, *121*, 11491–11502.

(171) Schmeltzer, J. M.; Porter, L. A.; Stewart, M. P.; Buriak, J. M. *Langmuir* **2002**, *18*, 2971–2974.

(172) Huck, L. A.; Buriak, J. M. *Langmuir* **2012**, *28*, 16285–16293.

(173) Holland, J. M.; Stewart, M. P.; Allen, M. J.; Buriak, J. M. *J. Solid State Chem.* **1999**, *147*, 251–258.

(174) Huck, L. A.; Buriak, J. M. *J. Am. Chem. Soc.* **2012**, *134*, 489–497.

(175) Veinot, J. G. C. *Chem. Commun.* **2006**, No. 40, 4160–4168.

(176) Buriak, J. M. *Chem. Commun.* **1999**, 1051–1060.

(177) Peng, W.; Rupich, S. M.; Shafiq, N.; Gartstein, Y. N.; Malko, A. V; Chabal, Y. J. *Chem. Rev.* **2015**, *115*, 12764–12796.

(178) Shirahata, N.; Hozumi, A.; Yonezawa, T. *Chem. Rec.* **2005**, *5*, 145–159.

(179) Yang, Z.; Iqbal, M.; Dobbie, A. R.; Veinot, J. G. C. *J. Am. Chem. Soc.* **2013**, *135*, 17595–17601.

(180) Yang, Z.; Dasog, M.; Dobbie, A. R.; Lockwood, R.; Zhi, Y.; Meldrum, A.; Veinot, J. G. C. *Adv. Funct. Mater.* **2014**, *24*, 1345–1353.

(181) Qian, C.; Sun, W.; Wang, L.; Chen, C.; Liao, K.; Wang, W.; Jia, J.; Hatton, B. D.; Casillas, G.; Kurylowicz, M. *J. Am. Chem. Soc.* **2014**, *136*, 15849–15852.

(182) Kehrle, J.; Hohlein, I. M. D.; Yang, Z.; Jochem, A. R.; Helbich, T.; Kraus, T.; Veinot, J. G. C.; Rieger, B. *Angew. Chemie. Int. Ed.* **2014**, *53*, 12494–12497.

(183) Yang, Z.; Gonzalez, C. M.; Purkait, T. K.; Iqbal, M.; Meldrum, A.; Veinot, J. G. C. *Langmuir* **2015**, *31*, 10540–10548.

(184) Kelly, J. A.; Shukaliak, A. M.; Fleischauer, M. D.; Veinot, J. G. C. *J. Am. Chem. Soc.* **2011**, *133*, 9564–9571.

(185) Zhai, Y.; Dasog, M.; Snitynsky, R. B.; Purkait, T. K.; Aghajamali, M.; Hahn, A. H.; Sturdy, C. B.; Lowary, T. L.; Veinot, J. G. C. *J. Mater. Chem. B* **2014**, *2*, 8427–8433.

(186) Tilley, R. D.; Warner, J. H.; Yamamoto, K.; Matsui, I.; Fujimori, H. *Chem. Commun.* **2005**, 1833–1835.

(187) Höhlein, I.; Kehrle, J.; Helbich, T.; Yang, Z.; Veinot, J. G. C.; Rieger, B. *Chem. Eur. J.* **2014**, *20*, 4212–4216.

(188) Purkait, T. K.; Iqbal, M.; Wahl, M. H.; Gottschling, K.; Gonzalez, C. M.; Islam, M. A.; Veinot, J. G. C. *J. Am. Chem. Soc.* **2014**, *136*, 17914–17917.

(189) Yu, Y.; Hessel, C. M.; Bogart, T. D.; Panthani, M. G.; Rasch, M. R.; Korgel, B. A. *Langmuir* **2013**, *29*, 1533–1540.

(190) Thissen, P.; Seitz, O.; Chabal, Y. J. *Prog. Surf. Sci.* **2012**, *87*, 272–290.

(191) Bateman, J. E.; Eagling, R. D.; Worrall, D. R.; Horrocks, B. R.; Houlton, A. *Angew. Chemie Int. Ed.* **1998**, *37*, 2683–2685.

(192) Sieval, A. B.; Demirel, A. L.; Nissink, J. W. M.; Linford, M. R.; Van der Maas, J. H.; De Jeu, W. H.; Zuilhof, H.; Sudhölter, E. J. R. *Langmuir* **1998**, *14*, 1759–1768.

(193) Panthani, M. G.; Hessel, C. M.; Reid, D.; Casillas, G.; José-Yacamán, M.; Korgel, B. A. *J.*

Phys. Chem. C **2012**, *116*, 22463–22468.

(194) Hirschman, K. D.; Tsybeskov, L.; Duttagupta, S. P.; Fauchet, Pm. *Nature* **1996**, *384*, 338–341.

(195) Dasog, M.; Yang, Z.; Regli, S.; Atkins, T. M.; Faramus, A.; Singh, M. P.; Muthuswamy, E.; Kauzlarich, S. M.; Tilley, R. D.; Veinot, J. G. C. *ACS Nano* **2013**, *7*, 2676–2685.

(196) Wang, D.; Buriak, J. M. *Langmuir* **2006**, *22*, 6214–6221.

(197) Wheeler, L. M.; Anderson, N. C.; Palomaki, P. K. B.; Blackburn, J. L.; Johnson, J. C.; Neale, N. R. *Chem. Mater.* **2015**, *27*, 6869–6878.

(198) Song, J. H.; Sailor, M. J. *J. Am. Chem. Soc.* **1998**, *120*, 2376–2381.

(199) Kim, N. Y.; Laibinis, P. E. *J. Am. Chem. Soc.* **1998**, *120*, 4516–4517.

(200) Perrine, K. A.; Teplyakov, A. V. *Chem. Soc. Rev.* **2010**, *39*, 3256–3274.

(201) Webb, L. J.; Lewis, N. S. *J. Phys. Chem. B* **2003**, *107*, 5404–5412.

(202) Boukherroub, R.; Morin, S.; Bensebaa, F.; Wayner, D. D. M. *Langmuir* **1999**, *15*, 3831–3835.

(203) Fidélis, A.; Ozanam, F.; Chazalviel, J.-N. *Surf. Sci.* **2000**, *444*, L7–L10.

(204) Höhlein, I. M. D.; Angi, A.; Sinelnikov, R.; Veinot, J. G. C.; Rieger, B. *Chem. - A Eur. J.* **2015**, *21*, 2755–2758.

(205) Dasog, M.; Veinot, J. G. C. *Phys. status solidi* **2014**, *251*, 2216–2220.

(206) Baldwin, R. K.; Pettigrew, K. A.; Garno, J. C.; Power, P. P.; Liu, G.; Kauzlarich, S. M. *J. Am. Chem. Soc.* **2002**, *124*, 1150–1151.

(207) Rogozhina, E.; Belomoin, G.; Smith, A.; Abuhassan, L.; Barry, N.; Akcakir, O.; Braun, P. V; Nayfeh, M. H. *Appl. Phys. Lett.* **2001**, *78*, 3711–3713.

(208) Li, Q.; He, Y.; Chang, J.; Wang, L.; Chen, H.; Tan, Y.-W.; Wang, H.; Shao, Z. *J. Am. Chem. Soc.* **2013**, *135*, 14924–14927.

(209) Wang, L.; Li, Q.; Wang, H.-Y.; Huang, J.-C.; Zhang, R.; Chen, Q.-D.; Xu, H.-L.; Han, W.;

Shao, Z.-Z.; Sun, H.-B. *Light Sci. Appl.* **2015**, *4*, e245.

(210) Bansal, A.; Li, X.; Lauermann, I.; Lewis, N. S.; Yi, S. I.; Weinberg, W. H. *J. Am. Chem. Soc.* **1996**, *118*, 7225–7226.

(211) Dasog, M.; Veinot, J. G. C. *Phys. Status Solidi Appl. Mater. Sci.* **2012**, *209*, 1844–1846.

(212) Dasog, M.; Bader, K.; Veinot, J. G. C. *Chem. Mater.* **2015**, *27*, 1153–1156.

(213) Shiohara, A.; Hanada, S.; Prabakar, S.; Fujioka, K.; Lim, T. H.; Yamamoto, K.; Northcote, P. T.; Tilley, R. D. *J. Am. Chem. Soc.* **2009**, *132*, 248–253.

(214) Zou, J.; Baldwin, R. K.; Pettigrew, K. A.; Kauzlarich, S. M. *Nano Lett.* **2004**, *4*, 1181–1186.

(215) Ruizendaal, L.; Pujari, S. P.; Gevaerts, V.; Paulusse, J. M. J.; Zuilhof, H. *Chem. Asian J.* **2011**, *6*, 2776–2786.

(216) Höhlein, I. M. D.; Kehrle, J.; Purkait, T. K.; Veinot, J. G. C.; Rieger, B. *Nanoscale* **2015**, *7*, 914–918.

(217) Liang, D.; Bowers, J. E. *Nat. Photonics* **2010**, *4*, 511–517.

(218) Daldosso, N.; Pavesi, L. *Laser Photon. Rev.* **2009**, *3*, 508–534.

(219) Littau, K. A.; Szajowski, P. J.; Muller, A. J.; Kortan, A. R.; Brus, L. E. *J. Phys. Chem.* **1993**, *97*, 1224–1230.

(220) Hybertsen, M. S. *Phys. Rev. Lett.* **1994**, *72*, 1514.

(221) Godefroo, S.; Hayne, M.; Jivanescu, M.; Stesmans, A.; Zacharias, M.; Lebedev, O. I.; Van Tendeloo, G.; Moshchalkov, V. V. *Nat. Nanotechnol.* **2008**, *3*, 174–178.

(222) Mitra, S.; Švrček, V.; Macias-Montero, M.; Velusamy, T.; Mariotti, D. *Sci. Rep.* **2016**, *6*, 27727.

(223) Sun, W.; Qian, C.; Chen, K. K.; Ozin, G. A. *ChemNanoMat* **2016**, *2*, 847–855.

(224) Pi, X. D.; Liptak, R. W.; Nowak, J. D.; Wells, N. P.; Carter, C. B.; Campbell, S. A.; Kortshagen, U. *Nanotechnology* **2008**, *19*, 245603.

(225) Gupta, A.; Swihart, M. T.; Wiggers, H. *Adv. Funct. Mater.* **2009**, *19*, 696–703.

(226) Wolf, O.; Dasog, M.; Yang, Z.; Balberg, I.; Veinot, J. G. C.; Millo, O. *Nano Lett.* **2013**, *13*, 2516–2521.

(227) Koch, F.; Petrova-Koch, V.; Muschik, T. *J. Lumin.* **1993**, *57*, 271–281.

(228) Yu, W.; Xu, Y.; Li, H.; Zhan, X.; Lu, W. *Appl. Phys. A* **2013**, *111*, 501–507.

(229) Wolkin, M. V; Jorne, J.; Fauchet, P. M.; Allan, G.; Delerue, C. *Phys. Rev. Lett.* **1999**, *82*, 197–200.

(230) Kanemitsu, Y.; Ogawa, T.; Shiraishi, K.; Takeda, K. *Phys. Rev. B* **1993**, *48*, 4883–4886.

(231) Prokes, S. M.; Carlos, W. E. *J. Appl. Phys.* **1995**, *78*, 2671–2674.

(232) Ondič, L.; Kůsová, K.; Ziegler, M.; Fekete, L.; Gärtnerová, V.; Cháb, V.; Holý, V.; Cibulka, O.; Herynková, K.; Gallart, M. *Nanoscale* **2014**, *6*, 3837–3845.

(233) Tsybeskov, L.; Vandyshev, J. V; Fauchet, P. M. *Phys. Rev. B* **1994**, *49*, 7821–7824.

(234) Dohnalová, K.; Žídek, K.; Ondič, L.; Kůsová, K.; Cibulka, O.; Pelant, I. *J. Phys. D. Appl. Phys.* **2009**, *42*, 135102.

(235) Locritani, M.; Yu, Y.; Bergamini, G.; Baroncini, M.; Molloy, J. K.; Korgel, B. A.; Ceroni, P. *J. Phys. Chem. Lett.* **2014**, *5*, 3325−3329.

(236) Kang, Z.; Tsang, C. H. A.; Wong, N.-B.; Zhang, Z.; Lee, S.-T. *J. Am. Chem. Soc.* **2007**, *129*, 12090–12091.

(237) Erogbogbo, F.; Lin, T.; Tucciarone, P. M.; LaJoie, K. M.; Lai, L.; Patki, G. D.; Prasad, P. N.; Swihart, M. T. *Nano Lett.* **2013**, *13*, 451–456.

(238) Sun, W.; Qian, C.; He, L.; Ghuman, K. K.; Wong, A. P. Y.; Jia, J.; Jelle, A. A.; O'Brien, P. G.; Reyes, L. M.; Wood, T. E. *Nat. Commun.* **2016**, *7*, 12553.

(239) Wheeler, L. M.; Neale, N. R.; Chen, T.; Kortshagen, U. R. *Nat. Commun.* **2013**, *4*, 2197.

(240) Park, Y.; Advincula, R. C. *Chem. Mater.* **2011**, *23*, 4273–4294.

(241) Lutich, A. A.; Pöschl, A.; Jiang, G.; Stefani, F. D.; Susha, A. S.; Rogach, A. L.; Feldmann, J. *Appl. Phys. Lett.* **2010**, *96*, 83109.

(242) Sun, B.; Snaith, H. J.; Dhoot, A. S.; Westenhoff, S.; Greenham, N. C. *J. Appl. Phys.* **2005**, *97*, 14914.

(243) Huynh, W. U.; Dittmer, J. J.; Alivisatos, A. P. *Science (80-.).* **2002**, *295*, 2425–2427.

(244) Saunders, B. R. *J. Colloid Interface Sci.* **2012**, *369*, 1–15.

(245) Tessler, N.; Medvedev, V.; Kazes, M.; Kan, S.; Banin, U. *Science (80-.).* **2002**, *295*, 1506–1508.

(246) Dabbousi, B. O.; Bawendi, M. G.; Onitsuka, O.; Rubner, M. F. *Appl. Phys. Lett.* **1995**, *66*, 1316–1318.

(247) Guo, F.; Yang, B.; Yuan, Y.; Xiao, Z.; Dong, Q.; Bi, Y.; Huang, J. *Nat Nano* **2012**, *7*, 798–802.

(248) Liao, G.; Chen, S.; Quan, X.; Chen, H.; Zhang, Y. *Environ. Sci. Technol.* **2010**, *44*, 3481–3485.

(249) Hessel, C. M.; Pattani, V. P.; Rasch, M.; Panthani, M. G.; Koo, B.; Tunnell, J. W.; Korgel, B. A. *Nano Lett.* **2011**, *11*, 2560–2566.

(250) Biju, V. *Chem. Soc. Rev.* **2014**, *43*, 744–764.

(251) Carregal-Romero, S.; Ochs, M.; Rivera-Gil, P.; Ganas, C.; Pavlov, A. M.; Sukhorukov, G. B.; Parak, W. J. *J. Control. release* **2012**, *159*, 120–127.

(252) Hong, J.; Lee, S.; Seo, J.; Pyo, S.; Kim, J.; Lee, T. *ACS Appl. Mater. Interfaces* **2015**, *7*, 3554–3561.

(253) Liu, C.-Y.; Holman, Z. C.; Kortshagen, U. R. *Nano Lett.* **2009**, *9*, 449–452.

(254) Meinardi, F.; Ehrenberg, S.; Dhamo, L.; Carulli, F.; Mauri, M.; Bruni, F.; Simonutti, R.; Kortshagen, U.; Brovelli, S. *Nat. Photonics* **2017**, *11*, 177–185.

(255) Dung, M. X.; Choi, J.-K.; Jeong, H.-D. *ACS Appl. Mater. Interfaces* **2013**, *5*, 2400–2409.

(256) Marinins, A.; Yang, Z.; Chen, H.; Linnros, J.; Veinot, J. G. C.; Popov, S.; Sychugov, I. *ACS Photonics* **2016**, *3*, 1575–1580.

(257) Gandhi, A.; Paul, A.; Sen, S. O.; Sen, K. K. *asian J. Pharm. Sci.* **2015**, *10*, 99–107.

(258) Li, Z. F.; Swihart, M. T.; Ruckenstein, E. *Langmuir* **2004**, *20*, 1963–1971.

(259) Tao, H.-C.; Yang, X.-L.; Zhang, L.-L.; Ni, S.-B. *J. Solid State Electrochem.* **2014**, *18*, 1989–1994.

(260) Yasar-Inceoglu, O.; Zhong, L.; Mangolini, L. *J. Phys. D. Appl. Phys.* **2015**, *48*, 314009.

(261) Park, M.; Lee, D.; Shin, S.; Kim, H.-J.; Hyun, J. *Carbohydr. Polym.* **2016**, *140*, 43–50.

(262) Mitra, S.; Cook, S.; Švrček, V.; Blackley, R. A.; Zhou, W.; Kovač, J.; Cvelbar, U.; Mariotti, D. *J. Phys. Chem. C* **2013**, *117*, 23198–23207.

(263) McCullough, R. D. *Adv. Mater.* **1998**, *10*, 93–116.

(264) Bousquet, A.; Awada, H.; Hiorns, R. C.; Dagron-Lartigau, C.; Billon, L. *Prog. Polym. Sci.* **2014**, *39*, 1847–1877.

(265) Haring, A. J.; Ahrenholtz, S. R.; Morris, A. J. *ACS Appl. Mater. Interfaces* **2014**, *6*, 4394–4401.

(266) Xu, J.; Wang, J.; Mitchell, M.; Mukherjee, P.; Jeffries-EL, M.; Petrich, J. W.; Lin, Z. *J. Am. Chem. Soc.* **2007**, *129*, 12828–12833.

(267) Boon, F.; Moerman, D.; Laurencin, D.; Richeter, S.; Guari, Y.; Mehdi, A.; Dubois, P.; Lazzaroni, R.; Clément, S. *Langmuir* **2014**, *30*, 11340–11347.

(268) Liu, J.; Tanaka, T.; Sivula, K.; Alivisatos, A. P.; Fréchet, J. M. J. *J. Am. Chem. Soc.* **2004**, *126*, 6550–6551.

(269) Senkovskyy, V.; Khanduyeva, N.; Komber, H.; Oertel, U.; Stamm, M.; Kuckling, D.; Kiriy, A. *J. Am. Chem. Soc.* **2007**, *129*, 6626–6632.

(270) Sontag, S. K.; Marshall, N.; Locklin, J. *Chem. Commun.* **2009**, No. 23, 3354–3356.

(271) Senkovskyy, V.; Tkachov, R.; Beryozkina, T.; Komber, H.; Oertel, U.; Horecha, M.; Bocharova, V.; Stamm, M.; Gevorgyan, S. A.; Krebs, F. C.; Kiriy, A. *J. Am. Chem. Soc.* **2009**, *131*, 16445–16453.

(272) Cho, K. S.; Park, N.-M.; Kim, T.-Y.; Kim, K.-H.; Sung, G. Y.; Shin, J. H. *Appl. Phys. Lett.* **2005**, *86*, 71909.

(273) Cheng, K.-Y.; Anthony, R.; Kortshagen, U. R.; Holmes, R. J. *Nano Lett.* **2011**, *11*, 1952–1956.

(274) Maier-Flaig, F.; Rinck, J.; Stephan, M.; Bocksrocker, T.; Bruns, M.; Kübel, C.; Powell, A. K.; Ozin, G. A.; Lemmer, U. *Nano Lett.* **2013**, *13*, 475–480.

(275) Gonzalez, C. M.; Iqbal, M.; Dasog, M.; Piercey, D. G.; Lockwood, R.; Klapötke, T. M.; Veinot, J. G. C. *Nanoscale* **2014**, *6*, 2608–2612.

(276) Ban, R.; Zheng, F.; Zhang, J. *Anal. Methods* **2015**, *7*, 1732–1737.

(277) Härting, M.; Zhang, J.; Gamota, D. R.; Britton, D. T. *Appl. Phys. Lett.* **2009**, *94*, 193509.

(278) Holman, Z. C.; Liu, C.-Y.; Kortshagen, U. R. *Nano Lett.* **2010**, *10*, 2661–2666.

(279) Kim, S.-K.; Kim, B.-H.; Cho, C.-H.; Park, S.-J. *Appl. Phys. Lett.* **2009**, *94*, 183106.

(280) Hirano, Y.; Sato, F.; Aihara, S.; Saito, N.; Miyazaki, S.; Hirose, M. *Appl. Phys. Lett.* **2001**, *79*, 2255–2257.

(281) Shieh, J.-M.; Lai, Y.-F.; Ni, W.-X.; Kuo, H.-C.; Fang, C.-Y.; Huang, J. Y.; Pan, C.-L. *Appl. Phys. Lett.* **2007**, *90*, 51105.

(282) Lin, T.; Liu, X.; Zhou, B.; Zhan, Z.; Cartwright, A. N.; Swihart, M. T. *Adv. Funct. Mater.* **2014**, *24*, 6016–6022.

(283) Liu, C.-Y.; Kortshagen, U. R. *Nanoscale Res. Lett.* **2010**, *5*, 1253–1256.

(284) Ding, Y.; Gresback, R.; Liu, Q.; Zhou, S.; Pi, X.; Nozaki, T. *Nano Energy* **2014**, *9*, 25–31.

(285) Peng, F.; Wang, J.; Ge, G.; He, T.; Cao, L.; He, Y.; Ma, H.; Sun, S. *Mater. Lett.* **2013**, *92*, 65–67.

(286) El-Demellawi, J. K.; Holt, C. R.; Abou-Hamad, E.; Al-Talla, Z. A.; Saih, Y.; Chaieb, S. *ACS Appl. Mater. Interfaces* **2015**, *7*, 13794–13800.

(287) Erogbogbo, F.; Yong, K.-T.; Roy, I.; Xu, G.; Prasad, P. N.; Swihart, M. T. *ACS Nano* **2008**,

2, 873–878.

(288) He, Y.; Su, Y.; Yang, X.; Kang, Z.; Xu, T.; Zhang, R.; Fan, C.; Lee, S.-T. *J. Am. Chem. Soc.* **2009**, *131*, 4434–4438.

(289) Tu, C.-C.; Chen, K.-P.; Yang, T.-A.; Chou, M.-Y.; Lin, L. Y.; Li, Y.-K. *ACS Appl. Mater. Interfaces* **2016**, *8*, 13714–13723.

(290) Xu, Z.; Wang, D.; Guan, M.; Liu, X.; Yang, Y.; Wei, D.; Zhao, C.; Zhang, H. *ACS Appl. Mater. Interfaces* **2012**, *4*, 3424–3431.

(291) Ji, X.; Peng, F.; Zhong, Y.; Su, Y.; Jiang, X.; Song, C.; Yang, L.; Chu, B.; Lee, S.; He, Y. *Adv. Mater.* **2015**, *27*, 1029–1034.

(292) Ohta, S.; Yamura, K.; Inasawa, S.; Yamaguchi, Y. *Chem. Commun.* **2015**, *51*, 6422–6425.

(293) Facchetti, A. *Chem. Mater.* **2011**, *23*, 733–758.

(294) Sekine, C.; Tsubata, Y.; Yamada, T.; Kitano, M.; Doi, S. *Sci. Technol. Adv. Mater.* **2014**, *15*, 34203.

(295) Li, G.; Zhu, R.; Yang, Y. *Nat. Photonics* **2012**, *6*, 153–161.

(296) Ghosh, B.; Masuda, Y.; Wakayama, Y.; Imanaka, Y.; Inoue, J.; Hashi, K.; Deguchi, K.; Yamada, H.; Sakka, Y.; Ohki, S. *Adv. Funct. Mater.* **2014**, *24*, 7151–7160.

(297) Yoshikawa, K.; Kawasaki, H.; Yoshida, W.; Irie, T.; Konishi, K.; Nakano, K.; Uto, T.; Adachi, D.; Kanematsu, M.; Uzu, H. *Nat. Energy* **2017**, *2*, 17032.

(298) Mangolini, L. *J. Vac. Sci. Technol. B, Nanotechnol. Microelectron. Mater. Process. Meas. Phenom.* **2013**, *31*, 20801.

(299) Song, T.; Lee, S.-T.; Sun, B. *J. Mater. Chem.* **2012**, *22*, 4216–4232.

(300) Kim, S.; Jeon, K.; Lee, J. C.; Swihart, M. T.; Yang, M. *Appl. Phys. Express* **2012**, *5*, 22302.

(301) Palaniappan, K.; Murphy, J. W.; Khanam, N.; Horvath, J.; Alshareef, H.; Quevedo-Lopez, M.; Biewer, M. C.; Park, S. Y.; Kim, M. J.; Gnade, B. E.; Stefan, M. C. *Macromolecules* **2009**, *42*, 3845–3848.

(302) He, M.; Qiu, F.; Lin, Z. *J. Phys. Chem. Lett.* **2013**, *4*, 1788–1796.

(303) Zhao, L.; Pang, X.; Adhikary, R.; Petrich, J. W.; Jeffries-EL, M.; Lin, Z. *Adv. Mater.* **2011**, *23*, 2844–2849.

(304) Wei, H.; Fang, Y.; Yuan, Y.; Shen, L.; Huang, J. *Adv. Mater.* **2015**, *27*, 4975–4981.

(305) Antoniadis, H.; Jiang, F.; Shan, W.; Liu, Y. In *Photovoltaic Specialists Conference (PVSC), 2010 35th IEEE*; IEEE, 2010; pp 1193–1196.

(306) Scardera, G.; Poplavskyy, D.; Abbott, M.; Lemmi, F. In *Photovoltaic Specialists Conference (PVSC), 2011 37th IEEE*; IEEE, 2011; pp 2202–2205.

(307) Ouyang, H.; Striemer, C. C.; Fauchet, P. M. *Appl. Phys. Lett.* **2006**, *88*, 163108.

(308) Gan, F.; Hou, L.; Wang, G.; Liu, H.; Li, J. *Mater. Sci. Eng. B* **2000**, *76*, 63–68.

(309) Takiguchi, Y.; Maruyama, H.; Kosugi, M.; Andoh, F.; Kato, T.; Tanioka, K.; Yamazaki, J.; Tsuji, K.; Kawamura, T. *IEEE Trans. Electron Devices* **1997**, *44*, 1783–1788.

(310) Chen, G.; Xu, Z.; Ding, H.; Sadler, B. M. *Opt. Express* **2009**, *17*, 3929–3940.

(311) Li, W.-D.; Chou, S. Y. *Opt. Express* **2010**, *18*, 931–937.

(312) Liu, C. Y.; Holman, Z. C.; Kortshagen, U. R. *Adv. Funct. Mater.* **2010**, *20*, 2157–2164.

(313) Gresback, R.; Kramer, N. J.; Ding, Y.; Chen, T.; Kortshagen, U. R.; Nozaki, T. *ACS Nano* **2014**, *8*, 5650–5656.

(314) Allard, S.; Forster, M.; Souharce, B.; Thiem, H.; Scherf, U. *Angew. Chemie Int. Ed.* **2008**, *47*, 4070–4098.

(315) Ridley, B. A.; Nivi, B.; Jacobson, J. M. *Science (80-.).* **1999**, *286*, 746–749.

(316) Panthani, M. G.; Korgel, B. A. *Annu. Rev. Chem. Biomol. Eng.* **2012**, *3*, 287–311.

(317) Lin, C.-C.; Ho, P.-H.; Huang, C.-L.; Du, C.-H.; Yu, C.-C.; Chen, H.-L.; Yeh, Y.-C.; Li, S.-S.; Lee, C.-K.; Pao, C.-W. *J. Phys. Chem. C* **2012**, *116*, 25081–25088.

(318) Gonzalez, C. M.; Veinot, J. G. C. *J. Mater. Chem. C* **2016**, *4*, 4836–4846.

(319) Iqbal, M.; Purkait, T. K.; Goss, G. G.; Bolton, J. R.; Gamal El-Din, M.; Veinot, J. G. C.

ACS Nano **2016**, *10*, 5405–5412.

(320) Zhang, Y.; Ziegler, D.; Salmeron, M. *ACS Nano* **2013**, *7*, 8258–8265.

(321) Forrest, S. R. *Nature* **2004**, *428*, 911–918.

(322) Guilbert, A. a Y.; Reynolds, L. X.; Bruno, A.; MacLachlan, A.; King, S. P.; Faist, M. a; Pires, E.; Macdonald, J. E.; Stingelin, N.; Haque, S. a; Nelson, J. *ACS Nano* **2012**, *6*, 3868–3875.

(323) Berggren, M.; Richter-Dahlfors, A. *Adv. Mater.* **2007**, *19*, 3201–3213.

(324) Waltman, R. J.; Bargon, J.; Diaz, a F. *J. Phys. Chem.* **1983**, *87*, 1459–1463.

(325) Yamamoto, T.; Sanechika, K.; Yamamoto, A. *J. Polym. Sci. Polym. Lett. Ed.* **1980**, *18*, 9–12.

(326) Kobayashi, M.; Chen, J.; Chung, T.-C.; Moraes, F.; Heeger, A. J.; Wudl, F. *Synth. Met.* **1984**, *9*, 77–86.

(327) Jen, K.-Y.; Miller, G. G.; Elsenbaumer, R. L. *J. Chem. Soc. Chem. Commun.* **1986**, *17*, 1346–1347.

(328) McCullough, R. D.; Lowe, R. D. *J. Chem. Soc. Chem. Commun.* **1992**, 70–72.

(329) Chen, T.-A.; Wu, X.; Rieke, R. D. *J. Am. Chem. Soc.* **1995**, *117*, 233–244.

(330) Beryozkina, T.; Senkovskyy, V.; Kaul, E.; Kiriy, A. *Macromolecules* **2008**, *41*, 7817–7823.

(331) Wu, S.; Huang, L.; Tian, H.; Geng, Y.; Wang, F. *Macromolecules* **2011**, *44*, 7558–7567.

(332) Niemi, V. M.; Knuuttila, P.; Österholm, J.-E.; Korvola, J. *Polymer (Guildf).* **1992**, *33*, 1559–1562.

(333) Perepichka, I. F.; Perepichka, D. F.; Meng, H.; Wudl, F. *Adv. Mater.* **2005**, *17*, 2281–2305.

(334) Jin, S.; Xue, G. *Macromolecules* **1997**, *30*, 5753–5757.

(335) Helgesen, M.; Sondergaard, R.; Krebs, F. C. *J. Mater. Chem.* **2010**, *20*, 36–60.

(336) Liu, R.; Liu, Z. *Chinese Sci. Bull.* **2009**, *54*, 2028–2032.

(337) Denmark, S. E.; Beutner, G. L.; Wynn, T.; Eastgate, M. D. *J. Am. Chem. Soc.* **2005**, *127*, 3774–3789.

(338) Denmark, S. E.; Barsanti, P. A.; Wong, K.-T.; Stavenger, R. A. *J. Org. Chem.* **1998**, *63*, 2428–2429.

(339) Ashby, E. C.; Bowers, J. R. *J. Am. Chem. Soc.* **1981**, *103*, 2242–2250.

(340) Yuan, C.; Fang, Q. *RSC Adv.* **2012**, *2*, 8055–8060.

(341) O'Leary, L. E.; Rose, M. J.; Ding, T. X.; Johansson, E.; Brunschwig, B. S.; Lewis, N. S. *J. Am. Chem. Soc.* **2013**, *135*, 10081–10090.

(342) Kern, W.; Soc, J. E. *J. Electrochem. Soc.* **1990**, *137*, 1887–1892.

(343) Mihailetchi, V. D.; Xie, H.; De Boer, B.; Koster, L. J. A.; Blom, P. W. M. *Adv. Funct. Mater.* **2006**, *16*, 699–708.

(344) Chang, J.-F.; Sun, B.; Breiby, D. W.; Nielsen, M. M.; Sölling, T. I.; Giles, M.; McCulloch, I.; Sirringhaus, H. *Chem. Mater.* **2004**, *16*, 4772–4776.

(345) He, G.; Kang, L.; Torres Delgado, W.; Shynkaruk, O.; Ferguson, M. J.; McDonald, R.; Rivard, E. *J. Am. Chem. Soc.* **2013**, *135*, 5360–5363.

(346) Cook, S.; Furube, A.; Katoh, R. *Energy Environ. Sci.* **2008**, *1*, 294–299.

(347) Hines, D. A.; Kamat, P. V. *ACS Appl. Mater. Interfaces* **2014**, *6*, 3041–3057.

(348) Freeman, R.; Girsh, J.; Willner, I. *ACS Appl. Mater. Interfaces* **2013**, *5*, 2815–2834.

(349) Kim, J. Y.; Voznyy, O.; Zhitomirsky, D.; Sargent, E. H. *Adv. Mater.* **2013**, *25*, 4986–5010.

(350) Islam, M. A.; Purkait, T. K.; Veinot, J. G. C. *J. Am. Chem. Soc.* **2014**, *136*, 15130–15133.

(351) Choi, H.; Chen, Y.-S.; Stamplecoskie, K. G.; Kamat, P. V. *J. Phys. Chem. Lett.* **2015**, *6*, 217–223.

(352) Wright, M.; Uddin, A. *Sol. Energy Mater. Sol. Cells* **2012**, *107*, 87–111.

(353) Sun, K.; Shen, S.; Liang, Y.; Burrows, P. E.; Mao, S. S.; Wang, D. *Chem. Rev.* **2014**, *114*, 8662–8719.

(354) Zhou, T.; Anderson, R. T.; Li, H.; Bell, J.; Yang, Y.; Gorman, B. P.; Pylypenko, S.; Lusk, M. T.; Sellinger, A. *Nano Lett.* **2015**, *15*, 3657–3663.

(355) Niesar, S.; Fabian, W.; Petermann, N.; Herrmann, D.; Riedle, E.; Wiggers, H.; Brandt, M. S.; Stutzmann, M. *Green* **2011**, *1*, 339–350.

(356) Saito, T.; Uchida, Y.; Misono, A.; Yamamoto, A.; Morifuji, K.; Ikeda, S. *J. Am. Chem. Soc.* **1966**, *88*, 5198–5201.

(357) Egerton, R. F. *Electron energy-loss spectroscopy in the electron microscope*, 2nd ed.; Plenum Press: New York and London, 1996.

(358) Banin, U.; Millo, O. *Annu. Rev. Phys. Chem.* **2003**, *54*, 465–492.

(359) Bakkers, E. P. A. M.; Hens, Z.; Zunger, A.; Franceschetti, A.; Kouwenhoven, L. P.; Gurevich, L.; Vanmaekelbergh, D. *Nano Lett.* **2001**, *1*, 551–556.

(360) Milliron, D. J.; Alivisatos, A. P.; Pitois, C.; Edder, C.; Frechet, J. M. J. *Adv. Mater.* **2003**, *15*, 58–61.

(361) Sontag, S. K.; Sheppard, G. R.; Usselman, N. M.; Marshall, N.; Locklin, J. *Langmuir* **2011**, *27*, 12033–12041.

(362) Lutich, A. A.; Jiang, G.; Susha, A. S.; Rogach, A. L.; Stefani, F. D.; Feldmann, J. *Nano Lett.* **2009**, *9*, 2636–2640.

(363) Nolasco, J. C.; Cabré, R.; Ferré-Borrull, J.; Marsal, L. F.; Estrada, M.; Pallarès, J. *J. Appl. Phys.* **2010**, *107*, 44505.

(364) Walters, R. J.; Bourianoff, G. I.; Atwater, H. A. *Nat. Mater.* **2005**, *4*, 143–146.

(365) Su, X.; Wu, Q.; Li, J.; Xiao, X.; Lott, A.; Lu, W.; Sheldon, B. W.; Wu, J. *Adv. Energy Mater.* **2014**, *4*, 1300882.

(366) Park, J.-H.; Gu, L.; Von Maltzahn, G.; Ruoslahti, E.; Bhatia, S. N.; Sailor, M. J. *Nat. Mater.* **2009**, *8*, 331–336.

(367) Xu, R.; Zhang, G.; Mai, J.; Deng, X.; Segura-Ibarra, V.; Wu, S.; Shen, J.; Liu, H.; Hu, Z.; Chen, L. *Nat. Biotechnol.* **2016**, *34*, 414–420.

(368) Sun, Q.-Y.; de Smet, L. C. P. M.; van Lagen, B.; Giesbers, M.; Thüne, P. C.; van Engelenburg, J.; de Wolf, F. A.; Zuilhof, H.; Sudhölter, E. J. R. *J. Am. Chem. Soc.* **2005**, *127*, 2514–2523.

(369) Flamm, D. L.; Donnelly, V. M. *Plasma Chem. Plasma Process.* **1981**, *1*, 317–363.

(370) Flamm, D. L.; Donnelly, V. M.; Ibbotson, D. E. *Basic principles of plasma etching for silicon devices*; Academic Press: Orlando, FL: New York, 1984.

(371) Manos, D. M.; Flamm, D. L. *Plasma etching: An introduction*; Auciello, O., Flamm, D. F., Ed.; Academic Press: London, 1989.

(372) Layadi, N.; Donnelly, V. M.; Lee, J. T. C. *J. Appl. Phys.* **1997**, *81*, 6738–6748.

(373) Kullmer, R.; Bäuerle, D. *Appl. Phys. A Mater. Sci. Process.* **1987**, *43*, 227–232.

(374) Wyman, D. P.; Wang, J. Y. C.; Freeman, W. R. *J. Org. Chem.* **1963**, *28*, 3173–3177.

(375) Olah, G. A.; Schilling, P.; Renner, R.; Kerekes, I. *J. Org. Chem.* **1974**, *39*, 3472–3478.

(376) Rivillon, S.; Chabal, Y. J.; Webb, L. J.; Michalak, D. J.; Lewis, N. S.; Halls, M. D.; Raghavachari, K. *J. Vac. Sci. Technol. A Vacuum, Surfaces, Film.* **2005**, *23*, 1100–1106.

(377) Solares, S. D.; Yu, H.; Webb, L. J.; Lewis, N. S.; Heath, J. R.; Goddard, W. A. *J. Am. Chem. Soc.* **2006**, *128*, 3850–3851.

(378) Yu, H.; Webb, L. J.; Solares, S. D.; Cao, P.; Goddard, W. A.; Heath, J. R.; Lewis, N. S. *J. Phys. Chem. B* **2006**, *110*, 23898–23903.

(379) Cao, P.; Yu, H.; Heath, J. R. *J. Phys. Chem. B* **2006**, *110*, 23615–23618.

(380) Avramov, P. V; Fedorov, D. G.; Sorokin, P. B.; Chernozatonskii, L. A.; Gordon, M. S. *J. Phys. Chem. C* **2007**, *111*, 18824–18830.

(381) Berberan-Santos, M. N.; Bodunov, E. N.; Valeur, B. *Chem. Phys.* **2005**, *315*, 171–182.

(382) Semonin, O. E.; Johnson, J. C.; Luther, J. M.; Midgett, A. G.; Nozik, A. J.; Beard, M. C. *J. Phys. Chem. Lett.* **2010**, *1*, 2445–2450.

(383) Tun, Z.-M.; Panzner, M. J.; Scionti, V.; Medvetz, D.; Wesdemiotis, C.; Youngs, W. J.;

Tessier, C. *J. Am. Chem. Soc.* **2010**, *132*, 17059–17061.

(384) Thorshaug, K.; Swang, O.; Dahl, I. M.; Olafsen, A. *J. Phys. Chem. A* **2006**, *110*, 9801–9804.

(385) Sychugov, I.; Juhasz, R.; Linnros, J.; Valenta, J. *Phys. Rev. B* **2005**, *71*, 115331.

(386) Poddubny, A. N.; Dohnalová, K. *Phys. Rev. B* **2014**, *90*, 245439.

(387) Grim, J. Q.; Manna, L.; Moreels, I. *Chem. Soc. Rev.* **2015**, *44*, 5897–5914.

(388) Kisch, H. *Angew. Chemie Int. Ed.* **2013**, *52*, 812–847.

(389) Yao, J.; Yang, M.; Duan, Y. *Chem. Rev.* **2014**, *114*, 6130–6178.

(390) Tan, Z.; Zhang, Y.; Xie, C.; Su, H.; Liu, J.; Zhang, C.; Dellas, N.; Mohney, S. E.; Wang, Y.; Wang, J. *Adv. Mater.* **2011**, *23*, 3553–3558.

(391) Kirchner, C.; Liedl, T.; Kudera, S.; Pellegrino, T.; Muñoz Javier, A.; Gaub, H. E.; Stölzle, S.; Fertig, N.; Parak, W. J. *Nano Lett.* **2005**, *5*, 331–338.

(392) Awada, H.; Medlej, H.; Blanc, S.; Delville, M.; Hiorns, R. C.; Bousquet, A.; Dagron-Lartigau, C.; Billon, L. *J. Polym. Sci. Part A Polym. Chem.* **2014**, *52*, 30–38.

(393) Wu, Y.; Zhang, X.; Jie, J.; Xie, C.; Zhang, X.; Sun, B.; Wang, Y.; Gao, P. *J. Phys. Chem. C* **2013**, *117*, 11968–11976.

(394) Denmark, S. E.; Wynn, T. *J. Am. Chem. Soc.* **2001**, *123*, 6199–6200.

(395) Denmark, S. E.; Heemstra, J. R. *Org. Lett.* **2003**, *5*, 2303–2306.

(396) Denmark, S. E.; Chung, W. *J. Org. Chem.* **2008**, *73*, 4582–4595.

(397) Rossi, S.; Benaglia, M.; Genoni, A. *Tetrahedron* **2014**, *70*, 2065–2080.

(398) Nuyken, O.; Pask, S. D. *Polymers (Basel).* **2013**, *5*, 361–403.

(399) Asandei, A. D.; Moran, I. W. *J. Am. Chem. Soc.* **2004**, *126*, 15932–15933.

(400) Luca, O. R.; Fenwick, A. Q. *J. Photochem. Photobiol. B Biol.* **2015**, *152*, 26–42.

(401) Skaff, H.; Sill, K.; Emrick, T. *J. Am. Chem. Soc.* **2004**, *126*, 11322–11325.

(402) Giro, R.; Caldas, M. J.; Galvao, D. S. *Int. J. Quantum Chem.* **2005**, *103*, 588–596.

(403) Liao, L. S.; Fung, M. K.; Lee, C. S.; Lee, S. T.; Inbasekaran, M.; Woo, E. P.; Wu, W. W. *Appl. Phys. Lett.* **2000**, *76*, 3582–3584.

(404) Marshall, N.; Sontag, S. K.; Locklin, J. *Macromolecules* **2010**, *43*, 2137–2144.

(405) Tkachov, R.; Senkovskyy, V.; Horecha, M.; Oertel, U.; Stamm, M.; Kiriy, A. *Chem. Commun.* **2010**, *46*, 1425–1427.

(406) Sanda, F.; Endo, T. *J. Polym. Sci. Part A Polym. Chem.* **2001**, *39*, 265–276.

(407) Hiraguri, Y.; Endo, T. *J. Am. Chem. Soc.* **1987**, *109*, 3779–3780.

(408) Bailey, W. J.; Ni, Z.; Wu, S. *J. Polym. Sci. Part A Polym. Chem.* **1982**, *20*, 3021–3030.

(409) Evans, R. A.; Rizzardo, E. *Macromolecules* **1996**, *29*, 6983–6989.

(410) Chinnathambi, S.; Chen, S.; Ganesan, S.; Hanagata, N. *Adv. Healthc. Mater.* **2014**, *3*, 10–29.

(411) Peng, F.; Su, Y.; Zhong, Y.; Fan, C.; Lee, S.-T.; He, Y. *Acc. Chem. Res.* **2014**, *47*, 612–623.

(412) Verma, A.; Uzun, O.; Hu, Y.; Hu, Y.; Han, H.-S.; Watson, N.; Chen, S.; Irvine, D. J.; Stellacci, F. *Nat. Mater.* **2008**, *7*, 588–595.

(413) Shin, S. H. R.; Lee, H.; Bishop, K. J. M. *Angew. Chemie Int. Ed.* **2015**, *54*, 10816–10820.

(414) Alkilany, A. M.; Nagaria, P. K.; Hexel, C. R.; Shaw, T. J.; Murphy, C. J.; Wyatt, M. D. *small* **2009**, *5*, 701–708.

(415) Joo, J.; Liu, X.; Kotamraju, V. R.; Ruoslahti, E.; Nam, Y.; Sailor, M. J. *ACS Nano* **2015**, *9*, 6233–6241.

(416) Pang, J.; Su, Y.; Zhong, Y.; Peng, F.; Song, B.; He, Y. *Nano Res.* **2016**, *9*, 3027–3037.

(417) Zhong, Y.; Peng, F.; Wei, X.; Zhou, Y.; Wang, J.; Jiang, X.; Su, Y.; Su, S.; Lee, S.; He, Y. *Angew. Chemie Int. Ed.* **2012**, *51*, 8485–8489.

(418) Ahire, J. H.; Behray, M.; Webster, C. A.; Wang, Q.; Sherwood, V.; Saengkrit, N.; Ruktanonchai, U.; Woramongkolchai, N.; Chao, Y. *Adv. Healthc. Mater.* **2015**, *4*, 1877–

1886.

(419) Song, C.; Zhong, Y.; Jiang, X.; Peng, F.; Lu, Y.; Ji, X.; Su, Y.; He, Y. *Anal. Chem.* **2015**, *87*, 6718–6723.

(420) Das, P.; Jana, N. R. *ACS Appl. Mater. Interfaces* **2014**, *6*, 4301–4309.

(421) Jiang, S.; Gnanasammandhan, M. K.; Zhang, Y. *J. R. Soc. Interface* **2010**, *7*, 3–18.

(422) Kang, B.; Kukreja, A.; Song, D.; Huh, Y.-M.; Haam, S. *J. Biol. Eng.* **2017**, *11*, 13.

(423) Seo, K.-I.; Haran, B.; Gupta, D.; Guo, D.; Standaert, T.; Xie, R.; Shang, H.; Alptekin, E.; Bae, D.-I.; Bae, G. In *VLSI Technology (VLSI-Technology): Digest of Technical Papers, 2014 Symposium on*; IEEE, 2014; pp 1–2.

(424) Myny, K. *Nat. Electron.* **2018**, *1*, 30–39.

(425) Yamamoto, Y.; Harada, S.; Yamamoto, D.; Honda, W.; Arie, T.; Akita, S.; Takei, K. *Sci. Adv.* **2016**, *2*, 1601473.

(426) Gates, B. D. *Science (80-.).* **2009**, *323*, 1566–1567.

(427) Zhao, J.; Guo, H.; Pang, Y. K.; Xi, F.; Yang, Z. W.; Liu, G.; Guo, T.; Dong, G.; Zhang, C.; Wang, Z. L. *ACS Nano* **2017**, *11*, 11566–11573.

(428) Rogers, J. A.; Bao, Z.; Baldwin, K.; Dodabalapur, A.; Crone, B.; Raju, V. R.; Kuck, V.; Katz, H.; Amundson, K.; Ewing, J.; Drzaic, P. *Proc. Natl. Acad. Sci.* **2001**, *98*, 4835–4840.

(429) Someya, T.; Sekitani, T.; Iba, S.; Kato, Y.; Kawaguchi, H.; Sakurai, T. *Proc. Natl. Acad. Sci. U. S. A.* **2004**, *101*, 9966–9970.

(430) Yokota, T.; Zalar, P.; Kaltenbrunner, M.; Jinno, H.; Matsuhisa, N.; Kitanosako, H.; Tachibana, Y.; Yukita, W.; Koizumi, M.; Someya, T. *Sci. Adv.* **2016**, *2*, 1501856.

(431) Ghosh, T. *Science (80-.).* **2015**, *349*, 382–383.

(432) Kenry; Yeo, J. C.; Lim, C. T. *Microsystems &Amp; Nanoeng.* **2016**, *2*, 16043.

(433) Kaltenbrunner, M.; Sekitani, T.; Reeder, J.; Yokota, T.; Kuribara, K.; Tokuhara, T.; Drack, M.; Schwödiauer, R.; Graz, I.; Bauer-Gogonea, S.; Bauer, S.; Someya, T. *Nature* **2013**, *499*,

458–465.

Appendices

Appendix A: Calculation of Yield of P3HT Presented in Experimental Chapter 2

The % Yield of P3HT can be calculated as follows:

% Yield = (experimental yield / theoretical yield) × 100

The molecular weight of 2-Bromo-3-hexyl-5-iodothiophene (Br-HT-I) starting material for the synthesis of 5-chloromagnesio-2-bromo-3-hexylthiophene monomer is 373.09 g/mol. The molecular weight of the hexylthiophene repeat unit (-HT-) is 166 g/mol. Therefore,

373.09 mg of Br-HT-I should theoretically yield 166 mg of -HT-.

So, X mg of Br-HT-I should theoretically yield (166 × X) / 373.09 mg of -HT-.

% Yield of P3HT in Cl-SiNC-Mediated Polymerization:

7.5 mmol of Br-HT-I = 2798.18 mg Br-HT-I.

Theoretical yield is (166 × 2798.18) / 373.09 mg = 1245 mg

Experimental yield of P3HT = 912 mg.

So, % Yield = (912 / 1245) × 100 = 73.

% Yield of P3HT in Cl-SiNC-Mediated Polymerization in the Absence of Light:

0.5 mmol of Br-HT-I = 186.55 mg Br-HT-I.

Theoretical yield is (166 × 186.55) / 373.09 mg = 83 mg

Experimental yield of P3HT = 47.5 mg.

So, % Yield = (47.5 / 83) × 100 = 57.

% Yield of P3HT in Cl-SiWF-Mediated Polymerization:

3.75 mmol of Br-HT-I = 1399.09 mg Br-HT-I.

Theoretical yield is (166 × 1399.09) / 373.09 mg = 622.5 mg

Experimental yield of P3HT = 410 mg.

So, % Yield = (410 / 622.5) × 100 = 66.

% Yield of P3HT in $SiCl_4$-Mediated Polymerization

3.75 mmol of Br-HT-I = 1399.09 mg Br-HT-I.

Theoretical yield is (166 × 1399.09) / 373.09 mg = 622.5 mg

Experimental yield of P3HT = 461 mg.

So, % Yield = (461 / 622.5) × 100 = 74.

% Yield of P3HT in the Comparison of Cl-SiNC, Cl-SiWF, and $SiCl_4$ Reactivity (Table 2-1):

0.5 mmol of Br-HT-I = 186.55 mg Br-HT-I.

Theoretical yield is (166 × 186.55) / 373.09 mg = 83 mg

Experimental yield of P3HT = 65.6, 15.8, and 26.6 mg for Cl-SiNC, Cl-SiWF, and $SiCl_4$ reactivity evaluations, respectively.

So, % Yield = 79, 19, and 32 for Cl-SiNC, Cl-SiWF, and $SiCl_4$ reactivity evaluations, respectively.

Appendix B: Calculation of Regioregularity of P3HT Presented in Experimental Chapter 2

The percentage of regioregular (head-to-tail: HT), and regiorandom (head-to-head: HH and tail-to-tail: TT) isomers of P3HT was evaluated on the basis of the integration of the area of the α-methylene proton resonance signals at 2.80 and 2.58 ppm, respectively.

% regioregular isomers = (area under resonance signal at 2.80 ppm / sum of area under resonance signals at 2.80 and 2.58 ppm) × 100

% regiorandom isomers = (100 − % regioregular isomers)

The ratios of area under resonance signals at 2.80 and 2.58 ppm are 2.13/1, 1.79/1, and 1.60/1 for P3HT synthesize *via* Cl-SiNC, Cl-SiWF, and $SiCl_4$ mediated polymerizations, respectively (Insets: Figures 2-3, 2-7 a,b). Therefore, the respective % of regioregular isomers are 68, 64, and 62 while that of regiorandom isomers are 32, 36, and 38.

Appendix C: Gas Chromatography-Mass Spectrometry Analysis Presented in Experimental Chapter 4

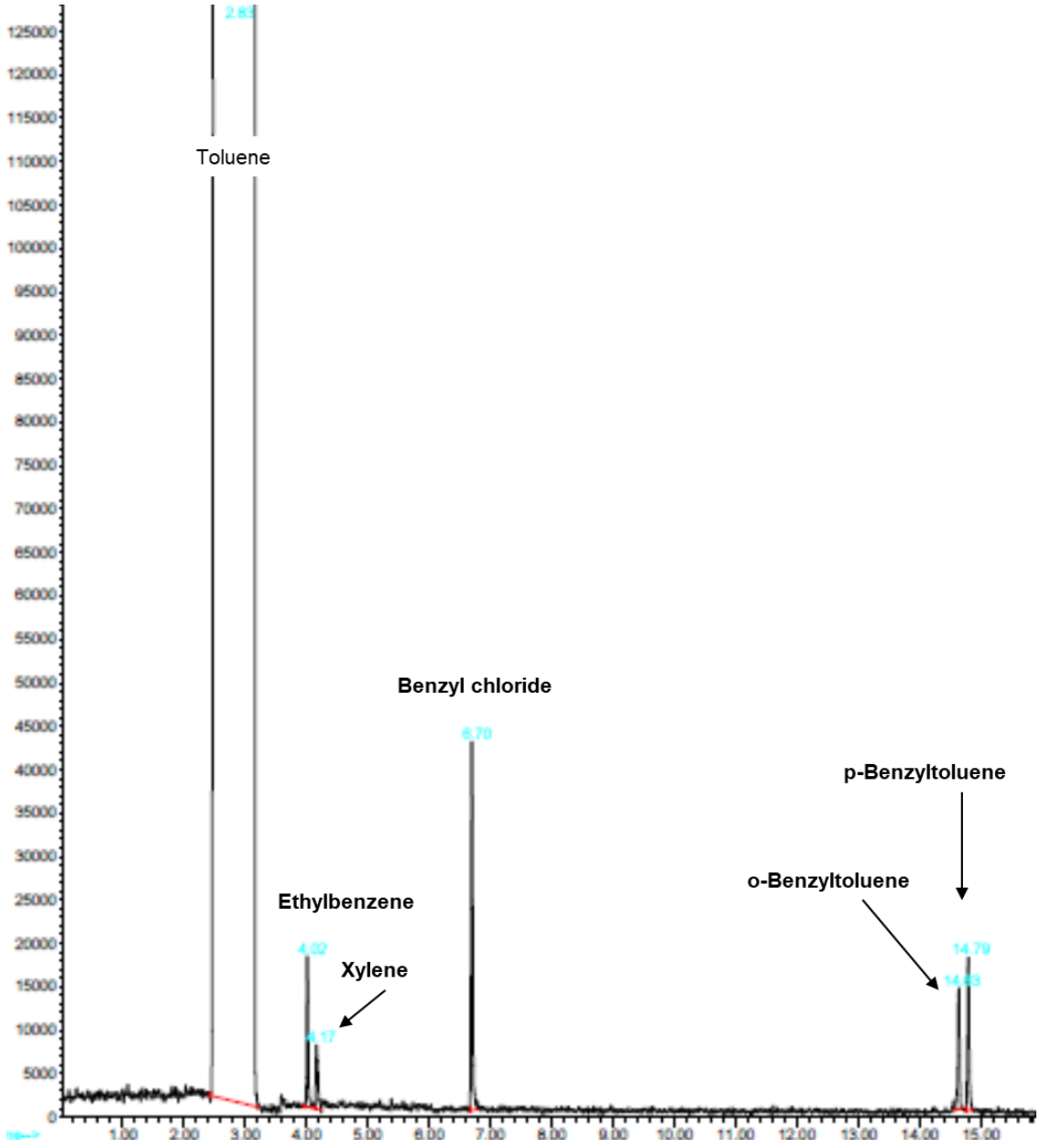

Figure A1. GC chromatogram of the supernatant from the reaction of d~3.4 nm H-SiNCs with PCl_5 in toluene showing some conversion of toluene into benzyl chloride, ortho-benzyltoluene and para-benzyltoluene. Ethyl benzene and xylene are the common impurities present in toluene.

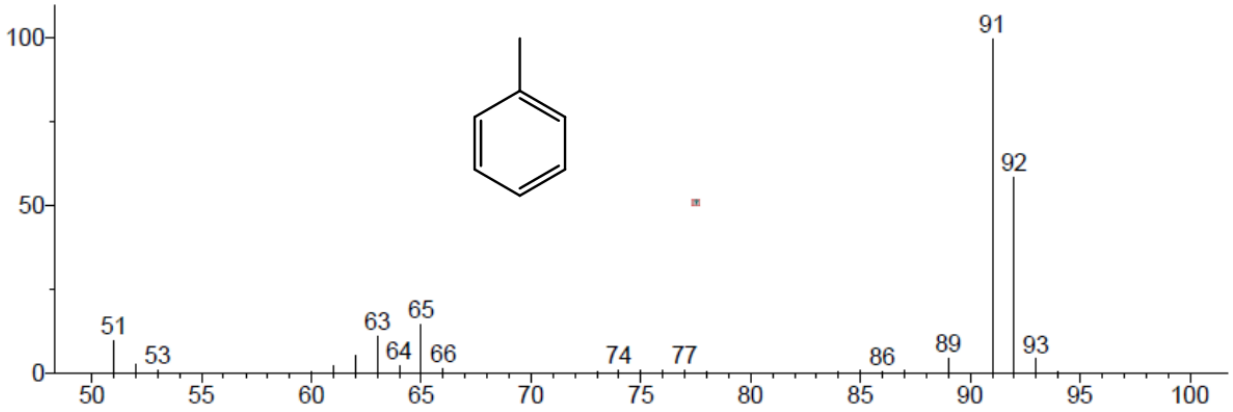

Figure A2. Fragmentation pattern of the toluene separated by GC from the supernatant of the reaction of d = 3.4 nm H-SiNCs with PCl_5 in toluene (same as the pattern in spectral library: CAS: 108-88-3; Lib: replib; ID: 12329).

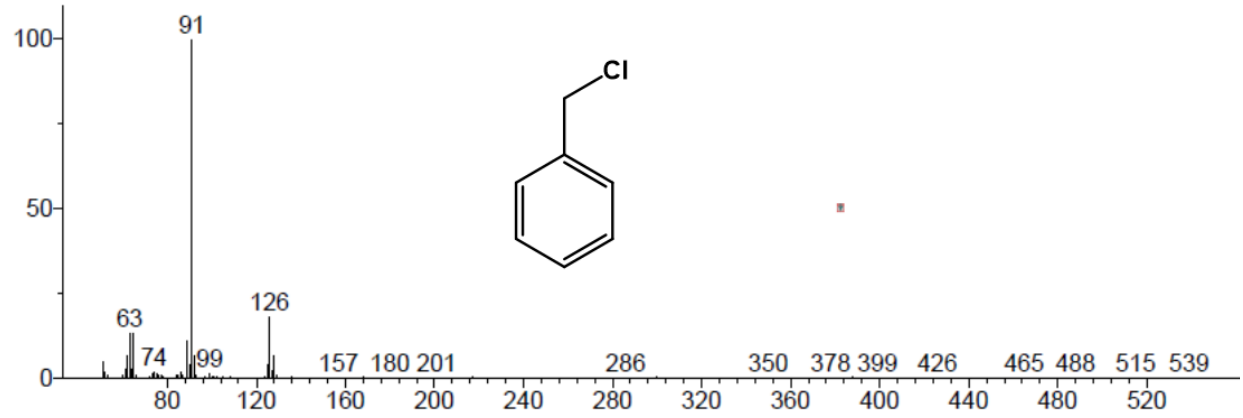

Figure A3. Fragmentation pattern of the benzyl chloride separated by GC from the supernatant of the reaction of d = 3.4 nm H-SiNCs with PCl_5 in toluene (same as the pattern in spectral library: CAS: 100-44-7; Lib: mainlib; ID: 56262).

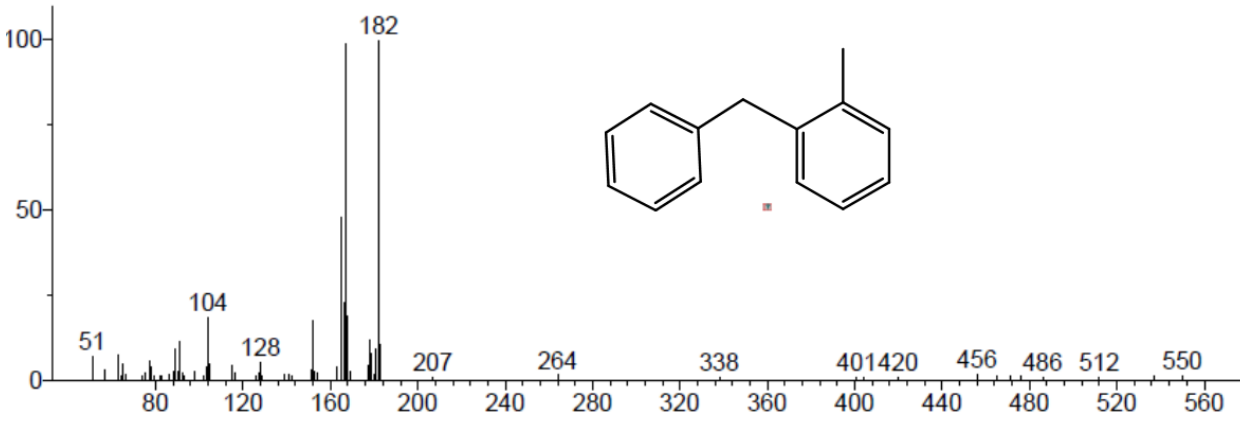

Figure A4. Fragmentation pattern of the ortho-benzyltoluene separated by GC from the supernatant of the reaction of d = 3.4 nm H-SiNCs with PCl_5 in toluene (same as the pattern in spectral library: CAS: 713-36-0; Lib: replib; ID: 23836).

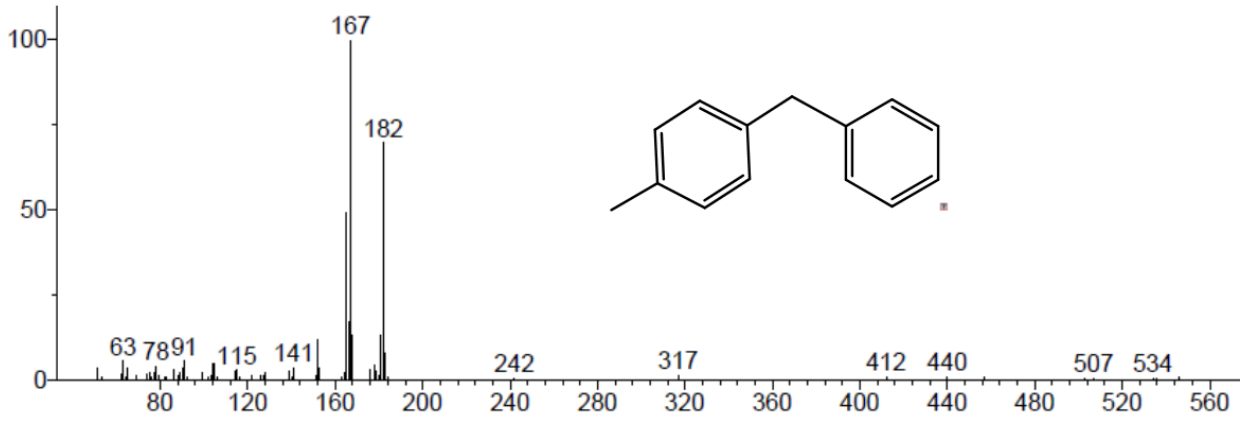

Figure A5. Fragmentation pattern of the para-benzyltoluene separated by GC from the supernatant of the reaction of d = 3.4 nm H-SiNCs with PCl_5 in toluene (same as the pattern in spectral library: CAS: 620-83-7; Lib: replib; ID: 23833).